Building a hierarchical tree of erythro-myeloid progenitor (EMP)-derived haematopoiesis

Lorea Iturri Torrea

Building a hierarchical tree of erythro-myeloid progenitor (EMP)-derived haematopoiesis

Doctoral thesis on Immunology,
Ecole doctoral Complexité du Vivant, Sorbonne université

Presented by
Lorea Iturri Torrea

Macrophages and Endothelial Cells,

Department of Stem Cell and Development, Department of Immunology,

Institut Pasteur

Directed by Elisa Gómez Perdiguero

Publicly presented and defended on 13th November 2020

In front of a jury composed of :

Dr Thierry Jaffredo	President of the Jury
Dr Berthold Göttgens	Reviewer
Dr Elaine Dzierzak	Reviewer
Dr James Palis	Examiner
Dr Ana Cumano	Examiner
Dr Elisa Gómez Perdiguero	PhD Supervisor

To my parents

ACKNOWLEDGEMENTS

This PhD study was carried out in 2016-2020 in the team Macrophages and Endothelial Cells, within the department of Stem Cells and Development and the department of Immunology at Institut Pasteur in Paris.

First of all, I would like to express my appreciation to each member of my thesis jury for accepting to be part of this event. I am grateful to Dr. Thierry JAFFREDO to be the president of my jury, as well as to Dr. Berthold GÖTTGENS and Dr. Elaine DZIERZAK for accepting to review the manuscript. I'm also thankful to Dr. Ana CUMANO and Dr. James PALIS to accept to be the examiners.

I owe a deep gratitude to my project supervisor, Dr. Elisa GÓMEZ PERDIGUERO for giving me the opportunity to work in her team. I'm thankful for her trust and guidance during these years.

I would also like to thank all the members of the lab for their support during these years. Specially, I would like to first thank Dr. Javier SÁENZ CORONILLA to help me build some confidence during the first two years and ending up becoming a true friend. I am very grateful to Dr. Laina FREYER, without whom the single cell project would not have happened. Thank you for always being so good-natured and helpful, thank you also for the endless discussions on populations and populations. I would like to thank Kémy ADÉ and Rebeca PONCE LANDETE for student support, specially Rebeca for the moral support I needed the last year. Also, I would like to thank Dr. Yvan LALLEMAND and Pascal DARDENNE for technical help and for showing me all I know about mice. Finally, I am very grateful to Dr. Anne BITON for the bioinformatic analysis.

I'm also grateful to Dr. Ana CUMANO and her team for the technical help and insightful discussions, specially to Dr. Ramy ELSAID for showing me techniques that I used throughout this work.

I am thankful to the members of my two Comité de Suivi de Thèse: Dr. Charles DURAND, Dr. Philippe HERBOMEL and Dr. Christian VOSSHENRICH for their attendance and pieces of advice during my thesis.

I would like to thank also the different platforms of Institut Pasteur for allowing me produce this work: the Cytometry & Biomarkers UTechS Platform, the Animal Facility and the Pasteur Single Cell Initiative, with special thanks to Dr. Yann LOE MIE and Dr. Baptiste SAUDEMONT for their help with the MARS-Seq pipeline. I'm also thankful to the ANR and the Labex REVIVE for fully funding my scholarship for these four years.

I would like to thanks my girls in Paris, Dr. Eva CONDE GARCÍA and Dr. Júlia TORNÉ CORTADA, for enduring with me these past 6 years and with whom I have shared more than flat (or two). I would like to thank the rest of my Spanish support team for the healing lunches in the cantine and the beer hours we have shared in The 25: Cristina FERNÁNDEZ MOLINA, Anna SEGÚ CRISTINA and MARÍA BENAVENTE DÍAZ.

Por último, me gustaría agradecer inmensamente a mis padres, Antxón ITURRI GAZTELU y Ana TORREA LARRAMENDI, por haberme empujado siempre hacia delante y por haberme permitido volar hasta donde estoy. I'm greatly appreciative to Haser SÜTÇU for taking so good care of me, this thesis would have been much more difficult without you by my side.

LIST OF CONTENTS

ACKNOWLEDGEMENTS **3**

LIST OF CONTENTS **5**

ABBREVIATIONS **9**

INTRODUCTION **11**

1.- Development of the hematopoietic system **11**

The generation of hematopoietic waves during embryonic development 12

1.1- First wave (primitive) 14

1.2 Second wave (Yolk sac definitive hematopoiesis) 16

1.2.1 Erythromyeloid progenitors 16

1.2.2 Lymphoid-primed precursors found in the early yolk sac 19

1.3- Third wave (hematopoietic stem cells) 21

2.- Emergence of EMPs **24**

2.1 Anatomy and development of the yolk sac 25

2.2 Endothelial to hematopoietic transition 29

2.2.1 EHT of hematopoietic stem cells 29

2.2.2 EHT of erythromyeloid progenitors 32

3. EMP-derived hematopoietic lineages **33**

3.1- Erythroid lineages 35

3.1.1- Red blood cells 35

Definitive RBC in development 37

3.1.2- Megakaryocytes 38

Mk in development 40

3.2- Myeloid lineages 40

3.2.1- Monocytes 40

Monocyte subsets 41

Monocyte development 41

Monocytes: a precursor for macrophages and dendritic cells 42
3.2.2- Resident macrophages 43
Functional diversity of ResMf 44
Developmental origins of resident macrophages 45
First wave of macrophage production in the yolk sac 45
Second wave of macrophage production in the fetal liver 47
Third wave of macrophage production from the fetal liver and bone marrow 47
3.2.3- Dendritic cells 48
DC heterogeneity 48
DC development 49
3.2.4- Granulocytes 50
Granulocyte heterogeneity 51
Granulocyte development 52
3.2.4- Mast cells 54
Mast cell development 54
AIMS AND OBJECTIVES 57
MATERIALS AND METHODS 59
Published protocol 61
RESULTS 71
Part 1. Yolk sac. Paper manuscript to be submitted 71
Part 2. Fetal liver 119
EMP derived cells in the fetal liver 119
Single cell expression analysis of EMP-derived progenitors of the yolk sac and fetal liver 122
DISCUSSION 133
1.- Phenotype of yolk sac definitive MEPs 133
Csf2rb/CD131 as a marker of early MEP commitment in the yolk sac 134
2.- EMP-derived megakaryopoiesis 136
3.- Production of macrophages by EMPs 138

Macrophage cluster in the single cell analysis 139

4. EMP-derived mast cell production 140

Differentiation hierarchy of mast cell progenitors 141

5. Similarities and differences between EMPs emerging at E8.5 and at E9.5 142

Phenotype of bona fide EMPs in the yolk sac 142

Observation of “early” and “late” emerging EMPs 143

REFERENCES 153

LIST OF FIGURES 178

LIST OF TABLES 179

ABSTRACT 180

English 180

Français 180

ABBREVIATIONS

AGM	Aorta-Gonads-Mesonephros
BaP	Basophil progenitor
BFU-E	Burst Forming Unit-Erythroid
BMP	Basophil and Mast cell progenitor
cDC	conventional DC
CDP	Common Dendritic cell Progenitor
CFC/CFU	Colony Forming Cells/Units
CFU-E	Colony Forming Unit-Erythroid
cMoP	common Monocyte Progenitor
CMP	Common Myeloid Progenitors
DC	Dendritic Cells
DETC	Dendritic Epidermal T Cells
E	Embryonic day (mouse development)
EHT	Endothelial to Hematopoietic Transition
EMP	Erythro-Myeloid Progenitor
EoP	Eosinophil Progenitor
FL	Fetal Liver
GMP	Granulocyte-Monocyte Progenitor
GW	Gestational weeks (human development)
HSC	Hematopoietic Stem Cell
HSPC	Hematopoietic Stem and Progenitor Cells
LTR	Long Term Reconstitution

MC	Mast Cells
MCp	Mast Cell progenitor
MDP	Monocyte and Dendritic Cell Progenitor
MEP	Megakaryocyte and Erythrocyte Progenitor
Mf	Macrophages
Mk	Megakaryocytes
Mo	Monocytes
MPP	Multipotent progenitors
NeuP	Neutrophil Progenitor
OHT	4-Hydroxy-Tamoxifen
pDC	plasmacytoid DC
pSp	para-aortic Splanchnopleura
RBC	Red Blood Cells
resMf	resident Macrophages
TAM	Tamoxifen
YS	Yolk Sac

INTRODUCTION

1.- Development of the hematopoietic system

The hematopoietic system is composed of a variety of blood cells that circulate through the body and the organs that are involved in their production and maturation: the bone marrow, spleen, thymus and lymph nodes in adulthood. Blood cells provide the necessary oxygen supply to the body (erythrocytes), prevent blood loss by clotting (platelets) and defend the host against internal aberrant cells and external pathogens by generating an immune response (myeloid and lymphoid cells).

Immune responses can be classified as part of the innate and adaptive immunity. Innate immune responses are fast, initiated within minutes or hours, and are not specific to pathogens. They embody a group of proteins and phagocytic cells that recognize conserved features of pathogens and become quickly activated to help destroy the invaders. Adaptive immune responses, on the other hand, are highly specific to the particular pathogen and provide long-lasting protection(Alberts et al., 2002).

Hematopoietic stem cells (HSCs) are responsible for the continuous blood cell production, a process known as hematopoiesis, while maintaining a pool of self-renewing stem cells, capable of long-term reconstitution activity. In the adult, hematopoiesis is localized in the bone marrow, spleen and thymus. However, not all the adult immune cells are produced by adult HSC.

Several studies to date have identified an additional layer of hematopoietic cells that are not produced by adult HSC, which includes tissue-resident macrophages and some lymphocyte subsets such as skin Vγ5+ γδT cells, also named dendritic epidermal-like T cells (DETC), and peritoneal B1a B cells(Beaudin et al., 2016; Elsaid et al., 2019). These immune

cell subsets are only produced during embryonic life and are maintained in their tissue of residency by self-renewal, independently of adult bone marrow hematopoiesis. Importantly, tissue-resident macrophages have further been shown to be able to develop from progenitors that are independent from HSC yet persist throughout adult life through localized self-renewal (Ginhoux et al., 2010; Gomez Perdiguero et al., 2015; Schulz et al., 2012). In order to better understand the respective contribution of HSC-derived and HSC-independent hematopoiesis, we need to further understand the events that happen in the early embryo and establish the foundation of the hematopoietic system.

The generation of hematopoietic waves during embryonic development

Groundbreaking studies described the existence of different waves of hematopoietic progenitor emergence that overlap in embryonic development in different model organisms, from invertebrates (D. melanogaster)(Evans et al., 2003; Holz et al., 2003), to amphibians (xenopus)(Ciau-Uitz et al., 2000; Turpen and Smith, 1985; Turpen et al., 1997), teleost fish (Danio rerio, zebrafish)(Bertrand and Traver, 2009; Davidson and Zon, 2004), avians (chicken, quail)(Dieterlen-Lievre, 1975; Sabin, 1920) and mammals (mouse and human)(Ivanovs et al., 2017; McGrath et al., 2015a; Müller et al., 1994; Russell and Seldon E. Bernstein, 1966). In mammalian embryos, blood cell production is observed in several successive niches: the extra-embryonic yolk sac, chorio-allantoic placenta, para-aortic splanchnopleura (pSp), aorta-gonad-mesonephros (AGM) region, fetal liver, spleen and the bone marrow (Dzierzak and Speck, 2008).

Historically, developmental hematopoiesis was subdivided into two main phases or waves, an embryonic or primitive wave, comprised of transitory hematopoietic cell populations located in the yolk sac; and a definitive wave, originating later in development and providing all mature hematopoietic cell lineages for the lifetime of the organism (Godin and Cumano, 2002). Subsequently, yolk sac hematopoiesis was further subdivided into two independent primitive and definitive waves, after careful examination of its erythropoietic component(Palis

et al., 1999; Wong et al., 1986); reviewed in(Palis and Yoder, 2001). Throughout this chapter, I will explain the characteristics of each of the three overlapping waves of mammalian embryonic hematopoiesis: primitive, yolk sac-definitive (EMP) and intraembryonic-definitive (HSC) hematopoiesis.

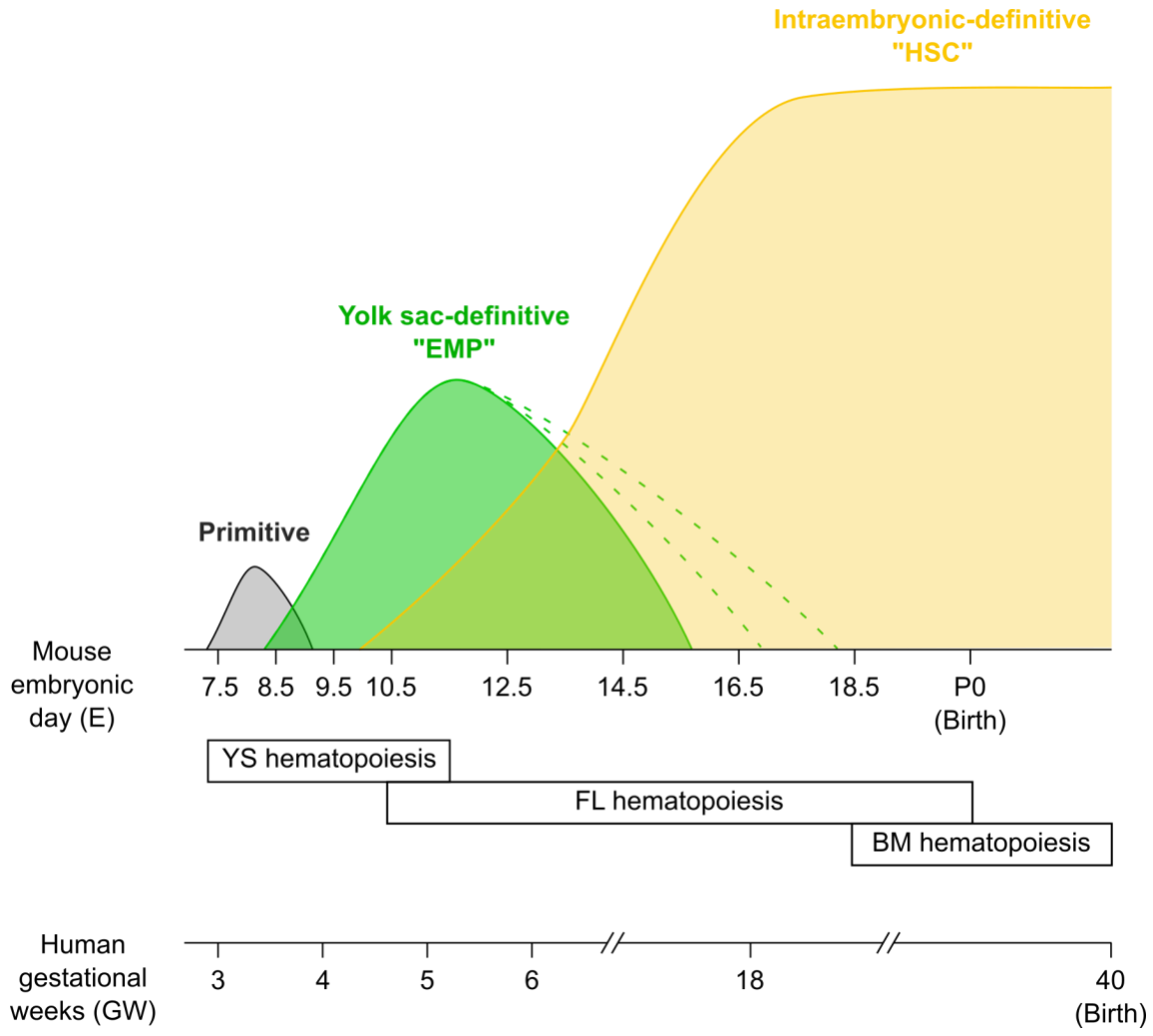

Figure 1. Illustration of the three hematopoietic waves during mammal development. A first transient primitive wave of progenitors emerges in the yolk sac at E7-7.5. The second wave of progenitors is composed of EMPs, that are found in the yolk sac and the fetal liver, and whose timing of exhaustion is still debated. Finally, HSCs take over fetal liver hematopoiesis and migrate to the bone marrow, where they will continue during adulthood. Progenitor numbers are represented by height of the peak. Approximate human hematopoietic timeline compared to mice from (Ivanovs et al., 2017; Mikkola and Orkin, 2006).

1.1- First wave (primitive)

Studies conducted in the beginning of the century observed that early mammalian embryos have specific blood cells compared to mid-late embryos (fetal liver) or adults (bone marrow). The concept of primitive hematopoiesis was intimately associated with the observation of nucleated erythropoiesis in young mammalian embryos that resemble those of birds, fish, reptiles, and amphibians (Gulliver, 1875; Migliaccio et al., 1986; Sabin, 1920). Also, macrophages had been observed with electron microscopy in the yolk sac starting from E9, thus before the appearance of monocytes or promonocytes (Enzan, 1986; Takahashi et al., 1989).

The first active hematopoietic site is located in the yolk sac, an extra-embryonic organ. The yolk sac (YS) produces clonogenic myeloid and erythroid progenitors that fail to long-term repopulate irradiated recipients (Dieterlen-Lievre, 1975; Lassila et al., 1978; Medvinsky and Dzierzak, 1996; Moore and Metcalf, 1970). Primitive monopotent precursors of erythrocytes, megakaryocytes and macrophages mature faster than their adult counterparts and are independent of the transcription factor Runx1, necessary for definitive hematopoietic emergence (Chen et al., 2009; Palis et al., 1999; Potts et al., 2014). This wave is characterized to emerge directly from the YS mesoderm and not through an endothelial intermediate like the following definitive waves. Importantly, targeted disruption of genes involved in primitive hematopoiesis regulation, such as *Scl/Tal1*, *Gata1* or *Lmo2*, causes embryonic death as early as E10.5, which highlight the importance of this wave to sustain early embryo growth (Fujiwara et al., 1996; Robb et al., 1995; Shivdasanl et al., 1995; Warren et al., 1994).

Primitive erythroid cells emerge in the yolk sac soon after gastrulation, at E7.5-8 in the mouse(Silver and Palis, 1997) and 18–19 days of gestation in humans(Bloom and Bartelmez, 1940; Luckett, 1978), and mature semi-synchronously in the bloodstream. Primitive erythroid precursors are also called EryP-CFC (CFC, colony forming cells) since they produce characteristic compact colonies of large erythroid cells in culture. EryP-CFC expand for 48

hours in the yolk sac and are rapidly extinguished by E9 (Palis et al., 1999). Primitive red blood cells can be distinguished from their definitive counterparts by their larger size and nuclei, as well as the expression of embryonic globins like the *εγ-* and *βH1-globin* genes in mouse (*ε-* and *γ-globin* genes in human)(Kingsley et al., 2006; Stamatoyannopoulos, 2005). At E12.5, primitive erythroid precursors cease dividing in the bloodstream and are rapidly substituted by the first definitive red blood cells released from the liver that quickly become the predominant cell type in circulation. Between E12.5 and E16.5 definitive red blood cells have been shown to enucleate and can remain in circulation several days (at least 5-7) after their enucleation (Fraser et al., 2007; Kingsley et al., 2004). Despite their dilution by definitive red blood cells, primitive erythrocytes can still be detected after birth in mice(Fraser et al., 2007; Kingsley et al., 2004).

Most platelets found before E10.5 are of maternal origin (Potts et al., 2014) and a few maternal-derived macrophages are transiently detected at E7.5-8. Both megakaryocyte and macrophage embryonic precursors emerge in the yolk sac at E7.5 (Palis et al., 1999). The first megakaryocytes of the yolk sac are observed at E8.5 and they form platelets by E10.5 (Potts et al., 2014). These primitive Mk are characterized by a faster rate of platelet production and lower ploidy (2-8N) (Palis et al., 1999; Tober et al., 2007; Xu et al., 2001). They are shown to be small, Runx1-independent, megakaryocytes that generate platelets very fast and have limited capacity to endoreplicate (Potts et al., 2014; Tober et al., 2007; Xu et al., 2001).

As for primitive macrophages, they have been observed in the vascular lumen of the yolk sac from E9.0, before the appearance of monocytes, and characterized by an expression of F4/80 and an immature phenotype of a round shape, a euchromatic nucleus with large nucleoli, poorly developed Golgi apparatus, few intracytoplasmic organelles, abundant polyribosomes, and the absence of peroxidase activity (Naito et al., 1989, 1996; Takahashi et al., 1989). Few monopotent macrophage precursors (2-9) have been observed in the E7.5 yolk sac, and their number rises to 100 precursors by E8.5 (Palis et al., 1999).

Nevertheless, it is still challenging to separate primitive macrophages and megakaryocytes from their definitive counterparts that arise in the definitive waves. We currently lack tools to perform specific genetic labelling to trace primitive megakaryocytes or macrophages separately from those derived later. Indeed, although primitive cells do not undergo an endothelial to hematopoietic transition (EHT, discussed later), EHT genes can be expressed throughout their development or maturation, as evidenced by the labelling of primitive erythroblasts using fate mapping approaches based on endothelial or EHT genes such as *Tie2/Tek* and *Runx1*(Samokhvalov et al., 2007; Stefanska et al., 2017; Tang et al., 2010). Indeed, Runx1-deficiency leads to lack of primitive macrophages(Lacaud et al., 2002), defective maturation of primitive erythrocytes (Yokomizo et al., 2008) and decreased number of primitive diploid megakaryocytes (Potts et al., 2014). We thus have a very limited understanding of the spatiotemporal pattern and functional contribution of primitive macrophages and megakaryocytes to development.

1.2 Second wave (Yolk sac definitive hematopoiesis)

1.2.1 Erythromyeloid progenitors

Colony forming assays demonstrated that a second wave of multipotent progenitors appeared at E8.25, containing definitive erythroid progenitors (BFU-E and CFU-E colonies) and multipotent myeloid progenitors (macrophage colonies were associated with mixed granulocyte, monocyte and mast cell colonies) (Palis et al., 1999). YS definitive progenitors were characterized as highly proliferative potential colony-forming cells (HPP-CFC) that give rise to macroscopic colonies when cultured in vitro (Palis et al., 2001). Such progenitors were named erythromyeloid progenitors (EMPs) as they have the potential to give rise to definitive hematopoietic cells from both the erythroid and myeloid lineages (Bertrand et al., 2007; Gomez Perdiguero et al., 2015; McGrath et al., 2015a). While EMPs are a transient population of progenitors, rescue experiments following the disruption of a Runx1 binding partner, *Cfbβ*, showed that they are required for fetal survival (Chen et al., 2011). Indeed, the first definitive erythrocytes

of the embryo are produced by EMPs in the E11.5 fetal liver (Gomez Perdiguero et al., 2015; McGrath et al., 2011) and defective EMP-derived erythropoiesis in *Myb*-deficient embryos is embryonic lethal by E15.5 (Mucenski *et al.*, 1991).

In the yolk sac, the expression of Kit and CD41 at E8.25 is associated with the onset of definitive hematopoiesis in the mouse(Ferkowicz et al., 2003), also in day 6 of cultured mouse and human embryoid bodies (EBs)(Garcia-Alegria et al., 2018; Mikkola et al., 2003), and are observed in co-expression in the YS hemogenic clusters(Frame et al., 2016). EMP potential has been shown to be enriched in the E9-10.5 YS Kit^+ $CD45^{low}$ $AA4.1^+$ fraction(Bertrand et al., 2005a; Gomez Perdiguero et al., 2015) and in the E9.5 YS Kit^+ $CD41^+$ $CD16/32^+$ fraction(McGrath et al., 2015a). However, a consensus has not been yet reached regarding the immunophenotypic definition of *bona fide* EMP at different stages.

It is known however that EMPs emerge from the yolk sac vasculature starting from E8.25 in the mouse, 4 GW in humans, in a Runx1-dependent endothelial to hematopoietic transition (EHT) (Chen et al., 2011; Frame et al., 2016; Gomez Perdiguero et al., 2015; Kasaai et al., 2017; Migliaccio et al., 1986). Hence, EMPs are yolk sac-derived multipotent progenitors that embody the first wave of definitive hematopoiesis. Contrary to hematopoietic stem cells, they do not give rise to lymphoid cells and are not capable of long-term reconstitution in irradiated mice. EMPs enter the bloodstream at E9-9.5 and colonize the fetal liver, where they massively expand and differentiate into erythrocytes, megakaryocytes, macrophages, monocytes, granulocytes and mast cells (Gentek et al., 2018a; Gomez Perdiguero et al., 2015; Hoeffel et al., 2015; Stremmel et al., 2018). Contrary to HSC, blood flow is not necessary for EMP emergence, as evidenced in embryos with targeted inactivation of the sodium-calcium exchanger (Ncx1) resulting in lack of heartbeat(Frame et al., 2016).

Interest in EMP biology was sparked recently by the discovery that they give rise to some adult resident myeloid populations. Tissue resident macrophages were shown to differentiate from EMPs in the early embryonic life and colonize the organs during gestation (Gomez

Perdiguero et al., 2015; Hoeffel et al., 2015). Further, these macrophages are not dependent on bone marrow HSC in steady state and self-maintain by local proliferation (Ajami et al., 2007; Bouwens et al., 1986; Chorro et al., 2009; Ghigo et al., 2013; Hashimoto et al., 2013; Jenkins et al., 2011; Yona et al., 2013). Similarly, EMP have also been proposed to give rise to adult mast cells in specific niches (Gentek et al., 2018a; Li et al., 2018).

Although it is now established from a variety of complementary studies that EMP differentiate into tissue resident macrophages, the extent of their contribution remains currently unclear. The gold standard to investigate ontogeny is through genetic fate mapping, but the temporal overlap with other hematopoietic waves and shared expression of genes used for Cre-driven strategies (*Runx1*, *Csf1r*, *Tie2*, *Kit* and *Cdh5*) makes it difficult to make definitive conclusions on the subject. Also, inducible Cre-driven labelling rarely reaches saturation (100%), which hinders the interpretation of results. It is proposed that the embryonic EMP contribution to adult pools depends on the niche availability and/or postnatal modifications, microglia being mostly constituted of embryonic self-renewing cells (Ginhoux et al., 2010; Gomez Perdiguero et al., 2015; Kierdorf et al., 2013) while lamina propria macrophages shift to adult HSC-derived origin during weaning (Bain et al., 2014).

It is tempting to hypothesize that EMP-like progenitor cells are present in the bone marrow in a quiescent state. A rare embryonic-like population of cells (Very Small Embryonic-Like Stem Cells, VSELs) have been identified in the adult bone marrow with the potential to regenerate damaged tissues and there seems to be an “EMP-like program” in the BM upon critical regeneration (Faltusová et al., 2020; Kucia et al., 2006). However, there is so far no evidence that VSELs are responsible for that program or that they are linked to *bona fide* embryonic EMPs. The current most reliable method to identify embryonic population progeny in the adult remains *in utero* genetic fate-mapping, which has failed to demonstrate any contribution of EMPs to adult bone marrow progenitor populations.

1.2.2 Lymphoid-primed precursors found in the early yolk sac

The discovery of lymphoid potential in the yolk sac at E9 raised the possibility that lymphoid precursors emerge in the yolk sac independently of hematopoietic stem cells(Liu and Auerbach, 1991; Yoder et al., 1997). Some lymphoid cells are tissue residents and self-maintain locally in the tissues by self-renewal, such as peritoneal B-1a B cells(Haas et al., 2005), skin γδT cells(Jameson et al., 2004; Payer et al., 1991) and lymphoid tissue inducer (LTi) cells, a subset of group 3 innate lymphoid cells (ILC3), in both lymphoid and non-lymphoid organs(Gasteiger et al., 2015). It has been suggested that these cells derive in fact from yolk sac-derived lymphoid-primed multipotent progenitors that emerge before definitive HSCs can be detected (Böiers et al., 2013; Yoshimoto et al., 2011). These studies have shown that a distinct lymphoid-primed progenitor population in the yolk sac, co-expressing classical lymphoid (*Rag1* and *Il7r)* and myeloid-associated genes, contribute to fetal lymphocytes and myeloid cells (but not to tissue resident macrophages). A subsequent study proposed that such progenitors give rise to epidermal γδ T cells (Gentek et al., 2018b) but this interpretation is not supported by another recent study, that claims their origin is, in fact, in embryonic HSC(Elsaid et al., 2019).

This population is distinct from EMP since it has been demonstrated that EMPs emerge prior to E9 and do not give rise to lymphocytes (Gomez Perdiguero et al., 2015; McGrath et al., 2015a). Additionally, B-lymphocyte potential prior to E9.5 is only found in the CD41 negative population of yolk sac cells, which is a key marker of EMPs at that stage (Yoshimoto et al., 2011).

It has not yet formally been proven whether these lymphoid-primed multipotent progenitors are generated *in situ* in the YS or if they are HSC-independent, as cells can reach the yolk sac through circulation at these stages. Indeed, lymphoid precursors appear inside the embryo proper earlier than they do in the yolk sac (Cumano et al., 1996; Godin et al., 1993; Tavian et al., 2001). Definitive LTR-HSC activity has been found in the AGM region at a time

slightly earlier than in the yolk sac and fetal liver (Cumano et al., 2001; Müller et al., 1994). It is also important to bear in mind that HSCs that emerge in the major arteries by E9.5 lack long term reconstitution capacity *in vivo* (thus named pre-HSC), but acquire it after culture (Cumano et al., 1996; Medvinsky and Dzierzak, 1996), which was not tested in the Yoshimoto and Böiers studies. It is thus not excluded that such lymphoid progenitors are in fact pre-HSC or multipotent progenitors generated from the earliest HSC.

The concept that some lymphoid-producing HSCs could be generated from yolk sac clusters was also claimed by a study that showed up to 10% of labelling of adult HSC when tamoxifen was administered at E7.5 in *Runx1*^{MerCreMer} embryos (Samokhvalov et al., 2007). However, the administration of tamoxifen (TAM) instead of the active form 4-hydroxy-tamoxifen (OHT) could lead to labelling of Runx1+ cells beyond E8.5. This distinction is key in lineage-tracing studies analysing such close-by events and is related to the pharmacological kinetics of tamoxifen in inducible Cre-lox strains. In those, a fusion gene is created between a bacterial Cre recombinase and the ligand binding domain of modified estrogen receptors (ER or Mer), which prevents the translocation of the produced protein into the nucleus(Metzger et al., 1995; Zhang et al., 1996). When TAM is administered, the reagent is metabolized by the liver into OHT, its active metabolite form with high binding affinity for estrogen receptor. OHT binds to the estrogen receptors, allowing translocation to the nucleus and initiation of Cre-mediated recombination. Administration of OHT by intraperitoneal injection ensures therefore a tighter temporal control of gene recombination events at the time of the injection.

Since the number of lymphoid precursors in the yolk sac at E9.5 and E10.5 is very small compared to the thousands of EMPs at that moment (Böiers et al., 2013; Gomez Perdiguero et al., 2015; Palis et al., 1999; Yoder et al., 1997; Yoshimoto et al., 2011) and their origin is still debated, we will consequently refer exclusively to EMP-derived hematopoiesis when discussing definitive yolk sac-hematopoiesis.

1.3- Third wave (hematopoietic stem cells)

Hematopoietic stem cells (HSC) are characterized by two main properties: multipotency and self-renewal. They are multipotent stem cells that can give rise to hematopoietic cells from the erythroid, myeloid and lymphoid lineages. They are also able to maintain an HSC pool by self-renewal, as assessed by the capacity of a single cell to reconstitute the hematopoietic system of an irradiated mouse in long term reconstitution (LTR) experiments.

Pioneering work in the 70s (Françoise Dieterlen-Lievre, 1975) demonstrated that the embryo proper, not the yolk sac, is the only source of HSC in the avian species, this was later proven true in mice(Cumano et al., 2001; Medvinsky and Dzierzak, 1996; Müller et al., 1994) and humans(Ivanovs et al., 2011; Tavian et al., 2001). The aorta has been shown to contain progenitor cells with erythroid, myeloid and lymphoid activity as early as E8(Cumano et al., 1996) and intra-aortic clusters can be observed from E9 up until E14 in the pSp, the AGM region and other major vessels (De Bruijn et al., 2002; Garcia-Porrero et al., 1995; Yokomizo and Dzierzak, 2010), also in a Runx1-dependent manner(Cai et al., 2000; North et al., 1999, 2002). The peak of cluster formation has been observed at E10.5, at the time in which cells with HSC capacity are first detected, and the largest clusters are found in the vitelline and umbilical artery, which connect the embryo with the yolk sac and placenta, respectively(Yokomizo and Dzierzak, 2010). Of note, human aortic clusters have been observed at 5-6 GW(Tavian et al., 1996). It is thought that little hematopoietic differentiation occurs locally (Godin et al., 1999; Kieusseian et al., 2012). HSC start to colonize the fetal liver from E10.5, where they mature, expand and ultimately give rise to myeloid, erythroid and lymphoid cells (Godin et al., 1999; Kieusseian et al., 2012).

HSCs dramatically expand in the fetal liver from E11.5 to E15.5, where they begin to establish an adult-like hierarchy of an expanding pool of multipotent progenitors (Ikuta et al., 1990; Morrison et al., 1995a). The fetal liver is the principal site of mid- and late-gestation

hematopoiesis in mice, and the shift towards bone marrow hematopoiesis is due to changes in the local hematopoietic microenvironment initiated by embryonic organogenesis (Mikkola and Orkin, 2006). The migration to the fetal bone marrow is essentially a progressive process that initiates at E16.5 and is finalized when the fetal liver hematopoiesis ceases at 2-4 days after birth (Christensen et al., 2004; Coşkun et al., 2014; Sasaki and Sonoda, 2000; Wolber et al., 2002). In humans, on the contrary, the fetal bone marrow starts to be colonized already at the end of the first trimester, at 10-11 GW, and becomes a second major location for hematopoiesis in the fetus during the second trimester, at 20-22 GW. Human fetal liver hematopoiesis is thought to decline in the third trimester and to cease soon after birth (Charbord et al., 1996; Golfier et al., 2000; Migliaccio et al., 1986). The difficulty to access mid and late gestation human tissues and the definition of HSC by their ability to LTR in irradiated hosts hampers the study of this key stage in humans, so most of our current understanding of late hematopoietic development comes from studies in the mouse. Although early ontogeny is largely conserved among mammals, it is thus important to keep in mind that midgestation hematopoietic events could differ, as does the onset of bone marrow hematopoiesis, between human and mouse.

HSC in the adult bone marrow perform differently than in the embryo. Indeed, adult HSC are quiescent cells that rarely enter the G1 stage of the cell cycle (Passegué et al., 2005). On the contrary, HSCs in the fetal liver are actively cycling and are more efficiently transplanted into irradiated mice, suggesting cell-intrinsic differences between HSCs in the fetus and adult bone marrow (Harrison et al., 1997; Morrison et al., 1995b; Rebel et al., 1996). Cell surface markers are also differently expressed in embryonic HSCs. Adult bone marrow HSC are defined by the lack of surface expression of lineage-specific markers and expression of Sca-1 and c-Kit (LSK population), they also downregulate CD34 expression by 10 weeks after birth (Ogawa et al., 2001). Conversely, embryonic HSC express lower levels of Sca-1 in the surface until E12.5, CD93/AA4.1 (an endothelial or B cell marker), VE-Cadherin (endothelial marker) and 50% are expressing Mac-1/CD11b (a myeloid marker)(Bertrand et al., 2005a; De Bruijn et

al., 2002; Sánchez et al., 1996). It is not known whether these molecules play a role in the behaviour of HSC during fetal life or if they are involved in their high expansion rate.

	Primitive	Yolk-sac definitive	Embryo definitive
Potential	Monopotent (E or Mk or Mf)	Multipotent (E/Mk-My)	Multipotent (E/Mk-My-Ly)
Time of emergence	E7.5-8.5 (?)	E8.25-E11.5	E9.5-E12.5
Niche of emergence	Yolk Sac	Yolk Sac	Embryo proper
EHT	No	Yes (vasculature)	Yes (arteries)
Globins in mice	ζ, βH1, εγ, α1, α2, β1 and β2	βH1(low), α1, α2, β1 and β2	α1, α2, β1 and β2
Fate mapping strategies	*Bh1-GFP* (only for erythrocytes)	*Csf1r*^{MiCM} OHT E8.5-9.5	*Csf1r*^{MiCM} OHT E10.5
		Cdh5^{CreERT2} OHT E7.5	*Cdh5*^{CreERT2} OHT E10.5
		Runx1^{MCM} OHT E7.5	*Runx1*^{MCM} OHT E8.5-9.5
	Kit^{MiCM} OHT E7.5(?)	*Kit*^{MiCM} OHT E7.5-8.5	*Kit*^{MiCM} OHT 8.5-9.5
	Tie2^{MCM} OHT E7.5(?)	*Tie2*^{MCM} OHT E7.5-E8.5	*Tie2*^{MCM} OHT E10.5
			Vav^{Cre}

Table 1. Summary of main characteristics of the three hematopoietic waves. MCM, MerCreMer; MiCM, MeriCreMer; OHT, 4-hydroxytamoxifen; ?, supposition, data available does not allow to define. The fate-mapping strategies that can label each wave are extensively explained in (Gentek et al., 2018a; Höfer et al., 2016; McGrath et al., 2015b; Stefanska et al., 2017)

Interestingly, studies on induced pluripotent stem cells (iPSC) and embryonic stem (ES) cells have further confirmed the emergence of overlapping waves of hematopoiesis. ES cells generate first unipotent primitive colonies —macrophage, erythroid and megakaryocyte— and secondly definitive colonies associated to endothelium —GM-CFC, BFU-E, mast cells and a second wave of megakaryocytes— (Fujimoto et al., 2003; Hadland et al., 2004; Irion et al., 2010; Kennedy et al., 2007; Zambidis et al., 2005). Additionally, murine ES cells grown as EBs can generate a population of immunophenotypic EMPs (Kit^+ $CD41^+$ $CD16/32^+$) with similar potential than *in vivo* (McGrath et al., 2015a) and without long-term reconstitution capacity. The mechanisms for which yolk sac but not AGM hematopoiesis can be mimicked in ES and iPS cells remain elusive to this day and need to be further investigated (Batta et al., 2014; Lacaud and Kouskoff, 2017).

2.- Emergence of EMPs

Central to the field of embryonic hematopoiesis is the generation of definitive progenitors from endothelial precursors. It is now well established from a variety of studies in several vertebrate model organisms that EMPs form hematopoietic cell clusters attached to the vessel walls of the yolk sac, in a manner similar to HSCs(Chen et al., 2011; Frame et al., 2016; Kasaai et al., 2017; Palis and Yoder, 2001). While the process of HSC emergence has been extensively studied in the last decades, especially in the dorsal aorta, less is known about the inherent mechanisms of EMP emergence. The understanding of their production is fundamental to understand EMP biology and could explain intrinsic differences between the two lineages.

This chapter provides an overview of the current knowledge on EMP emergence, starting by introducing the anatomy of the yolk sac and following with the key aspects of the process.

2.1 Anatomy and development of the yolk sac

Although the mammalian ovum contains virtually no yolk, its development is homologous to avians and reptilians whose yolk is abundant, and the yolk sac constitutes an important nutritive organ in small rodents, exercising both absorptive and secretory functions (Snell and Stevens, 1966; Wislocki et al., 1946). It is also the niche of origin of the first hematopoietic cells of the embryo.

The yolk sac (YS) is a splanchnopleuric organ composed of a double cell layer formed by extraembryonic mesoderm and endoderm. The endoderm of the yolk sac is an villous epithelium that absorbs and digests maternal blood-derived macromolecules (Jollie, 1990), a function later assumed by the definitive endoderm-derived gut and liver, while the adjacent mesoderm cells produce the first vasculature and blood cells of the embryo. It has long been accepted that he association of these structures, an absorption machinery coupled to a capillary network, makes the yolk sac an organ of fetal-mother exchange prior to the formation of the allantoic placenta (Everett, 1935).

The formation of the yolk sac begins during gastrulation at E6.5-7 of murine development when the primitive streak generates a layer of extraembryonic mesodermal cells under the visceral endoderm. At E7.5, the yolk sac is a limited structure forming the central portion of the egg cylinder, but it rapidly expands and form an extensive band enveloping the amnion and the exocoelomic cavity of the ovoid egg. The yolk sac vasculature arises from extraembryonic mesoderm and is initially composed of two sequential and independent vasculogenesis events that are then inter-twined, the development of blood islands (clusters

of primitive erythroblasts surrounded by an endothelial covering) and the formation of the vascular plexus.

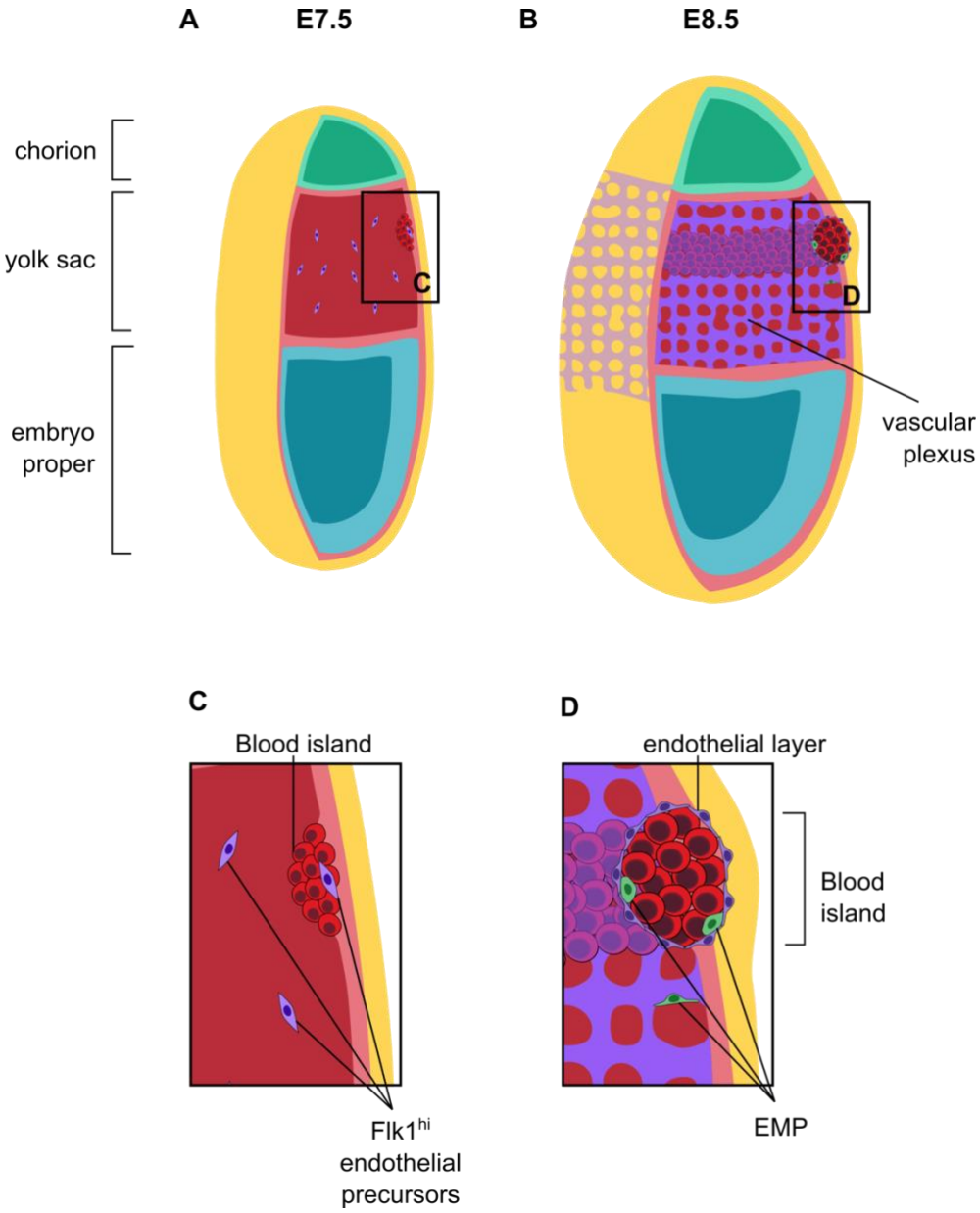

Figure 2. Illustrations of murine yolk sacs after gastrulation. (A) At E7.5, the yolk sac is located proximal to the embryo, few endothelial precursors are sparse throughout the yolk sac. (B) At E8.5, endothelial cells fuse into a honeycomb-like vascular plexus, the blood islands surround the proximal yolk sac. (C) Close up of a E7.5 mesodermal mass. Erythroid precursors expand in the mesoderm forming cell masses that will turn into blood islands. (D) Close up of E8.5 blood islands. Morphologically distinguishable erythroblasts are surrounded by a layer of endothelial cells that connects them with the developing vasculature. EMPs start to emerge both inside the blood islands and in the proximal part of the yolk sac. Inspired from (Ferkowicz and Yoder, 2005).

Blood island precursors are morphologically evident in the yolk sac mesoderm from the time of its formation, at E7-7.5, as proliferative masses that express *Scl/Tal1* and low levels of *Flk1 (*also known as *Vegfr2*) (Drake and Fleming, 2000; Palis, 2006). Angioblasts coexpressing *Tal1* and high levels of *Flk1* are visible at E7.5-8 throughout the yolk sac surrounding blood clusters, but not in the embryo proper. At E8, the process of yolk sac vasculogenesis is initiated in the proximal part of the yolk sac where angioblasts fuse and begin forming a vascular plexus that extends towards the blood islands until both entities merge around E8.25, when the primitive heart begins pumping (Lopez et al., 2015). By E8.5, the mesodermal cell masses have turned into morphologically distinguishable red blood cells that do not express *Flk1* and are surrounded by an endothelium (Palis, 2006).

Morphogenesis of the vascular plexus vessels follows a sequential pattern of gene expression in which *Tal1/Scl* and *Flk1* are coexpressed first, then *Pecam-1* (CD31), *CD34*, *Cdh5 (*VE-Cad) and later *Tie2*. *Tal1* is later downregulated as part of the endothelial cell maturation(Drake and Fleming, 2000). When the blood circulation is established, the yolk sac vasculature starts to remodel into a hierarchical network of branched vessels until E9.5 (Lucitti et al., 2007; Udan et al., 2013).

The release of erythroblasts increases the viscosity of blood flow, producing a hemodynamic force that is necessary to induce vasculature remodelling, and arterial specification in particular. This proved evident in *Mlc2a*-deficient embryos with impaired heart contractility (Flamme et al., 1997; Lucitti et al., 2007), in which plasma pumped by the heart was responsible for the release of erythroblasts and allowed them to promote yolk sac remodelling. Arterial specification can be observed at this stage by change of morphology and the expression of nuclear Sox17(Corada et al., 2013). Live hemodynamic analysis with doppler OCT indicates a robust blood velocity in the yolk sac vessels of 1-3mm/s on the different phases of the heartbeat cycle, although slower than in the dorsal aorta, where the velocity reaches 1-8mm/s (Garcia et al., 2015).

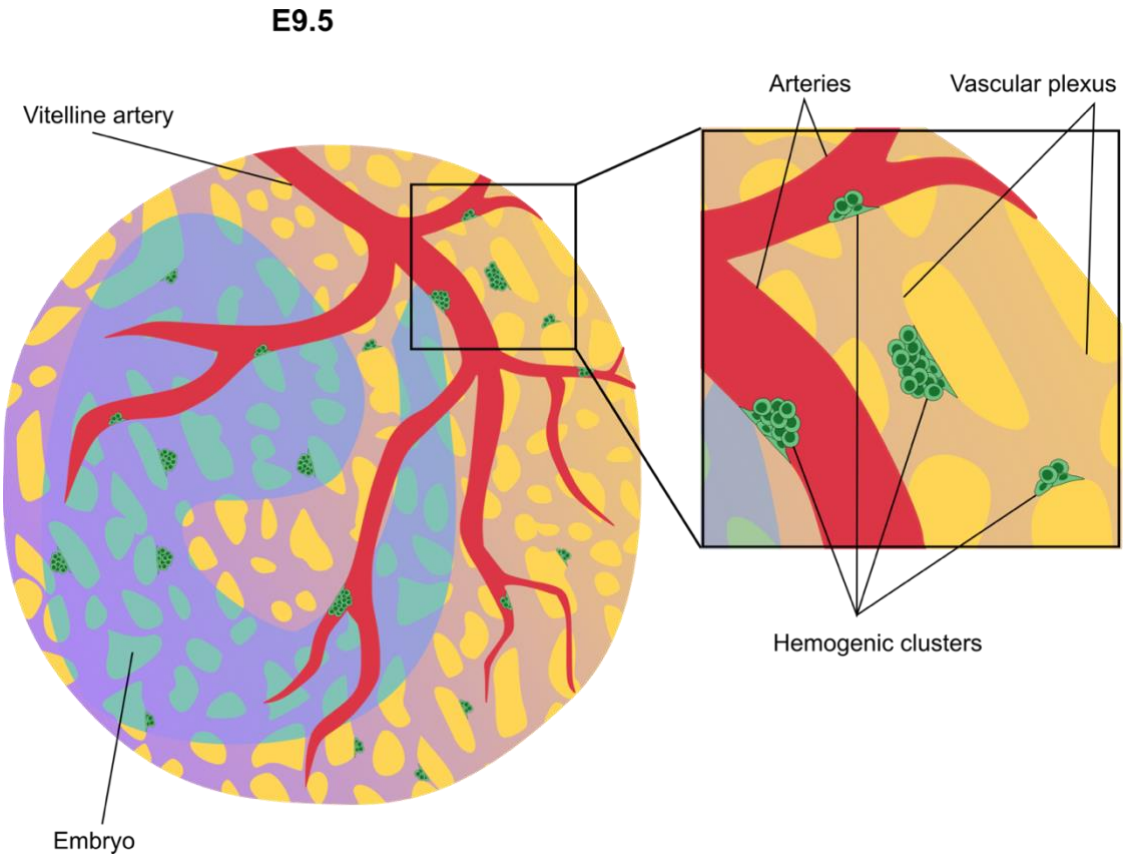

Figure 3. Illustration of E9.5 murine embryo. The embryo has turned and is contained inside the yolk sac. Arterial specification has occurred and the vitelline artery receives the circulation from the embryo. In the close up, numerous hemogenic clusters containing EMPs are emerging from both the arterial and venous vasculature.

Meanwhile, between E8.5 and E9, the mouse embryo turns and is enveloped by the yolk sac together with the amnion, remaining connected to the yolk sac the walls of the midgut enclosing the vitelline artery and vein. From E9.5 onwards, the vessel remodelling is finished and hematopoietic cell clusters are visible in the vessel walls of both the arterial and venous side(Frame et al., 2016). The process of mouse embryo turning is very different from other mammals like the human, in which the embryo is enveloped only by the amnion while the yolk sac is displaced alongside and then absorbed after 8 GW. If the yolk sac and the vitelline duct are not properly absorbed (in non-murine species) they cause an intestinal anomaly called Meckel's diverticulum(Downard et al., 2004). After E11.5, the murine yolk sac is no longer hematopoietic (Frame et al., 2016) but it is not discarded until birth, its sole function is thought to be the physical protection of the fetus.

2.2 Endothelial to hematopoietic transition

Extensive research has focused on the generation of hematopoietic stem/progenitor cells (HSPCs) from endothelial cells lining the major arteries of the vertebrate embryo in a process termed endothelial to hematopoietic transition (EHT). EHT consists of a switch in cell morphology and the break of tight junctions with neighbouring cells, generating characteristic clusters of cells attached to the vessel walls (De Bruijn et al., 2002; Jaffredo et al., 1998; Kissa and Herbomel, 2010; Oberlin et al., 2002).

2.2.1 EHT of hematopoietic stem cells

The specification of hemogenic endothelium in the embryonic aorta is a process extensively studied that depends on the transcriptional network of *Runx1*, both Notch and Wnt signaling pathways, blood flow and inflammatory signals. Embryos deficient for *Runx1* lack hematopoietic clusters, HSCs and definitive progenitor cells (Cai et al., 2000; North et al., 1999; Okuda et al., 1996). Runx1 is considered to be the master regulator of the onset of EHT, as it is in charge of reorganizing transcription factors to regulate the fate decision of endothelial cells and is therefore key for the process (Lichtinger et al., 2012; Narula et al., 2013; Yzaguirre et al., 2017).

Both Notch and Wnt/β-catenin signalling pathways are activated during aortic EHT (Bigas et al., 2013). While several Notch proteins are expressed during HSC emergence, Notch1 has been shown to be located specifically in the nucleus of endothelial cells of the dorsal aorta and cells of the clusters, and it was proven key to promote aortic specification and HSC emergence, together with *Gata2* (Kumano et al., 2003; Robert-Moreno et al., 2005, 2008). On the other hand, canonical Wnt/β-catenin signaling pathway has also been proven to be fundamental to the process. β-catenin can also be observed in the nucleus of the cells in the aortic endothelium and seems to be involved in arterial specification via Notch (Corada et al., 2010; Ruiz-Herguido et al., 2012). Other transcription factors involved in the Wnt

signaling pathway are regulated in the process, for instance, the downregulation of Sox17 maintains arterial identity and prevents commitment into HSC (Corada et al., 2013). In addition Wnt signaling is implicated in cell-cell junctions, which are remodelled during EHT as observed by live imaging (Bertrand et al., 2010; Boisset et al., 2010; Lancino et al., 2018).

Key studies demonstrated that blood flow is also required for hemogenic cluster formation as a result of hemodynamic forces and nitric oxide signaling, which ultimately regulates *Runx1* expression(Adamo et al., 2009; North et al., 2009). Higher nitric oxide concentrations increased HSC numbers by increasing blood flow, while lower concentrations impeded cluster generation. Finally, recent studies have similarly found that pro-inflammatory signals such as tumor necrosis factor (TNF) and interferons (IFNs) could enhance HSC emergence in the zebrafish and mouse aorta. It is proposed that those signals are provided by yolk sac-macrophages (Espín-Palazón et al., 2014; Li et al., 2014b; Mariani et al., 2019; Sawamiphak et al., 2014).

Whether HSC are generated from putative hemogenic endothelial cells or they acquire endothelial markers when they are emerging from the underlying tissue has been debated for the past few decades. Since *Runx1* is expressed in mesenchymal cells underlying the endothelial layer of the aorta, which are not labelled with VE-Cad and that have some HSC activity, it has been suggested that hematopoietic progenitors emerge from those mesenchymal cells (North et al., 2002) or from subaortic patches expressing *Gata2* and *CD93*/*AA4.1* (Bertrand et al., 2005a). This could also be explained by an egress into the lumen, which has been observed In avian and fish embryos. In chick embryos, the ability to uptake acetylated low-density lipoprotein (AcLDL) by endothelial cells has been used for lineage tracing, and labelled cells have been found in the underlaying mesenchyme of the aorta, suggesting that endothelial cells could ingress into the tissue (Jaffredo et al., 2000). In zebrafish embryos, live imaging showed that EHT does not release the HSC into the vascular lumen but into the underlying mesenchyme(Bertrand et al., 2010; Kissa and Herbomel, 2010).

Maturation steps have been identified inside intra-aortic clusters expressing *Runx1*, *Pecam-1*, *Kit* and *Ly6a/Sca-1*(De Bruijn et al., 2002; Yokomizo and Dzierzak, 2010). Flow cytometry and cell sorting allowed the characterization of the different stages of cell maturation starting from immature HSCs to fully matured HSC with reconstitution potential: from pro-HSC (VE-Cad^{+} CD41^{lo}), to pre-HSC I (VE-Cad^{+} CD41^{lo} CD43^{+}), to pre-HSC II (VE-cad^{+} CD41^{lo} CD43^{+} CD45^{+}) to HSC (or dHSC) (Rybtsov et al., 2011; Taoudi et al., 2008). Recently, scRNA-seq analysis studies have further supported the notion of a hemogenic endothelium and have allowed to further dissect the steps of HSC maturation inside the clusters, providing markers for arterial cell specification programs (Neurl3(Hou et al., 2020)) and for HSC commitment (CD201(Zhou et al., 2016), CD44(Oatley et al., 2020), Gata2 and CD27 (Vink et al., 2020)).

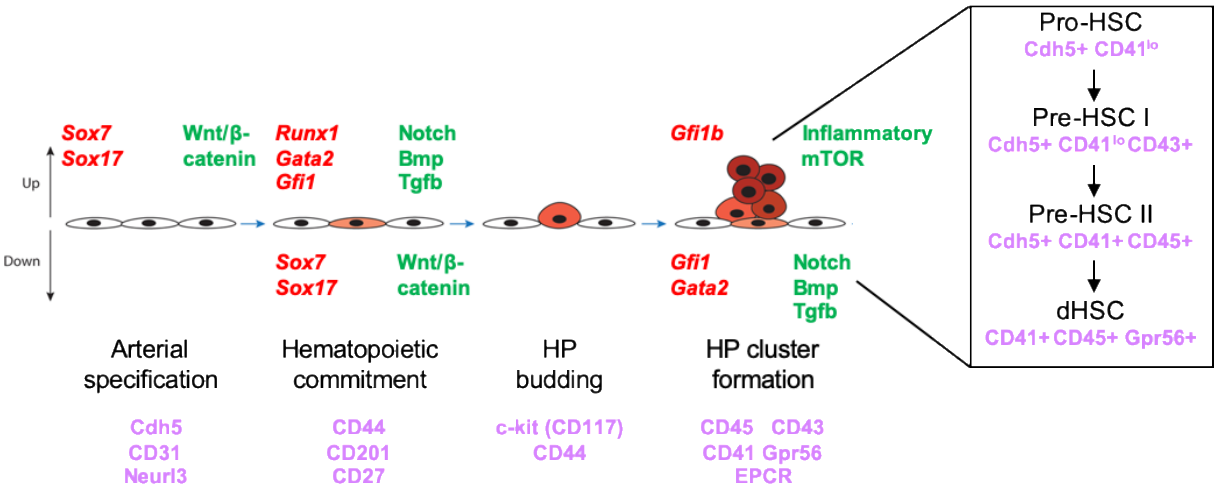

Figure 4. Illustration of events taking place in EHT. Key transcription factors involved in the EHT are shown in red and key signalling pathways in green. Cell surface markers characteristic for each stage are shown in purple. Up-regulated genes during the process are shown on top of the cells and down-regulated genes are showed below the cells HP, hematopoietic progenitor. Image adapted from (Ottersbach, 2019).

It is worth remembering that although HSCs mature into multipotential progenitors with long term reconstitution capacity in the aorta, they are not able to differentiate into mature cells within their niche of origin, as shown by the lack of differentiated precursors in the AGM(Godin et al., 1999; Kieusseian et al., 2012). It is not known whether this is due to the lack of support for hematopoiesis by the aortic niche or to an intrinsic temporal need for maturation of HSCs.

2.2.2 EHT of erythromyeloid progenitors

The initiation of EHT is concomitant with yolk sac vasculature remodelling and precedes the acquisition of aortic fate. Hemogenic cell clusters can be observed in the yolk sac vessel walls from E9 to E11 (Frame et al., 2016; Samokhvalov et al., 2007). The number of individual clusters reaches its maximum at E9.5, but the clusters tend to be overall larger from E10.5, exemplified by the appearance of clusters composed of 50 cells or more(Frame et al., 2016). YS hematopoietic clusters express endothelial cell surface markers such as Flk1, CD34, VE-Cadherin, Pecam-1 and CD105 (Frame et al., 2016; Lee et al., 2016; McGrath et al., 2015a). Similarly to intra-embryonic EHT, YS EHT is dependent on the transcription factor Runx1, whose expression is found in the nucleus of hemogenic endothelial cells (Chen et al., 2011; Frame et al., 2016; North et al., 1999; Samokhvalov et al., 2007). Furthermore, YS AcLDL$^+$ endothelial cells gave rise to EMPs, which were shown to emerge directly from the endothelium in a live-imaging set up of fate-mapped cells (Kasaai et al., 2017). Similar to HSC generation, EMP cluster generation is dependent on the Wnt/β-catenin signaling pathway (Frame et al., 2016).

However, essential differences have been reported concerning the EHT generation of EMP versus HSC. EMP emergence begins in the blood islands prior to the remodelling of the vascular plexus, EMP clusters show no preference for arterial versus venous vasculature and they appear equally abundant in both large and small vessels(Frame et al., 2016). Additionally, studies on ES cells proposed the existence of an hemogenic wave independent of Notch1, endowed with erythromyeloid potential and no LTR capacity (Hadland et al., 2004; McGrath et al., 2015a).

Furthermore, the lack of blood flow does not disrupt EMP emergence. Normal cluster morphology and localization were observed in the yolk sacs of *Ncx1-/-* mutants that lack a beating heart although nitric oxide enhanced the formation of clusters (Frame et al., 2016; Kasaai et al., 2017; Lux et al., 2008). Whether inflammatory signals are needed for the

emergence of EMPs is currently unknown, but macrophages that are located both inside and outside the vessels during EHT could potentially contribute to the process, as has been proposed for intra-embryonic EHT.

Finally, EMPs differ from their HSC counterparts in their capacity to differentiate within their niche of emergence. EMPs have been shown to produce macrophages *in situ* that are *Runx1*-dependent and that can be labelled with an inducible Cre under control of the *Cdh5* (VE-Cadherin) promoter pulsed at E7.5(Gentek et al., 2018a). It is not yet clear whether the yolk sac constitutes a supportive niche for hematopoietic differentiation or whether this capacity is an inherent characteristic of EMPs that is distinct from HSCs.

3. EMP-derived hematopoietic lineages

EMPs have been demonstrated to give rise to the first innate immune cells of the embryo. They are the first multipotent hematopoietic progenitors, with the potential to give rise to cells from the erythroid lineage (erythrocytes and megakaryocytes) and myeloid lineage (macrophages, monocytes, granulocytes, dendritic cells and mast cells)(Gomez Perdiguero et al., 2015; McGrath et al., 2015a). The extent of their contribution to fetal and adult hematopoietic systems is still unclear but there is a growing body of literature that recognises their key role in fetal erythropoiesis and the production of certain adult resident myeloid populations.

While not much is yet known on how lineage choice is regulated in EMPs, we do have substantial data on the process from HSC-derived progenitors. In the adult bone marrow, common myeloid progenitors (CMP) hold the potential to from myeloid and erythroid lineages, and could be thus considered as a functional equivalent to EMP. HSC give rise to CMP through sequential steps of commitment in which they lose the self-renewal capacity to become multipotent progenitors (MPP) and further loose lymphoid potential (Akashi et al., 2000; Debili et al., 1996). CMPs then differentiate into megakaryocyte/erythrocyte progenitors (MEP) and

into granulocyte/monocyte progenitors (GMP) to give rise to all erythroid and myeloid lineages (Figure 5). A similar hierarchical differentiation tree has been proposed to occur during fetal liver HSC-derived hematopoiesis(Traver et al., 2001).

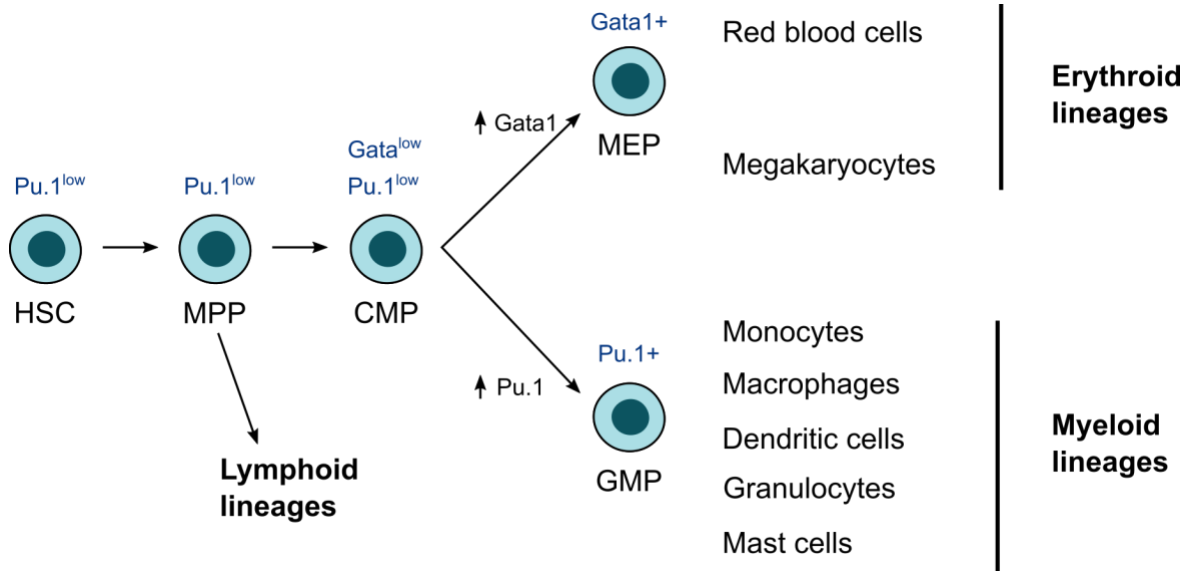

Figure 5. Schematic illustration of commitment steps of HSC towards erythroid and myeloid lineages. Expression of Pu.1 and Gata1 transcription factors is indicated in blue for gene and black for protein levels. HSC, hematopoietic stem cell; MPP, multipotent progenitor; CMP, common myeloid progenitor; MEP, megakaryocyte/erythrocyte progenitor; GMP, granulocyte/monocyte progenitor.

Erythroid/myeloid lineage decision seems to be governed by the transcription factors Gata1 and Pu.1, although the process to that leads to lineage choice is still an intense debate. Gata1 is essential for the differentiation of the erythroid lineage (Zhang et al., 2000), while Pu.1 is necessary for the differentiation of myeloid cells and the maintenance of stem and progenitor cells during hematopoiesis (Iwasaki and Akashi, 2007; Nerlov and Graf, 1998). Pu.1 and Gata1 both inhibit each other and activate themselves. In the literature, a stoichiometric model for erythroid versus myeloid commitment in HSCs was proposed where randomly fluctuating Gata1 and Pu.1 cross-antagonise each other until a threshold of expression is surpassed (Graf and Enver, 2009; Nerlov et al., 2000; Orkin and Zon, 2008; Zhang et al., 2000). However, a recent study failed to observe a reproducible Pu.1–Gata1 double-positive stage in live imaging

of single cells(Hoppe et al., 2016), which led the authors to propose that Pu.1 and Gata1 were not lineage-decision driving but rather executing transcription factors.

In order to better understand the lineage decisions and the hierarchy of EMP-derived hematopoiesis, I will review the different classes of cells that they can give rise to, with special emphasis on the current knowledge on their differentiation steps, mostly obtained from adult hematopoiesis.

3.1- Erythroid lineages

3.1.1- Red blood cells

Red blood cells (RBC), also called erythrocytes, are the cells responsible for transport of oxygen and carbon dioxide between the lungs and the rest of the body. They are the most abundant cell type in the body, around 70% of the cell count in humans(Bianconi et al., 2013), and they are constantly produced in the erythroblastic islands of the bone marrow at an approximate rate of 2 x 10^{11} RBC per day(Palis, 2014). Once released into circulation, they have an average lifespan of 45 days in adult mouse, 115 days in human(Franco, 2012; Palis, 2014) and are ultimately cleared in the spleen by resident red pulp macrophages (Bratosin et al., 1998; Burger et al., 2012; Mebius and Kraal, 2005) and to a minor extent by resident macrophages (Kupffer cells) in the liver. Splenic red pulp macrophages recycle the iron, which is returned to new erythroid precursors (Dautry Varsat et al., 1983; Hentze et al., 2010; Leimberg et al., 2008).

Mammalian RBCs are highly specialised in gas transportation. The lack of nucleus and organelles makes them small and biconcave, which yields an increased surface-to-volume ratio for a more efficient gas exchange(Blatter et al., 2017). It also provides deformability to traverse small capillaries and allows to increase hemoglobin capacity, the oxygen transportation molecule, and (Ji et al., 2011; Morera and MacKenzie, 2011).

Hemoglobin is a metalloprotein composed of 4 protein subunits, globins, each carrying one iron containing molecule, the haem or heme, that binds to one oxygen molecule. There are different types of globins, which have different affinity to oxygen. In adult mice, these are α1-, α2-, β1-, and β2-globins, but primitive erythroid cells also express type ζ-, βH1-, and εγ-globins(Trimborn et al., 1999). The switch from γ-globin to adult β-globin occurs when fetal liver erythropoiesis begins. In humans, two globin gene switches occur during development, the embryonic (ε or ζ) to fetal (γ) switch correlates with yolk sac to fetal liver erythropoiesis, while a second fetal to adult (β) switch occurs at birth. Human fetal hemoglobin is thus composed of $\alpha_2\gamma_2$ (called HbF) while adult hemoglobin is composed of $\alpha_2\beta_2$ (called HbA) or, less frequently, $\alpha_2\delta_2$ (called HbA_2)(Peschle et al., 1985; Stamatoyannopoulos, 2005; Stamatoyannopoulos and Nienhuis, 1983).

The production of RBCs is effectuated through a series of more differentiated highly proliferating progenitors. In the adult bone marrow, megakaryocyte/erythrocyte progenitors (MEP) differentiate sequentially into lineage committed burst-forming unit erythroid (BFU-E) and colony-forming unit erythroid (CFU-E). These populations were defined by their ability to form erythroid colonies *in vitro*. The transcription factor Myb supports erythropoiesis through the transactivation of Kruppel-Like Factor 1 (*Klf1*) and LIM Domain Only 2 (*Lmo2*) expression(Bianchi et al., 2010). CFU-E requires the cytokine erythropoietin (EPO) for their survival and expansion (Koury and Bondurant, 1990, 1992) and proper maturation. BFU-E develop into morphologically identifiable precursors that gradually progress by accumulating haemoglobin, decreasing cell size, condensing their chromatin (nuclear pyknosis) and finally decreasing their RNA content (Figure 6). After, the erythroblast enucleates and turns into a reticulocyte. Finally, the reticulocyte further matures by removing all residual cytoplasmic organelles, including mitochondria and ribosomes by autophagy and exocytosis, acquiring a biconcave elastic shape (Palis, 2014).

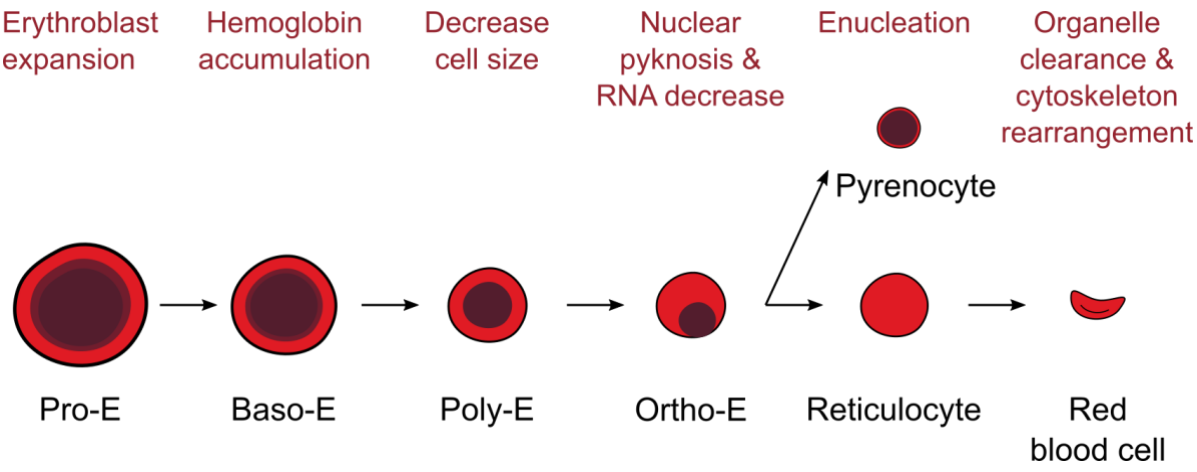

Figure 6. Maturation steps of definitive erythroid precursors deriving from BFU-E progenitors. Precursors are defined morphologically through the maturation steps. ProE, proerythroblast; BasoE, basophilic erythroblast; PolyE, polychromatic erythroblast; OrthoE, orthochromatic erythroblast. Pyrenocytes are cleared by macrophages during the maturation process, and reticulocytes and red blood cells are released into circulation.

The final maturation step of definitive erythroblasts occurs within erythroblastic islands of the fetal liver and the bone marrow, where a central macrophage surrounded by erythroblasts phagocytes the extruded nuclei surrounded by a cell membrane (pyrenocytes) (Yoshida et al., 2005).

Definitive RBC in development

During murine development, the first definitive red blood cells are produced by E11.5 in the fetal liver, after rapid and local expansion of EMP and EMP-derived progenitors (Gomez Perdiguero et al., 2015; McGrath et al., 2015a). Release into circulation starts at E12.5, probably to respond to the increasing demands of the developing embryo, and they rapidly become the most common cell type in circulation. Defective EMP-derived erythropoiesis in *Myb*-deficient embryos is embryonic lethal by E15.5 (Mucenski *et al.*, 1991). A similar rapid burst of enucleated erythrocytes has been observed in the human embryo from 4 to 6 weeks of gestation, at the moment in which EMPs have emerged and colonize the fetal liver (Migliaccio et al., 1986; Oberlin et al., 2002). It should be mentioned that, although terminal differentiation occurs only in the fetal liver, the observation of both BFU-E and CFU-E forming cells in the

yolk sac and circulation by E10.5 suggests a maturation of erythroid progenitors already in their niche of emergence(Palis et al., 1999).

The erythrocytes that EMP and HSC produce are morphologically identical: they are enucleated and ovoid and they express large quantities of β- and α-globins. Although EMP-derived erythrocytes do not express primitive εγ-globin, low levels of embryonic βH1-globin transcripts can be detected during early fetal erythropoiesis(McGrath et al., 2011). Importantly, EMP-derived erythropoiesis, although transient, can support murine embryo during gestation, as evidenced in experiments in which HSCs were selectively depleted(Chen et al., 2011).

Further interesting differences have been noticed among erythroblasts of the EMP-lineage with respect to both primitive and bone marrow-derived erythroblasts. While the latter fail to self-maintain in culture, it was demonstrated that yolk sac-derived erythroblasts can proliferate in culture and be maintained for several months(England et al., 2011). Another difference between EMP- and HSC-derived erythropoiesis is the expression of the pan-hematopoietic marker CD45. While loss of CD45 expression at the surface of erythrocytes is secondary and occurs during the BFU-E stage in bone marrow erythropoiesis(Boulais et al., 2018; Li et al., 2014a), a recent preliminary report demonstrated that EMP-derived MEP are CD45 negative (Soares-da-Silva et al., 2020). Additionally, this manuscript also showed that EMP-derived erythrocytes require lower concentration of EPO than HSC-derived erythrocytes, which might provide a competitive advantage during fetal erythropoiesis(Soares-da-Silva et al., 2020).

3.1.2- Megakaryocytes

Megakaryocytes (Mk) are large cells that produce platelets, small cell fragments whose function is to prevent blood loss by aggregating to induce blood coagulation. Platelets are the second most abundant cell type in the blood and they are constantly replenished since they have a lifespan of a few days. In humans, it was quantified that 10^{11} platelets are produced per

day in humans to maintain homeostasis(Branehög et al., 1975). Adult Mks are situated close to bone marrow sinusoids, to ensure a fast release of platelets into circulation when needed(Stegner et al., 2017).

Megakaryopoiesis in the adult bone marrow occurs through hierarchical steps of differentiation, from HSC, multipotent progenitor (MPP), common myeloid progenitor (CMP) and megakaryocyte-erythroid progenitor (MEP)(Akashi et al., 2000; Debili et al., 1996). However, there is evidence that Mks are also produced from an alternative route prior to the CMP stage, from VWF+ long term-HSC (quiescent, expressing CD150)(Grover et al., 2016; Sanjuan-Pla et al., 2013) and MPP2(Cabezas-Wallscheid et al., 2014; Pietras et al., 2015; Rodriguez-Fraticelli et al., 2018). Extensive research over the last decade has shown that these populations contain Mk-primed cells and can differentiate directly into Mks, thus bypassing the intermediate shared progenitors CMP and MEP. This direct differentiation was demonstrated in different conditions, such as thrombopoietin (TPO) induction, inflammation and after expression of a tyrosyl-tRNA synthetase variant (YRS^{ACT}), as well as in steady state(Carrelha et al., 2018; Haas et al., 2015; Kanaji et al., 2018; Rodriguez-Fraticelli et al., 2018). VWF+ HSCs are spatially located alongside Mks, which induce their proliferation and repopulation capacity via CXCL4(Pinho et al., 2018).

Mks undergo endomitosis as they mature, acquiring a polyploid nucleus of 16N on average. They then follow a series of elaborate remodelling events to produce platelets. They extend long cytoplasmic protrusions along the sinusoidal blood vessels of the bone marrow (proplatelets) that release 1 to 2 µm platelets into the blood vasculature(Avecilla et al., 2004; Bender et al., 2015; Stegner et al., 2017). Restructuring of the Mk cytoskeleton is conducted by a massive microtubule reorganization(Bender et al., 2015; Italiano et al., 1999; Patel et al., 2005). The cytokine thrombopoietin (TPO) is the primary regulator of platelet production, since it supports the survival, proliferation and differentiation of the precursors(Hitchcock and Kaushansky, 2014). Additionally, CXCL12 and its receptor CXCR4 increase the mobility of

terminally differentiated Mks and facilitate the interaction with sinusoidal endothelial cells (Grozovsky et al., 2015).

Mk in development

Embryonic platelets play a critical role in the closure of blood and lymphatic vasculatures as Mk-devoid embryos display blood-filled lymphatic vessels at E10.5, in *Meis1*-deficient embryos and after targeted ablation of platelets carrying diphtheria toxin receptor (DTR) (Bertozzi et al., 2010; Carramolino et al., 2010). EMPs can differentiate into megakaryocytes but the extent of their contribution is currently unknown (Gomez Perdiguero et al., 2015; McGrath et al., 2015a). During development, Mk production shifts from the yolk sac to the FL at E11.5 and Mk production in the YS has been defined as belonging to the primitive wave. However, it is difficult to rule out Mk production from definitive EMPs in the YS, as there are currently no distinctive features between primitive and definitive megakaryocytes, such as globin genes in the erythroid lineage.

3.2- Myeloid lineages

3.2.1- Monocytes

Monocytes are myeloid circulating cells found in the bone marrow, spleen and blood that mediate initiation and resolution of inflammation, and they have diverse roles in tissue homeostasis. Their recruitment to sites of tissue injury and inflammation requires trafficking across the blood vessel wall, which is mediated by their chemokine receptors and adhesion molecules(Auffray et al., 2009; Swirski et al., 2009). They are also the precursors of infiltrating macrophages and, in some instances, dendritic cells. However, monocytes, and patrolling monocytes in particular, can also have intravascular effector functions (Carlin et al., 2013) and as such may not be considered as only precursor cells.

Monocyte subsets

Murine monocytes are generally divided into two subsets: classical or inflammatory and patrolling monocytes, regarding their phenotype and functions.

Classical monocytes are defined as CD115 (Csf1r)+ Gr1/Ly6C^{+} (CD14^{hi} CD16$^{+/-}$ in humans). They express *Ccr2*, which is required for their egress form the BM into circulation, and low levels of *Cx3cr1* (a fractalkine receptor) and are rapidly recruited in various situations of tissue injury or infection, where they differentiate into macrophages (Dunay et al., 2010; Peters et al., 2004; Samstein et al., 2013; Serbina et al., 2003; Traynor et al., 2000; Wojtasiak et al., 2010). Of note, the granulocyte receptor-1 (Gr1) antigen is comprised of the two structurally related GPI-anchored proteins: Ly-6C (expressed by the monocyte lineage) and Ly-6G (expressed by granulocyte lineage).

Patrolling monocytes are CD115+ Gr1/Ly6C^{neg} (CD14^{dim} CD16^{+} in humans), do not express *Ccr2* but high levels of *Cx3cr1*. They patrol blood vessels to mediate early responses and promote wound healing and angiogenesis(Auffray et al., 2007; Carlin et al., 2013; Nahrendorf et al., 2007).

Monocyte development

As for most immune cells, classical monocytes are produced through progressively more restricted progenitors (Figure 7), starting from the common myeloid progenitor (CMP), to the granulocyte/monocyte progenitor (GMP) to the monocyte/dendritic cell progenitor (MDP) to the common monocyte progenitor (cMoP) that differentiates into Ly6C^{+} monocytes, which later can differentiate into Ly6C^{neg} monocytes (Geissmann et al., 2010; Guilliams et al., 2018; Hettinger et al., 2013). However, recent studies have challenged this differentiation pathway and have proposed that monocytes are produced through different developmental programs in steady state, which may explain their functional diversity. Some MDPs can be found within the phenotypic characterization of CMP, and recent reports based on adoptive transfer and

fate-mapping experiments have proposed that Ly6C^{hi} monocytes can differentiate directly from GMPs under inflammatory conditions(Ikeda et al., 2018; Liu et al., 2019; Yáñez et al., 2017).

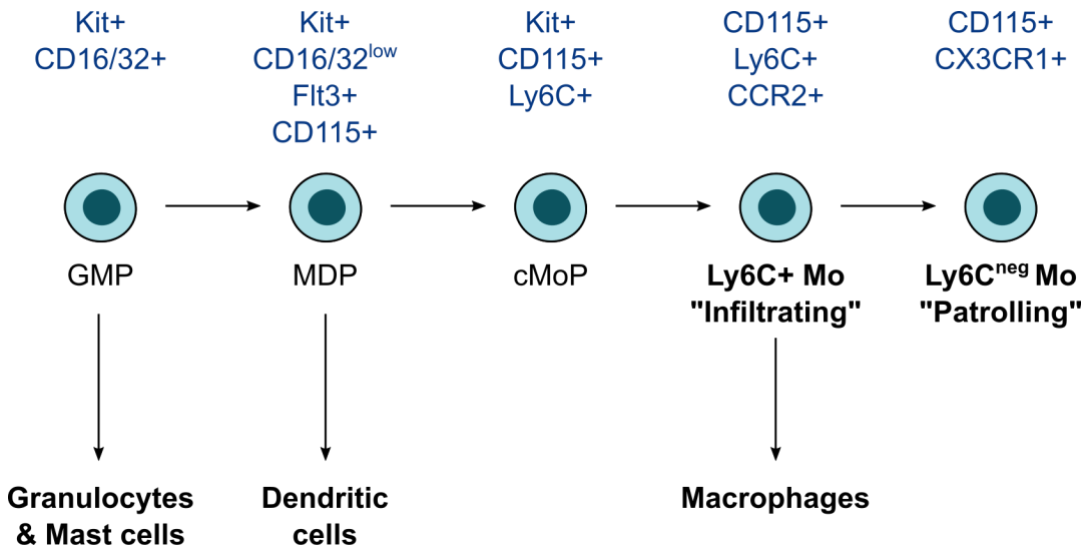

Figure 7. Schematic illustration of progenitor steps leading to the production of monocytes. Surface marker phenotype is indicated in blue. GMP, granulocyte/monocyte progenitor; MDP, monocyte/dendritic cell progenitor; cMoP, common monocyteprogenitor; Mo, monocyte.

In the embryo, the first monocytes are produced in the fetal liver starting from E12.5 and they are products of EMP hematopoiesis (Gomez Perdiguero et al., 2015). This first wave of monocytes is proposed to be responsible for a second wave of resident macrophage production (Hoeffel et al., 2012, 2015) (discussed below). Monocytes are then produced from HSC later in the fetal liver and the bone marrow, and HSC are responsible for all monocyte production during adult life(Boyer et al., 2011).

Monocytes: a precursor for macrophages and dendritic cells

Monocytes have been historically considered as the obligatory circulating precursors of all macrophages(van Furth et al., 1972). Ly-6C+ monocytes are indeed a major source for macrophage differentiation in response to tissue injury and monocyte-derived macrophages are required for infection defense and tissue repair. Ly-6C+ monocyte-derived macrophages can adopt a very wide range of phenotypes in response to the stimuli present but they are

usually classified into two main categories: inflammatory macrophages (or M1) and alternatively activated macrophages (M2)(Murray et al., 2014).

Finally, monocytes can also differentiate into dendritic cells (DCs) under inflammatory conditions and infection. Although monocyte-derived dendritic cells (MoDCs or infDCs) display DC-like properties *in vivo*, they do not depend on FLT3 but on Csf1/M-CSF (Karsunky et al., 2003; Louis et al., 2015). Monocytes have been shown to give rise to antigen presenting cells resembling dendritic cells *in vitro*, when they are cultured with IL-4 and Csf2 (also known as GM-CSF) (Briseño et al., 2016). MoDCs share a similar surface phenotype with conventional dendritic cells (cDCs) and macrophages but they can be identified by coexpression of CD64 and FcεRI (Plantinga et al., 2013; Segura and Amigorena, 2013).

3.2.2- Resident macrophages

The term resident macrophage (resMf) refers to a heterogeneous family of innate immune cells that play a central role in tissue inflammation and homeostasis. They are found in all organs and body cavities, where they display tissue-specific phenotypes, functions and gene expression profiles(Gautier et al., 2012; Lavin et al., 2014), as exemplified by liver Kupffer cells, brain microglia, splenic red pulp macrophages and epidermal Langerhans cells. They are professional phagocytic cells that are essential players in the homeostasis of their tissue of residency by releasing growth factors, cytokines and extracellular matrix (ECM)-modifying enzymes(Okabe and Medzhitov, 2016). ResMf populations, at steady-state, are characterized by a low input rate from bone marrow-derived monocytes, in stark contrast to other myeloid populations. Instead, they are long-lived and self-maintain by proliferation (Chorro et al., 2009; Epelman et al., 2014; Hashimoto et al., 2013; Kierdorf et al., 2013; Schulz et al., 2012; Yona et al., 2013; Zigmond et al., 2014).

Functional diversity of ResMf

ResMf are regularly spaced in many tissues such as the brain, the peritoneal serosa, the muscles, the epidermis, and the liver and this arrangement has been hypothesized to be regulated by mutual repulsion and growth factor availability(Hume et al., 2019). They exhibit long elongated processes or dendrites that build up a 3D network-like structure throughout each organ(Chopin and Nutt, 2015; Nimmerjahn et al., 2005) and which allows them to behave as tissue sentinels. Among their multiple functions, they regulate tissue homeostasis by scavenging of macromolecules, tissue debris, senescent and apoptotic cells and production of bioactive molecules, fight infections by uptaking invading pathogens and finally, they have key functions in tissue repair and regeneration(Kierdorf et al., 2015; Wynn and Vannella, 2016).

Specifically during development, they are involved in organogenesis of the brain (Paolicelli *et al.*, 2011; Nguyen *et al.*, 2020), limbs, lung (Blackwell et al., 2011; Muñoz-Espín et al., 2013), mammary glands (Ingman et al., 2006), testis (DeFalco et al., 2014) and pancreas (Banaei-Bouchareb et al., 2004). They also contribute to HSPC emergence (Mariani et al., 2019) and blood and lymphatic vessel branching (Fantin et al., 2010; Gordon et al., 2010; Kubota et al., 2009). In line with such highly diverse and tissue-specific functions, resMf have tissue-specific transcriptomic, epigenetic and metabolic profiles (Lavin et al., 2014), for which the transcription factors responsible have been identified in some tissues. This is the case for Gata6 for peritoneal macrophages(Okabe and Medzhitov, 2014; Rosas et al., 2014) and SpiC for red pulp macrophages(Kohyama et al., 2009). Acquisition of these tissue-specific macrophage phenotypes occurs after tissue colonization during organogenesis and their maturation continues during development (Mass et al., 2016; Matcovitch-Natan et al., 2016; Summers and Hume, 2017). Interestingly, it has been reported that the transcription factor Zeb2 is necessary to maintain those tissue-specific identities as well as maintaining the macrophage pool (Scott et al., 2018).

Developmental origins of resident macrophages

The past decade has seen an increasingly growing body of literature in the field of resident macrophages. A series of seminal studies evidenced the embryonic origin of some adult resident macrophages (Ginhoux et al., 2010; Gomez Perdiguero et al., 2015; Hoeffel et al., 2015; Schulz et al., 2012) and renewed interest in these resident homeostatic cells and in the potential role of different lineage contributions in a phenotypically homogenous population. However, the precise ontogeny of these cells has been the subject of intense debate because of the limitations of the different fate-mapping systems, including temporal overlap of hematopoietic waves, low labelling efficiencies and lack of specificity of the promoters used. The current framework proposes the existence of three waves of macrophages that sequentially colonize tissues. After a first wave of yolk sac-derived *Myb*-independent macrophages, a second wave of fetal liver-derived embryonic monocytes can give rise to tissue macrophages. Finally, HSC-derived monocytes can infiltrate specific tissues during postnatal development, in steady state or after tissue inflammation. In terms of ontogeny, the first macrophage wave could derive from primitive and/or EMPs while the second could originate from EMP and/or HSC. The contribution of each wave to the resMf pool in each tissue is suggested to be dependent on both niche availability and accessibility(Guilliams and Scott, 2017). It should be noted at this point that some confusion currently exists in the macrophage field, as the term “primitive” was often (and in some cases still is) used to qualify immature or ancestral cells or to express that they are the earliest or first of its kind, with no regards to their ontogeny. As such, yolk sac macrophages are often called “primitive” for these reasons, and not because they are deriving from primitive progenitors.

First wave of macrophage production in the yolk sac

The potential to produce macrophages in the yolk sac resides in EMPs and monopotent progenitors/precursors (Bertrand et al., 2005b). Yolk sac macrophages have no monocyte intermediates and their generation is independent of the transcription factor c-Myb (Bertrand

et al., 2005b; Naito et al., 1989; Schulz et al., 2012; Takahashi et al., 1989). Currently, we lack lineage-specific markers or tools to discriminate between primitive and EMP-derived macrophages in the early yolk sac. In particular, it is not possible yet to determine the quantitative contribution of primitive progenitors vs EMP into microglia, the central nervous system resident macrophages. While such distinction has been studied in the developing zebrafish (Ferrero et al., 2018), it has yet to be clarified whether mouse microglia are of primitive, EMP or mixed origin. Unfortunately, studies to date have been unable to isolate a yolk sac macrophage primitive precursor, and the use of Cx3cr1-GFP reporter in combination with Kit marker in the E8 yolk sac showed that the macrophage forming cells at this stage are associated with erythromyeloid colonies, pointing towards an EMP origin for mouse microglia (Kierdorf et al., 2013). Further, ResMf and their progenitors can be fate mapped when targeting cells expressing *VE-Cad/Cdh5*(Gentek et al., 2018a), *Runx1*(Ginhoux et al., 2010), *Tie2/Tek*(Gomez Perdiguero et al., 2015) and *Csf1r*(Gomez Perdiguero et al., 2015; Kasaai et al., 2017) early in development, thus strongly arguing for an origin of resMf progenitors from hemogenic endothelium. This does not exclude that primitive macrophage precursors could contribute in part to the monocyte-independent macrophage wave, as they could express these genes in the course of their generation.

As EMP commit towards their myeloid progeny, they lose Kit expression while they concomitantly upregulate the expression of macrophage genes like *Cx3cr1*, *Csf1r* and *Irf8* (Bertrand et al., 2005b; Kierdorf et al., 2013; Mass et al., 2016). EMP-derived macrophages enter in circulation as soon as it is established and colonize all the tissues from E8.5 to E12.5 (Gomez Perdiguero et al., 2015; Stremmel et al., 2018). The primary target for YS-produced EMP macrophages is the yolk sac and the developing brain (neuroectoderm) by E9.5, probably due to the early establishment of the vascular network in this niche (Ginhoux et al., 2010; Gomez Perdiguero et al., 2015; Kierdorf et al., 2013; Stremmel et al., 2018).

Second wave of macrophage production in the fetal liver

Later on, EMPs produce monocytes in the fetal liver and release them into circulation, which leads to colonization of all tissues but the brain(Gomez Perdiguero et al., 2015; Hoeffel et al., 2012, 2015). The inducible recombination of progenitor cells under the control of *Tie2/Tek* promoter proved essential to address the ontogeny of this wave. Indeed, while E7.5 and E8.5 tamoxifen (TAM) pulses highly labelled tissue resMf populations, tissue resMf were barely labelled when pulsed at E9.5 but other myeloid and lymphoid cells (together with HSC) were highly labelled. This demonstrated that resMf progenitors originated from hemogenic progenitors present before E9.5 and not from HSCs(Gomez Perdiguero et al., 2015).

Third wave of macrophage production from the fetal liver and bone marrow

The majority of tissue macrophage populations are established prenatally during mouse development and can be maintained by proliferation independently of bone marrow monocyte input in *steady state*(Hashimoto et al., 2013; Yona et al., 2013).

However, EMP-derived resMf can be replaced by a wave of HSC-derived infiltrating monocytes in a manner dependent on the tissue and that is impacted by tissue challenge and aging. Gradual replacement by HSC-derived monocytes can occur in steady state in specific organs and has been proposed to progressively increase with age. During steady state, resMf of the gut lamina propia are entirely dependent from bone marrow Ly6C^{+} monocytes after weaning(Bain et al., 2014). Other resMf are partly dependent on bone marrow monocytes for their maintenance, such as macrophages from the lung (Gomez Perdiguero et al., 2015; Hashimoto et al., 2013), liver (Scott et al., 2016), heart(Epelman et al., 2014; Molawi et al., 2014), pancreas(Calderon et al., 2015), dermis(Tamoutounour et al., 2013), adipose tissue(Kanda et al., 2006; Weisberg et al., 2006), and peritoneum(Parwaresch and Wacker, 1984; Yona et al., 2013).

Tissue resMf can also be replaced after specific tissue challenges. It has been long reported that γ-radiation provokes replacement of epidermal Langerhans cells(Katz et al., 1979) and spleen red pulp macrophages(Fogg et al., 2006) with bone marrow derived monocytes. Also, liver Kupffer cells can be replaced with HSC-derived cells, after cell ablation (DT mediated or clodronate)(Scott et al., 2016), bacterial and viral infection(Blériot et al., 2015; Borst et al., 2018) and following lipid overload during non-alcoholic steatohepatitis(Tran et al., 2020). Much less is known about the impact that this replacement over age or after specific challenges has on the ability of resMf to perform their functions, which could have major implications in physiological tissue homeostasis, as infections and wounds are frequent during lifetime.

3.2.3- Dendritic cells

Dendritic cells (DC) are specialized antigen-presenting myeloid cells. They are highly phagocytic and migratory cells that process antigens in peripheral and lymphoid tissues (spleen and lymph nodes). After activation in peripheral tissues, they migrate to the T and B cell zones of lymphoid tissues (spleen and lymph nodes) to expose the antigen via afferent lymphatics and high endothelial venules and thus have major functions in the initiation and regulation of adaptive immunity. Adult DC production is located in the bone marrow and depends on the ligand of the receptor tyrosine kinase fms-like tyrosine kinase 3 (FLT3)(Liu et al., 2009; McKenna et al., 2000; Waskow et al., 2008). It is a heterogeneous group classified by transcription factor and cell surface marker expression, but their surface markers also represent activation stages(Boltjes and van Wijk, 2014; Geissmann et al., 2010).

DC heterogeneity

Conventional DCs (cDCs) are generally short-lived, 3-6 days, and can be subdivided into cDC1 and cDC2, regarding distinct sets of transcription factors required for their development (equivalent to human CD141/BDCA3$^+$ and CD1c/BDCA1$^+$ cDCs(Collin and

Bigley, 2018)). cDCs can be identified in several tissues by their general expression of CD11c and CD24 and the lack of CD64 (marker that separates them from macrophages)(Guilliams et al., 2016). cDC1 development is dependent on the basic leucine zipper transcriptional factor ATF-like 3 (Batf3) and display a phenotype of $CD26^{hi}CADM1^{hi}CD11b^{lo}CD172a^{lo}$. On the other hand, cDC2 development is dependent on the interferon-regulatory factor 4 (IRF4) and are defined by expression of $CD11b^{hi}CD172a^{hi}F4/80^{lo\text{-}int}CD64^{lo\text{-}int}$. Additionally, they can express tissue and function specific markers such as CD4 in the spleen or CD207 in the dermis(Guilliams et al., 2014, 2016).

Plasmacytoid DCs (pDCs) are present in all peripheral organs and are relatively long-lived (14 days) (O'Keeffe et al., 2002). pDCs display a characteristic surface phenotype of expressing low levels of MHC class II and co-stimulatory molecules, and they contain a highly developed secretory compartment(Reizis et al., 2011). pDCs can act as antigen presenting cells but their main function is to respond to viral infections with a massive production of type I interferons (IFN-α and IFN-β), 100 to 1000-fold more potent than any other cell type(Siegal et al., 1999). Neonate pDCs however show an immature morphology and reduced capacity to produce IFN-α)(Schüller et al., 2013)

DC development

DCs are produced in a series of hierarchically and increasingly restricted progenitors. The arise from common myeloid progenitors (CMP) to monocyte/macrophage progenitors (MDP) up to common dendritic progenitors (CDP). CDPs express *Flt3* and *Zbtb46*(Satpathy et al., 2012) and give rise to pDCs and pre-cDCs(Naik et al., 2006; Onai et al., 2007). The precursor of cDCs, pre-DCs, circulate in the bloodstream and develop into the two subsets of cDCs in the tissues. However, reports using single cell transcriptome analysis have proposed previously overlooked committed precursors already present in the CDP (Schlitzer et al., 2015) and pre-cDC compartments(Grajales-Reyes et al., 2015). To further complicate the matter,

lymphoid progenitors have been reported to produce pDCs in steady state(Rodrigues et al., 2018), and cDCs under ablation conditions(Salvermoser et al., 2018).

Very little is currently known about DC development during fetal life. Small numbers of DCs (CD11c+ cells) have been observed in the thymus at E17.5 and the spleen at postnatal day (P)1(Dakic et al., 2004) but the absence of detection could come from a lack of activation from T cells before that stage, as most DC-markers are only expressed later in development. At birth, DCs are still only 0.2% of the spleen but reach 30% after 3 weeks of age and stabilise at 10% in the adult (Sun et al., 2003). It is currently unknown when the first DCs are produced during fetal life. In humans, DCs have been observed within fetal spleen, skin, thymus, and lung by 13WG with the capacity to induce T cell stimulationc(McGovern et al., 2017), and recent scRNAseq has identified putative DCs clusters in human fetal liver relatively as early as 7 GW(Popescu et al., 2019). However, such identification is solely based on expression of general myeloid markers and lack of other myeloid lineage genes, and as such it would need further investigation for this cell annotation to be confirmed. EMP contribution to this population during development remains to be investigated.

3.2.4- Granulocytes

The term granulocyte embodies a heterogeneous group of innate immune cells that are distinguished by a polylobed nucleus, multiple granules in the cytoplasm and specific cell surface markers. There are three types of granulocytes; basophils, eosinophils and neutrophils that are distinguished based on their nucleus structure and granule content. Neutrophils contain a multilobed nucleus with acidic granules; eosinophils contain a bi-lobed nucleus and crystalloid acidic granules; finally, basophils have a large bi- or tri-lobed nucleus with big basic granules. They are relatively short-lived cells, produced in the bone marrow, where they form and mature the granules before they are released into the peripheral blood.

Granulocyte heterogeneity

Neutrophils are the most abundant type of granulocytes and also of immune cells. Nearly 60% of bone marrow leukocytes are neutrophil precursors(Kennedy and Deleo, 2009). They are the first cells that are mobilized to the sites of infection where they degrade pathogenic bacteria and fungi by releasing proteolytic and antimicrobial granules, reactive oxygen species as well as their nuclear content forming nuclear extra-cellular traps (NET) (Brinkmann et al., 2004; Mantovani et al., 2011). Furthermore, neutrophils produce cytokines to recruit immune cells and regulate the inflammatory responses(Soehnlein et al., 2017). They remain 6-12h in the blood and stay in tissues an average of 1-2 days before undergoing apoptosis (Athens et al., 1961; Bainton et al., 1971; Cronkite and Fliedner, 1964; Summers et al., 2010) and being cleared by tissue macrophages(Savill et al., 1989b, 1989a). 1-2x10^{11} neutrophils are released daily into circulation in humans to maintain their numbers (Athens et al., 1961; Summers et al., 2010). Their production is controlled by granulocyte colony-stimulating factor (G-CSF or Csf3), granulocyte/macrophage colony-stimulating factor (GM-CSF or Csf2), and interleukin 3 (IL3).

Eosinophils can be found in mucosal tissues, the lung, the gastrointestinal tract and the bone marrow; and only a minor part is found in the peripheral blood. They are considered very short-lived, as they only stay in the blood for 18h of average before seeding tissues(Williams and Hellewell, 1995). Their main function is to respond to parasites and allergic responses(Costa, 1997). They are recruited to sites of inflammation in Th2-type responses where they produce an array of cytokines and lipid mediators and release toxic granule proteins and superoxide radicals(Kita, 2011). They express the high affinity receptor for IgE (FcεRI), CD80/CD86 and MHC II.

Basophils are a rare cell type in circulation (0.5% of leukocytes) and have a short lifespan of 1-2 days. Under inflammatory conditions, however, they rapidly proliferate in the bone marrow and migrate to sites of inflammation(Karasuyama and Yamanishi, 2014; Min et

al., 2012), where they play a role in parasite infections (Lantz et al., 1998) and allergic reactions (Gibbs, 2005; Prussin and Metcalfe, 2006). They express FcεRI and are the main producers of IL-4 during primary helminth infection (van Panhuys et al., 2011). They also secrete IL-4 in allergic reactions in response to IL-3 or FcεRI cross-linking (Denzel et al., 2008).

Granulocyte development

All granulocytes derive from a granulocyte/monocyte progenitor (GMP) in a highly controlled process that involves the C/EBP (CCAAT/enhancer binding proteins) transcription factor family: C/EBP-α(Johansen et al., 2001; Ma et al., 2014), -β(Hirai et al., 2006, 2015), and -ε(Bartels et al., 2015; Paul et al., 2015). Further differentiation produces lineage-committed progenitors like eosinophil progenitor (EoP) and basophil/mast cell progenitor (BMCP) (Figure 8). The upregulation of Gata1 is key to produce EoP, while the acetylation of C/EBP-ε at specific lysines causes neutrophil differentiation (Bartels et al., 2015; Fiedler and Brunner, 2012). An early neutrophil-restricted progenitor (proNeu1) has only recently been proposed in mice, using single-cell transcriptional analysis, that is contained within the GMP population, expresses CD68 and low levels of *Mac-1/CD11b* and requires CEBP-ε to further differentiate into neutrophil precursors (Kwok et al., 2020).

Under resting conditions, granulopoiesis is regulated by a number of physiological processes, such as diurnal oscillation, metabolic activity and aging. In response to stress conditions, like an infection, granulopoiesis is rapidly activated and enter in emergency granulopoiesis mode. Emergency granulopoiesis enhances the production of granulocytes to meet the demand for neutrophils during severe infection when these cells are consumed in large quantities during the innate immune response and is regulated by granulocyte colony-stimulating factor (G-CSF), C/EBP-α and specially by C/EBP- β(Manz and Boettcher, 2014; Yvan-Charvet and Ng, 2019).

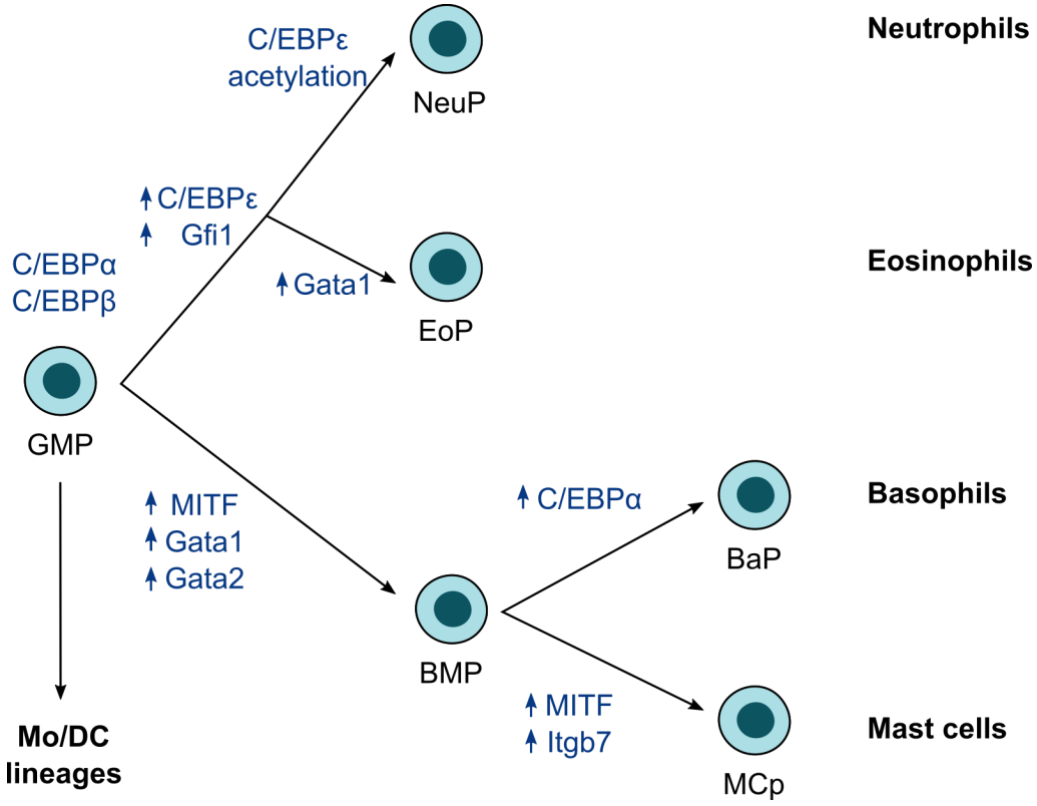

Figure 8. Schematic illustration of the development of the three types of granulocytes and mast cells in steady state. Expressed genes are in blue. GMP, granulocyte/monocyte progenitor; NeuP, neutrophil progenitor; EoP, eosinophil progenitor; BMP, basophil and mast cell progenitor; BaP, basophil progenitor; MCp, mast cell progenitor

During mouse embryonic development, rare neutrophils have been observed as early as E11.5 in circulation. These cells show normal maturation and are produced by EMPs in the fetal liver at least until E16.5 (Gomez Perdiguero et al., 2015; McGrath et al., 2015a). The fetal liver from E12.5 to E14.5 has mostly immature granulocyte precursors and no eosinophil peroxidase (*Epx*) or basophil FcεRI expression (McGrath et al., 2015a). In human fetal development, mature neutrophils clusters were observed in the bone marrow at 12-15 weeks of gestation, but lower number were found in the fetal liver at this stage(Ohls et al., 1995; Slayton et al., 1998). These observations are consistent with a recent human fetal liver single cell transcriptomic analysis, which failed to detect mature neutrophils, basophils and eosinophils at 17 GW (Popescu et al., 2019). It is not known whether this apparent discrepancy is due to the scarcity of neutrophils in the fetal liver in comparison with the fetal erythroid and

monocyte/macrophage cell abundance, observed also in the mouse, or whether human embryonic granulopoiesis is distinctly located in the bone marrow.

3.2.4- Mast cells

Mast cells (MCs) are innate resident mononuclear granular myeloid cells that play a key role in allergies but also have tissue specific homeostatic functions such as promoting (i) uterine spiral artery remodeling during pregnancy (Meyer et al., 2017; Woidacki et al., 2013), (ii) cardiomyocyte contractility following myocardial infarction (Ngkelo et al., 2016), (iii) corneal vasculature and (iv) neuronal network development (Liu et al., 2015). Their cytoplasm contains hundreds of large granules that store histamine, heparin, a variety of cytokines, chondroitin sulfate and proteases. They are widely distributed throughout vascularized tissues, particularly near surfaces exposed to the external environment, including the skin, airways, and gastrointestinal tract, but not in circulation (Galli et al., 2005). Consistent with their role in allergic reactions, they share expression of FcεRI with eosinophils and basophils, however they additionally express Kit/CD117, ST2 and IL-33Rα (Allakhverdi et al., 2007).

MCs are long lived cells that self-maintain in the tissues by local precursors (Dahlin and Hallgren, 2015; Matsuda et al., 1981) and have minimal contribution from the bone marrow in steady state (Gentek et al., 2018a; Hatanaka et al., 1979; Kitamura et al., 1977). Interestingly, it was shown that bone marrow progenitors contribute to skin MC only when the host is MC-deficient (Hatanaka et al., 1979). More recently, it was shown that bone marrow progenitors did not contribute significantly to MC replenishment in RMB mice (which express the human diphtheria toxin receptor under the control of the 3′ UTR of the FcεRI gene) after DT treatment, despite niche availability and vasculature proximity (Gentek et al., 2018a).

Mast cell development

In the adult bone marrow, MCs come from granulocyte/macrophage progenitor (GMP) that differentiate into a bipotent basophil/mast cell progenitor (BMP) that further commits to

MC progenitors (MCp) (Arinobu et al., 2005; Iwasaki et al., 2006; Qi et al., 2013). The bone marrow releases immature MCp that differentiate into MCs in peripheral tissues. The migration of MCp to tissues is a regulated process that is stimulated by inflammation (Dahlin and Hallgren, 2015). Gata1 and Gata2 are also involved in the maturation from MCp into mature MCs (Harigae et al., 1998; Migliaccio et al., 2003).

Much less is known about the development of MC during development. MC potential have been observed in the E8.5 mouse yolk sac and reach maximum at E11.5 (Palis et al., 1999; Sonoda et al., 1983). This is followed by an increase in MC potential in the fetal liver from E11 to E15, and in the skin until E17 (Gentek et al., 2018a; Hayashi et al., 1985). Similarly to resMf, adult MC have been recently shown to be partially derived from EMPs that are not completely replaced from bone marrow MCp in young animals (Gentek et al., 2018a; Li et al., 2018). Importantly, embryonic MCs have a different phenotype compared with their adult counterparts; they lack FcεR1 and MHCII surface expression but acquire them in the adulthood, which makes the observation of MC during development challenging (McGrath et al., 2015a). A recent study reported that adult-like MC could be generated by mouse or human ESC populations enriched in *Gata2* expression when cultured for two weeks(Kauts et al., 2018). This suggests that, rather than depending on the lineage, the acquisition of adult phenotype depends on a steady maturation in time.

AIMS AND OBJECTIVES

Extensive research over the last two decades has established the importance of EMP hematopoiesis for embryo development and for the generation of adult tissue resident macrophages. However, one of the main obstacles in developmental hematopoiesis, and specifically when studying EMPs, is the inability to distinguish EMP-derived from HSC-derived hematopoietic cells, since they coexist in different tissues while sharing surface markers and gene expression patterns. As a result, very little is known about EMP differentiation process and the contribution of EMP-derived erythroid and myeloid lineages to the embryo.

A better understanding of EMP-derived lineage decisions is critical to comprehend embryonic hematopoiesis and could have important translational significance, since defects in EMP development could affect infancy related hematopoietic disorders and/or result in long-term defects of tissue resident macrophages.

The main questions that I addressed during my PhD are the following:

Aim 1. Identify the *in vivo* differentiation patterns of EMPs

Aim 2. Characterize a unique phenotype and gene expression pattern of EMPs and EMP-derived progenitors in the yolk sac and the fetal liver

Aim 3. Assess the contribution of EMPs to the fetal hematopoietic system to ultimately build an EMP lineage tree.

In pursuit of these aims, I based my experiments on the precise genetic *Csf1r*^{MeriCreMer} fate mapping system, that has been demonstrated to label exclusively EMP and EMP progeny but not HSC when pulsed at E8.5(Gomez Perdiguero et al., 2015). I combined flow cytometry, cell sorting and single cell gene expression analysis in order to determine surface markers and molecular pathways of EMPs throughout embryonic development.

MATERIALS AND METHODS

The materials and methods used during this work are contained in the form of a manuscript in the results section.

The differences in the single-cell RNA-Sequencing data analysis for the figures 10-14 are explained here

Experimental design for scRNA-Seq. YFP+ single cells from E9.5 yolk sac *Csf1r*^{iCre} *Rosa*^{YFP} (n=3 litters, 27-29sp), E10.5 yolk sac *Csf1r*^{MeriCreMer} *Rosa*^{YFP} (n=6 litters, 34-38sp), E10.5 fetal liver *Csf1r*^{MeriCreMer} *Rosa*^{YFP} (n=6 litters, 34-38sp) and E12.5 fetal liver *Csf1r*^{MeriCreMer} *Rosa*^{YFP} (n=2 litters) embryos pulsed at E8.5 were index-sorted into 384-well plates with a lysis mix containing UPW, 10% Triton X-100 and RNasin plus 40U/µl (Promega N2611) with MARS-seq barcodes (made by etc) and immediately placed in dry ice after sorting. Plates were stored until processing at -80°C.

The plates were processed following the MARS-Seq pipeline (Jaitin et al., 2014) and sequenced in a Illumina NextSeq 500 sequencer using NextSeq® 500/550 High Output Kit v2 (75 cycles) (Illumina). 22 plates were sequenced in three independent sequencing runs, megakaryocytes and macrophages were sorted in the first run (Figure 10)

Cell and gene filtering for scRNA-Seq analysis. Cells for which mitochondrial genes took up more than 5% of the total UMI counts, and that had less than 3,000 detected genes were filtered out. We excluded 241 cells that were detected as doublet by the scDblFinder R package (Germain, 2020) using default parameters and running the analysis for each plate separately. In total, we analysed 5002 cells from 8360 sorted. The genes detected in less than 5% of the cells of each condition (E9.5 YS, E10.5 YS, E10.5 FL and E12.5 FL), the ERCC-spike-ins, and all mitochondrial genes were excluded. In total, 9,467 genes were kept. 797

and 1,257 cells were selected in the E9.5 and E10.5 YS conditions, respectively, and 1,686 and 1,456 cells were selected in the E10.5 and E12.5 FL conditions, respectively.

Batch effect correction. Batch effects were removed by hierarchically merging the samples using the 'reduceMNN' function of the batchelor R package(Haghverdi et al., 2018) on 50 principal components calculated with the multiBatchPCA function from the HVGs only. Plates were first merged within each sequencing run (using auto.merge=TRUE), and then across sequencing runs by descending number of plates.

The corrected low-dimensional coordinates of each cell returned by fastMNN were used as input for computation of clustering and UMAP (Uniform Manifold Approximation and Projection for Dimension Reduction) for visualization. UMAPs were calculated using the 'runUMAP' function of the Seurat package(Stuart et al., 2019) with the default parameters

Cell Clustering. A shared nearest-neighbor graph (SNN) was built using the 'buildSNNGraph' function of the scran R package. Communities were searched for in the SNN graph using the method of random walks implemented in the `cluster_walktrap` function of the igraph v1.2.5 package. The number k of nearest neighbors used in the SNN graph containing both tissues was k = 11.

Gene differential expression between clusters. Differential expression analyses were performed by computing pairwise t-tests using the 'findMarkers' function in the scran R package. The option 'pval.type="some"' was used to only consider markers differential in at least half of the pairwise comparisons between clusters.

Cell cycle quantification. Cells were classified into their cell cycle phases based on their gene expression data using the 'cyclone' function(Scialdone et al., 2015) of the scran package with default parameters.

Published protocol

Additionally, the fate-mapping and flow cytometry method that is used in this work are more extensively explained in the form of a published protocol in The Journal of Visualized Experiments (JoVE) attached to this section (Iturri et al., 2017). Of note, the day of the experiment the digestion buffer or mix, PBS containing 1mg/ml Collagenase D, 100 U/ml Deoxyribonuclease I (DNAseI) and 3% fetal bovine serum (FBS), is prepared before starting dissection and stored at 4 °C, as the yolk sac is transferred before the blood collection.

Video Article

Identification Of Erythromyeloid Progenitors And Their Progeny In The Mouse Embryo By Flow Cytometry

Lorea Iturri[1,2], Javier Saenz Coronilla[1], Yvan Lallemand[1], Elisa Gomez Perdiguero[1]

[1]Department of Developmental and Stem Cell Biology, CNRS UMR3738, Department of Immunology, Institut Pasteur

[2]Cellule Pasteur UPMC, University Pierre et Marie Curie

Correspondence to: Elisa Gomez Perdiguero at elisa.gomez-perdiguero@pasteur.fr

URL: https://www.jove.com/video/55305
DOI: doi:10.3791/55305

Keywords: Developmental Biology, Issue 125, Macrophages, yolk sac, definitive hematopoiesis, hematopoietic stem and progenitor cells, mouse embryos, FACS, fate mapping

Date Published: 7/17/2017

Citation: Iturri, L., Saenz Coronilla, J., Lallemand, Y., Gomez Perdiguero, E. Identification Of Erythromyeloid Progenitors And Their Progeny In The Mouse Embryo By Flow Cytometry. *J. Vis. Exp.* (125), e55305, doi:10.3791/55305 (2017).

Abstract

Macrophages are professional phagocytes from the innate arm of the immune system. In steady-state, sessile macrophages are found in adult tissues where they act as front line sentinels of infection and tissue damage. While other immune cells are continuously renewed from hematopoietic stem and progenitor cells (HSPC) located in the bone marrow, a lineage of macrophages, known as resident macrophages, have been shown to be self-maintained in tissues without input from bone marrow HSPCs. This lineage is exemplified by microglia in the brain, Kupffer cells in the liver and Langerhans cells in the epidermis among others. The intestinal and colon lamina propria are the only adult tissues devoid of HSPC-independent resident macrophages. Recent investigations have identified that resident macrophages originate from the extra-embryonic yolk sac hematopoiesis from progenitor(s) distinct from fetal hematopoietic stem cells (HSC). Among yolk sac definitive hematopoiesis, erythromyeloid progenitors (EMP) give rise both to erythroid and myeloid cells, in particular resident macrophages. EMP are only generated within the yolk sac between E8.5 and E10.5 days of development and they migrate to the fetal liver as early as circulation is connected, where they expand and differentiate until at least E16.5. Their progeny includes erythrocytes, macrophages, neutrophils and mast cells but only EMP-derived macrophages persist until adulthood in tissues. The transient nature of EMP emergence and the temporal overlap with HSC generation renders the analysis of these progenitors difficult. We have established a tamoxifen-inducible fate mapping protocol based on expression of the macrophage cytokine receptor Csf1r promoter to characterize EMP and EMP-derived cells *in vivo* by flow cytometry.

Video Link

The video component of this article can be found at https://www.jove.com/video/55305/

Introduction

There are several successive but overlapping waves of hematopoietic progenitors during development whose myeloid progeny remain into adulthood. First, unipotent "primitive" progenitors emerge in the mouse yolk sac [1,2] between E7.5-E8.25 and give rise to embryonic macrophages without any monocytic intermediate. Whether macrophages derived from primitive progenitors persist in the adult brain as microglia remains a subject of active investigation. Second, Erythro-Myeloid Precursors (EMPs) arise in the yolk sac at E8.5, enter the bloodstream and colonize the embryo. EMPs emerge from the yolk sac hemogenic endothelium in a Runx1-dependant endothelial-to-hematopoietic transition [3,4]. While EMP can differentiate into macrophages within the yolk sac, they also colonize the fetal liver from embryonic day (E)9[5] and differentiate into erythrocytes, megakaryocytes, macrophages, monocytes granulocytes and mast cells [6]. The macrophages that derive from EMPs exhibit proliferative capacity in developmental and adult tissues. Whether EMP-derived macrophages bypass the monocyte stage of differentiation is still controversial as very little is known about their differentiation pathway [7,8]. Finally, Hematopoietic Stem Cells (HSCs) emerge at E10.5 within the embryo proper from the aorta-gonad-mesonephros region and migrate to the fetal liver. HSCs with long-term repopulation capacity are only detected after E11 (at the 42 somite pair stage)[9]. There, they expand and differentiate from E12.5 until definitive hematopoiesis begins to shift to the bone marrow, which becomes the predominant site of blood cell production for the duration of postnatal life [10].

The spatial and temporal overlap in emergence, as well as shared immuno-phenotypic markers has thus far hampered our ability to distinguish the specific contributions of these waves of embryonic hematopoietic progenitors. While both EMP and HSC are generated in a Runx1-dependent manner and express the transcription factor Myb and the growth factor receptor Csf1r (Colony-Stimulating Factor 1 Receptor, also known as Macrophage Colony Stimulating Factor Receptor) among others, EMPs can be distinguished from HSCs by their lack of lymphoid potential, both *in vitro* and *in vivo*, their lack of long-term repopulating potential and lack of surface expression of the lineage marker Sca-1 [11]. Genetic fate mapping models are required to characterize macrophage ontogeny since they allow targeting embryonic progenitors in a cell-specific and time-specific manner. Here we present the fate-mapping protocol used in our laboratory to discriminate between the two lineages of macrophages found in most adult tissues: HSC-derived infiltrating macrophages and HSC-independent resident macrophages.

Tissue resident macrophages have been traced back to Myb-independent precursor cells expressing the cytokine receptor Csf1r[12] and are present in the embryo at E8.5-E10.5 using three complementary fate-mapping strategies [6]. In order to study yolk sac hematopoiesis without

labeling fetal HSCs, we use a transgenic strain, *Csf1r*^{MeriCreMer}, expressing a tamoxifen-inducible fusion protein of 'improved' Cre recombinase and two mouse estrogen receptors (Mer-iCre-Mer) under the control of the Csf1r promoter. Hence, the Cre recombinase will be active in *Csf1r*-expressing cells during a limited time-window. When used with a reporter strain containing a fluorescent protein downstream of a lox-STOP-lox cassette (Rosa26$^{LSL-eYFP}$), it will lead to the permanent genetic labeling of the cells present at the time of induction but also of their progeny. Administration at E8.5 of the active form of tamoxifen, 4-hydroxytamoxifen (OH-TAM), labels EMPs and macrophages, without labeling yolk sac unipotent "primitive" progenitors or fetal HSCs. Thereby, we have characterized the immunophenotype of EMPs and their progeny during embryonic development, as well as assessed the contribution of yolk sac-derived macrophages to the adult macrophage pools. Further work is required to characterize whether primitive progenitor-derived macrophages are also labeled using this approach and whether they can contribute to adult macrophage pools.

Protocol

Animal procedures were performed in accordance with the approved institutional animal care and use committee of the Institut Pasteur (CETEA).

1. *In Utero* Pulse Labeling in *Csf1r* ^{MeriCreMer} *Rosa* $^{LSL-YFP}$ Embryos

1. **Prepare the stock solution of 4-hydroxytamoxifen (OH-TAM, 50 mg/mL).**
    1. Under the fumehood, open the 25 mg vial of OH-TAM and add 250 µL ethanol (100%).
    2. Transfer the OH-TAM solution to a 2 mL microcentrifuge tube with a truncated tip and vortex at maximum speed for 10 min.
    3. Sonicate 30 min in a sonicator bath.
    4. Add 250 µL of PEG-35 castor oil under the fumehood to obtain a 50 mg/mL stock solution.
    NOTE: PEG-35 castor oil is a solvent with amphiphilic properties that binds hydrophobic molecules and solubilizes them in aqueous solvents.
    5. Vortex for approximately 5 min at maximum speed and sonicate 30 min in a sonicator bath.
    6. Aliquot 90 µL (4.5 mg) per microcentrifuge tube (1 aliquot per injection).
    7. Store at 4 °C for 1 week or at -20 °C for long term as previously described [13].

2. **Prepare the stock solution of Progesterone (10 mg/mL)**
    1. Add 250 µL of 100% Ethanol to 25 mg of progesterone to prepare a 10 mg/100 µL suspension under the fumehood. Vortex gently.
    2. Add 2250 µL autoclaved sunflower oil to make 10 mg/ml progesterone solution under the hood.
    3. Vortex for approximately 5 min at maximum speed, aliquot and store at 4 °C. Note that the solution is clear when stored.

3. **Tamoxifen administration**
    NOTE: Embryonic development was estimated considering the day of vaginal plug formation as Embryonic day (E) 0.5. Recombination is induced by single injection at E8.5 into pregnant *Csf1r*^{MeriCreMer}*females* [12]. Supplement OH-TAM with 37.5 µg per g of Progesterone to reduce abortion rates after tamoxifen administration. Inject at 1 pm (for vaginal plug observed in the morning).
    1. On the morning of injection, sonicate an aliquot of the OH-TAM solution for 10 min (or until completely resuspended).
    2. Add 360 µL NaCl 0.9% under the fumehood to obtain a 10 mg/mL OH-TAM solution and vortex thoroughly. Sonicate until the solution is clear and completely resuspended (at least 30 min).
    3. Pre-warm progesterone to room temperature.
    4. Mix 450 µL of OH-TAM and 225 µL of progesterone in a microcentrifuge tube. Vortex.
    5. Sonicate at least 10 min and load on to a 1 mL syringe with a 25G needle.
    6. In the animal facility, weigh the pregnant female (*Csf1r*^{MeriCreMer} females are in an inbred FVB genetic background and typical weigh between 25 and 33 g).
    7. Perform an intra-peritoneal injection by slowly injecting the calculated volume into the mouse. After withdrawing the needle, gently press on the puncture wound and massage the abdomen to distribute the OH-TAM.
    NOTE: The OH-TAM injection dose is 75 mg/kg and the Progesterone dose is 37.5 mg/kg. **Table 1** provides the volume to inject into pregnant females.

Mouse weight (g)	Total volume to inject from the mix (µL)
25	281
26	292
27	303
28	315
29	326
30	338
31	348
32	360
33	371
34	382
35	394

Table 1: Injection volume of 4-OH-tamoxifen (OH-TAM). Volume required for a single injection at E8.5 of 75 µg per g (body weight) of OH-TAM supplemented with 37.5 µg per g of progesterone.

2. Dissection of the Yolk Sac (YS) and Fetal Liver (FL)

NOTE: Rigorous sterile techniques are not necessary when manipulating embryos unless if they are going to be used for long-term culture. Nevertheless, the working area must be clean and covered in foil under absorbent paper.

1. Prepare ice-cold phosphate buffered saline (PBS) and digestion mix (PBS containing 1 mg/mL collagenase D, 100 U/mL Deoxyribonuclease I (DNase I) and 3% fetal bovine serum).
2. Sacrifice pregnant females by cervical dislocation at the required gestation day (*e.g.* embryonic stage E10.5).
3. Pinch the skin just over the genitals and make a small incision at the midline with scissors. Pull the skin toward the head to expose completely the body wall without fur. Cut the abdominal muscles to expose the internal organs and push the gut to expose the two uterine horns.
4. With middle-sized blunt forceps, grab the fat-pad attached to the ovary and gently pull the uterus. Cut at the cervical level of the uterine horns and lift the horns from the peritoneal cavity. Remove the fat-pad to completely free the uterine horns and cut the horns from the ovary on each side.
5. Put the horns into ice-cold PBS in a 10 mm Petri dish. Rapidly grip the uterus muscle layers at one extremity (cervical end) and slide fine scissors between the muscle layer and the decidual tissue to release the embryos with the surrounding decidual tissue.
   NOTE: Muscle tend to rapidly contract after the extraction, so this step must be as quick as possible.
6. Use one pair of fine forceps to cut off the Reichert's membrane and the placenta.
7. **Gently remove the yolk sac and place it in a 24-well tissue culture plate with 0.5 mL of digestion mix.**
   NOTE: At this step, embryonic blood can be collected.
   1. Immediately after severing the umbilical and vitelline vessels, transfer the embryo into a 12-well tissue culture plate containing 10 mM ice-cold ethylenediaminetetraacetic acid (EDTA). Decapitate the embryo using sharp fine scissors, trying to limit as much as possible tissue dilaceration. Incubate on ice for 10-15 min and collect the EDTA containing the blood.
8. Remove the amnion surrounding the embryo.
9. For stages <E11.5, count the number of somite pairs for better staging of embryos and a better time resolution (each somite pair develops in ~1 h 30 min).
10. Cut the head of the embryo using forceps or fine scissors. Transfer the head to a 24-well plate with 0.5 mL digestion mix.
    NOTE: The neuroectoderm and brain at later stages are further dissected for flow cytometry analysis; carefully remove the surrounding vascular plexus.
11. Cut the embryo above the hindlimb and remove the forelimbs.
12. **To isolate the liver, open the thorax using a pair of fine forceps. Pinch anteriorly to the heart and gently pull while using the second forceps to free the organs from the body.**
    1. Carefully separate the fetal liver from the heart and gut. Transfer the fetal liver to a 24-well plate with 0.5 mL digestion mix. Carefully monitor the transfer under the dissecting microscope.
13. Collect the tail region (or any other embryo part) for genotyping by polymerase chain reaction assay (PCR).
    NOTE: Other tissues and organs can be harvested from E10.5 embryos for a similar analysis using flow cytometry. Blood, head skin, aorta-gonad-mesonephros region (AGM), heart and neuroectoderm can be collected at E10.5. At later stages, lung, kidney, spleen and pancreas can also be collected. A detailed description of the dissection of the AGM at different developmental stages has been previously described [14].

3. Processing of Embryonic Tissues for Flow Cytometry

1. Incubate the organs (placed in the digestion mix) for 30 min at 37 °C.
2. Transfer the tissue and enzymatic solution onto a 100 µm strainer placed in a 6-well tissue culture plate filled with 6 ml of FACS buffer (0.5% Bovine Serum Albumin (BSA) and 2 mM EDTA in 1x PBS). Mechanically dissociate by gently mashing with the black rubber piston of a 2 mL syringe to obtain a single-cell suspension.

NOTE: From now on, all steps should be performed at 4 °C.

3. Collect the cell suspension with a Pasteur pipette and transfer into a 15 mL tube.
4. Spin for 7 min at 320 x g at 4 °C. Discard the supernatant by aspiration.
5. **Resuspend the pellet in 60 µL Fc-blocking buffer (CD16/CD32 blocking antibody diluted 1/50 in FACS buffer).**
    1. Transfer 50 µL of the single-cell suspension per well in a round bottom 96 multi-well plate. Incubate for at least 15 min on ice.
    NOTE: The staining can also be performed in 5 mL polystyrene FACS tubes when handling a small number of samples.
    2. Transfer the remaining 10 µL into a 5 mL polystyrene FACS tube to obtain a pool of the samples from each tissue. This pool will serve as the controls (*i.e.* unstained samples and fluorescent minus one (FMO) controls for each fluorochrome). Transfer 50 µL of the pool for each fluorescent minus one (FMO) control (one per fluorochrome) to the 96 multi-well plate.
    NOTE: Each FMO control contains all the fluorochrome-coupled antibodies from the antibody panel, except for the one that is being measured. FMOs are used to identify gate boundaries and to control for the spectral overlap in multicolor panels. To correctly address the variations in background and autofluorescence between different tissues, it is important to prepare these controls from the pool of samples of each tissue. The appropriate control for YFP expression will be the samples from Cre-negative embryos, which are confirmed by PCR genotyping.

4. Surface Antigen Staining

1. **Prepare the antibody mix in FACS buffer (Table 2). Prepare 50 µL of antibody mix per sample.**
    1. Use the following fluorochrome-coupled antibodies: anti-CD45.2 (clone 104); anti-CD11b (clone M1/70); anti-F4/80 (clone BM8); anti-AA4.1 (clone AA4.1); anti-Kit (clone 2B8); and anti-Ter119 (clone Ter119).
    2. Prepare six antibody mixes for the FMO controls in FACS buffer. Prepare 50 µL of antibody mix per control sample.
    NOTE: The antibody dilution in the antibody mix is two times more concentrated than the final concentration indicated in the materials table. For a panel with six fluorochrome-coupled antibodies, 6 FMO controls are prepared. **Table 2** provides the composition of the antibody mix and FMO controls for one tube.

		Volume (µL) of antibody (Final Volume 50 µL)						
Antibody	Clone	Antibody Mix	FMO CD45.2	FMO CD11b	FMO F4/80	FMO AA4.1	FMO Kit	FMO Ter119
anti-CD45.2	104	1	0	1	1	1	1	1
anti-CD11b	M1/70	0.5	0.5	0	0.5	0.5	0.5	0.5
anti-F4/80	BM8	1	1	1	0	1	1	1
anti-AA4.1	AA4.1	1	1	1	1	0	1	1
anti-Kit	2B8	0.5	0.5	0.5	0.5	0.5	0	0.5
anti-Ter119	Ter119	0.5	0.5	0.5	0.5	0.5	0.5	0
FACS buffer		45.5	46.5	46	46.5	46.5	46	46

Table 2: Volume of antibodies using for staining and Fluorescent minus one (FMO) controls. Volume (µL) of antibody required for a final volume of 50 µL.

2. Add 50 µL of the antibody mix to the samples in the 96-multiwell plate (final volume during staining is 100 µL). Gently pipette up and down twice and incubate on ice for 30 min.
3. Spin the 96-multiwell plate for 7 min at 320 x g at 4 °C and discard the supernatant. Resuspend in 200 µL of FACS buffer.
4. Repeat wash procedure (step 4.3) twice with 150 µL FACS buffer.
5. Filter the samples and the controls (FMOs and unstained pool samples) into 5 ml polystyrene tubes through a 70 µm strainer. Store on ice until acquisition.

5. Identification of EMPs and YS-derived Macrophages by Flow Cytometry

NOTE: This protocol was optimized using a 4 laser flow cytometer equipped with a 405 nm Violet laser, a 488 nm Blue laser, a 562 nm Yellow laser and a 638 nm Red laser.

1. Prepare compensation beads for each coupled antibody following the manufacturer's instructions. Use unstained samples and compensation beads to optimize laser intensities.
2. To identify gate boundaries, use FMO (Fluorescence minus one) controls for each antibody.
3. In order to exclude dead cells, add 1 µL of DAPI (1 mg/ml) to the tube (containing 200 µL of stained cell suspension) 1 min before acquisition. Use the strong DAPI signal and the forward-scattered parameter (FSC) to perform exclusion of dead cells and debris.
NOTE: Use software from the flow cytometer to draw gates during acquisition. Compensation matrix and analysis can be performed after sample acquisition using other commercially available software.
4. Use forward and side scatter (FSC vs SSC) to perform live cell and doublet discrimination from total events.
5. Create fluorescence dot plots in log-scale axis and draw daughter gates to, first, exclude erythrocytes ($Ter119^+$) and, then, to identify progenitor cells (Kit^+) and hematopoietic cells ($CD45^+$ Kit^{neg}) (See **Figure 1**).
6. Create fluorescence histograms to quantify the labeling efficiency of YFP among the different identified populations in the YS (**Figure 2**), fetal liver (**Figure 3**) and brain (**Figure 4**).

Representative Results

Genetic fate mapping was achieved by administration at E8.5 of OH-TAM into Csf1r-Mer-iCre-Mer females mated with males carrying a Rosa26-LSL-eYFP reporter. In the presence of OH-TAM, excision of the stop cassette leads to the permanent expression of YFP in the cells expressing *Csf1r*. We collected two hematopoietic tissues: the yolk sac and the fetal liver and a non-hematopoietic tissue, the neuroectoderm, from the embryos at E10.5. Single-cell suspensions were obtained by enzymatical and mechanical dissociation and samples were analyzed by flow cytometry after staining with fluorescent-coupled antibodies. After exclusion of dead cells and doublets, single cell suspensions were analyzed (**Figure 1**). All gates were defined using Fluorescence Minus One (FMO) controls. It is recommended to also perform an erythrocyte exclusion (Ter119^{+} cells) to improve clarity of the analysis (**Figure 1B**). Using the cell surface markers Kit (progenitor marker) and CD45 (hematopoietic cells marker), we were able to distinguish three populations of cells of interest: Kit^{+} CD45^{neg}; Kit^{+} CD45^{low} and Kit^{neg} CD45^{+} (**Figure 1**). Progenitors were further analyzed based on their expression of AA4.1 (**Figures 2-4**). Indeed, AA4.1 is a surface marker that allows the enrichment of the progenitor population within erythromyeloid progenitors in the yolk sac, as demonstrated in colony forming assays [15]. Once the populations of interest were identified, we quantified the YFP labeling efficiency in each population using histograms. Among the yolk sac Kit^{+} progenitors, both CD45^{neg} (**Figure 2A**) and CD45^{low} (**Figure 2B**) cell populations contain AA4.1^{+} YFP^{+} cells. However, AA4.1^{+} YFP^{+} cells in the liver and brain are only found in the Kit^{+} CD45^{low} progenitor population (**Figure 3B** and **4B**). Since, the brain is not an active site of hematopoiesis, progenitors found in this tissue could correspond to circulating progenitors. This also suggests a process of progenitor maturation as they migrate from the yolk sac to the fetal liver and the peripheral tissues. Kit^{+} progenitors first express AA4.1, irrespectively of CD45 expression, but by the time they reach circulation and the fetal liver, all AA4.1^{+} YFP^{+} progenitors express detectable levels of cell surface CD45. Macrophages, defined as F4/80^{bright} CD11b^{+}, were found in the Kit^{neg} CD45^{+} gate (**Figure 2-4**). Macrophages in the E10.5 yolk sac, liver and brain were efficiently labeled (60 to 80% of F4/80^{bright} CD11b^{+} cells are YFP^{+}) by a single OH-TAM administration at E8.5 (**Figure 2C**, **3C** and **4C**).

To compare labeling efficiency between litters, we recommend that an internal control for recombination efficiency is used. Variability in the level of expression of the reporter can be observed between experiments, due to variations in developmental timing between litters and mouse strains when OH-TAM is injected *in utero*. Hence, we recommend that embryo staging from E8.5 to E11.5 embryos is performed by somite pair counting. In this protocol, we propose to use the labeling efficiency in the brain resident macrophages (microglia) as a reference to compare the efficiency of Cre recombination between different experiments and strains (**Figure 4C**). Other resident macrophages could be used, however microglia were the first cells to be described as yolk sac-derived macrophages [16] and they represent the most abundant population of tissue resident macrophages at E10.5. Thus, YFP labeling in microglia can be used to assess the fate-mapping efficiency in each experiment and compare data from different litters.

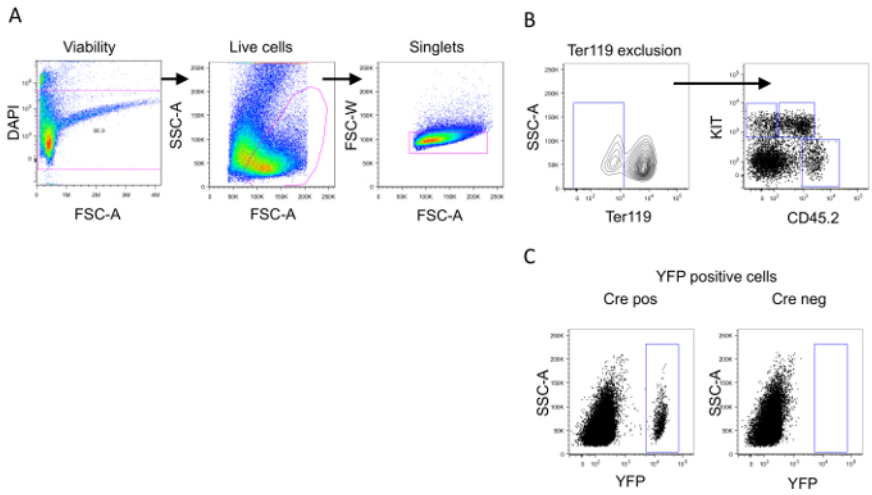

Figure 1: Gating strategy to identify progenitor cells (Kit^{+} CD45^{neg} and Kit^{+} CD45^{low}) and differentiated hematopoietic cells (Kit^{neg} CD45^{+}). (**A**) Discrimination of live cells and singlets is performed using DAPI staining and Forward and Side scatter (FSC/SSC) parameters. (**B**) Following red blood cell exclusion (Ter119^{neg}), three populations of cells of interest are identified based on cell surface expression of Kit and CD45: Kit^{+} CD45^{neg}; Kit^{+} CD45^{low} and Kit^{neg} CD45^{+} cells. (**C**) Csf1r-expressing cells present when OH-TAM is injected and their progeny are identified in Cre-recombinase positive embryos as expressing YFP compared to the Cre-recombinase negative embryos (confirmed later by polymerase chain reaction assay, PCR). Please click here to view a larger version of this figure.

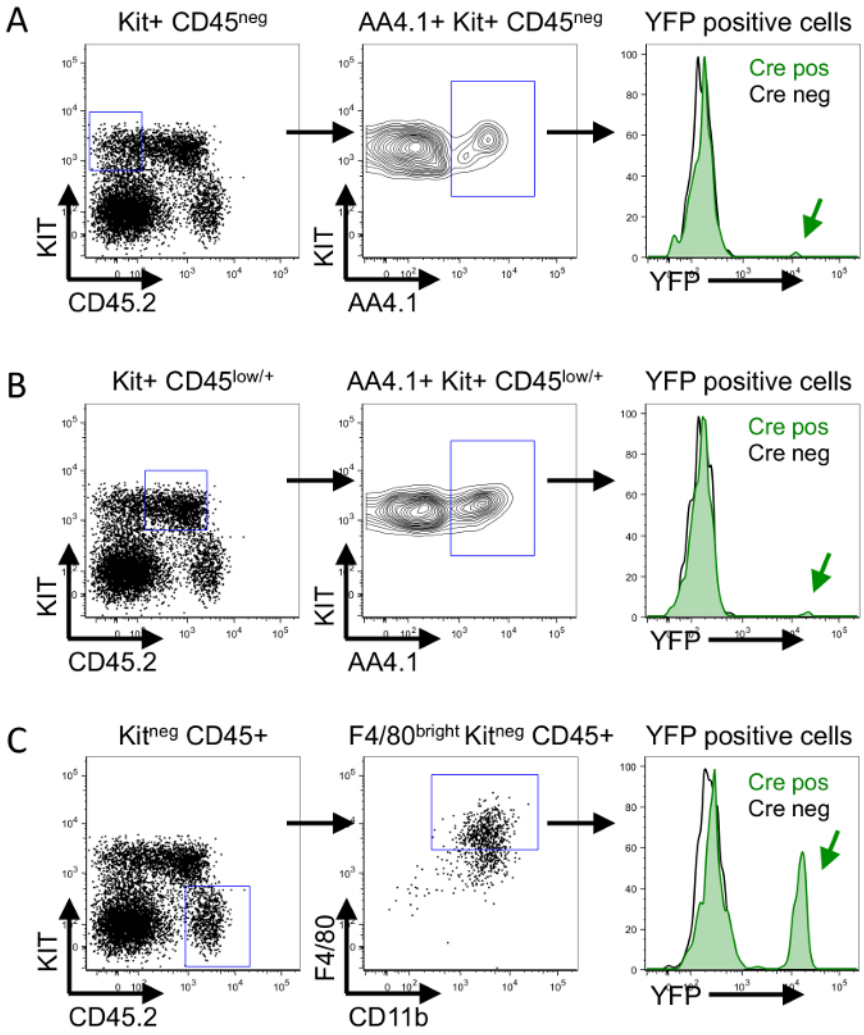

Figure 2: Labeling efficiency in the yolk sac from E10.5 Csf1r^{MeriCreMer} Rosa26$^{LSL-eYFP}$ embryospulsed with OH-TAM at E8.5. (**A**) Kit^{+} CD45^{neg} cells are gated based on Kit and CD45 expression on live yolk sac cells (blue gate, left panel). AA4.1 and Kit expression on Kit^{+} CD45^{neg} cells. Blue gate encloses AA4.1^{+} Kit^{+} CD45^{neg} cells (middle panel). Comparison of YFP labeling in AA4.1^{+} Kit^{+} CD45^{neg} cells (right panel) in Cre negative controls (black) and Cre positive samples (green). Histograms represent the percentage of cells (y-axis) positive for YFP signal (x-axis). (**B**) Kit^{+} CD45^{low} cells are gated based on Kit and CD45 expression (blue gate, left panel). AA4.1 and Kit expression on Kit^{+} CD45^{low} cells. Blue gate encloses EMP, as defined as AA4.1^{+} Kit^{+} CD45^{low} cells (middle panel). Comparison of YFP labeling in AA4.1^{+} Kit^{+} CD45^{low} cells (right panel) in Cre negative controls (black) and Cre positive samples (green). Histograms represent the percentage of cells (y-axis) positive for YFP signal (x-axis). (**C**) Hematopoietic cells are defined as Kit^{neg} CD45^{+} and gated in blue (left panel). F4/80 and CD11b expression on Kit^{neg} CD45^{+} cells. Macrophages are defined as F4/80^{bright} CD11b^{+} cells (middle panel). Comparison of YFP labeling in F4/80^{bright} CD11b^{+} macrophages (right panel) in Cre negative controls (black) and Cre positive samples (green). Histograms represent the percentage of cells (y-axis) positive for YFP signal (x-axis). Please click here to view a larger version of this figure.

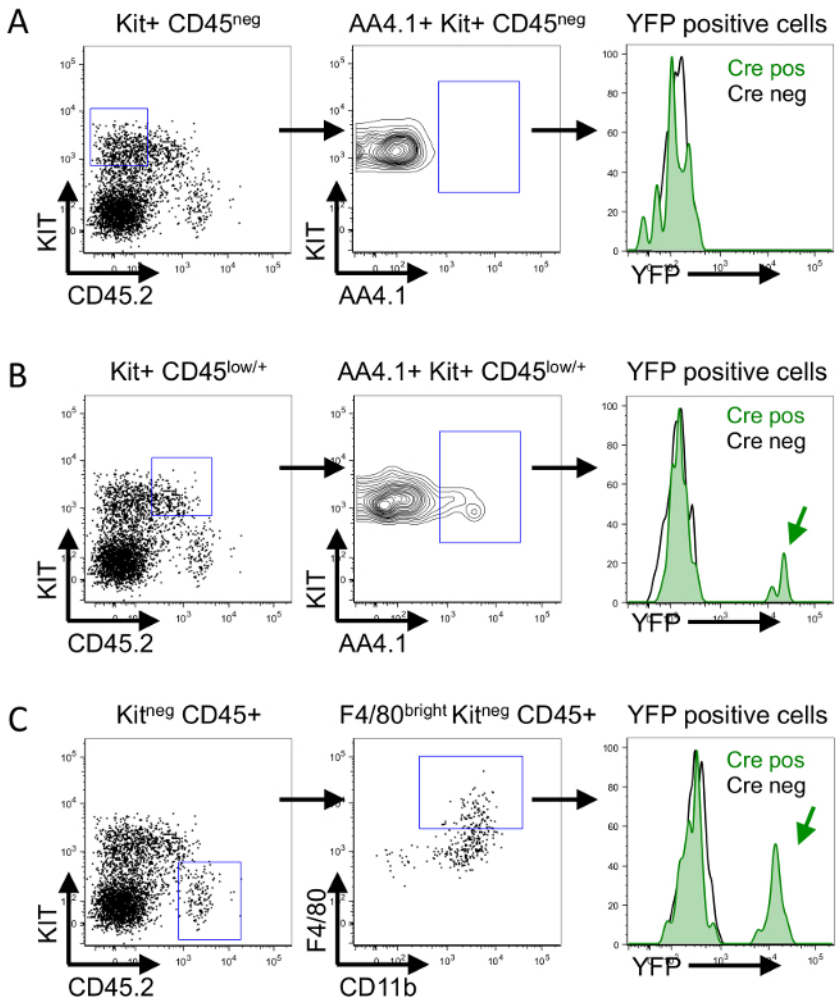

Figure 3: Labeling efficiency in the liver from E10.5 Csf1r^{MeriCreMer} Rosa26$^{LSL-eYFP}$ embryospulsed with OH-TAM at E8.5. (**A**) Kit^{+} CD45^{neg} cells are gated based on Kit and CD45 expression on live liver cells (blue gate, left panel). AA4.1 and Kit expression on Kit^{+} CD45^{neg} cells. Blue gate encloses AA4.1^{+} Kit^{+} CD45^{neg} cells (middle panel). Comparison of YFP labeling in AA4.1^{+} Kit^{+} CD45^{neg} cells (right panel) in Cre negative controls (black) and Cre positive samples (green). Histograms represent the percentage of cells (y-axis) positive for YFP signal (x-axis). (**B**) Kit^{+} CD45^{low} cells are gated based on Kit and CD45 expression (blue gate, left panel). AA4.1 and Kit expression on Kit^{+} CD45^{low} cells. Blue gate encloses EMP, as defined as AA4.1^{+} Kit^{+} CD45^{low} cells (middle panel). Comparison of YFP labeling in AA4.1^{+} Kit^{+} CD45^{low} cells (right panel) in Cre negative controls (black) and Cre positive samples (green). Histograms represent the percentage of cells (y-axis) positive for YFP signal (x-axis). (**C**) Hematopoietic cells are defined as Kit^{neg} CD45^{+} and gated in blue (left panel). F4/80 and CD11b expression on Kit^{neg} CD45^{+} cells. Macrophages are defined as F4/80^{bright} CD11b^{+} cells (middle panel). Comparison of YFP labeling in F4/80^{bright} CD11b^{+} macrophages (right panel) in Cre negative controls (black) and Cre positive samples (green). Histograms represent the percentage of cells (y-axis) positive for YFP signal (x-axis). Please click here to view a larger version of this figure.

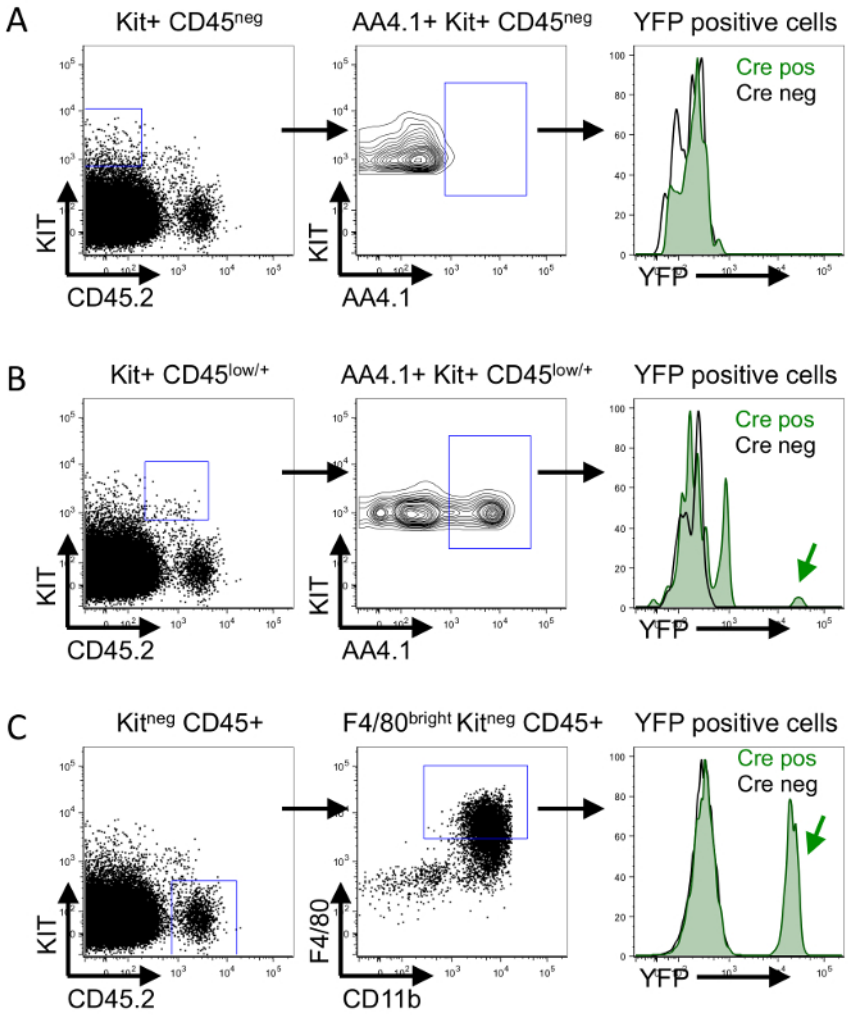

Figure 4: Labeling efficiency in the brain from E10.5 Csf1r^{MeriCreMer} Rosa26$^{LSL-eYFP}$ embryospulsed with OH-TAM at E8.5. (**A**) Kit^{+} CD45^{neg} cells are gated based on Kit and CD45 expression on live brain cells (blue gate, left panel). AA4.1 and Kit expression on Kit^{+} CD45^{neg} cells. Blue gate encloses AA4.1^{+} Kit^{+} CD45^{neg} cells (middle panel). Comparison of YFP labeling in AA4.1^{+} Kit^{+} CD45^{neg} cells (right panel) in Cre negative controls (black) and Cre positive samples (green). Histograms represent the percentage of cells (y-axis) positive for YFP signal (x-axis). (**B**) Kit^{+} CD45^{low} cells are gated based on Kit and CD45 expression (blue gate, left panel). AA4.1 and Kit expression on Kit^{+} CD45^{low} cells. Blue gate encloses EMP, as defined as AA4.1^{+} Kit^{+} CD45^{low} cells (middle panel). Comparison of YFP labeling in AA4.1^{+} Kit^{+} CD45^{low} cells (right panel) in Cre negative controls (black) and Cre positive samples (green). Histograms represent the percentage of cells (y-axis) positive for YFP signal (x-axis). (**C**) Hematopoietic cells are defined as Kit^{neg} CD45^{+} and gated in blue (left panel). F4/80 and CD11b expression on Kit^{neg} CD45^{+} cells. Macrophages are defined as F4/80^{bright} CD11b^{+} cells (middle panel). Comparison of YFP labeling in F4/80^{bright} CD11b^{+} macrophages (right panel) in Cre negative controls (black) and Cre positive samples (green). Histograms represent the percentage of cells (y-axis) positive for YFP signal (x-axis). Please click here to view a larger version of this figure.

Discussion

The different waves of hematopoietic precursor cells partially overlap within a short time frame, which makes the analysis of the contribution of each wave of developmental hematopoiesis to immune cells technically very challenging.

Tamoxifen-inducible Cre systems offer the opportunity to tag specific cells in a temporally inducible manner and to perform lineage analysis in embryos or adults, without the need for *ex vivo* or *in vitro* culture or transplantation. In tamoxifen-inducible Cre strains, a fusion gene is created between a bacterial Cre recombinase and a mutant form of the ligand binding domain of the human estrogen receptor (CRE-ER) or between an improved single-point mutant Cre and two mouse estrogen receptors (Mer-iCre-Mer). Fusion of Cre with estrogen receptors leads to the cytoplasmic sequestration of Cre by Hsp90, thereby preventing nuclear Cre-mediated recombination. Tamoxifen (TAM) is metabolized by the liver into 4-hydroxytamoxifen (OH-TAM), its active metabolite with high binding affinity for estrogen receptor. OH-TAM binding to the fusion Cre leads to the disruption of the interaction with Hsp90, permitting its translocation to the nucleus and initiation of Cre-mediated recombination. Injection of TAM or OH-TAM *in utero* into pregnant females has been shown to activate recombination in the developing embryo. Tamoxifen administration during pregnancy can lead to abortion and thus reduces litter size but it also prevents birth if delivered after mid-gestation, in

which case pup delivery through a caesarean operation is required. To counterbalance tamoxifen effects during pregnancy, we supplement OH-TAM administration with a half-dose of progesterone, in order to improve survival of embryos and reduce the risk of abortions [17].

Several routes can be employed to deliver TAM or OH-TAM into pregnant females. Currently oral gavage or intra peritoneal (ip) injection is used for tamoxifen. OH-TAM has the advantage to be immediately available, as it does not require to be metabolized by the liver of the pregnant dam. However, while tamoxifen is very easy to dissolve in corn oil, OH-TAM is very difficult to prepare using the same technique and results in an emulsion. This has been a limiting step in employing OH-TAM for *in utero* pulse labeling. We have adapted the protocol for preparation of OH-TAM developed by the group of J.F. Nicolas [13], where they use PEG-35 castor oil, a solvent with amphiphilic properties to solubilize OH-TAM, as tamoxifen dissolution is one of the most critical steps in the procedure. This allows for reproducible and optimal preparation of OH-TAM and considerably shortens the time of tamoxifen preparation. Further, it is necessary to adapt the concentration of OH-TAM to inject when using different inducible Cre strains. The combination of a viability dye (DAPI) and size (FSC) is critical to remove dead cells and cellular debris, respectively. Dead cells and debris are highly autofluorescent in most of the violet, blue and red laser detectors, and can hamper flow cytometric analysis. Further, we do not recommend fixing the cells after staining prior to analysis with the flow cytometer. Fixation can lead to changes in cell morphology and thus renders difficult size discrimination based on Forward and Side Scatter (FSC vs. SSC). Further, fixation of samples with PFA leads to a significant loss of YFP fluorescent intensity.

The main limitation within this protocol is that the populations are not tested on their functionality and differentiation potential. In order to overcome this, cells can be sorted following a similar protocol using a Fluorescently-activated cell sorter (FACS) to perform colony-forming assay. In this case, the procedure must be performed under sterile conditions and use of fetal bovine serum (FBS) in the FACS buffer, instead of BSA, is highly recommended. The low labeling efficiency achieved with this technique and the consequently low number of YFP^+ cells of interest per embryonic tissue is a major challenge in the study of EMP phenotype. This protocol uses a 4-laser flow cytometer. A flow cytometer with 3 lasers can also be used but it is important to adapt the antibody panel to take into account the increased spectral overlap between dyes. Additionally, titration of antibodies is required to find the appropriate concentration when changing the antibody panel and we recommend performing titration of antibodies and validation of the new antibody panel in a pilot experiment where all embryos per tissue are pooled, in order to increase the number of cells analyzed per tissue.

The field of developmental biology has been revolutionized by the Cre/Lox method, which allows permanent labeling of cells *in situ*. This approach achieves tissue- or cell type -specificity through expression of the Cre recombinase under the control of a specific promoter. In our case, we chose to study the expression of the Cre recombinase under the control of the promoter of Csf1r (Colony Stimulating Factor 1 Receptor), an important mitogenic and growth factor receptor for macrophages and their progenitors, using a strain developed by the group of J. Pollard [18]. The advantage of a fate mapping strategy based on Csf1r expression compared to other published strategies is that it allows the labeling of yolk sac-derived cells (EMP and macrophages) without labeling any fetal HSCs [12]. The $Cx3cr1^{CreERT2}$ strain can also label yolk sac cells without labeling HSCs [19], however it can only label macrophages and macrophage precursors but it does not label EMP progenitors [1]. The $Cx3cr1^{CreERT2}$ strain has the same caveat as the $Csf1r^{MerCreMer}$ line, since it cannot distinguish between macrophages derived from unipotent primitive macrophage progenitors or from EMP. When tamoxifen is administered as early as E7.5 in both $Runx1^{MerCreMer16}$ and $Kit^{MerCreMer20}$, peripheral blood cells are always labeled in adults, albeit at a very low efficiency, thus demonstrating labeling of HSCs during development. Further, $Kit^{MerCreMer}$ fate mapping labels yolk sac Kit^+ $Sca1^+$ progenitors while EMP are Kit^+ Sca1 negative [11]. The $Csf1r^{MeriCreMer}$ strain is not a knock-in but it was generated by classical additive transgenesis, thus expression of the Cre may not fully recapitulate endogenous expression of Csf1r. However, this has the advantage to avoid any potential developmental defects due heterozygous expression of Csf1r. This is an important factor to take to account when analyzing other fate mapping strategies used for developmental hematopoiesis studies, such as $Runx1^{MerCreMer}$, $Kit^{MerCreMer}$ and $Cx3cr1^{CreERT2}$, where the inducible Cre is inserted-in the endogenous locus. For both $Runx1^{MerCreMer}$ and $Kit^{MerCreMer}$, developmental hematopoietic defects have been described in heterozygous embryos. Collectively, the method presented here allows to investigate yolk sac EMP biology during development and also yolk sac-derived macrophages found in adult tissues and distinct from HSC-derived macrophages. This will improve our current understanding of this lineage of resident macrophages and their specific functions in adulthood. The immunophenotypic characterization of EMPs has been improved recently using cell sorting and colony forming assays, demonstrating that yolk sac EMP specifically express CD41 and CD16/32 in early stages of development [11]. However, the specificity of expression of CD41 and CD16/32 needs further characterization from E10.5 onwards, especially in the fetal liver niche, using fate-mapping models. Indeed, whether CD41 and CD16/32 expression is still specific to EMP when compared to fetal HSCs and HSC-derived progenitors in the E10.5 to E14.5 fetal liver need to be elucidated. The presented method allows to label EMP generated in the yolk sac and to follow them during embryonic development and it will contribute to a more detailed characterization of EMP phenotype when they seed the fetal liver.

This method could be important in the near future to study EMP differentiation pathways. While EMPs emerge from the yolk sac endothelium from E8.5 to E10.5 4, this method only allows to label a fraction of the progenitors emerging between E8.5-E9.5. Therefore, a limitation of this method is that only a small fraction of EMP is labeled, thus rendering difficult the analysis in classical loss-of-function studies with floxed alleles for candidate genes. Alternatively, sparse labeling could become an advantage in clonal studies of EMP differentiation *in vivo*, using clonal reporter. Nevertheless, the labeling efficiency needs to be characterized for each floxed reporter or floxed allele used, as recombination efficiency of floxed constructs depends on genomic locus (floxed alleles) or the Rosa26 reporter construct. Indeed, different Rosa26 reporter lines are available with different promoters and it is reported that $Rosa26^{tdTomato}$ and $Rosa26^{mTmG}$ strain have higher recombination efficiency than the $Rosa26^{LSL\text{-}eYFP}$ line. The reporter mouse strain used in this protocol is $Rosa26^{LSL\text{-}eYFP}$ line, which cannot provide information regarding the dynamic process of progenitor maturation mentioned in the results section. The question of maturation process can be partially addressed using different reporter strains like the $Rosa26^{mTmG}$. In such strain, cells can be distinguished based on the time elapsed since the recombination event. All cells in the $Rosa26^{mTmG}$ strain express membrane-bound tdTomato fluorescent protein and Cre recombination excises the tdTomato cassette and allows for expression of membrane-bound GFP. Since tdTomato has a long half-life, cells that still contain tdTomato but have started to express the GFP (shortly after recombination) are $tdTomato^+$ $GFP^{low/int}$ and can be distinguished from $tdTomato^{neg}$ GFP^+ cells that do not express tdTomato anymore and express higher levels of GFP (later after recombination).

As discussed above, OH-TAM preparation is a critical step to consistently deliver similar doses of OH-TAM between experiments and to reduce tamoxifen side effects. Progesterone co-administration is also useful to limit deleterious effect of tamoxifen on pregnancy. Another critical element of the protocol is the viability of the single-cell suspension obtained from different embryonic tissues. We usually obtain >90% viable cells for flow cytometric analysis. To achieve this, it is critical to follow all the steps rapidly and to maintain all samples on ice after tissue

collection. Appropriate controls such as unstained samples, single stains and fluorescent minus one (FMO) controls are required to identify gate boundaries and to control for the spectral overlap in multicolor panels. Changes in the antibody need to be validated in terms of antibody titration and spectral overlap. Finally, the choice of the Rosa26 reporter strain needs to be adapted to the scientific question that is investigated.

Disclosures

The authors have nothing to disclose.

Acknowledgements

The authors thank Prof Frederic Geissmann and Prof Christian Schulz for insightful discussions; Dr Hannah Garner for critical reading of the manuscript, Dr Xavier Montagutelli and Dr Jean Jaubert and the staff of the Institut Pasteur animal facility for support with mouse husbandry; and Pascal Dardenne and Vytaute Boreikaite, an Amgen Scholar, for their technical assistance. Research in the E.G.P. laboratory is funded by the Institut Pasteur, the CNRS, the Cercle FSER (FRM and a starting package from the Institut Pasteur and the REVIVE consortium. L.I. is supported by a PhD fellowship from the REVIVE consortium.

References

1. Bertrand, J. Y. *et al.* Three pathways to mature macrophages in the early mouse yolk sac. *Blood.* **106** (9), 3004-3011 (2005).
2. Palis, J., Robertson, S., Kennedy, M., Wall, C., & Keller, G. Development of erythroid and myeloid progenitors in the yolk sac and embryo proper of the mouse. *Development.* **126** (22), 5073-5084 (1999).
3. Chen, M. J. *et al.* Erythroid/myeloid progenitors and hematopoietic stem cells originate from distinct populations of endothelial cells. *Cell Stem Cell.* **9** (6), 541-552 (2011).
4. Frame, J. M., Fegan, K. H., Conway, S. J., McGrath, K. E., & Palis, J. Definitive Hematopoiesis in the Yolk Sac Emerges from Wnt-Responsive Hemogenic Endothelium Independently of Circulation and Arterial Identity. *Stem Cells.* (2015).
5. Kieusseian, A., Brunet de la Grange, P., Burlen-Defranoux, O., Godin, I., & Cumano, A. Immature hematopoietic stem cells undergo maturation in the fetal liver. *Development.* **139** (19), 3521-3530 (2012).
6. Gomez Perdiguero, E. *et al.* Tissue-resident macrophages originate from yolk-sac-derived erythro-myeloid progenitors. *Nature.* **518** (7540), 547-551 (2015).
7. Hoeffel, G. *et al.* C-Myb(+) erythro-myeloid progenitor-derived fetal monocytes give rise to adult tissue-resident macrophages. *Immunity.* **42** (4), 665-678 (2015).
8. Kierdorf, K., Prinz, M., Geissmann, F., & Gomez Perdiguero, E. Development and function of tissue resident macrophages in mice. *Semin Immunol.* **27** (6), 369-378 (2015).
9. Houssaint, E. Differentiation of the mouse hepatic primordium. II. Extrinsic origin of the haemopoietic cell line. *Cell Differ.* **10** (5), 243-252 (1981).
10. Cumano, A., & Godin, I. Ontogeny of the hematopoietic system. *Annu Rev Immunol.* **25** 745-785 (2007).
11. McGrath, K. E. *et al.* Distinct Sources of Hematopoietic Progenitors Emerge before HSCs and Provide Functional Blood Cells in the Mammalian Embryo. *Cell Rep.* **11** (12), 1892-1904 (2015).
12. Schulz, C. *et al.* A lineage of myeloid cells independent of Myb and hematopoietic stem cells. *Science.* **336** (6077), 86-90 (2012).
13. Chevalier, C., Nicolas, J. F., & Petit, A. C. Preparation and delivery of 4-hydroxy-tamoxifen for clonal and polyclonal labeling of cells of the surface ectoderm, skin, and hair follicle. *Methods Mol Biol.* **1195** 239-245 (2014).
14. Bertrand, J. Y., Giroux, S., Cumano, A., & Godin, I. Hematopoietic stem cell development during mouse embryogenesis. *Methods Mol Med.* **105** 273-288 (2005).
15. Bertrand, J. Y. *et al.* Characterization of purified intraembryonic hematopoietic stem cells as a tool to define their site of origin. *Proc Natl Acad Sci U S A.* **102** (1), 134-139 (2005).
16. Ginhoux, F. *et al.* Fate mapping analysis reveals that adult microglia derive from primitive macrophages. *Science.* **330** (6005), 841-845 (2010).
17. Nakamura, E., Nguyen, M. T., & Mackem, S. Kinetics of tamoxifen-regulated Cre activity in mice using a cartilage-specific CreER(T) to assay temporal activity windows along the proximodistal limb skeleton. *Dev Dyn.* **235** (9), 2603-2612 (2006).
18. Qian, B. Z. *et al.* CCL2 recruits inflammatory monocytes to facilitate breast-tumour metastasis. *Nature.* **475** (7355), 222-225 (2011).
19. Yona, S. *et al.* Fate mapping reveals origins and dynamics of monocytes and tissue macrophages under homeostasis. *Immunity.* **38** (1), 79-91 (2013).
20. Sheng, J., Ruedl, C., & Karjalainen, K. Most Tissue-Resident Macrophages Except Microglia Are Derived from Fetal Hematopoietic Stem Cells. *Immunity.* **43** (2), 382-393 (2015).

RESULTS

Part 1. Yolk sac. Paper manuscript to be submitted

Two sequential and independent pathways of erythromyeloid progenitor commitment in their niche of emergence

Authors

Lorea Iturri[1-2], Laina Freyer[1], Anne Biton[3], Pascal Dardenne[1], Yvan Lallemand[1] and Elisa Gomez Perdiguero[1].

[1]Institut Pasteur, Macrophages and endothelial cells, Department of Developmental and Stem Cell Biology, UMR3738 CNRS, F-75015 Paris, France; [2]Sorbonne Université, Collège Doctoral, F-75005 Paris, France ; [3]Institut Pasteur, Bioinformatics and Biostatistics Hub (C3BI), Paris, France.

Correspondence: elisa.gomez-perdiguero@pasteur.fr

Key points

- EMP commitment towards myeloid and erythroid lineages revealed at the single cell level in the yolk sac niche.
- Mk develop directly from EMPs in a Myb-independent manner and then from EMP-derived CD131+ *Myb*-dependent-MEP progenitors.

Abstract:

The extra-embryonic yolk sac contains the first definitive multipotent cells of the embryo that are denominated as erythromyeloid progenitors (EMP). EMPs emerge in the yolk sac vasculature prior to the intraembryonic generation of Hematopoietic Stem Cells (HSCs) and they give rise to erythroid, monocyte/granulocytes, mast cells and macrophages, the latter in a *Myb*-independent manner. Different groups have isolated yolk sac EMPs in their niche of origin according to a phenotype that is based on membrane markers. Whereas these classical immunophenotyping approaches only capture late megakaryocyte and erythroid commitment at these early developmental stages, bona fide EMPs can be distinguished from their committed derived progenitors at the single cell gene expression level. Here, we uncover the heterogeneity and progressive commitment of yolk sac HSC-independent EMP progenitors into myeloid, megakaryocyte and erythroid fates in their niche of emergence, prior to colonization and expansion in the fetal liver. We further demonstrate that EMPs commit and differentiate within the yolk sac not only into macrophages but also into megakaryocytes (Mks). EMPs first commit towards Mk in a Myb-independent manner that does not require a shared Mk-E common progenitor. Such shared Mk-E progenitor (or MEP) is produced later by EMPs in the yolk sac and is absent in *Myb*-deficient embryos. We identified CD131 (Csf2rb) as a novel marker of these EMP-derived *Myb*-dependent MEPs in the yolk sac that colonize the fetal liver and differentiate there into Mk but mostly erythrocytes.

Introduction

Erythromyeloid progenitors (EMPs) are developmentally restricted hematopoietic progenitors that emerge from the hemogenic endothelium of the yolk sac and have the potential to give rise to definitive hematopoietic cells from both the erythroid and myeloid lineages (Frame et al., 2016; Gomez Perdiguero et al., 2015; Kasaai et al., 2017; McGrath et al., 2015). While the extent of their contribution to fetal and adult hematopoietic systems is still under investigation, EMP-derived hematopoiesis is required for embryo survival through

erythrocyte production (Chen et al., 2011) and for the generation of certain adult resident macrophage populations, such as brain microglia, liver Kupffer cells and epidermal Langerhans cells (Ginhoux et al., 2010; Schulz et al., 2012) and adult resident mast cells (Gentek et al., 2018; Li et al., 2018).

EMPs emerge from the yolk sac vasculature from E8.25 to E11.5, where they are observed as intravascular cell clusters (Frame *et al.*, 2016). In contrast to Hematopoietic Stem Cells (HSCs), EMP emergence is regulated by canonical Wnt signalling but does not require Notch signalling (Hadland et al., 2004) or blood flow (Frame et al., 2016; Kasaai et al., 2017). Importantly, while HSCs need to colonize the fetal liver in order to differentiate (Godin et al., 1999; Kieusseian et al., 2012), EMPs can also differentiate *in situ* in the yolk sac at least into macrophages, but other lineages have not been formally investigated. EMPs then enter the bloodstream at the beginning of circulation and colonize the fetal liver, where they expand and differentiate into erythrocytes, megakaryocytes, macrophages, monocytes, granulocytes and mast cells (Gentek et al., 2018; Gomez Perdiguero et al., 2015; Hoeffel et al., 2015; McGrath et al., 2015; Stremmel et al., 2018).

Another key difference between EMPs and HSCs is their dependence on the transcription factor Myb. While both progenitors express *Myb* (Hoeffel et al., 2015; Mukouyama et al., 1999), only HSCs require Myb for their survival and self-renewal (Mukouyama et al., 1999; Sumner et al., 2000). Consequently, *Myb*-deficient embryos lack HSC and HSC-derived cells (Mucenski et al., 1991) but still possess normal EMP-derived resident macrophages (Schulz et al., 2012).

EMPs have been characterized by different groups by the expression of Kit, CD41 and CD16/32(McGrath et al., 2015) or Kit, AA4.1 and low levels of CD45 (Bertrand et al., 2005; Gomez Perdiguero et al., 2015), which can all be expressed by HSC themselves or HSC-derived progenitors. Indeed, from E9.5-10.5 onwards, HSCs emerge from the dorsal aorta hemogenic endothelium and contribute to circulating and fetal liver progenitor pools. As such,

the study of EMP-derived hematopoiesis requires control of progenitor labelling in a short temporal window. Unfortunately, most tamoxifen-inducible Cre/lox fate mapping strategies based on targeting of hemogenic endothelium (*Runx1*^{MeriCreMer}; *Cdh5*^{CreERT2}; *Tie2*^{MerCreMer}) lead to labelling of both EMPs and HSCs, even when tamoxifen or 4-hydroxytamoxifen (OHT) is delivered very early in development (E6.5-E7.5)(Gentek et al., 2018; Gomez Perdiguero et al., 2015; Samokhvalov et al., 2007). We thus decided to employ the *Csf1r*^{MeriCreMer} fate mapping strategy, as it has been demonstrated that it labels EMPs without any HSC labeling when OHT is administered at E8.5 (Gomez Perdiguero et al., 2015).

HSC erythro-myeloid commitment and differentiation is a process relatively well understood. In the adult bone marrow, HSC give rise to common myeloid progenitors (CMP) after sequentially losing self-renewal (multipotent progenitor, MPP) and lymphoid potential (Debili et al., 1996; Akashi et al., 2000). CMP hold the potential to form myeloid and erythroid lineages, and could be thus considered as a functional equivalent to EMP. CMPs then differentiate into megakaryocyte/erythrocyte progenitors (MEP) and granulocyte/monocyte progenitors (GMP). Lineage-determining transcription factors orchestrate the activation of specific gene expression programs that lead to commitment and differentiation (Orkin and Zon, 2008), such as Pu.1 for myeloid fate (Scott et al., 1994) and Gata1 for erythroid lineages (Pevny et al., 1991), and their interplay is essential for myeloid versus erythroid lineage choice (Hoppe et al., 2016; Nerlov et al., 2000; Zhang et al., 2000).

Nevertheless, the dynamics and differentiation steps by which EMP give rise to diverse blood and immune cell types in development are currently unclear. The paucity of progenitor cells, the coexistence with HSC and the limited expression of specific cell surface markers at these stages have to date hampered the faithful characterization of definitive yolk sac progenitors. We thus embarked in an unbiased characterization of yolk sac progenitor heterogeneity by combining high-parameter flow cytometry, single cell RNA-sequencing

(scRNA-seq) and functional potency assays together with fate mapping analysis of wild type and *Myb* mutant embryos.

Methods

Animals. *Csf1r*^{MeriCreMer} (Qian et al., 2011), PU.1^{eYFP}GATA1^{mCherry}(Hoppe et al., 2016), c-*myb mutant*(Mucenski et al., 1991) and *Rosa*^{YFP}(Srinivas et al., 2001) reporter mice have been previously described. *Csf1r*^{MeriCreMer} mice were on FVB background, other mice were on C57BL/6 background. *Csf1r*^{MeriCreMer} mice were generated by J. W. Pollard. *Myb-/-* mice were generated by M. L. Mucenski and were a kind gift from F. Geissmann, Centre for Molecular and Cellular Biology of Inflammation (CMCBI), King's College London, London SE1 1UL, UK. *Rosa*^{YFP} (B6.129X1-Gt(ROSA)26Sortm1(EYFP)Cos/J) reporter mice were purchased from The Jackson Laboratory. Embryonic development was estimated considering the day of vaginal plug formation as 0.5 day embryonic day (E0.5), and staged by developmental criteria. Animals procedures were performed in accordance with the Care and Use Committee of the Institut Pasteur (CETEA) guidelines and with their approval.

PCR genotyping of *Csf1r*^{MeriCreMer} (Qian et al., 2011), PU.1^{eYFP}GATA1^{mCherry}(Hoppe et al., 2016) and *c-myb mutant*(Mucenski et al., 1991) embryos was performed according to protocols described previously. No randomization method was used and the investigators were blinded to the genotype of the animals during the experimental procedure. Results are displayed as mean ± s.e.m. All experiments included littermate controls.

In utero **pulse labelling of Csf1r+ haematopoietic progenitors.** Heterozygous *Csf1r*^{MeriCreMer} females were crossed to homozygous *Rosa*^{YFP} reporter males in the case of figures 2-5. Heterozygous *Myb*$^{+/-}$ females were crossed with males homozygous for *Csf1r*^{MeriCreMer}*;Rosa*^{YFP} and heterozygous for *Myb*$^{+/-}$ in the case of figure 6. Recombination was induced by single injection at E8.5 or E9.5 of 75 µg/g (body weight) of 4-hydroxytamoxifen

(Sigma) into pregnant females. The 4-hydroxytamoxifen was supplemented with 37.5 µg per g (body weight) progesterone (Sigma).

Processing of tissues for flow cytometry. Pregnant females were euthanized by cervical dislocation and embryos ranging from embryonic day (E) 8 to E14.5 were dissected out from the uterus and washed in 4°C phosphate buffered saline (PBS, Invitrogen). Harvest of embryonic blood was performed by severing the umbilical and vitelline vessels and immediately transferring the embryo into a 12-well tissue culture plate filled with 2 mM 4°C EDTA, embryos smaller than E11.5 were decapitated in the well. Organs were dissected in PBS at 4°C and digested for 30 minutes at 37°C in with 0.5 ml digestion solution (PBS containing 1mg/ml Collagenase D (Roche), 100 U/ml DNAse I (Sigma) and 3% fetal calf serum (Invitrogen)). Tissues were then mechanically disrupted with a 2ml-syringe piston on top of 100 µm filters to obtain a single cell suspension in FACS buffer containing PBS with 0.5% bovine serum albumin (BSA) and 2mM ethylene-diamine-tetra-acetic acid (EDTA).

Flow cytometric analysis of embryonic tissues and cell sorting. Cells were centrifuged at 320g for 7 min, resuspended in 4°C FACS buffer, plated in multi-well round-bottom plates and immunolabelled for FACS analysis. After 15 min incubation with purified anti-CD16/32 (FcγRIII/II) diluted 1/50 or ChromPure Mouse IgG diluted 1/20, antibody mixes were added and incubated for 30 min. Where appropriate, cells were further incubated with streptavidin conjugates for 20 min.

Samples were acquired using a Beckman Coulter CytoFLEX LX or a BD Symphony A5 cell analyser. Cells were sorted using a BD FACSAria III cell sorter. All data was analysed using FlowJo 10.7. t-Distributed Stochastic Neighbour Embedding (t-SNE) representation was obtained using FlowJo 10.7 default parameters. Cell density was calculated using the following formula: Cells/tissue = Count x V_{sample}/V_{acq} x V_{block}/V_{plated}; with Count, quantification by FlowJo; V_{sample}, volume of the analysed sample; V_{acq}, volume acquired by cytometer; V_{block},

volume in antibody blocking buffer after first centrifugation; V_{plated}, volume of V_{block} plated with antibody mix.

Table1: Antibodies used for flow cytometry and cell sorting

Antigen	Conjugate	Clone	Company
AA4.1	PE-CF594	AA4.1	eBioscience
CD131	BV421	JORO50	BD Pharmingen
CD131	PE	JORO50	BD Pharmingen
CD16/32	BV605	2.4G2	BD Biosciences
CD16/32	FITC	2.4G2	BD Biosciences
CD16/CD32 (Fc Block™)		2.4G2	BD Biosciences
CD19	Biotin	1D3	BD Biosciences
CD3	Biotin	145-2C11	BD Biosciences
CD34	Biotin	RAM34	ThermoFisher
CD34	BV421	RAM34	BD Biosciences
CD4	Biotin	H129	BD Biosciences
CD41	BV510	MWReg30	Biolegend
CD41	PE	MWReg30	SONY
CD45	BUV395	30-F11	BD Biosciences
CD45.2	APC-Cy7	104	Sony
CD61	PE-Cy7	2C9.G2	BD Biosciences
CD71	AF647	C2	BD Biosciences
CD8	Biotin	53-6.7	Biolegend
ChromPure Mouse IgG			Jackson ImmunoResearch
F4/80	Biotin	BM8	Biolegend
F4/80	BV421	BM8	SONY
Gr1	Biotin	RB6-8C5	BD Pharmingen
Gr1	APC	RB6-8C5	BD Pharmingen
Kit	APC-Cy7	2B8	SONY
Kit	PE	2B8	BD Pharmingen
Streptavidin	BUV737		BD Pharmingen
Streptavidin	BV785		BD Pharmingen
Streptavidin	PE-Cy7		Biolegend
Ter119	Biotin	TER-119	Biolegend
Ter119	PerCP-Cy5.5	TER-119	Biolegend

Colony forming assays. Colony-forming-unit-culture (CFU-C) assays were performed sorting single cells into 96-well Nunc™ UpCell™ Microplates (ThermoFisher) in complete medium OPTI-MEM with 10% FCS, penicillin (50 units/ml), streptomycin (50 µg/ml) and β-mercaptoethanol (50 µM) 493 supplemented with a saturating amount of the following

cytokines: M-CSF (5 ng/ml), GM-CSF (2.5 ng/ml), SCF in saturation, EPO (2ng/ml) and TPO (5ng/ml) for myeloid and erythroid differentiation. SCF was obtained from the supernatant of myeloma cell lines (provided by F. Melchers) transfected with cDNA encoding those cytokines.

Cultures were grown at 37°C with 5% CO2 and colonies scored after 12 days. Plates were incubated at 4°C for 20 minutes and colonies were transferred into multi-well round-bottom plates and washed once with FACS buffer. Wells were stained following same protocol with antibodies against Ter119, CD41, CD11b, F4/80 and Gr-1 and analysed by flow cytometry using a Beckman Coulter CytoFLEX LX.

Experimental design for scRNA-Seq. Yolk sac YFP+ single cells from E9.5 Csf1riCre RosaYFP (n=3 litters, 27-29sp) and E10.5 Csf1rMeriCreMer RosaYFP (n=6 litters, 34-38sp) embryos pulsed at E8.5 were stained with fluorescent antibodies for the populations A, B, C D, Mf and Mk. Cells were index-sorted into 384-well plates with a lysis mix containing UPW, 10% Triton X-100 and RNasin plus 40U/µl (Promega N2611) with MARS-seq barcodes (prepared by Baptiste Saudemont (Keren-Shaul et al., 2019)) and immediately placed in dry ice after sorting. Plates were stored until processing at -80°C.

The plates were processed following the MARS-Seq pipeline (Jaitin et al., 2014) and sequenced in a Illumina NextSeq 500 sequencer using NextSeq® 500/550 High Output Kit v2 (75 cycles) (Illumina). Nine plates were sequenced in three independent sequencing runs, megakaryocytes and macrophages were sorted in the first run (Figure S3A-E)

Cell and gene filtering for scRNA-Seq analysis. Cells for which mitochondrial genes took up more than 5% of the total UMI counts, and that had less than 2,750 detected genes were filtered out. We excluded 38 cells out of 1990 that were detected as doublet by the scDblFinder R package (Germain, 2020) using default parameters and running the analysis for each plate separately. In total, we analysed 1952 cells from 3420 sorted. The genes detected in less than 5% of the cells of each condition (E9.5 and E10.5), the ERCC-spike-ins, and all mitochondrial

genes were excluded. In total, 10,188 genes were kept and 781 and 1,234 cells were selected in the E9.5 and E10.5 conditions, respectively.

Data normalization. Cells were pre-clustered within each plate with the 'quickCluster' function of the scran R package(Lun et al., 2016) using a minimum cluster size of 50 cells. Size factors were calculated using the 'computeSumFactors' function from the scran R package. Size factors were then rescaled to adjust for differences in sequencing depth between plates and used to normalize the UMI counts of each cell using the multiBatchNorm function of the R batchelor package(Haghverdi et al., 2018). The resulting normalized and log-transformed counts were used for further processing.

Selection of highly variable genes. A mean-variance trend was fitted for each gene using the 'modelGeneVar' and 'combineVar' functions from the scran R package using plate as a blocking factor. The top 3,000 genes with larger variance than the fitted trend were retained as the highly variable genes (HVGs).

Batch effect correction. Batch effects were removed by hierarchically merging the samples using the 'reduceMNN' function of the batchelor R package(Haghverdi et al., 2018) on 50 principal components calculated with the multiBatchPCA function from the HVGs only. The samples were first merged across plates within each sequencing run for each condition (E9.5 and E10.5) separately, then across sequencing runs for each condition, and finally across conditions from the oldest (E10.5) to youngest (E9.5) time point. The E9.5 condition contained three batches: two plates with >300 cells from the same sequencing run and one plate with ~80 cells from a different sequencing run. We thus first merged the two plates with the largest number of cells that were coming from the same sequencing run and then merged them with the third plate that had a smaller number of cells in order to make sure we were maximising the number of similar cells during the merging.

The corrected low-dimensional coordinates of each cell returned by fastMNN were used as input for computation of clustering and UMAP (Uniform Manifold Approximation and Projection for Dimension Reduction) for visualization. UMAPs were calculated using the 'runUMAP' function of the Seurat package(Stuart et al., 2019) with 16 neighbouring points (neighbours = 16) and 0.32 as the minimal distance to be considered (min.dist = 0.32).

Cell Clustering. A shared nearest-neighbor graph (SNN) was built using the 'buildSNNGraph' function of the scran R package. Communities were searched for in the SNN graph using the method of random walks implemented in the `cluster_walktrap` function of the igraph v1.2.5 package. The number k of nearest neighbors used in the SNN graph differed depending on the dataset under consideration: k = 13 was used for the full yolk sac dataset and k = 9 for the E9.5 yolk sac dataset.

Gene differential expression between clusters. Differential expression analyses were performed by computing pairwise t-tests using the 'findMarkers' function in the scran R package. The option 'pval.type="some"' was used to only consider markers differential in at least half of the pairwise comparisons between clusters.

Gene set enrichment analysis. Using the genes detected as differentially expressed between each cluster and at least half of the other clusters (FDR < 1%), we performed an over-representation analysis using the MSigDB (http://software.broadinstitute.org/gsea/msigdb) and the GeneSetDB databases (https://www.genesetdb.auckland.ac.nz/haeremai.html).

Pseudotime analysis. Cell lineage trajectories were inferred using the R package slingshot v1.4.0 (Street et al., 2018). The UMAP coordinates and the cell clustering assignments were used as inputs. The EMP1 cluster was used as the root node and the 'My' ,'Mk2', and 'pEry2' clusters as ending points of the trajectories. We used 'shrink.method="density"' and the parameter "extend='n'" was used in the 'getCurves' function in order to ask for the trajectories

to not extend beyond the center of the endpoint clusters. In order to find genes associated with each trajectory, a general additive model (GAM) was fitted to each gene as recommended in the slingshot vignette, p-values were corrected using the Bonferroni method.

Results

Spatio-temporal dynamics of yolk sac progenitor subpopulations endowed with progressive commitment to erythroid lineages

We sought to further characterize the heterogeneity among yolk sac (YS) definitive progenitors using high parameter flow cytometry with fluorescently-conjugated antibodies against well-known hematopoietic and progenitor markers. We probed expression of CD45 (pan-hematopoietic marker), AA4.1/CD93 (C-type lectin like type I transmembrane protein; endothelial/progenitor marker), CD16/32 (Fc receptor, myeloid/progenitor marker), CD34 (transmembrane phosphoglycoprotein, hematopoietic progenitor marker excluding MEPs), CD61 (Integrin b3, binding partner to the Mk marker CD41), and CD71 (transferrin receptor, erythroid precursor marker) at the surface of Kit^+ $CD41^+$ progenitor cells in the yolk sac (gating strategy in Figure S1).

We selected AA4.1, CD34 and CD45 as they were the most discriminating markers and used them to further subdivide YS progenitor cells into four major subsets (A, B, C and D). The four subsets of cells can be visualized in two dimensions with respect to their expression of the three markers using a t-Distributed Stochastic Neighbour Embedding (t-SNE) plot (Figure 1A-B and S1B). We next performed a timecourse analysis of the emergence and dynamics of these populations in the three main developmental locations of EMPs, the yolk sac, blood and fetal liver (FL) (Figure 1C).

Population A, defined as $AA4.1^+$ $CD34^+$ $CD45^+$, was detected in the yolk sac from E8 (6-8sp stage), albeit at very low numbers (21.21± 5.35 cells per yolk sac) and increased by

54-fold by E9.5 (1146.6± 133.94 cells per yolk sac) (Figure 1B and quantification in 1C). Population A can be detected from E9.5 onwards in blood while it was only detected in the FL from E10.5, suggesting that A was generated in the YS and reached and seeded the FL through circulation. Although A was $CD45^{neg}$ at E8, it gained expression of CD45 at its cell surface from E8.75 (Figure S1C). B, defined as $AA4.1^{neg}$ $CD34^{+}$ $CD45^{+}$, followed a similar trend to A in dynamics and cell numbers, but delayed, as no B cells could be detected yet at E8.

Population C, defined as $AA4.1^{neg}$ $CD34^{neg}$ $CD45^{+}$, and D, $AA4.1^{neg}$ $CD34^{neg}CD45^{neg}$, only appeared in the YS at E9.5 and expressed higher levels of the erythroid lineage marker CD71 (Figure 1B and S1B). In blood and FL, it were only detected after E10.5 and represented the most abundant subset in the FL.

These population dynamics combined with the enrichment of CD71 in C-D suggested that A gave rise to B and then to erythroid committed progenitors (C and D). Indeed, CFU assays confirmed that, while all populations had a similar cloning efficiency, multipotent progenitors were enriched in A and B while C and D contained almost strictly erythroid/megakaryocyte potential. Thus *bona fide* multipotential EMPs are found in A and B while C and D correspond to already committed progenitors toward E/Mk lineages.

Lineage relationship between yolk sac progenitor subsets

To further characterize these temporal dynamics between the different subpopulations, we investigated whether E/Mk-committed progenitors (C and D) developed from EMPs (A and B). We performed pulse-and-chase experiments in the transgenic fate-mapping mouse line $Csf1r^{MeriCreMer}$ $Rosa^{YFP}$ by administering OHT *in utero* at E8.5 or E9.5 (Figure 2A) and analysing the labelling efficiency of the different subsets of yolk sac progenitors 24, 48 and 72h after pulse (Figure 2A-C). A and B were equally labelled 24 hours after pulse, albeit at different extents depending on the timing of the pulse (40% in OHT E8.5

and 10% in OHT E9.5). Importantly, A was barely labelled 48h after pulse, whereas B labelling efficiency was maintained. These results clearly showed that YFP-labelled A cells differentiated into B progenitors within 24 hours, regardless of the timing of their labelling ("early" at E8.5 vs "late" at E9.5). Erythroid-committed progenitors (C and D) were only labelled 48h after pulse and labelling efficiency of C equilibrated with B, indicating that C and D correspond to EMP-derived E/Mk-committed progenitors and that transiting from A/B into C also took 24 hours or less.

Interestingly, we also observed differences in erythroid progenitor labelling between E8.5 and E9.5 OHT pulse and this was reflected in the YFP labelling of mature Mk and erythrocytes (Figure 2C and D). Early E8.5 pulse labelling led to equal labelling of C and D at E10.5 (48h post pulse) and significant labelling (peaking at 30%) of mature Mks in YS and blood until E11.5 and E14.5, respectively (Figure 2C). However, the E9.5 pulse barely labelled mature cells in the yolk sac and blood, and YFP+ Mks in the FL preceded circulating YFP+ Mks, suggesting that the YFP+ Mks found in FL were locally produced (Figure 2D). In conclusion, early-pulsed EMPs make mature circulating Mks within 24-48h in the yolk sac while late E9.5 pulsed EMPs require the fetal liver to produce Mks. Thus, it appeared there were two megakaryopoiesis pathways from EMPs: a YS pathway, in which Mk differentiation occurred rapidly from early-pulsed EMPs *in situ* in the yolk sac with Mks released immediately into circulation, and a second FL pathway where late-pulsed EMPs differentiated more slowly into Mk and later release them into circulation.

As previously published (Gomez Perdiguero et al., 2015), no erythrocytes were labelled in the yolk sac (Figure 2E) and the first EMP-derived (YFP^+) erythrocytes were found in the FL four days after pulse. EMP-derived erythrocytes were consistently found in the blood 5 days after pulse at the earliest in both pulses, suggesting it takes 5 days for yolk sac EMPs to commit and fully differentiate into circulating blood erythrocytes, regardless of time of pulse. Altogether, these results suggested that the *in vivo* erythroid output of EMPs changed over

time while their cell intrinsic potential was unchanged: first EMPs differentiate rapidly into mature Mks in the yolk sac, while red blood cell production is gradual and becomes predominant in the fetal liver.

Single cell expression analysis reveals lineage commitment and differentiation among fate-mapped progenitors

In order to further unravel the relationships between the different progenitor populations, we performed gene expression analysis of single EMP-derived progenitor cells in the yolk sac. We index-sorted yolk sac YFP$^+$ single cells from E9.5 *Csf1r^{iCre} Rosa^{YFP}* and E10.5 *Csf1r^{MeriCreMer} Rosa^{YFP}* embryos pulsed at E8.5 in order to analyse the different populations at key stages. The cells were stained with fluorescent antibodies for the previously described populations and processed following the MARS-Seq pipeline (Jaitin et al., 2014). After quality control and doublet exclusion, we analysed a total of 781 E9.5 cells and 1234 E10.5 cells (Figure S3A and S3B). Among those, 1952 cells were Kit$^+$ CD41$^+$ progenitors, 13 macrophages and 64 megakaryocytes (Figure 3C). After normalization and data merging to minimize batch effects generated during plate processing and sequencing runs, dimensionality reduction was conducted using Uniform Manifold Approximation and Projection (UMAP) (see figure S3C-E). Random walk clustering (Pons and Latapy, 2006) allowed us to identify 13 well-defined cell states or clusters among sorted cells which were annotated as followed: Macrophages (Mf), Myeloid progenitors (My), undifferentiated erythro-myeloid clusters EMP1, EMP2 and EMP3, megakaryocyte/ erythrocyte progenitors (MEP), mast cell/mast cell progenitor (MCp-MC), Mk progenitors (pMk1 and pMk2), megakaryocytes (Mk1, Mk2) and erythroid progenitors (pEry1, pEry2) (Figure 3A). Clusters were annotated on the basis of literature-established lineage genes (Figure 3B), top differentially expressed genes of each pairwise comparison (Figure S3F) and index sorting information (Figure 3C).

The expression of two key hematopoietic master regulators, the transcription factors Sfpi1(Pu.1) and Gata1 for myeloid and erythroid lineages, respectively, were key for

determining the identity of the clusters (Figure 3B). At the gene expression level, EMP1 expressed *Pu.1* but *Gata1* expression was not detected. In accordance with progressive erythroid commitment, *Pu.1* expression was down regulated from EMP1 to MEP while *Gata1* expression was upregulated from EMP3 to fully committed progenitors (pEry2 and pMk2). Concurrently, *Pu.1* expression was upregulated along myeloid/macrophage differentiation (Figure 3B).

Surface marker annotations allowed us to show that population A was mainly restricted to EMP1 and part of EMP2 and EMP3 clusters, while population B was a very heterogeneous population that corresponded to EMP2 and EMP3, myeloid progenitors (My), MEP and megakaryocyte progenitors (pMk1 and pMk2) (Figure 3C). As expected, C and D were restricted to the E/Mk clusters (MEP, pEry1 and pMk1) although D corresponded principally to the most committed erythroid clusters (pEry1 and pEry2). Thus, in accordance with the pulse-and-chase experiments (Figure2), A is mostly composed of multipotent EMPs, B is a mixed population of committed or lineage-primed progenitors, C contains E/Mk-committed progenitors and D is mostly composed of fully committed erythroid progenitors.

To confirm at the protein level, we analysed the expression of Pu.1 and Gata1 proteins tagged with fluorescent proteins in *Pu.1-YFP Gata1-mCherry* embryos(Hoppe et al., 2016) (Figure 3D). As expected, population A (EMP1) expressed only Pu.1-YFP both at E9.5 and E10.5 and population B contained cells expressing Pu.1, Gata1 or coexpressing both markers, consistent with the transcriptional heterogeneity observed in the scRNASeq dataset. Pu.1-YFP cells were not detected in populations C and D. Finally, gene set enrichment analysis (GSEA) uncovered in specific clusters innate immunity (clusters My and Mf), platelet activation/degranulation and coagulation (clusters pMk1 to Mk2) and heme synthesis (clusters pEry1 and pEry2) pathways, thus further confirming the cluster annotations (Figure 3E).

Importantly, there was a striking difference in the contribution of the two analysed timepoints to the committed clusters (Figure S3E). Myeloid (My) and Mk (pMk1 and pMk2)

progenitor clusters were composed of cells from both E9.5 and E10.5. However, erythroid clusters (pEry1 and pEry2) were almost exclusively composed of E10.5 cells. Altogether, the results confirmed at the single cell level that the *in vivo* output of EMPs changed over time in regards to the Mk/E balance, with erythroid differentiation only starting after E9.5.

Trajectory analysis of yolk sac progenitors reveals an E9.5-specific Mk lineage pathway

We then performed trajectory analysis of the lineages that were annotated in the dataset with the Slingshot package(Street et al., 2018). Starting from cluster EMP1, three trajectories were generated: (i) a megakaryocyte lineage trajectory (Mk trajectory, black); (ii) an erythroid trajectory (E trajectory, red) and (iii) a shorter myeloid trajectory (My trajectory, blue) (Figure 4A). 1468, 2246 and 431 genes were associated with the megakaryocyte, erythrocyte and myeloid trajectories, respectively (p-value < 0.01). The trajectory analysis suggested that among EMP clusters, EMP2 corresponded to myeloid-primed EMPs while EMP3 to erythroid-primed EMPs. This was supported by higher expression of myeloid genes in EMP2 (*Pu.1*, *Csf1r*, *Irf8*) and lower expression of E/Mk genes (*Gata1*, *Klf1*) (Figure 3B and S3F). Conversely, EMP3 had higher expression levels of E/Mk genes (*Gata1*, *Klf1* and *Gata2*).

In the E and Mk shared trajectory, leading from EMP1 to MEP*, Cebpb*, *Lcp1*, *Coro2a* and *Cd34* were downregulated while *Gata1*, *Zfpm1*, *Cited4* and *Mfsd2b* were upregulated at the MEP level (Figure 4B-C). In the Mk trajectory, the first genes specific for megakaryopoiesis to be upregulated in MEP were *Fermt3*, *Itga2b*(CD41), *F2r* and *Rap1b*. A large number of genes was upregulated in more differentiated progenitors (pMk1 and pMk2) and in mature Mks, such as *Thbs1*, *Pf4*, *Treml1*, *F2rl2* and components of the platelet von Willebrand factor (vWF) receptor (*Gp1bb*, *Gp5* and *Gp9*). Interestingly, few C and D cells were part of the trajectory, but B cells, especially from E9.5, were found in the committed pMk1 and pMk2 clusters (Figure 4B). The F trajectory had two sets of genes that clustered depending on the timing of upregulation. The first set of genes that was upregulated early corresponded to MEP

differentiation genes (*Gata1*, *Zfpm1*, *Cited4* and *Mfsd2b)*. The second set of genes was upregulated in more mature progenitors (pEryp1 and pEry2) at E10.5 and included genes linked to erythrocyte function such as *Alad*, *Epor*, *Cpox* and *Ermap* (Figure 4C).

The Myeloid trajectory was characterized by a first large gene set upregulated in EMP2 that included innate immune and myeloid genes (*Emb*, *Tspo* and *Mpo)* and then a second set of upregulated genes in the My cluster, containing a macrophage specific transcription factor (*Irf8*), genes involved in peroxisomal or lysosomal activity (*Abcd2*) and cathepsin-encoding genes (*Ctsz* and *Ctsc)*.

Since E9.5 progenitors seemed particularly enriched in megakaryocyte but not erythroid clusters (Figure 3SE and 4C) and as the erythroid trajectory was mostly composed of E10.5 progenitors, we analysed separately the E9.5 progenitors and annotated three cell states or clusters on the basis of gene expression (Figure 4E). A distinct megakaryocyte progenitor cluster was observed at E9.5 (Figure 4B S4A and S4B). We performed trajectory analysis starting from the EMP cluster at E9.5 and observed a Mk-differentiation trajectory that involved the significant regulation of 586 genes (p-value<0.01). These included the downregulation of multiple myeloid genes such as *Sfpi1*, *Cebpb*, *Emb* and *Cd34*, the upregulation of *Tal1* starting in the EMP cluster and a later upregulation of Mk lineage genes such as *Gata1*, *Podxl*, *Gp1bb*, *F2r* and *Itga2b*(CD41) in the pMk cluster. This gene set upregulation was also closely correlated with the loss of AA4.1 at the surface (phenotype A to B, Figure S4E) and suggested the existence of a rapid yolk sac megakaryopoiesis that does not involve a MEP intermediate (Figure 4E).

CD131 is a novel marker of MEP commitment in the yolk sac

In order to resolve the erythroid/megakaryocyte commitment steps in the yolk sac, we performed pairwise comparison of the genes that were differentially expressed by E9.5 and E10.5 cells from the MEP cluster. We observed that E10.5 MEPs distinctly expressed *Csf2rb*

(the common β chain of GM-CSF, IL-3 and IL-5 receptors) (Fig5A). Importantly, while cells in EMP and myeloid clusters also expressed *Csf2rb* at a lower level, the highest *Cs2rb*-expressing cells were those of the MEP cluster. Further, *Cs2rb*-expressing were effectively located in the UMAP region where E10.5 cells were most abundant (Figure 5B and S3E).

We proceeded to verify the expression of CD131 at the surface of YS progenitor populations and we observed few $CD131^+$ cells at E9.5 (27.51± 6.69 sem) but considerably more at E10.5 (188.8± 28.6 sem) (Figure 5C-D). $CD131^+$ cells were $CD45^+$ $AA4.1^{neg}$ and expressed CD34 at a lower level than B, and as such could correspond to phenotypic intermediates between B and C populations (Figure S5). Since most $CD131^+$ cells were found in B (49.36%) and C (41.87%) (Figure 5E) and expressed Gata1-mCherry (46%) (Figure 5F), we hypothesized they corresponded to an erythroid-committed progenitor. We therefore sorted E10.5 $CD131^+$ yolk sac cells for colony forming assays to investigate their differentiation potential. The enrichment in highly proliferative erythroid colonies and mixed erythroid and megakaryocyte colonies suggested an early Mk/E committed progenitor (Figure 5G). Altogether, the results identified CD131 as a novel marker of early yolk sac MEP produced at E10.5.

Deletion of the transcription factor Myb blocks production of yolk sac MEP but allows direct megakaryocyte differentiation

We next analysed *Csf1r*^{MeriCreMer} *Rosa*^{YFP} *Myb*$^{-/-}$ embryos pulsed at E8.5 in order to follow the fate of EMP and EMP-derived cells in the absence of the hematopoietic transcription factor Myb. Erythroid-committed progenitors C and D were completely absent in *Myb*-deficient embryos at all stages analysed (Figure 6A). While there were no significant differences in A and B numbers at E9.5, A and B were reduced from E10.5 onwards in *Myb*-deficient yolk sacs and no gene dosage effects were observed (Figure 6B). Pulse-labelled YFP^+ *Myb*-deficient progenitors followed the same trend as all cells, therefore showing no difference of YFP^+ and YFP^{neg} progenitors with regard to *Myb*-dependence (Figure S6A) and by E11.5, only a few

YFP$^+$ cells were still present in the yolk sac, and had a B phenotype. Further, CD131$^+$ cells were also absent both at E10.5 and E11.5 in *Myb*-deficient yolk sacs, suggesting an early blockage at the MEP level during YS hematopoiesis (Figure 6C). Altogether, this complete lack of E/Mk-committed progenitors in *Myb*-deficient embryos should result in the lack of definitive YFP$^+$ E and Mk mature cells. It is indeed the case for erythrocytes (Figure 6D), as no YFP$^+$ red blood cells were observed in the fetal liver and blood of *Myb*-deficient embryos. However, yolk sac EMP-derived megakaryopoiesis remained unaffected until E12.5 (Figure 6D and S6B). Moreover, Mk labelling was normal in *Myb*-deficient embryos in the blood until E11.5 and in the fetal liver at E10.5, but strongly decreased thereafter (Figure 6D). These results suggested that EMP-derived Mks found in blood and fetal liver at these early stages bypassed the MEP intermediate and were produced in the yolk sac until E12.5. No EMP-derived Mk production was observed in the FL after E11.5, coinciding with the lack of production of mature red blood cells and the absence of MEPs in *Myb*-deficient embryos (Figure 6B-D).

Altogether these results demonstrated the existence of two successive and independent waves of Mk production from EMPs. In the yolk sac, EMPs were able to provide the first burst of definitive megakaryocytes in circulation in a *Myb*-independent manner from E9.5 until at least E12.5, which were later replaced by a wave of MEP-produced Mk. EMP-derived MEPs were produced in the yolk sac after E9.5 in a *Myb*-dependent manner and they terminally differentiated in the fetal liver before Mk were released into circulation.

Discussion

Kit and CD41 coexpression in the yolk sac is considered a marker of definitive hematopoiesis and both are expressed in the hemogenic clusters in this niche (Frame et al., 2016). While it is known that EMPs in the yolk sac locally differentiate into macrophages and that the other erythromyeloid lineages are found in the fetal liver (Gomez Perdiguero et al., 2015; McGrath et al., 2015), less is known about the spatio-temporal dynamic of EMP

hematopoiesis. The presence of cells able to produce BFU-E and CFU-E type colonies from E9.5 in the yolk sac also led to the hypothesis that some maturation occurs in this niche before liver colonization (Palis et al., 1999) and implied that intermediate progenitors can be present in the yolk sac. We therefore decided to decipher the EMP-derived hematopoiesis in the yolk sac focusing in the progenitor heterogeneity among Kit and CD41 expressing cells.

While McGrath and colleagues proposed a yolk sac EMP phenotype based on CD16/32 expression, Gomez Perdiguero and colleagues used AA4.1 and CD45 low expression, as initially defined by Bertrand and colleagues (Bertrand et al., 2005). We here showed that at least four populations of EMP-derived progenitors are present in the yolk sac before fetal liver colonization, that can be distinguished by the surface expression of AA4.1, CD34 and CD45 and that have different potential. In particular, the sequential loss of CD34 and CD45 enriched for yolk sac definitive megakaryocyte and erythroid progenitors (MEP) (C and D). We did not select CD16/32 expression for further analysis, as it also labelled many already committed erythroid progenitors (C and to a minor extent D) and it did not help to unravel the progenitor heterogeneity at E10.5.

Pulse-and-chase experiments in *Csf1r*^{MeriCreMer} *Rosa*^{YFP} embryos showed that A (AA4.1^{+} CD34^{+} CD45^{+}) gave rise to the other subsets, and that these progenitors could only be traced for 24 hours before downregulating AA4.1 and pursuing differentiation. Single cell transcriptomic analysis further revealed the heterogeneity of yolk sac progenitors and confirmed that A (AA4.1^{+} CD34^{+} CD45^{+}) was the most undifferentiated multipotent population, and expressed Pu.1 but not Gata1. We showed that population B (AA4.1^{neg} CD34^{+} CD45^{+}) was very heterogeneous and contained mostly committed or lineage-primed myeloid, megakaryocytic and early erythroid progenitors. Finally, C enriched in E/Mk-committed progenitors and D was mostly composed of more committed erythroid progenitors. The notion of differentiation from A towards myeloid, megakaryocyte and erythroid committed progenitors was further supported by trajectory inference. Since E9.5 and E10.5 cells segregated inside

the MEP (megakaryocyte and erythroid progenitors) cluster and contributed differently to the trajectories of megakaryocyte and erythrocytes, we proceeded to resolve E/Mk pathways of differentiation in the yolk sac.

We were able to further refine the identification of the intermediate steps in the E/Mk pathway thanks to a cell surface marker identified with the scRNA-seq analysis by pairwise statistical comparison of E9.5 and E10.5 cells from the MEP cluster. *Csf2rb* was found to be expressed 2.4-fold more in E10.5 cells and it was also expressed higher in E10.5 MEP when compared to other clusters. This gene encodes for the high affinity receptor subunit CD131/ βc, the common β chain shared among granulocyte-macrophage colony-stimulating factor (GM-CSF/CSF2), interleukin-3 (IL-3) and interleukin 5 (IL-5) receptors, and is involved in the differentiation and survival of progenitor cells and the growth and differentiation of myeloid cells and megakaryocytes (Scott and Begley, 1999). The expression of CD131 was recently described in the literature to enrich in E/Mk biased progenitors of the bone marrow (Drissen et al., 2019) and the cytokine GM-CSF is used in culture to promote the initial proliferation of progenitors of the erythroid and megakaryocyte lineage, although it is not required for the terminal cell divisions in these pathways (Metcalf et al., 1980). In this study, we showed that EMPs differentiate at E10.5 in the yolk sac into functional and transcriptomic MEPs, characterized first by the expression of CD131 and defined by *in vitro* clonal differentiation potential. CD131 is thus a marker of MEP commitment in the yolk sac that is situated upstream of CD34 loss at the cell surface.

We also showed that this differentiation pathway was dependent on the expression of *Myb*. Embryos lacking the hematopoietic transcription factor *Myb* have normal number of tissue resident macrophages (Schulz et al., 2012) but fetal liver erythropoiesis is blocked (Mucenski et al., 1991). While AA4.1^{+} EMPs emerge normally in *Myb-/-* embryos, their AA4.1^{neg} CD34+ CD45+ (B) progeny is rapidly reduced from E10.5 onwards and all the E/Mk intermediates (CD131+ MEP, C and D) are completely absent at all stages. No EMP-derived

erythrocyte production was consequently found in *Myb-/-* embryos, however EMP-derived megakaryopoiesis was unaffected in the yolk sac at all stages. After E10.5, EMP-derived Mk were severely reduced in the fetal liver, suggesting that Mk production through a *Myb*-dependent MEP intermediate occurred primarily in the fetal liver niche.

It was proposed that normal Mk numbers in the *Myb*-deficient embryos derived from primitive hematopoiesis (Tober et al., 2008). However, by combining *Myb* deficiency with EMP pulse labelling, we can clearly demonstrate that EMPs emerge normally in *Myb-/-* embryos and differentiate directly into megakaryocytes bypassing yolk sac CD131+ MEP progenitors. Importantly, this novel direct MEP-independent megakaryopoiesis uncovered in *Myb*-deficient embryos is also found in *Myb*-competent embryos, as evidenced during EMP fate mapping and scRNAseq studies. Yolk sac MEP-independent megakaryopoiesis started rapidly after EMP emergence in a limited time window, as evidence by the fact that yolk sac Mks are only labeled when EMP are pulsed at E8.5 and not at E9.5. This yolk sac-specific direct megakaryopoiesis is faster than the MEP-derived counterpart, as mature Mks were found in the yolk sac and blood 24-48h after EMP pulse labeling, and Mks were released into circulation as soon as they were produced. Further scRNAseq analysis of yolk sac progenitors confirmed the existence of a megakaryocyte differentiation pathway at E9.5 that differed from the adult-like MEP-dependent differentiation, which is predominant at E10.5. Collectively, our results demonstrate that *Myb*-deficient Mk progenitors are not just a restricted form of definitive megakaryopoiesis (Tober et al., 2008), in which $Myb^{-/-}$ EMP retain the capability to give rise to Mks as they fail to differentiate into MEP in the absence of *Myb*. Rather, megakaryopoiesis *in Myb*-deficient embryos corresponds to the first wave of rapid and local Mk production from EMPs before the production of CD131 MEPs, that later mature into a second EMP-derived wave of Mk in the fetal liver. This is reminiscent of local macrophage differentiation in the yolk sac that is proposed to bypass monocytic intermediates (Naito et al., 1996; Takahashi et al., 1989).

In regards to the differences in EMP output depending on the timing of pulse-labelling, the production of red blood cells also displayed different dynamics. While the labelling efficiency of red blood cells produced from E9.5-pulsed EMPs peaked 5 days after pulse, those pulsed at E8.5 peaked 4 days after pulse. Interestingly, regardless of the time of pulse labelling, EMP-derived red blood cells were only found in circulation at E13.5, even if labeled EMP-derived red blood cells were present and accumulating in the fetal liver since E11.5. This suggests that erythrocyte release into circulation is not passive event but rather a highly regulated process in the fetal liver. The differences in EMP output between pulses could be explained by a temporal specialization of progenitors in the yolk sac in response to changes in the different signals provided by the hematopoietic niches over time (cell extrinsic hypothesis) or by the emergence of two waves of EMP progenitors (cell intrinsic hypothesis). In regards to the latter, comparison of E9.5 and E10.5 yolk sac progenitors did not reveal any major differences at the scRNA-seq level in the EMP clusters.

Altogether, these results demonstrate that EMPs can differentiate into megakaryocytes in the yolk sac very rapidly (in 24-48h) and that they do not depend on a MEP intermediate to do so. These results uncover two pathways to produce definitive megakaryocytes: a direct yolk sac-specific pathway that starts at E9.5 directly from EMP progenitors in a *Myb*-independent manner, and a second adult-like pathway, where EMP produce first MEP in the yolk sac in a *Myb*-dependent manner and that terminally differentiate into both erythrocytes and megakaryocytes in the fetal liver. These MEP progenitors seed the fetal liver starting from E10.5 and are responsible for the rapid production of millions of definitive red blood cells that are released into circulation from E12.5. Commitment of erythroid progenitors occurs at E10.5 and it is characterized by the acquisition of CD131 at the surface and a sequential loss of CD34 and CD45.

Acknowledgements

We are thankful for insightful discussions, technical support, and critical reading of the manuscript by Ana Cumano. We gratefully acknowledge the Plateforme de Cytometrie (Sophie Novault) at the Center for Innovation and Technological Research of the Institut Pasteur for support in conducting this study. We thank Yann Loe Mie and Baptiste Saudemont for their help with the MARS-Seq pipeline. This work was supported by recurrent funding from the Institut Pasteur, the CNRS and Revive (Investissement d'Avenir; ANR-10-LABX-73) and by an ERC investigator award (2016-StG-715320) from the European Research Council to E.G.P. E.G.P. also acknowledges financial support from the Fondation Schlumberger (FRM FSER 2017) and the Emergence(s) program from Ville de Paris (2016 DAE 190). L.I. was supported by a fellowship from the Revive Labex and L.F. by a Florence Gould-Pasteur Foundation fellowship.

Authorship Contributions

Conceptualization: LI and EGP; Methodology and data collection: LI, LF, PD, YL and EGP; scRNA-seq data analysis: LI, LF and AB; Writing - Original Draft: LI and EGP; Writing - Review & Editing: LI, LF, AB, YL and EGP; Funding Acquisition: EGP; Supervision: EGP.

The authors declare no competing financial interests and no conflicts of interest.

References

Bertrand, J.Y., Giroux, S., Golub, R., Klaine, M., Jalil, A., Boucontet, L., Godin, I., and Cumano, A. (2005). Characterization of purified intraembryonic hematopoietic stem cells as a tool to define their site of origin. Proc. Natl. Acad. Sci. U. S. A. *102*, 134–139.

Chen, M.J., Li, Y., De Obaldia, M.E., Yang, Q., Yzaguirre, A.D., Yamada-Inagawa, T., Vink, C.S., Bhandoola, A., Dzierzak, E., and Speck, N.A. (2011). Erythroid/myeloid progenitors and hematopoietic stem cells originate from distinct populations of endothelial cells. Cell Stem Cell *9*, 541–552.

Drissen, R., Thongjuea, S., Theilgaard-Mönch, K., and Nerlov, C. (2019). Identification of two distinct pathways of human myelopoiesis. Sci. Immunol. *4*, 7148.

Frame, J.M., Fegan, K.H., Conway, S.J., McGrath, K.E., and Palis, J. (2016). Definitive Hematopoiesis in the Yolk Sac Emerges from Wnt-Responsive Hemogenic Endothelium Independently of Circulation and Arterial Identity. Stem Cells *34*, 431–444.

Gentek, R., Ghigo, C., Hoeffel, G., Bulle, M.J., Msallam, R., Gautier, G., Launay, P., Chen, J., Ginhoux, F., and Bajénoff, M. (2018). Hemogenic Endothelial Fate Mapping Reveals Dual Developmental Origin of Mast Cells. Immunity *48*, 1160-1171.e5.

Germain, P.-L. (2020). scDblFinder: scDblFinder. R package version 1.1.8.

Ginhoux, F., Greter, M., Leboeuf, M., Nandi, S., See, P., Gokhan, S., Mehler, M.F., Conway, S.J., Ng, L.G., Stanley, E.R., et al. (2010). Fate mapping analysis reveals that adult microglia derive from primitive macrophages. Science (80-.). *330*, 841–845.

Godin, I., Garcia-Porrero, J.A., Dieterlen-Lièvre, F., and Cumano, A. (1999). Stem cell emergence and hemopoietic activity are incompatible in mouse intraembryonic sites. J. Exp. Med. *190*, 43–52.

Gomez Perdiguero, E., Klapproth, K., Schulz, C., Busch, K., Azzoni, E., Crozet, L., Garner, H., Trouillet, C., De Bruijn, M.F., Geissmann, F., et al. (2015). Tissue-resident macrophages originate from yolk-sac-derived erythro-myeloid progenitors. Nature *518*, 547–551.

Hadland, B.K., Huppert, S.S., Kanungo, J., Xue, Y., Jiang, R., Gridley, T., Conlon, R.A., Cheng, A.M., Kopan, R., and Longmore, G.D. (2004). A requirement for Notch1 distinguishes 2 phases of definitive hematopoiesis during development. Blood *104*, 3097–3105.

Haghverdi, L., Lun, A.T.L., Morgan, M.D., and Marioni, J.C. (2018). Batch effects in single-cell RNA-sequencing data are corrected by matching mutual nearest neighbors. Nat. Biotechnol. *36*, 421–427.

Hoeffel, G., Chen, J., Lavin, Y., Low, D., Almeida, F.F., See, P., Beaudin, A.E., Lum, J., Low, I., Forsberg, E.C., et al. (2015). C-Myb+ Erythro-Myeloid Progenitor-Derived Fetal Monocytes Give Rise to Adult Tissue-Resident Macrophages. Immunity *42*, 665–678.

Hoppe, P.S., Schwarzfischer, M., Loeffler, D., Kokkaliaris, K.D., Hilsenbeck, O., Moritz, N., Endele, M., Filipczyk, A., Gambardella, A., Ahmed, N., et al. (2016). Early myeloid lineage choice is not initiated by random PU.1 to GATA1 protein ratios. Nature *535*, 299–302.

Jaitin, D.A., Kenigsberg, E., Keren-Shaul, H., Elefant, N., Paul, F., Zaretsky, I., Mildner, A., Cohen, N., Jung, S., Tanay, A., et al. (2014). Massively Parallel Single-Cell RNA-Seq for Marker-Free Decomposition of Tissues into Cell Types. Science (80-.). *343*, 776 LP – 779.

Kasaai, B., Caolo, V., Peacock, H.M., Lehoux, S., Gomez-Perdiguero, E., Luttun, A., and Jones, E.A.V. (2017). Erythro-myeloid progenitors can differentiate from endothelial cells and modulate embryonic vascular remodeling. Sci. Rep. *7*, 1–12.

Keren-Shaul, H., Kenigsberg, E., Jaitin, D.A., David, E., Paul, F., Tanay, A., and Amit, I. (2019). MARS-seq2.0: an experimental and analytical pipeline for indexed sorting combined with single-cell RNA sequencing. Nat. Protoc. *14*, 1841–1862.

Kieusseian, A., de la Grange, P.B., Burlen-Defranoux, O., Godin, I., and Cumano, A. (2012). Immature hematopoietic stem cells undergo maturation in the fetal liver. Dev. *139*, 3521–3530.

Li, Z., Liu, S., Xu, J., Zhang, X., Han, D., Liu, J., Xia, M., Yi, L., Shen, Q., Xu, S., et al. (2018). Adult Connective Tissue-Resident Mast Cells Originate from Late Erythro-Myeloid Progenitors. Immunity *49*, 640-653.e5.

Lun, A.T.L., McCarthy, D.J., and Marioni, J.C. (2016). A step-by-step workflow for low-level analysis of single-cell RNA-seq data with Bioconductor. F1000Research *5*, 2122.

McGrath, K.E., Frame, J.M., Fegan, K.H., Bowen, J.R., Conway, S.J., Catherman, S.C., Kingsley, P.D., Koniski, A.D., and Palis, J. (2015). Distinct Sources of Hematopoietic Progenitors Emerge before HSCs and Provide Functional Blood Cells in the Mammalian Embryo. Cell Rep. *11*, 1892–1904.

Metcalf, D., Johnson, G.R., and Burgess, A.W. (1980). Direct stimulation by purified GM-CSF of the proliferation of multipotential and erythroid precursor cells. Blood *55*, 138–147.

Mucenski, M.L., McLain, K., Kier, A.B., Swerdlow, S.H., Schreiner, C.M., Miller, T.A., Pietryga, D.W., Scott Jr., W.J., and Potter, S.S. (1991). A functional c-myb gene is required for normal murine fetal hepatic hematopoiesis. Cell *65*, 677–689.

Mukouyama, Y., Chiba, N., Mucenski, M.L., Satake, M., Miyajima, A., Hara, T., and Watanabe, T. (1999). Hematopoietic cells in cultures of the murine embryonic aorta-gonad-mesonephros region are induced by c-Myb. Curr. Biol. *9*, 833–836.

Naito, M., Umeda, S., Yamamoto, T., Moriyama, H., Umezu, H., Hasegawa, G., Usuda, H., Shultz, L.D., and Takahashi, K. (1996). Development, differentiation, and phenotypic heterogeneity of murine tissue macrophages. J. Leukoc. Biol. *59*, 133–138.

Nerlov, C., Querfurth, E., Kulessa, H., and Graf, T. (2000). GATA-1 interacts with the myeloid PU.1 transcription factor and represses PU.1-dependent transcription. Blood *95*, 2543–2551.

Orkin, S.H., and Zon, L.I. (2008). Hematopoiesis: An Evolving Paradigm for Stem Cell Biology. Cell *132*, 631–644.

Palis, J., Robertson, S., Kennedy, M., Wall, C., and Keller, G. (1999). Development of erythroid and myeloid progenitors in the yolk sac and embryo proper of the mouse. Development *126*, 5073–5084.

Pevny, L., Simon, M.C., Robertson, E., Klein, W.H., Tsai, S.F., D'Agati, V., Orkin, S.H., and Costantini, F. (1991). Erythroid differentiation in chimaeric mice blocked by a targeted mutation in the gene for transcription factor GATA-1. Nature *349*, 257–260.

Pons, P., and Latapy, M. (2006). Computing communities in large networks using random walks. J. Graph Algorithms Appl. *10*, 191–218.

Qian, B.Z., Li, J., Zhang, H., Kitamura, T., Zhang, J., Campion, L.R., Kaiser, E.A., Snyder, L.A., and Pollard, J.W. (2011). CCL2 recruits inflammatory monocytes to facilitate breast-tumour metastasis. Nature *475*, 222–225.

Samokhvalov, I.M., Samokhvalova, N.I., and Nishikawa, S.I. (2007). Cell tracing shows the contribution of the yolk sac to adult haematopoiesis. Nature *446*, 1056–1061.

Schulz, C., Perdiguero, E.G., Chorro, L., Szabo-Rogers, H., Cagnard, N., Kierdorf, K., Prinz, M., Wu, B., Jacobsen, S.E.W., Pollard, J.W., et al. (2012). A Lineage of Myeloid Cells Independent of Myb and Hematopoietic Stem Cells. Science (80-.). *336*, 86 LP – 90.

Scott, C.L., and Begley, C.G. (1999). The beta common chain (βc) of the granulocyte macrophage-colony stimulating factor, interleukin-3 and interleukin-5 receptors. Int. J. Biochem. Cell Biol. *31*, 1011–1015.

Scott, E.W., Simon, M.C., Anastasi, J., and Singh, H. (1994). Requirement of transcription factor PU.1 in the development of multiple hematopoietic lineages. Science (80-.). *265*, 1573–1577.

Srinivas, S., Watanabe, T., Lin, C.S., William, C.M., Tanabe, Y., Jessell, T.M., and Costantini, F. (2001). Cre reporter strains produced by targeted insertion of EYFP and ECFP into the ROSA26 locus. BMC Dev. Biol. *1*, 1–8.

Street, K., Risso, D., Fletcher, R.B., Das, D., Ngai, J., Yosef, N., Purdom, E., and Dudoit, S. (2018). Slingshot: Cell lineage and pseudotime inference for single-cell transcriptomics. BMC Genomics *19*, 477.

Stremmel, C., Schuchert, R., Wagner, F., Thaler, R., Weinberger, T., Pick, R., Mass, E., Ishikawa-Ankerhold, H.C., Margraf, A., Hutter, S., et al. (2018). Yolk sac macrophage progenitors traffic to the embryo during defined stages of development. Nat. Commun. *9*, 75.

Stuart, T., Butler, A., Hoffman, P., Hafemeister, C., Papalexi, E., Mauck, W.M., Hao, Y., Stoeckius, M., Smibert, P., and Satija, R. (2019). Comprehensive Integration of Single-Cell Data. Cell *177*, 1888-1902.e21.

Sumner, R., Crawford, A., Mucenski, M., and Frampton, J. (2000). Initiation of adult myelopoiesis can occur in the absence of c-Myb whereas subsequent development is strictly dependent on the transcription factor. Oncogene *19*, 3335–3342.

Takahashi, K., Yamamura, F., and Naito, M. (1989). Differentiation, maturation, and proliferation of macrophages in the mouse yolk sac: A light-microscopic, enzyme-cytochemical, immunohistochemical, and ultrastructural study. J. Leukoc. Biol. *45*, 87–96.

Tober, J., McGrath, K.E., and Palis, J. (2008). Primitive erythropoiesis and megakaryopoiesis in the yolk sac are independent of c-myb. Blood *111*, 2636–2639.

Zhang, P., Zhang, X., Iwama, A., Yu, C., Smith, K.A., Mueller, B.U., Narravula, S., Torbett, B.E., Orkin, S.H., and Tenen, D.G. (2000). PU.1 inhibits GATA-1 function and erythroid differentiation by blocking GATA-1 DNA binding. Blood *96*, 2641–2648.

Figures

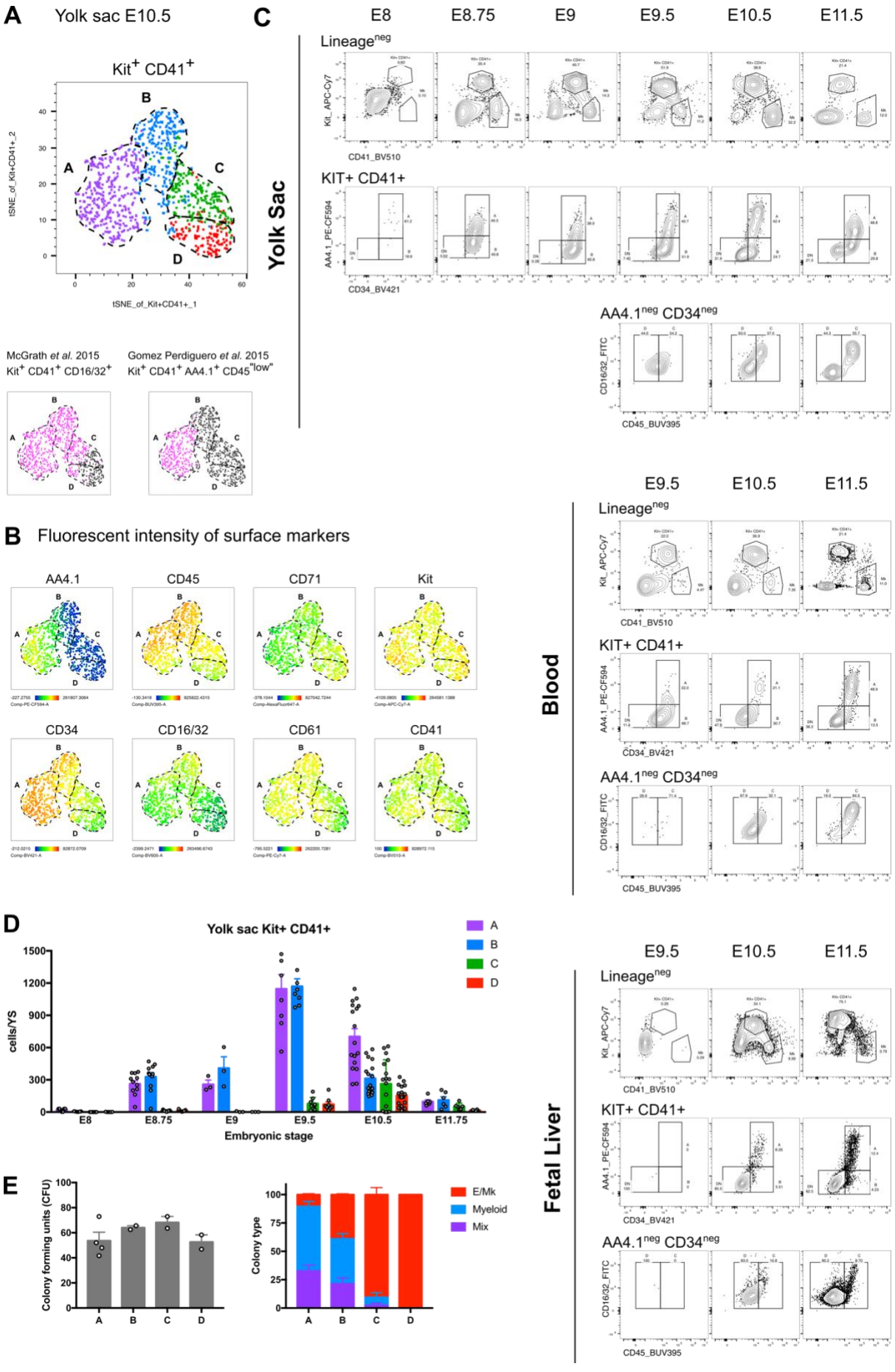
A
Yolk sac E10.5
Kit+ CD41+
tSNE_of_Kit+CD41+_2
tSNE_of_Kit+CD41+_1
McGrath et al. 2015
Kit+ CD41+ CD16/32+
Gomez Perdiguero et al. 2015
Kit+ CD41+ AA4.1+ CD45"low"
B
Fluorescent intensity of surface markers
AA4.1
CD45
CD71
Kit
CD34
CD16/32
CD61
CD41
C
E8
E8.75
E9
E9.5
E10.5
E11.5
Yolk Sac
Lineageneg
Kit_APC-Cy7
CD41_BV510
KIT+ CD41+
AA4.1_PE-CF594
CD34_BV421
AA4.1neg CD34neg
CD16/32_FITC
CD45_BUV395
Blood
Fetal Liver
D
Yolk sac Kit+ CD41+
cells/YS
Embryonic stage
A
B
C
D
E
Colony forming units (CFU)
Colony type
E/Mk
Myeloid
Mix

Figure 1. Spatio-Temporal dynamics of yolk sac progenitor subsets endowed with progressive commitment to erythroid lineages.

(A) Yolk sac E10.5 CD41+ Kit+ cells can be subdivided in a tSNE representation (upper panel) into 4 populations A, B, C and D (dashed lines). (lower panel) Overlay of previous phenotypic definitions of EMPs (pink) on the t-SNE space (grey). (B) t-SNE representation of the fluorophore intensity of AA4.1, CD45, CD71, Kit, CD34, CD16/32, CD61 and CD41 in the four subsets. (C) Representative contour plots of Kit and CD41 expression among lineage negative cells, of AA4.1 and CD34 among Kit+ CD41+ progenitor cells and of CD16/32 and CD45 among AA4.1neg CD34neg cells from E8 to E11.5 in the yolk sac (upper panel), blood (middle panel) and fetal liver (bottom panel). (D) Quantification of the number of cells per yolk sac in each population from E8.5 to E11.5. n=3 at E8(6-8 somite pairs - sp), 11 at E8.75 (16-28 somite pairs - sp); 3 at E9 (20-21sp); 7 at E9.5 (27-29 sp); 17 at E10.5 (34-38sp) and 5 at E11.75 (51-53sp). Bars represent mean$\pm$ sem. (E) Colony forming units (CFU-C) assays of sorted A, B, C and D populations and analyzed 12 days after. Cloning efficiency (left) and frequency of colony types (E/Mk, erythroid and/or Mk; Myeloid and Mix colonies) (right); mean$\pm$ sem. Data from 6 embryos.

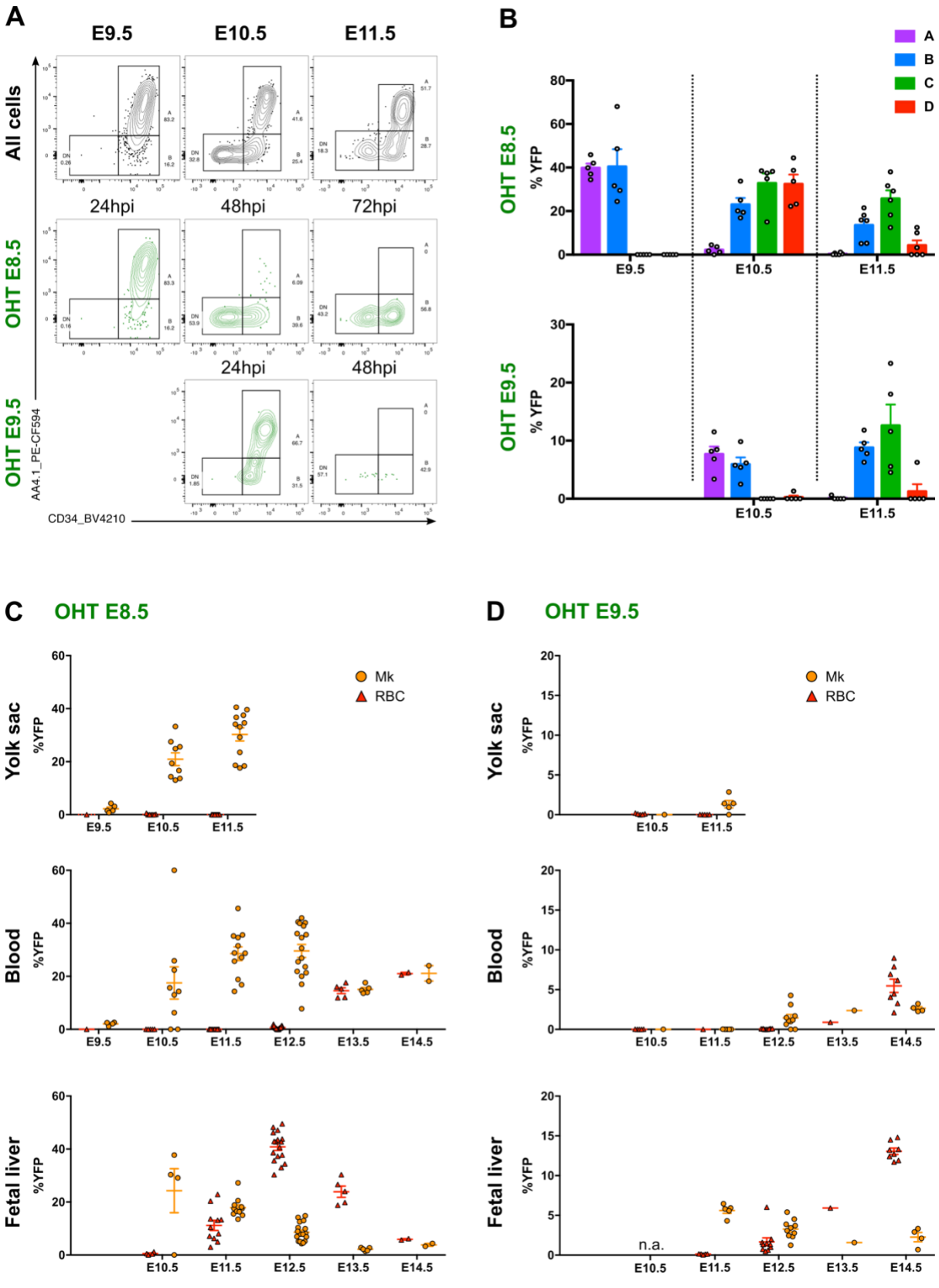
A
E9.5
E10.5
E11.5
All cells
24hpi
48hpi
72hpi
OHT E8.5
24hpi
48hpi
OHT E9.5
AA4.1_PE-CF594
CD34_BV4210
B
A
B
C
D
OHT E8.5
% YFP
E9.5
E10.5
E11.5
OHT E9.5
% YFP
E10.5
E11.5
C
OHT E8.5
Mk
RBC
Yolk sac
%YFP
E9.5
E10.5
E11.5
Blood
%YFP
E9.5
E10.5
E11.5
E12.5
E13.5
E14.5
Fetal liver
%YFP
E10.5
E11.5
E12.5
E13.5
E14.5
D
OHT E9.5
Mk
RBC
Yolk sac
%YFP
E10.5
E11.5
Blood
%YFP
E10.5
E11.5
E12.5
E13.5
E14.5
Fetal liver
%YFP
n.a.
E10.5
E11.5
E12.5
E13.5
E14.5

Figure 2. Lineage relationship between yolk sac progenitor subpopulations.

(A) Flow cytometric analysis of Kit+ CD41+ cells from *Csf1r*^{MeriCreMer} *Rosa*^{YFP} embryos pulsed at E8.5 (middle panel) and E9.5 (bottom panel) and analyzed 24, 48 and 72h after. (B) Labelling efficiency (% of YFP+ cells) of A, B, C and D progenitor subsets after E8.5 (upper) or E9.5 pulse (bottom). 4-OHT at E8.5: n=5 at E9.5; 9 at E10.5 and 12 at E11.5. 4-OHT at E9.5: n=6 at E10.5 and 5 at E11.5. Bars represent mean± sem. (C) Labelling efficiency (% of YFP+ cells) of megakaryocytes (Mk) and red blood cells (RBC) in the yolk sac, blood and fetal liver after an E8.5 pulse. n=5 at E9.5; 9 at E10.5; 12 at E11.5; 17 at E12.5; 5 at E13.5 and 2 at E14.5 (D) Labelling efficiency of Mk and RBC in the yolk sac, blood and fetal liver after a E9.5 pulse. n=6 at E10.5; 5 at E11.5; 10 at E12.5; 5 at E13.5 and 4-8 at E14.5

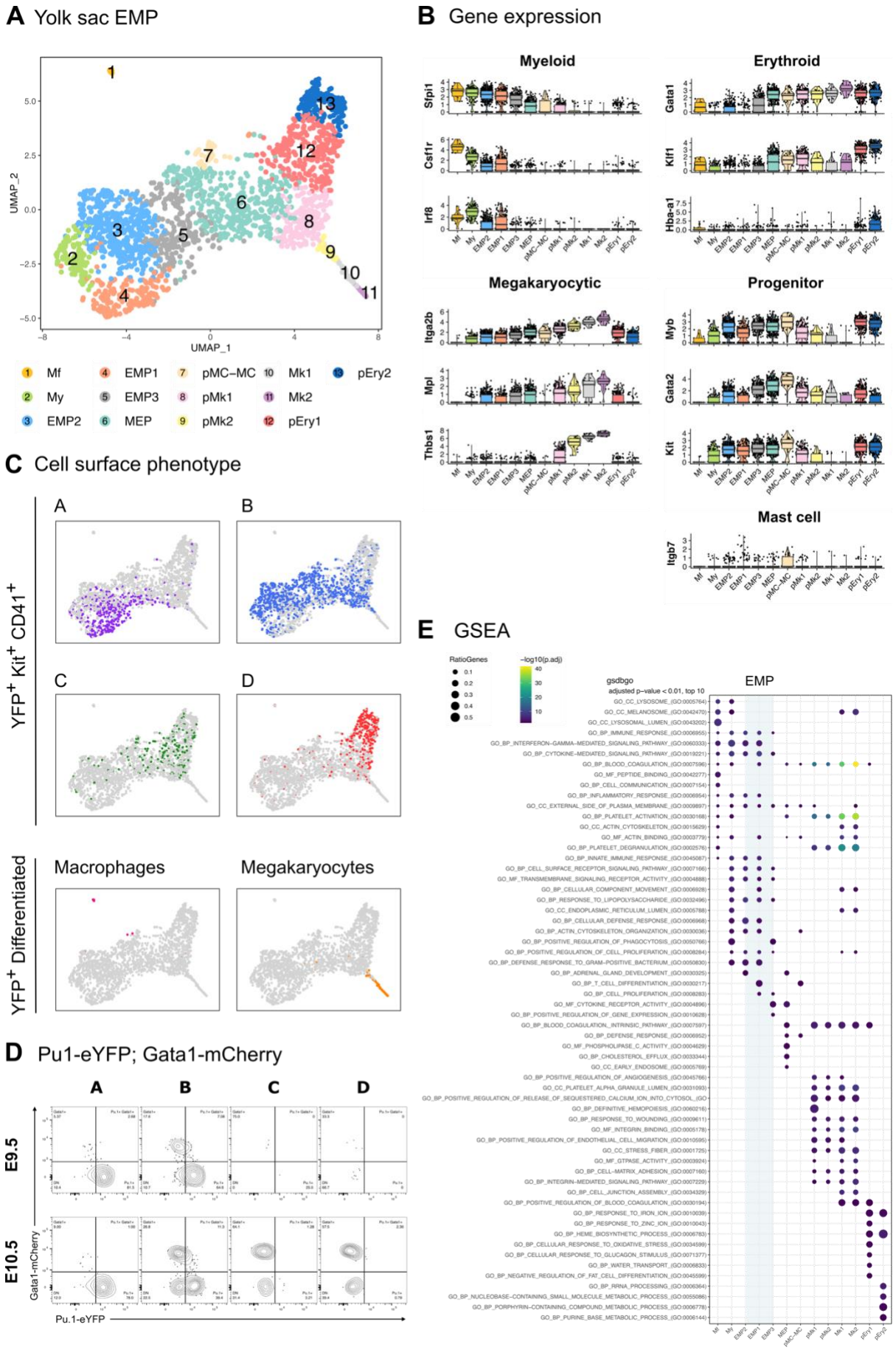
A Yolk sac EMP
UMAP_1
UMAP_2
1 Mf
2 My
3 EMP2
4 EMP1
5 EMP3
6 MEP
7 pMC–MC
8 pMk1
9 pMk2
10 Mk1
11 Mk2
12 pEry1
13 pEry2
B Gene expression
Myeloid
Erythroid
Megakaryocytic
Progenitor
Mast cell
Sfpi1
Csf1r
Irf8
Gata1
Klf1
Hba-a1
Itga2b
Mpl
Thbs1
Myb
Gata2
Kit
Itgb7
C Cell surface phenotype
YFP+ Kit+ CD41+
YFP+ Differentiated
Macrophages
Megakaryocytes
D Pu1-eYFP; Gata1-mCherry
E9.5
E10.5
Gata1-mCherry
Pu.1-eYFP
E GSEA
RatioGenes
−log10(p.adj)
gsdbgo
adjusted p−value < 0.01, top 10
EMP

Figure 3. Single cell expression profiling of fate mapped progenitors supports heterogeneity based on membrane markers and reveal different transcriptional states.

(A) UMAP representation of 1965 yolk sac YFP+ cells from E9.5 *Csf1r*^{iCre}*Rosa*^{YFP} and E10.5 *Csf1r*^{MeriCreMer} *Rosa*^{YFP} pulsed at E8.5, index-sorted and processed with the MARS-Seq pipeline. Clustering was performed using shared nearest-neighbor graph (SNN) and random walks method (FAST-MNN). Clustering was performed using random walks clustering on a shared nearest-neighbor graph (SNN) built using 13 nearest neighbors. Mf, macrophage; My, myeloid progenitor; MEP, megakaryocyte-erythroid progenitor; pMC-MC, mast cell progenitor/mast cell; pMK, Mk progenitor; pEry, erythroid progenitor. (B) Violin plot representation of key lineage-associated gene expression by the hematopoietic clusters. (C) UMAP representation of the cells colored by index sorting. A (purple), B (blue), C (green), D (red), macrophages (Kit^{neg} CD16/32^{high}, pink) and megakaryocytes (Kit^{neg} CD41^{high}, orange). (D) Representative contour plots showing expression of Gata1-mCherry and Pu.1-EYFP among E9.5 (upper) and E10.5 (bottom) yolk sac progenitor subsets. n=9 and 3 at E9.5 and E10.5, respectively. (E) Gene set enrichment analysis (GSEA) of the hematopoietic clusters. Dot color indicates adjusted p-value and dot size indicates the percentage of genes that are expressed from the pathway. Only the top 10 Gene Ontology (GO) pathways with Benjamini and Hochberg adjusted p-value < 0.1 in at least one cluster are represented. The three GO categories were used simultaneously (BP (Biological process), CC (Cellular component), MF (Molecular Function)).

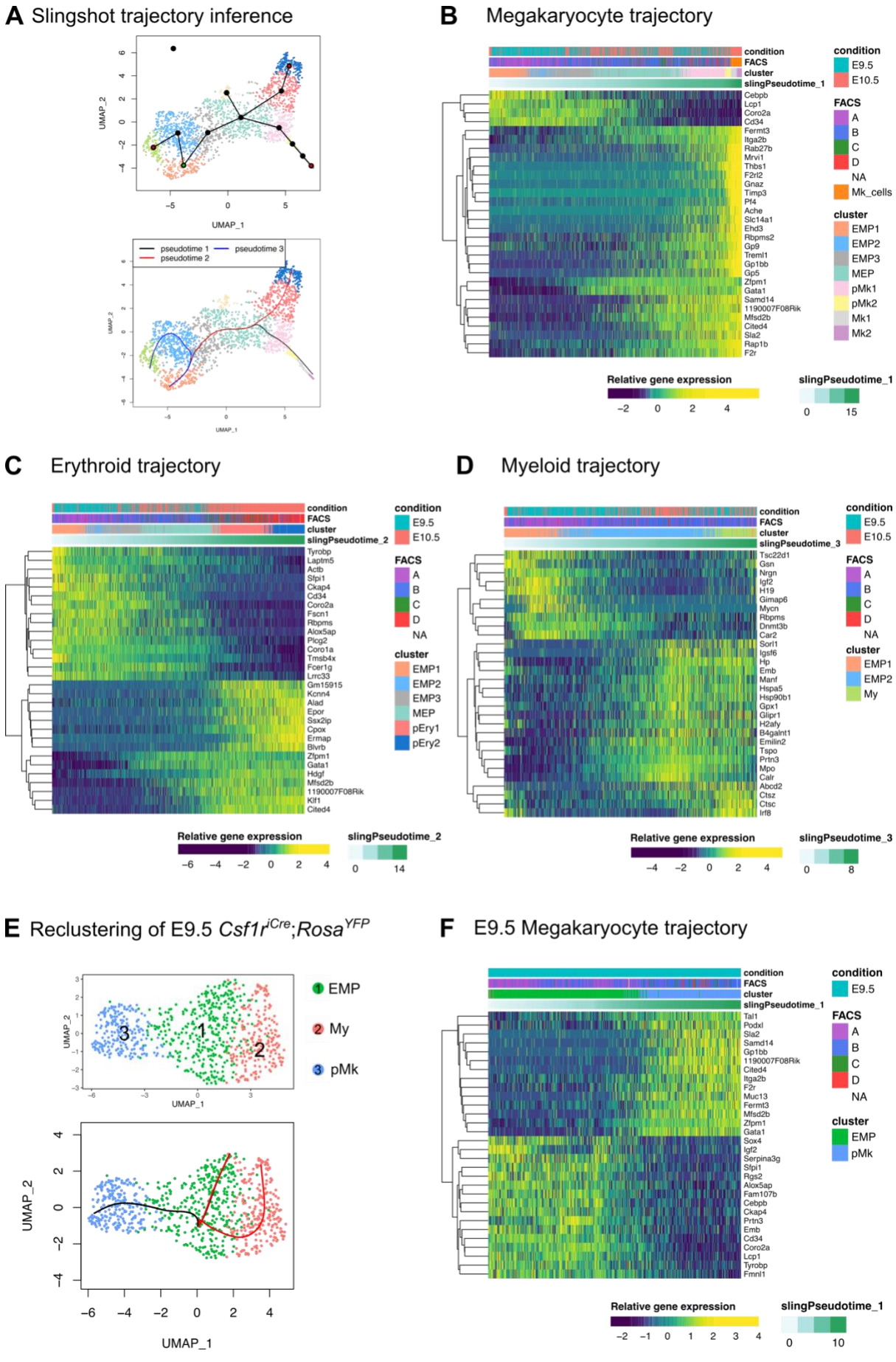
A Slingshot trajectory inference
UMAP_1
UMAP_2
pseudotime 1
pseudotime 2
pseudotime 3
B Megakaryocyte trajectory
condition
FACS
cluster
slingPseudotime_1
Cebpb
Lcp1
Coro2a
Cd34
Fermt3
Itga2b
Rab27b
Mrvi1
Thbs1
F2rl2
Gnaz
Timp3
Pf4
Ache
Slc14a1
Ehd3
Rbpms2
Gp9
Tremll
Gp1bb
Gp5
Zfpm1
Gata1
Samd14
1190007F08Rik
Mfsd2b
Cited4
Sla2
Rap1b
F2r
E9.5
E10.5
A
B
C
D
NA
Mk_cells
EMP1
EMP2
EMP3
MEP
pMk1
pMk2
Mk1
Mk2
Relative gene expression
slingPseudotime_1
C Erythroid trajectory
slingPseudotime_2
Tyrobp
Laptm5
Actb
Sfpi1
Ckap4
Cd34
Coro2a
Fscn1
Rbpms
Alox5ap
Plcg2
Coro1a
Tmsb4x
Fcer1g
Lrrc33
Gm15915
Kcnn4
Alad
Epor
Ssx2ip
Cpox
Ermap
Blvrb
Zfpm1
Gata1
Hdgf
Mfsd2b
1190007F08Rik
Klf1
Cited4
pEry1
pEry2
D Myeloid trajectory
slingPseudotime_3
Tsc22d1
Gsn
Nrgn
Igf2
H19
Gimap6
Mycn
Rbpms
Dnmt3b
Car2
Sorl1
Igsf6
Hp
Emb
Manf
Hspa5
Hsp90b1
Gpx1
Glipr1
H2afy
B4galnt1
Emilin2
Tspo
Prtn3
Mpo
Calr
Abcd2
Ctsz
Ctsc
Irf8
My
E Reclustering of E9.5 Csf1r^iCre;Rosa^YFP
1 EMP
2 My
3 pMk
F E9.5 Megakaryocyte trajectory
Tal1
Podxl
Sla2
Samd14
Gp1bb
1190007F08Rik
Cited4
Itga2b
F2r
Muc13
Fermt3
Mfsd2b
Zfpm1
Gata1
Sox4
Igf2
Serpina3g
Sfpi1
Rgs2
Alox5ap
Fam107b
Cebpb
Ckap4
Prtn3
Emb
Cd34
Coro2a
Lcp1
Tyrobp
Fmnl1

Figure 4. Lineage trajectories of EMP in the yolk sac.

(A) Slingshot infers three lineage trajectories starting from EMP1 towards pEry2 (red), Mk2 (black) and My clusters (blue). (B) Trajectory from EMP1 to Mk2. Heatmap representing the differentially expressed genes along the trajectory. Top 30 genes (30 smallest p-values) for the trajectory are represented. (C) Trajectory from EMP1 towards Erythroid progenitors (pEry2). Top 30 genes (30 smallest p-values) for the trajectory are represented. (D) Trajectory from EMP1 to Myeloid progenitor cluster (My). Top 30 genes (30 smallest p-values) for the trajectory are represented. (E) Upper panel, UMAP representation of YS E9.5 *Csf1r*^{iCre} *Rosa*^{YFP} YFP+ Kit+ cells allows the identification of an EMP (green), Myeloid (red) and Mk progenitor (blue) cluster. Lower panel, Slingshot infers two trajectories starting from EMP towards pMk or My. (F) Trajectory of E9.5 EMP to Megakaryocyte progenitors (pMk). Top 30 genes (30 smallest p-values) for the trajectory are represented.

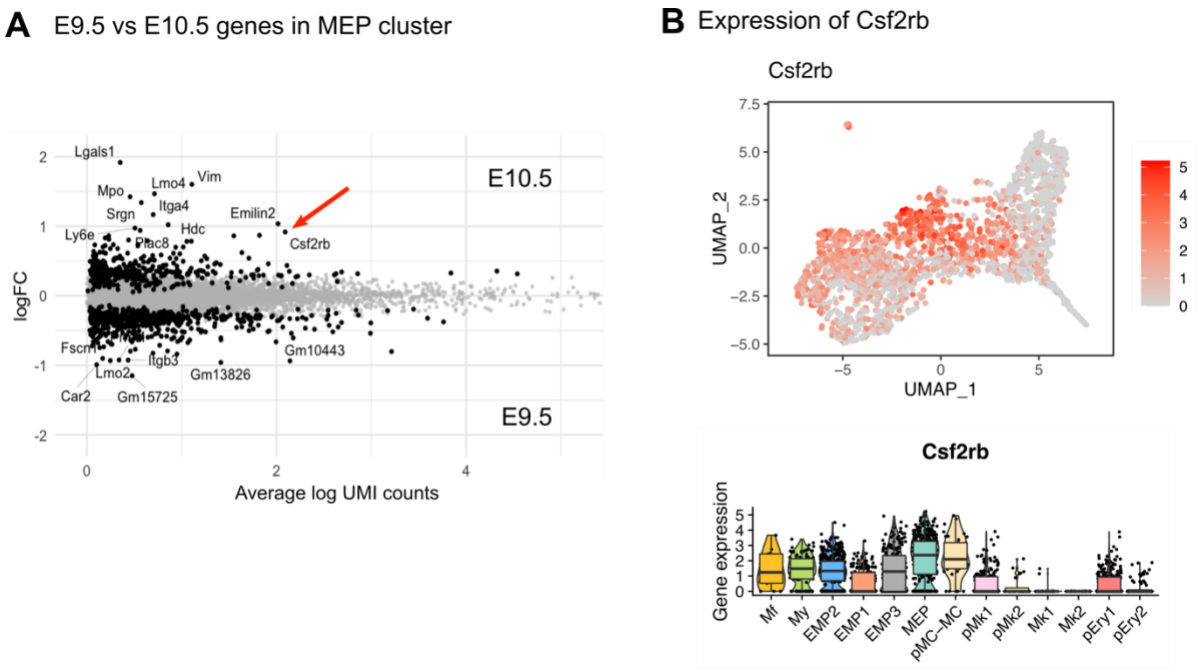
A
E9.5 vs E10.5 genes in MEP cluster
E10.5
E9.5
logFC
Average log UMI counts
Lgals1
Lmo4
Vim
Mpo
Itga4
Srgn
Emilin2
Ly6e
Hdc
Ptac8
Csf2rb
Fscn1
Itgb3
Gm10443
Lmo2
Gm13826
Car2
Gm15725
B
Expression of Csf2rb
Csf2rb
UMAP_2
UMAP_1
Csf2rb
Gene expression
Mf
My
EMP2
EMP1
EMP3
MEP
pMC–MC
pMk1
pMk2
Mk1
Mk2
pEry1
pEry2
C
Kit+ CD41+
E9.5
E10.5
CD131_BV421
CD34_PE-Cy7
D
CD131+ cells
Cells/YS
E9.5
E10.5
E
Phenotype of CD131+
5.86% A
49.36% B
41.87% C
2.90% D
F
Pu.1-YFP; Gata1-mCherry
CD131+
E9.5
E10.5
Gata1-mCherry
Pu.1-EYFP
G
Colony forming assay
CFU %
A
CD131+
Colony type %
Mk
E
E/Mk
Gr1
MF
MF/Gr1
EMP

Figure 5. CD131 is a marker of EMP to erythroid commitment in the yolk sac.

(A) MA-plot of the MEP cluster comparing E9.5 to E10.5 cells. The genes that are differentially expressed with FDR < 1% are shown as black dots, and the names of the genes with FDR < 1% and logFC > 0.9 are shown. (B) Upper panel, expression of *Csf2rb* in the UMAP. Lower panel, violin plot representation with boxplots of *Csf2rb* expression in all hematopoietic clusters. (C) Representative contour plots showing cytometric analysis of CD131+ cells among YS Kit+ CD41+ cells at E9.5 and E10.5. (D) Quantification of the number of CD131+ cells per YS at E9.5 and E10.5. n=15 and 11 at E9.5 and E10.5, respectively. Bars represent mean± sem. (E) Pie chart indicating the proportion of CD131+ cells among A-D progenitor subsets. (F) Expression of Gata1-mCherry and Pu.1-EYFP among E9.5 and E10.5 YS CD131+ progenitors. n=9 and 3 at E9.5 and E10.5, respectively. (G) Colony forming units (CFU-C) assays of sorted CD131+ progenitors compared to population A and analyzed 12 days after. Cloning efficiency (left) and frequency of colony types (Mk, Megakaryocyte; E, erythroid; E/Mk, E and Mk; Gr1, granulocytes; MF, macrophages; MF/Gr1, MF and Gr; EMP, mixed colonies) (right); mean± sem. Data from 6 embryos.

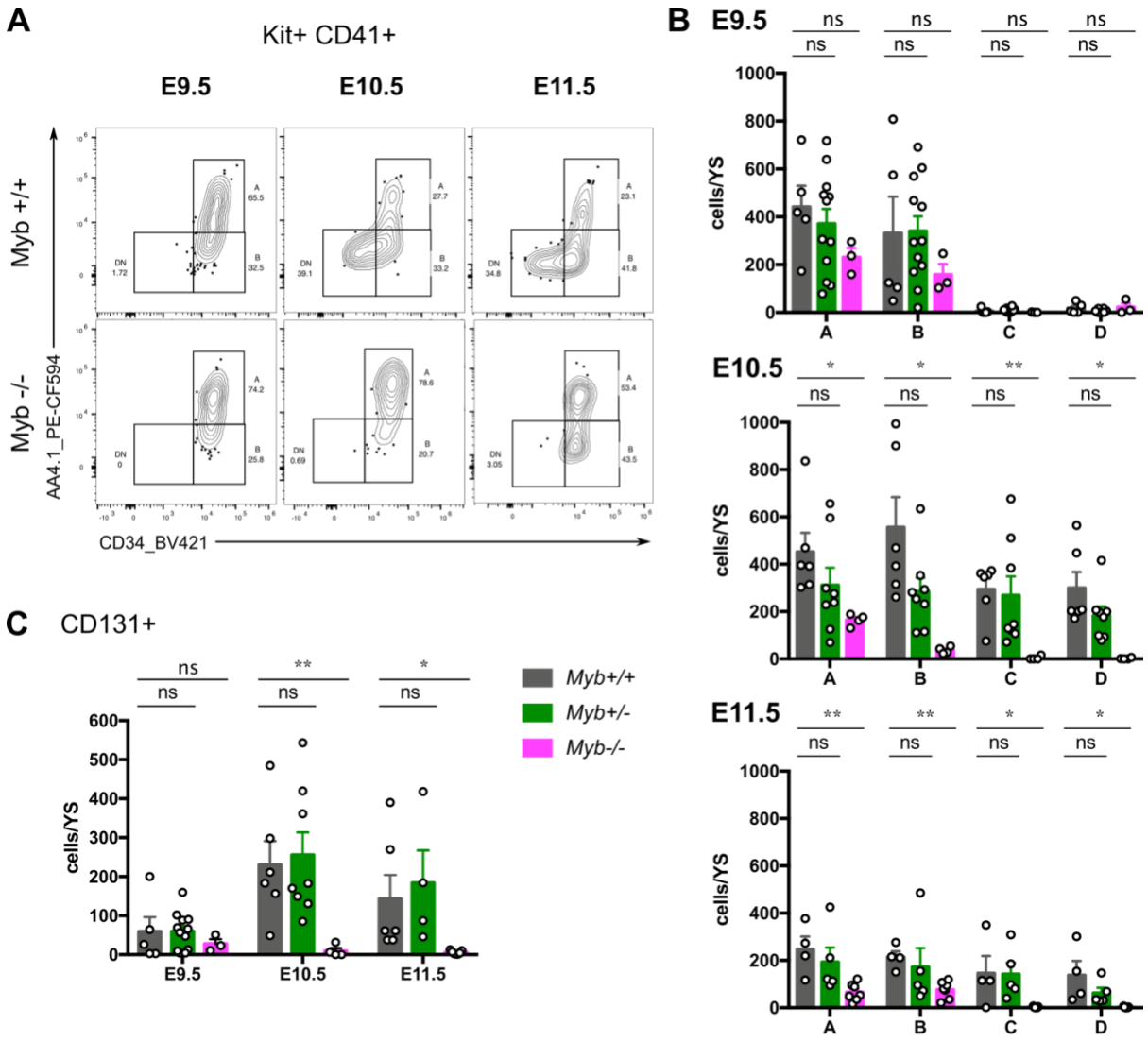
A
Kit+ CD41+
E9.5
E10.5
E11.5
Myb +/+
Myb -/-
AA4.1_PE-CF594
CD34_BV421
B
E9.5
E10.5
E11.5
cells/YS
ns
*
**
A
B
C
D
C
CD131+
Myb+/+
Myb+/-
Myb-/-
cells/YS
E9.5
E10.5
E11.5
D
Csf1r MeriCreMer Rosa YFP Myb-/- OHT E8.5
Red blood cells
Megakaryocytes
Yolk Sac
Blood
Fetal liver
% YFP
%YFP
E9.5
E10.5
E11.5
E12.5
E13.5
E14.5
Myb+/+
Myb+/-
Myb-/-

Figure 6. Deletion of the transcription factor Myb specifically results in a blockage of yolk sac erythroid progenitors but does not affect megakaryocyte differentiation.

(A) Flow cytometric analysis of Kit+ CD41+ cells from *Myb*-deficient embryos and *wt* littermates from E9.5 to E11.5. (B) Number of cells per yolk sac in each population in *Myb*+/+, *Myb* +/- and *Myb*-/- at E9.5, E10.5 and E11.5. Results from 3 independent litters per stage. Bars represent mean± sem. ns, not significant; *, p<0.1; **, p<0.01. (C) Number of CD131+ cells per yolk in *Myb*+/+, *Myb* +/- and *Myb*-/- at E9.5, E10.5 and E11.5. Results from 3 independent litters per stage. Bars represent mean± sem. ns, not significant; *, p<0.1; **, p<0.01. (D) Labelling efficiency (% of YFP+ cells) of red blood cells (RBC) and megakaryocytes (Mk) in the yolk sac, blood and fetal liver of $Csf1r^{MeriCreMer}$ $Rosa^{YFP}$ *Myb*-/- embryos pulsed at E8.5. Results from 3 independent litters per stage. Bars represent mean± sem. Statistical analysis compared *wt* and Myb-deficient groups: *, p<0.1.

Supplemental Figures (6)

A Gating strategy for EMPs in the yolk sac

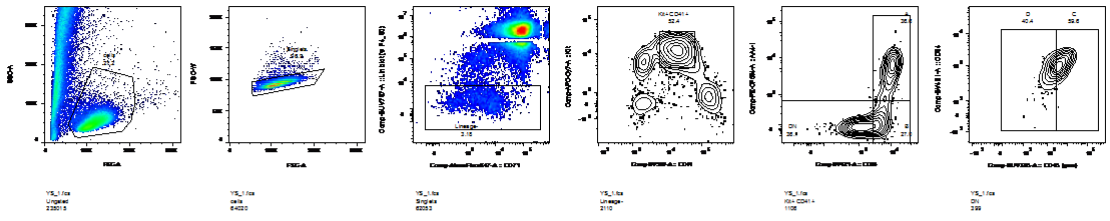

B Phenotype of Kit+ CD41+ at E10.5

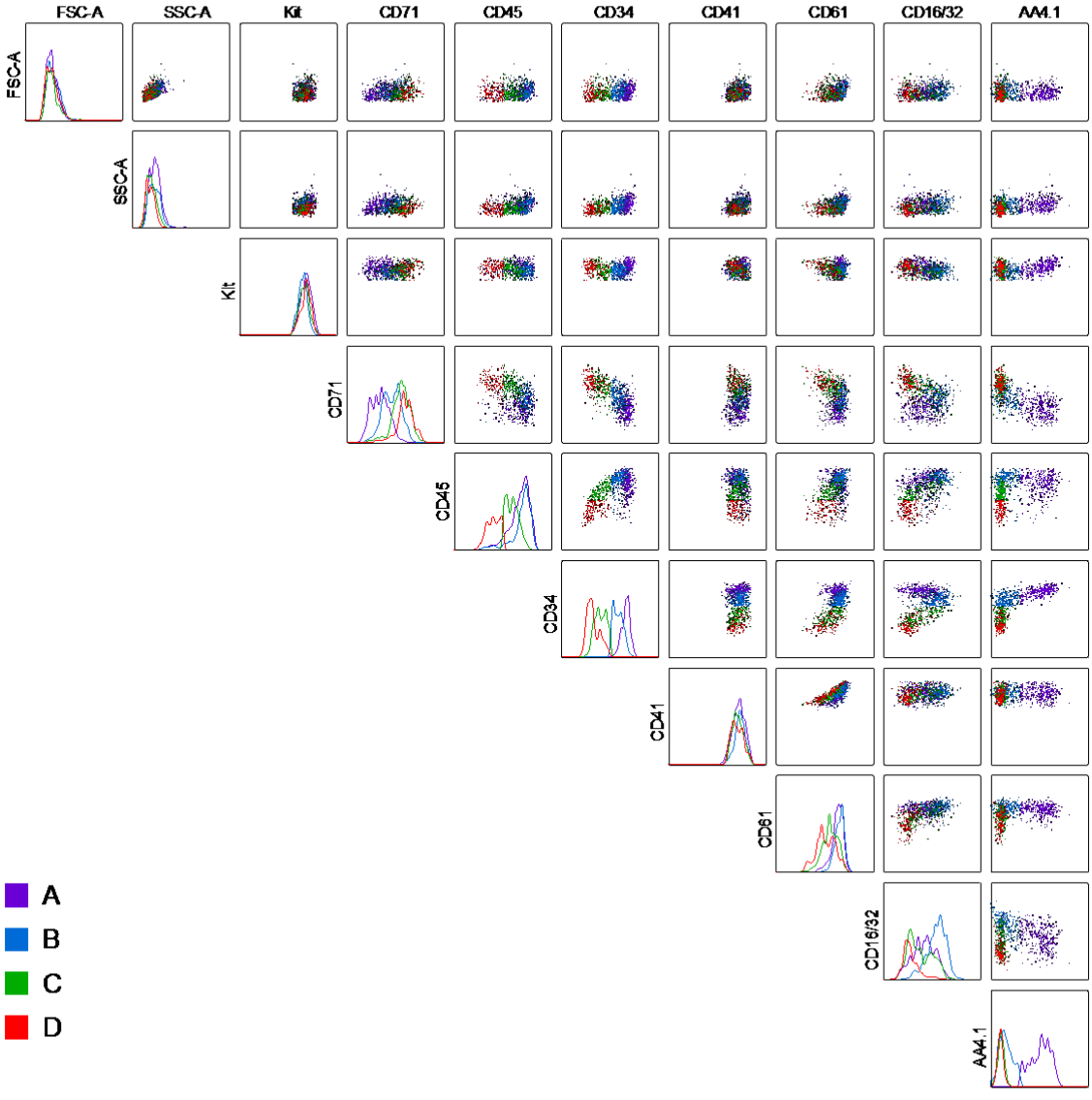

C Expression of CD45 in A

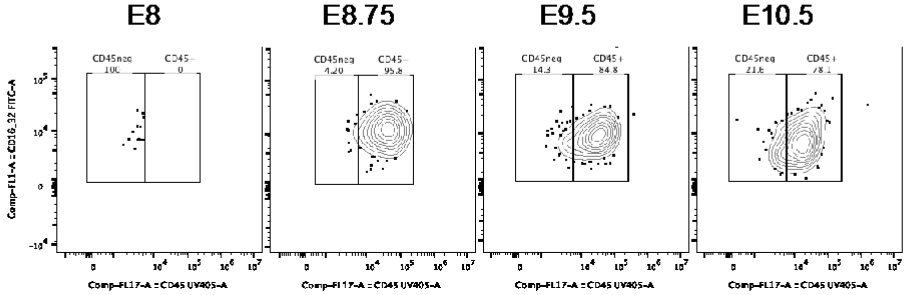

Figure S1. (A) Gating strategy for EMP subsets in the E10.5 yolk sac. Cells were gated based on size (FSC-A) and scatter (SSC-A). After doublet exclusion, lineage negative cells were selected and EMPs were gated using expression of Kit and CD41. Among Kit+ CD41+ cells, A was defined as AA4.1+ CD34+ and B as AA4.1^{neg} CD34+. In the AA4.1^{neg} CD34^{neg} gate (DN), C and D were identified based on CD45 expression. (B) Immunophenotype of E10.5 yolk sac Kit+ CD41+ cells with the markers used for the t-SNE analysis. Histogram of individual markers and dot plots with overlay of A (purple), B (blue), C (green) and D (red) populations. (C) Expression of CD45 on A (Kit+ CD41+ AA4.1+ CD34+) cells in the yolk sac over time, from E8 to E10.5.

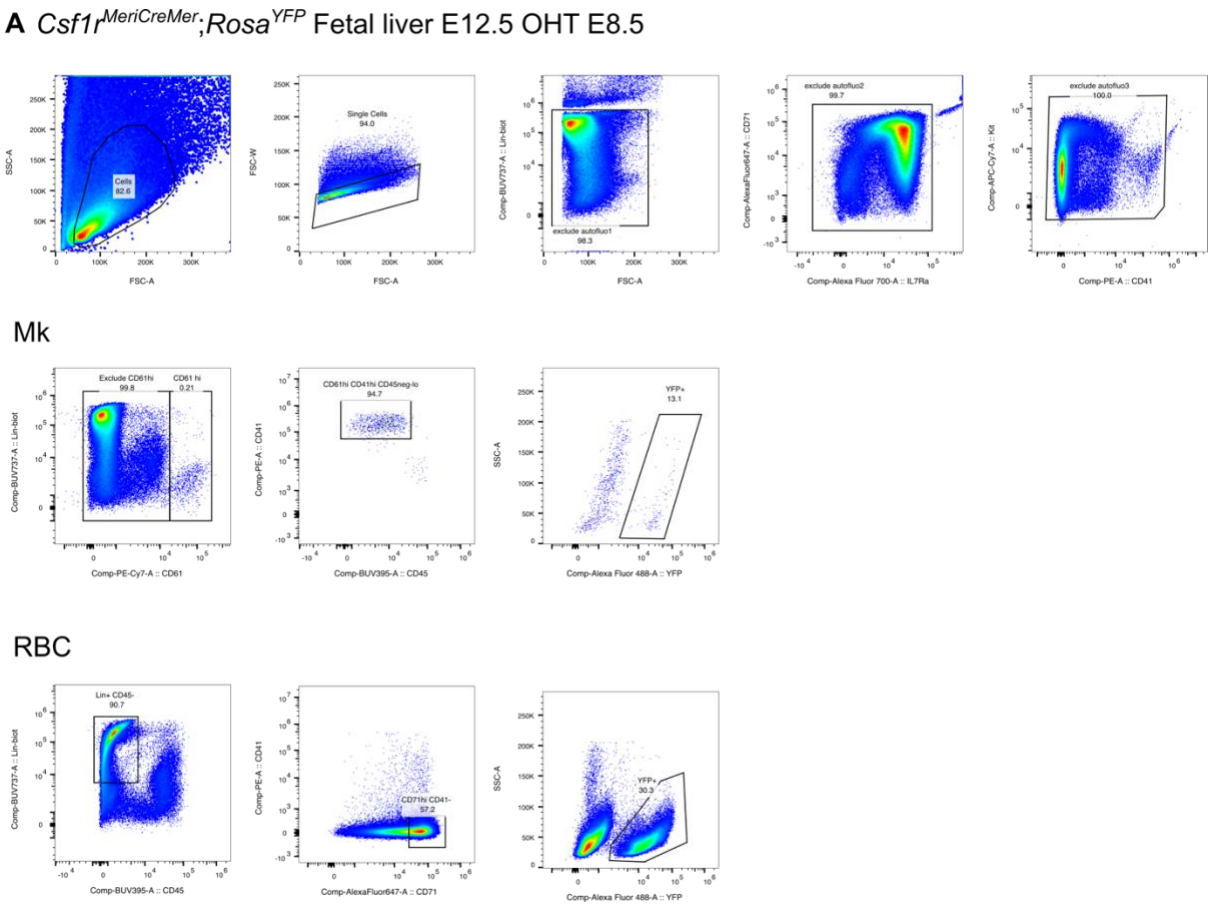

Figure S2. Gating strategy for Megakaryocytes (Mks) and red blood cells (RBC) in the E12.5 fetal liver of *Csf1r*^{MeriCreMer} *Rosa*^{YFP} embryos pulsed at E8.5. Cells were gated based on size (FSC-A) and scatter (SSC-A). After exclusion of doublets and autofluorescent debris, CD61^{hi} cells were selected and Mks were gated using expression of CD45 and CD41. For RBC, CD71^{hi} CD41^{neg} cells were gated among Lineage+ CD45^{neg} cells. YFP labelling was then analyzed in Mks (CD61^{hi} CD41+ CD45^{neg}) and RBC (Lineage+ CD71^{hi} CD45^{neg} CD41^{neg}).

A

Sequencing run	Stage	Plate	Halfplate	Cells after QC
1	E10.5	E10.5_02	A	45
			H	58
	E10.5	E10.5_07	A	176
			H	179
	E10.5	E10.5_09	A	183
			H	175
2	E9.5	E10.5_11	A	46
			H	39
	E10.5	E10.5_15	A	discarded
			H	discarded
	E10.5	E10.5_16	A	42
			H	38
3	E10.5	E10.5_03	A	186
			H	187
	E9.5	E9.5_01	A	174
			H	179
	E9.5	E9.5_02	A	183
			H	178

B

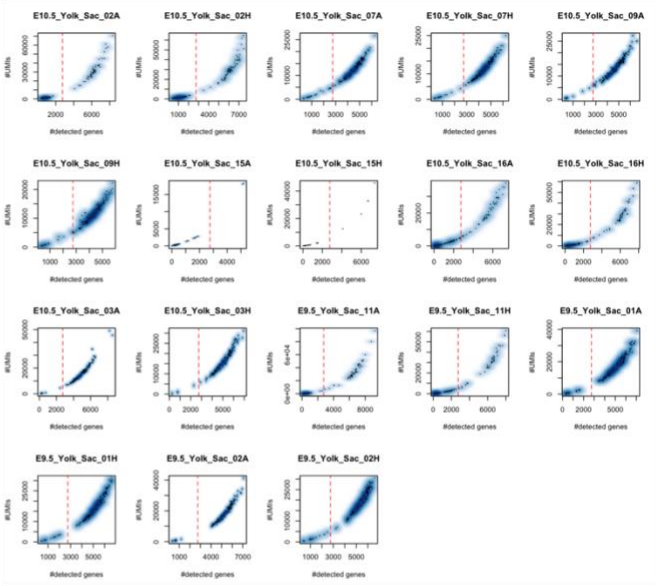

C

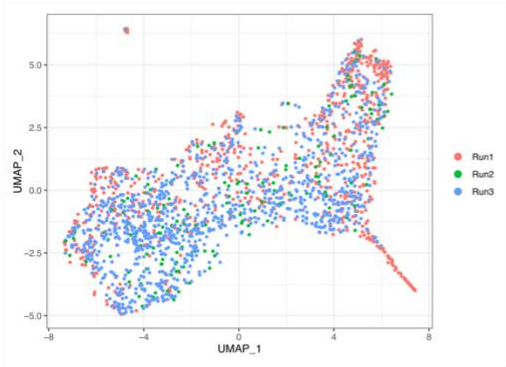

D

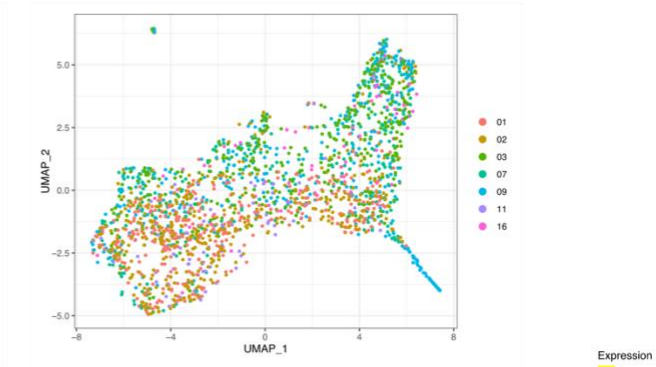

E

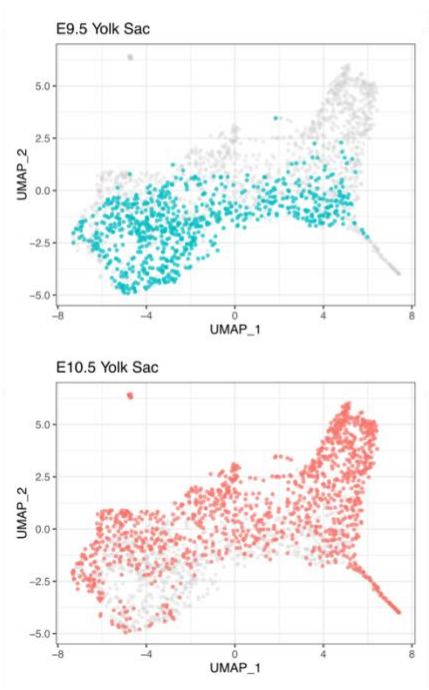

F

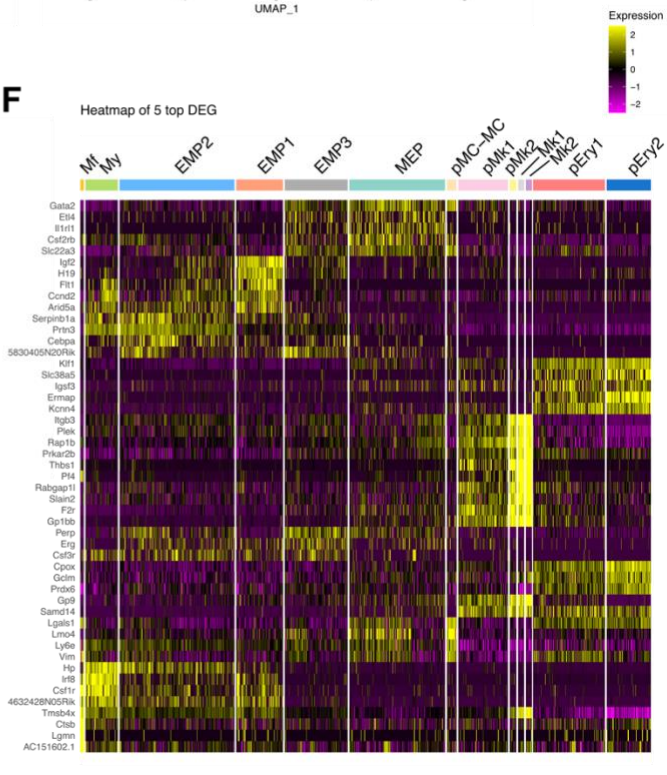

Figure S3. (A) Table summarizing the sequencing runs, sorted 384-well plates, separately processed half-plates and the number of cells that passed the quality control in each half plate. (B) Graphical representation of the number of UMI per number of detected genes in each cell from each processed half-plate and with the threshold at 2750 detected genes for the QC (red dotted line). (C) Representation of the three sequencing runs in the UMAP. (D) Representation of the seven independently sorted plates in the UMAP. (E) Representation of the two developmental time points (E9.5, turquoise, and E10.5, red) in the UMAP. (F) Heatmap representing the top 5 differentially expressed genes (DEG) out of each pairwise cluster comparison among the 13 clusters identified in the scRNA-seq analysis.

A Expression of lineage genes in E9.5 clusters

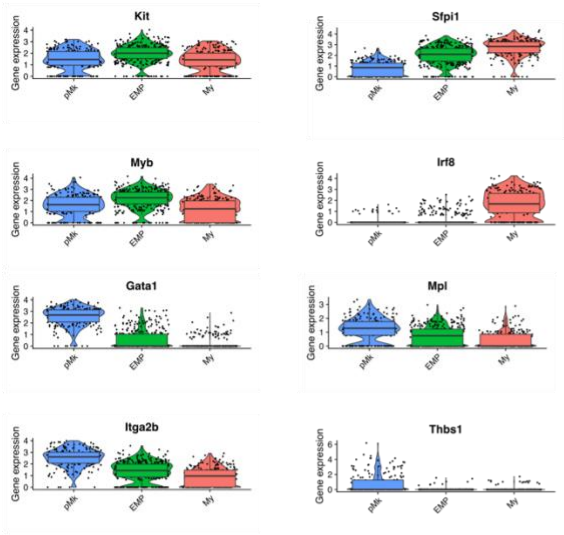

B Top 5 DEG in E9.5 clusters

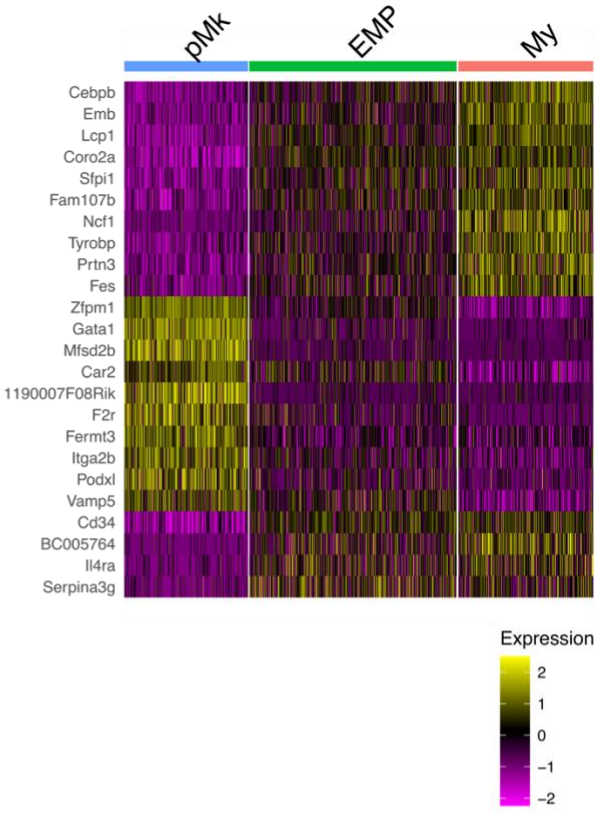

C FACS progenitor annotation along trajectories

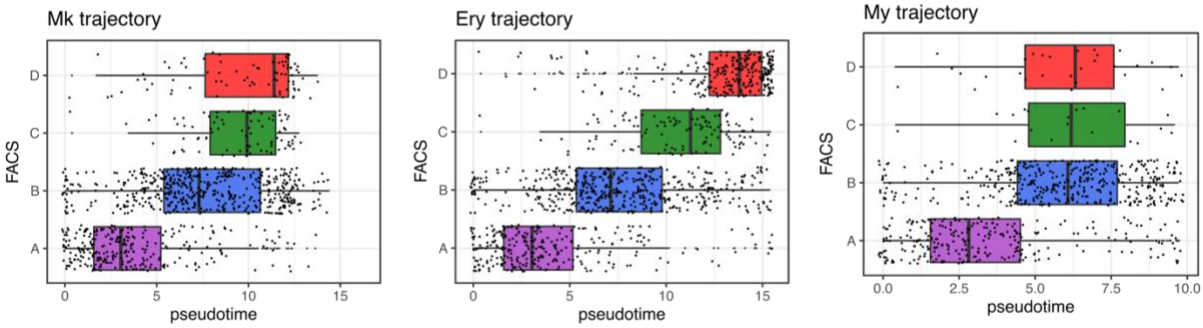

D Slingshot parameters in E9.5 dataset

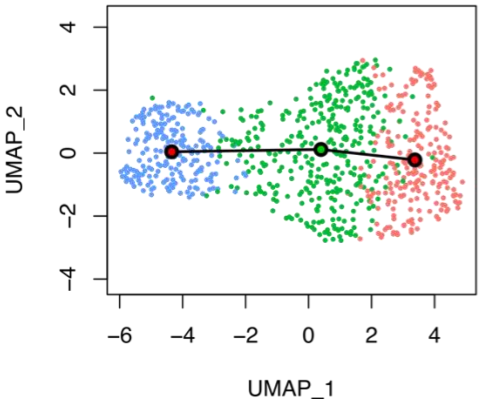

E FACS progenitor annotation in E9.5 dataset

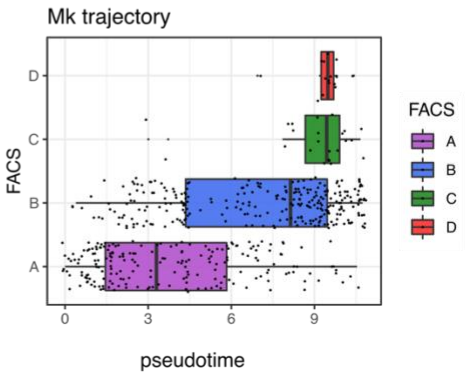

Figure S4. (A) Violin plot representing expression of Kit, key transcription factors (Myb, Gata1, Spf1(Pu.1), Irf8) and Mk-associated genes (Itg2b, Mpl, Thbs1) by the 3 hematopoietic clusters at E9.5. (B) Heatmap representing the 10 top differentially expressed genes (DEG) among the 3 clusters identified at E9.5. pMk, Mk progenitor; My, Myeloid progenitor. (C) Representation of the progenitor phenotype (A, purple; B, blue; C, green; D, red) of the cells belonging to each of the three trajectories along the pseudotime value. (D) UMAP representation of YS E9.5 *Csf1r*^{iCre} *Rosa*^{YFP} YFP+ Kit+ cells and the three clusters used for trajectory analysis with Slingshot. (E) Representation of the progenitor phenotype (A, purple; B, blue; C, green; D, red) of the cells belonging to the megakaryocyte trajectory in E9.5 dataset alone along the pseudotime value.

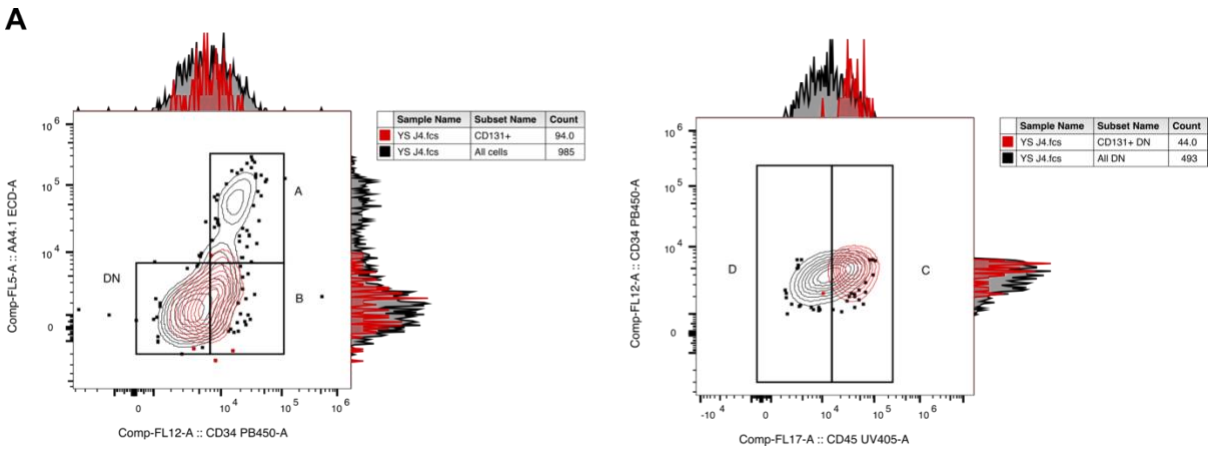

Figure S5. Phenotype of CD131+ cells in the E10.5 yolk sac in regards to progenitor subsets A-D. CD131+ cells (red) are overlaid on top of all CD41+ Kit+ progenitors.

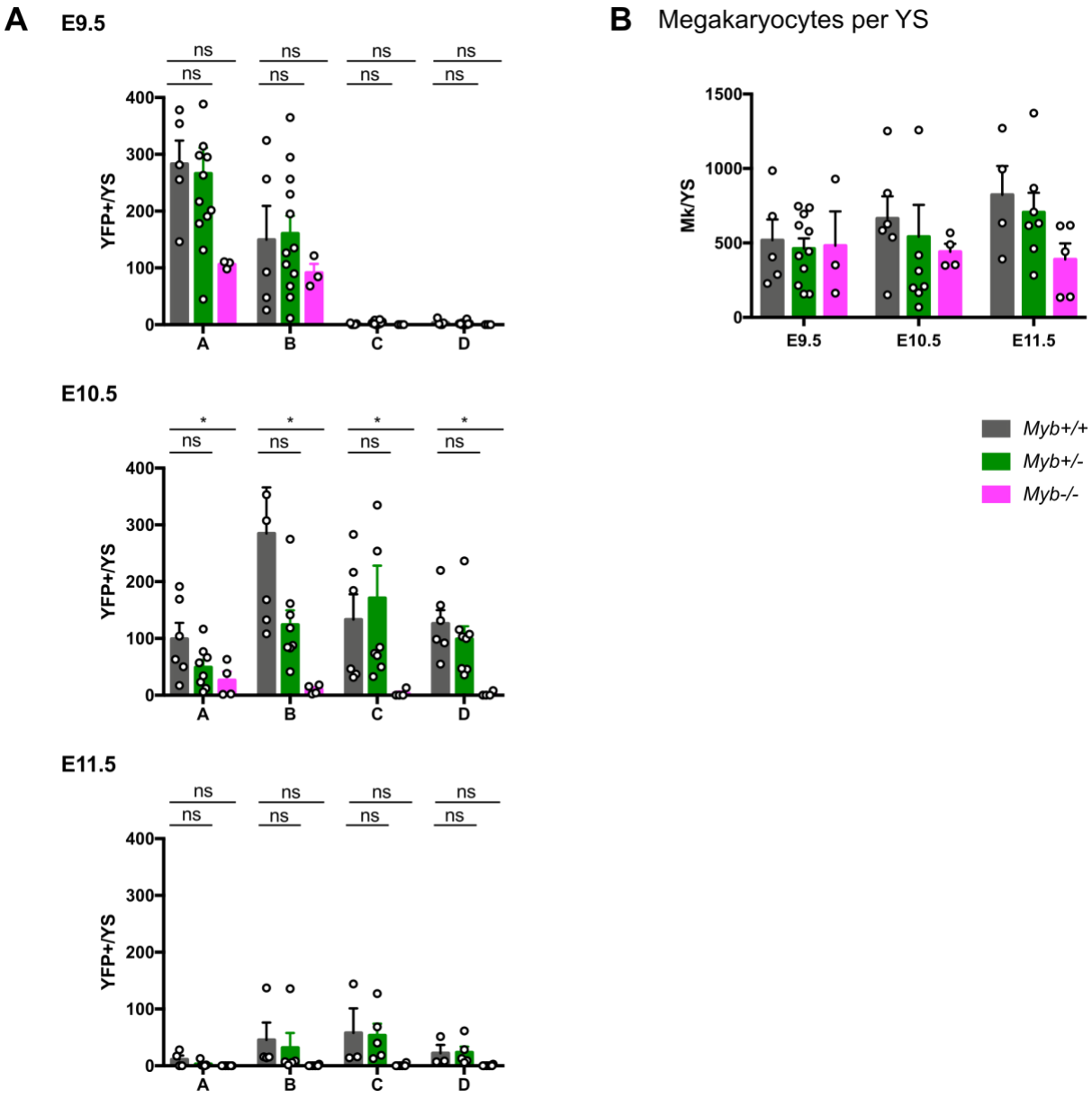

Figure S6. (A) Number of YFP+ cells per yolk sac in each EMP subset (A-B-C-D) in *Myb*+/+, *Myb* +/- and *Myb*-/- at E9.5, E10.5 and E11.5. Results 3 independent litters. Bars represent mean± sem; ns, not significant; *, p<0.1. (B) Number of Mk cells per yolk sac in *Myb*+/+, *Myb* +/- and *Myb*-/- at E9.5, E10.5 and E11.5. Results from 3 independent litters. Bars represent mean± sem.

Part 2. Fetal liver

In order to further investigate the differentiation dynamics of EMPs, we followed pulsed-labelled EMP and EMP-derived progenitors in the fetal liver at different stages.

EMP derived cells in the fetal liver

First, we performed high parameter flow cytometry from E12.5 FL and identified myeloid progenitors as annotated in the bone marrow, since they have similar potential in the E14.5 fetal liver(Traver et al., 2001). Lineage^{neg} KIT+ Sca-1^{neg} cells can be subdivided into three progenitor populations, based on CD34 and CD16/32 expression: CMP (Common Myeloid Progenitor, CD34+ CD16/32^{neg}), GMP (Granulocyte and Macrophage progenitor, CD34+ CD16/32+) and MEP (Megakaryocyte and erythrocyte progenitor, CD34^{neg} C16/32^{neg}). The E12.5 FL contains a CD16/32+ CD34^{neg} population that is not readily apparent in the bone marrow and we named it P1 (Figure 9A). We performed dimensionality reduction (t-SNE) and observed that the differences in surface marker expression did separate these four populations. We observed that MEPs were characterized by an increase in CD71 and a decrease in CD45 and ultimately CD41 at the surface. Also, we saw that GMPs have higher CD61 (figure 9B).

We then used *Csf1r*^{MeriCreMer} *Rosa*^{YFP} embryos pulsed *in utero* at E8.5 or E9.5 to observe EMPs and EMP-derived progenitor phenotype in the fetal liver from E10.5 to E14.5 (Figure 9C). In total cells, we observed an acquisition of BM phenotype, since P1 was very abundant at E10.5 but less apparent by E14.5 and GMP and CMP clearly separated from E11.5 onwards. Pulsed EMPs gave rise to a majority of MEPs in both pulses (from 80% at E10.5 to 98% of labelled progenitors at E14.5) and to GMPs and P1 cells. Pulse at E8.5 showed non-MEP labelled progenitors until E13.5 and MEPs until E14.5 (Figure 9C) but there was a rapid decrease of labelling efficiency in all progenitors from E11.5 (Figure 9D). Pulse labelling at E8.5 suggested that CMP was not produced from EMP. Further, labeling efficiency equilibrated

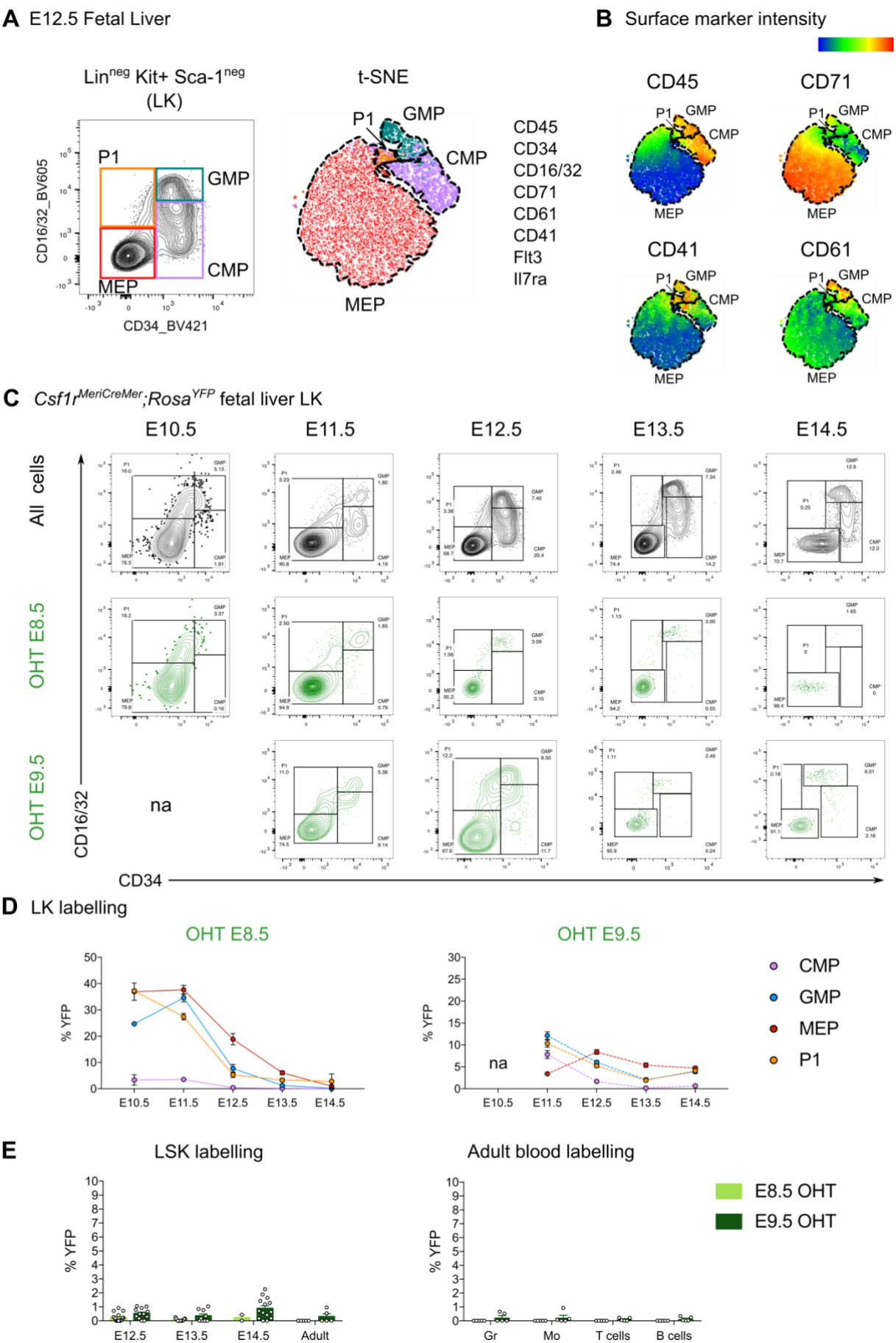
A E12.5 Fetal Liver
Lin^neg Kit+ Sca-1^neg (LK)
P1
GMP
CMP
MEP
CD16/32_BV605
CD34_BV421
t-SNE
CD45
CD34
CD16/32
CD71
CD61
CD41
Flt3
Il7ra
B Surface marker intensity
CD45
CD71
CD41
CD61
C Csf1r^MeriCreMer;Rosa^YFP fetal liver LK
E10.5
E11.5
E12.5
E13.5
E14.5
All cells
OHT E8.5
OHT E9.5
na
CD16/32
CD34
D LK labelling
OHT E8.5
OHT E9.5
% YFP
CMP
GMP
MEP
P1
E LSK labelling
Adult blood labelling
E8.5 OHT
E9.5 OHT
Gr
Mo
T cells
B cells
Adult

Figure 9. Erythroid and/or myeloid progenitor populations in the fetal liver. (A) Left, Representative dotplot of Lineage^{neg} Kit+ Sca-1^{neg} (LK) cells in E12.5 fetal liver, showing CD34 and CD16/32 expression. Four populations can be distinguished, CMP (purple), GMP (blue), MEP (red) and a novel population denominated P1 (orange). Right, t-SNE representation of E12.5 FL LK cells, created with the expression of the surface markers on the right of the t-SNE. (B) Surface marker intensity of CD45, CD71, CD41 and CD61 on the different populations. (C) LK cells from *Csf1r^{MeriCreMer} Rosa^{YFP}* FL at different stages showing representative dotplots of all LK cells (top), YFP+ cells pulsed at E8.5 (middle) and YFP+ cells pulsed at E9.5 (bottom). (D) YFP labelling in the different populations when pulsed at E8.5 (left) and at E9.5 (right). (E) Labelling of Lineage^{neg} Kit+ Sca-1+ (LSK) cells at different stages (left) and labelling of blood populations from adult (2 month-old) mice (left) after pulse-labelling at E8.5 (light green) or E9.5 (dark green). Bars represent mean± sem. n.a., not acquired. Results from 3 independent litters per stage.

at all time points between GMP, P1 and MEP, suggesting they share a common origin that does not progresses through a CMP intermediate, in stark contrast to adult progenitors (Figure 9D). Pulse at E9.5 showed a much lower labelling (10%) in all populations but, interestingly, MEP labelling increased between E11.5 and E12,5 and stayed constant until at least E14.5, which implies a high proliferation rate since it is when the FL is growing exponentially (Figure 9D). Labelling efficiency of non-MEP progenitors pulsed at E9.5 also decreased progressively over time as when pulsed at E8.5, with the notable difference of CMP labelling.

We verified the labelling among LSK (Lin^{neg} Kit^{+} Sca-1^{+} cells), which include HSC and MPP, in embryos and in adult bone marrow. Although the difference in labelling was not significant, some E9.5 pulsed embryos and adults did have 1% of LSK labelled, and this was observed also in circulating populations of adult (2 months) mice (Figure 9E). However, no circulating YFP+ cells were ever detected when pulsed at E8.5.

Single cell expression analysis of EMP-derived progenitors of the yolk sac and fetal liver

In order to further characterize EMP and EMP-derived progenitors, we also index-sorted *Csf1r*^{MeriCreMer} *Rosa*^{YFP} fetal liver YFP+ cells that were pulsed at E8.5 to perform single cell expression analysis using the MARS-Seq pipeline. Kit+ YFP+ cells from E10.5 and E12.5 fetal liver were analysed and merged to the yolk sac cells that were previously analysed (Figure 10A-B). When sorting E12.5 fetal liver progenitors, in order to enrich the dataset in myeloid cells (98% of YFP cells are MEP, Figure 9), we sorted half of the plate of “non-MEP” progenitors, defined as double negative cells for CD34 and CD16/32. This allowed us to decrease the frequency of MEPs to 77% of average (Figure 10A). 5002 YFP+ cells were sorted in total, including 64 yolk sac megakaryocytes and 29 macrophages from yolk sac and fetal liver (Figure 10B). The objective of this analysis was to observe differences in the differentiation dynamics of EMPs across different niches, the yolk sac and the fetal liver, and stages, from E9.5 to E12.5.

Normalization and data merging were performed to minimize batch effects generated during plate processing and sequencing runs (collaboration with Anne Biton, bioinformatician at the C3BI, Institut Pasteur), and data was represented in UMAP (Figure 10C). The enrichment for certain stages among certain cell types is biologically relevant feature that is observed in the plate distribution in the UMAP (will be explained later, Figure 14) due to the uneven distribution of stages among the sequencing runs (FL E12.5 were only analysed from first run, E10.5 fetal liver were mostly from third run, and E9.5 yolk sac was mostly in the third run). Importantly, cells from each sequencing run did locate in all parts of the UMAP although up to different proportions.

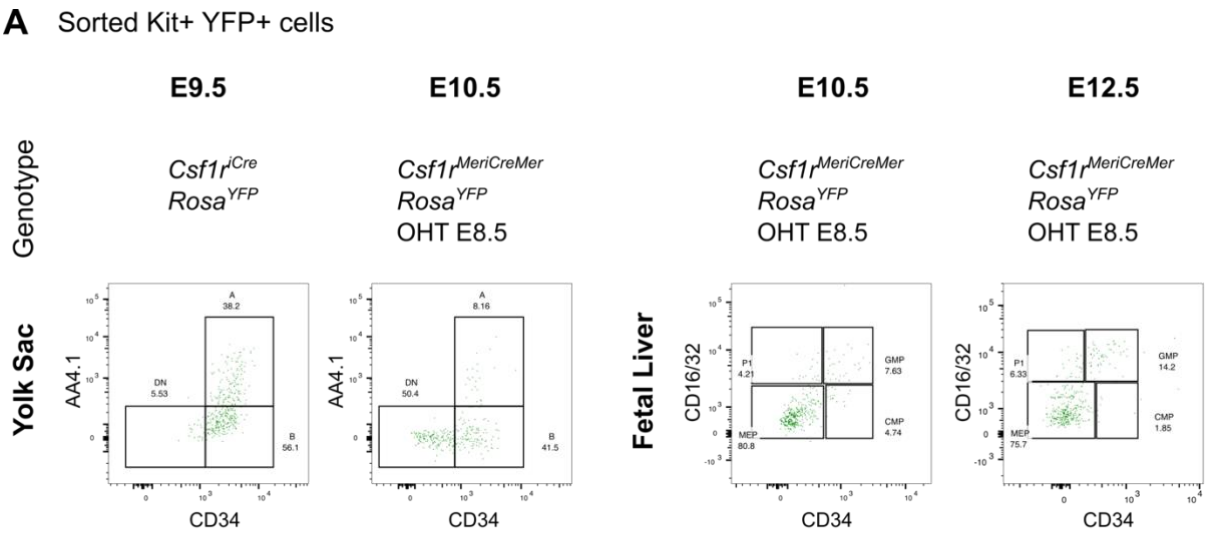

B Summary of sequenced plates

Sequencing run	Stage	Tissue	Genotype	Plate	Halfplate	Cells after QC
1	E12.5	Fetal Liver	*Csf1r*^{MeriCreMer} ; *Rosa*^{YFP}	E12.5_YS_01	A	183
					H	177
	E10.5	Yolk Sac	*Csf1r*^{MeriCreMer} ; *Rosa*^{YFP}	E10.5_YS_02	A	44
					H	58
	E12.5	Fetal Liver	*Csf1r*^{MeriCreMer} ; *Rosa*^{YFP}	E12.5_YS_03	A	133
					H	130
	E12.5	Fetal Liver	*Csf1r*^{MeriCreMer} ; *Rosa*^{YFP}	E12.5_YS_04	A	109
					H	115
	E12.5	Fetal Liver	*Csf1r*^{MeriCreMer} ; *Rosa*^{YFP}	E12.5_YS_05	A	151
					H	137
	E12.5	Fetal Liver	*Csf1r*^{MeriCreMer} ; *Rosa*^{YFP}	E12.5_YS_06	A	133
					H	136
	E10.5	Yolk Sac	*Csf1r*^{MeriCreMer} ; *Rosa*^{YFP}	E10.5_YS_07	A	172
					H	174
	E10.5	Fetal Liver	*Csf1r*^{MeriCreMer} ; *Rosa*^{YFP}	E10.5_YS_08	A	116
					H	122
	E10.5	Yolk Sac	*Csf1r*^{MeriCreMer} ; *Rosa*^{YFP}	E10.5_YS_09	A	172
					H	167
	E10.5	Fetal Liver	*Csf1r*^{MeriCreMer} ; *Rosa*^{YFP}	E10.5_YS_10	A	169
					H	155
2	E9.5	Yolk Sac	*Csf1r*^{iCre} ; *Rosa*^{YFP}	E9.5_YS_11	A	45
					H	37
	E10.5	Fetal Liver	*Csf1r*^{MeriCreMer} ; *Rosa*^{YFP}	E10.5_FL_14	A	discarded
					H	44
	E10.5	Yolk Sac	*Csf1r*^{MeriCreMer} ; *Rosa*^{YFP}	E10.5_YS_15	A	discarded
					H	discarded
	E10.5	Fetal Liver	*Csf1r*^{MeriCreMer} ; *Rosa*^{YFP}	E10.5_FL_15	A	30
					H	27
	E10.5	Yolk Sac	*Csf1r*^{MeriCreMer} ; *Rosa*^{YFP}	E10.5_YS_16	A	40
					H	38
	E10.5	Fetal Liver	*Csf1r*^{MeriCreMer} ; *Rosa*^{YFP}	E10.5_FL_16	A	discarded
					H	discarded
3	E9.5	Yolk Sac	*Csf1r*^{iCre} ; *Rosa*^{YFP}	E9.5_YS_01	A	169
					H	175
	E9.5	Yolk Sac	*Csf1r*^{iCre} ; *Rosa*^{YFP}	E9.5_YS_02	A	182
					H	136
	E10.5	Yolk Sac	*Csf1r*^{MeriCreMer} ; *Rosa*^{YFP}	E10.5_YS_03	A	182
					H	179
	E10.5	Fetal Liver	*Csf1r*^{MeriCreMer} ; *Rosa*^{YFP}	E10.5_YS_04	A	179
					H	173
	E10.5	Fetal Liver	*Csf1r*^{MeriCreMer} ; *Rosa*^{YFP}	E10.5_YS_05	A	168
					H	140
	E10.5	Fetal Liver	*Csf1r*^{MeriCreMer} ; *Rosa*^{YFP}	E10.5_YS_06	A	159
					H	146
					Total	5002

C Merging and UMAP representation

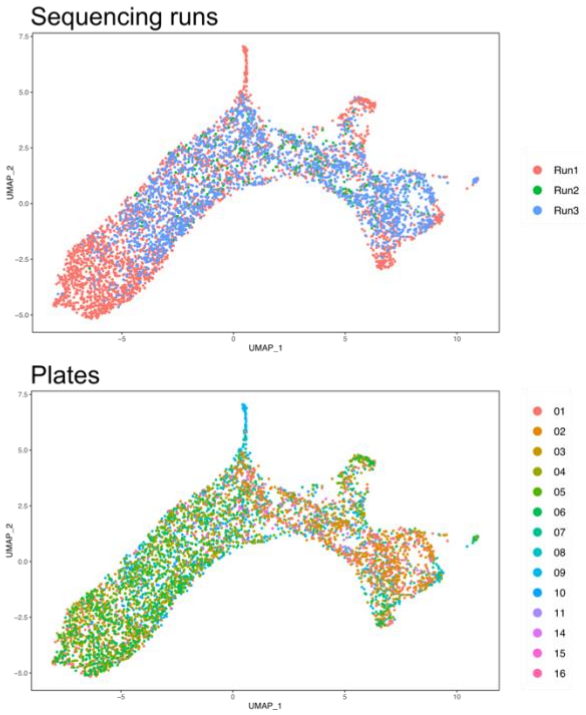

Figure 10. Single cell RNA-Sequencing of yolk sac and fetal liver EMP-derived progenitors. (A) Representative dotplots of the four sorted conditions. YS E9.5, E10.5 and FL E10.5 dotplots correspond to the sorted cells from plates 02, 03 and 04 of Run1, respectively, and FL E12.5 dotplot corresponds to plate04 of Run1. (B) Summary of processed plates following MARS-Seq pipeline and number of cells that were used for analysis per half-plate after quality control (QC) and doublet exclusion. (C) Projection of the dataset after merging and dimensionality reduction with Uniform Manifold Approximation and Projection (UMAP). Upper panel shows the different sequencing runs and lower panel shows the different processed plates.

Next, we clustered the cells using nearest-neighbour graph (SNN) and random walks method (Pons and Latapy, 2006) and identified 13 well-defined cell states or clusters among the cells which were annotated as followed: erythroid progenitors 1, 2 and 3 (pEry1, pEry2, pEry3); megakaryocytes 1 and 2 (Mk1 and Mk2); megakaryocyte progenitor (pMk); erythromyeloid progenitors 1 and 2 (EMP1, EMP2); mast cell (MC); mast cell progenitor (pMC), erythromyeloid progenitor (EMP); granulocyte/monocyte progenitor (GMP); macrophage progenitor (pMf); and macrophage (Mf) (Figure 9) Clusters were annotated on the basis of the expression of lineage specific genes (Figure 9B) and of differentially expressed genes of each pairwise comparison (Figure 10).

EMP1 and EMP2 did not express specific lineage genes although they were distinct from each other. EMP1 expressed high Pu.1 (*Sfpi1*) and C/EBP-β (*Cebpb*) and no *Gata1*. EMP2 expressed higher levels of Gata2 and low levels of *Gata1*, together with lower expression of *Cd34* and *Sfpi1*, suggesting an erythroid-biased erythromyeloid progenitor. They both expressed *Notch1* and *Gpr56* (not shown).

Erythroid progenitors (pEry1, 2 and 3) progressively acquired erythroid-specific genes. pEry1 significantly expressed *Gata1* and *Gata2* and lower levels of *CD34*. pEry2 had lost the expression of *Gata2*, but acquired more *Klf1* and erythropoietin receptor (*Epor*). By pEry3, the expression of haemoglobin genes such as *Hba-a1* was evident (Figure 9B).

Megakaryocyte progenitor (pMk) expressed key megakaryocyte genes such as *Rap1b*, integrin subunit Beta 3/CD61 (*Itgb3*), Integrin subunit alpha 2b/CD41 (*Itgba2b*) and thrombospondin (*Thbs1*). pMk differed from fully mature megakaryocytes (Mk1 and 2) in that it expressed megakaryocytic genes at a lower level and retained expression of progenitor genes such as *Kit* and *Gata2* (Figure 9B).

A Clustering

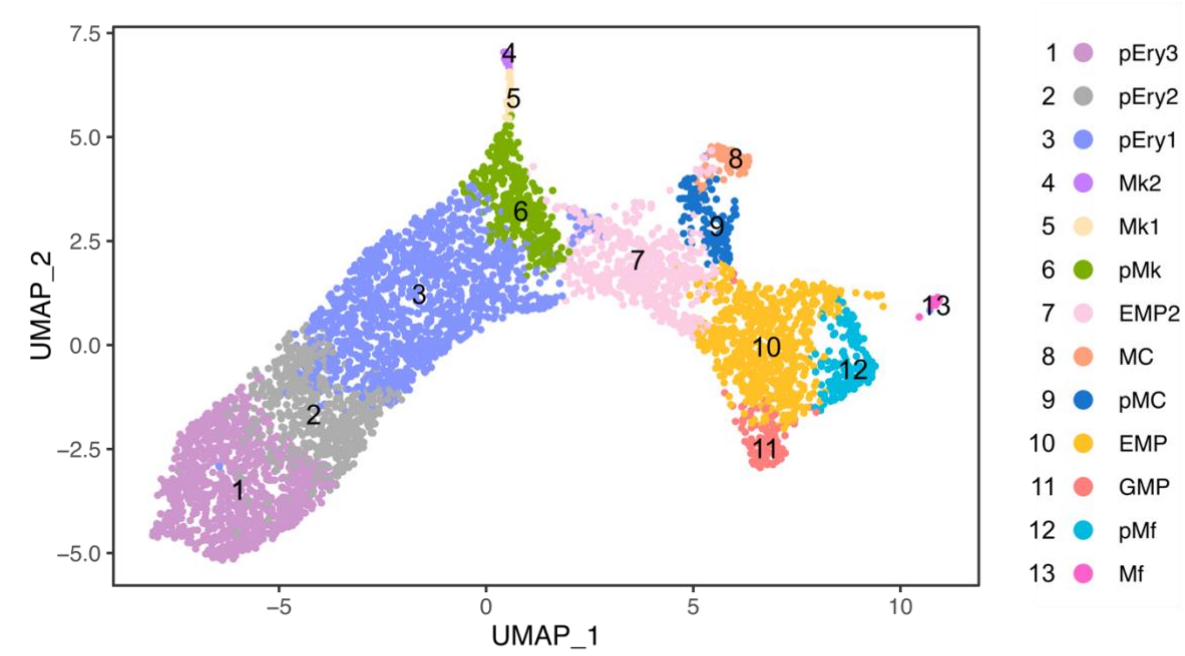

B Lineage genes

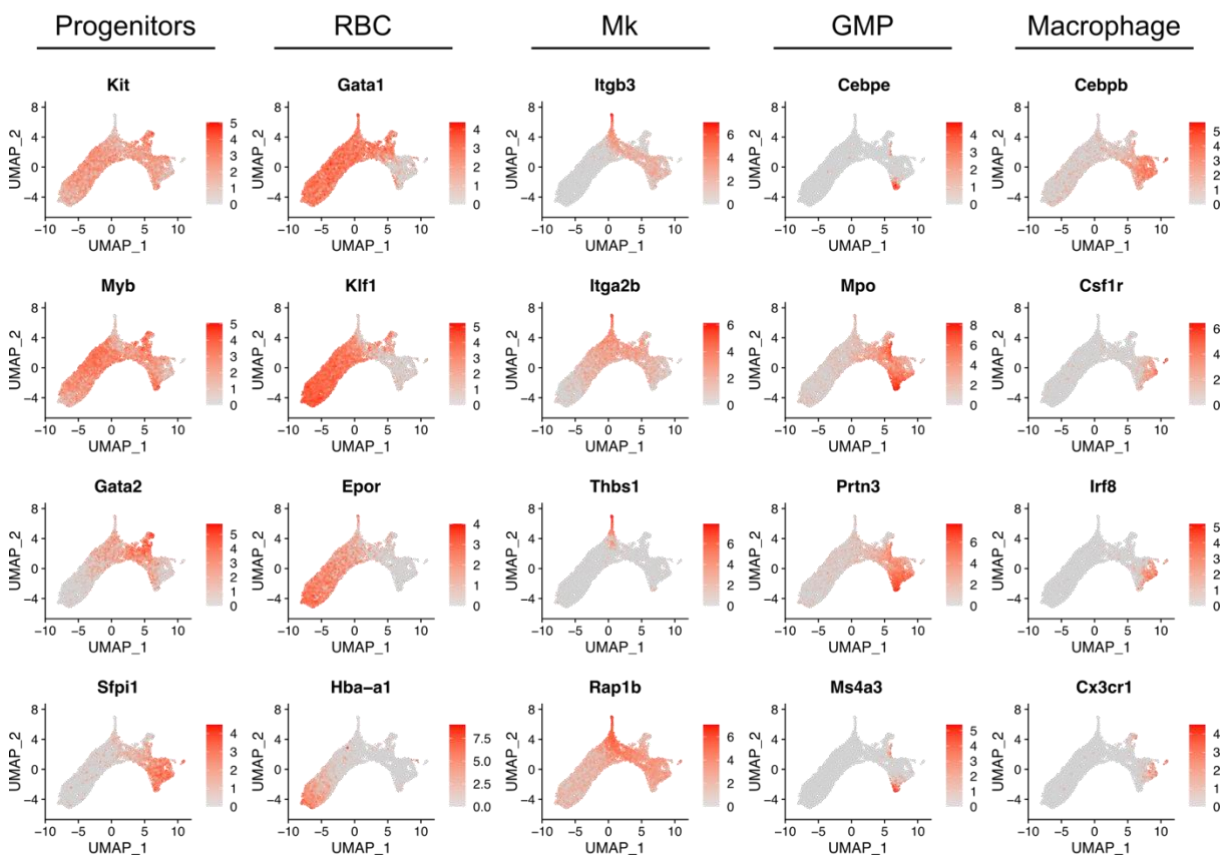

Figure 11. Distribution of clusters in the UMAP and expression of manually picked genes. (A) Clustering is shown in UMAP representation. (B) Expression of manually picked lineage genes in UMAP.

Genes are divided in five columns, depending on the gene type. RBC, red blood cell; Mk, megakaryocyte; GMP, Granulocyte/Monocyte progenitors.

The cell cluster annotated as GMP, for Granulocyte/Monocyte progenitors, expressed *Cd34* and PU.1 (*Sfpi1*), as the other myeloid progenitor cells. These cells expressed low levels of the CCAAT/enhancer binding protein (C/EBP)-β (*Cebpb*), but high levels of myeloperoxidase (*Mpo*). Further, they are the sole cells expressing C/EBP-ε (*Cepbe*), which could be indicative of neutrophil differentiation. They also expressed neutrophil granule proteases such as proteinase 3 (*Prtn3*), elastase (*Elane*) and cathepsin G (*Ctsg*) (*Prtn3* shown in Figure 12B as example) and the proteinase inhibitor *Serpinb1a* was also significantly more expressed in this cluster. Additionally, we detected in this cluster membrane spanning 4-domains A3 (*Ms4a3*), which has been recently proposed to be a distinct marker for early myeloid progenitors in the adult bone marrow (Liu et al., 2019). Granule proteoglycan serglycin (*Srgn*), marker of granulocyte and mast cell, was significantly expressed in both GMP and MC clusters. While we termed this cluster GMP in accordance to current consensus from adult myeloid progenitors, it did mostly express granulocyte genes and no “monocyte” genes (or at very low level), such as *Csf1r* or *Cx3cr1*.

Macrophage progenitors (pMf) were annotated on the basis of their high expression of Colony Stimulating Factor 1 Receptor (*Csf1r*), Interferon Regulatory Factor 8 (*Irf8*) and C-X3-C Motif Chemokine Receptor 1 (*Cx3cr1*). Together with EMP1, they expressed higher levels of C/EBP-β (*Cebpb*) and Myocyte Enhancer Factor 2C (*Mef2c*)(Schüler et al., 2008) than the GMP cluster, which is indicator of monocyte and macrophage differentiation. pMf progenitors, together with pMk, expressed lower levels of *Myb* compared to GMP, pMC and pEry.

Heatmap of top 3 DEG

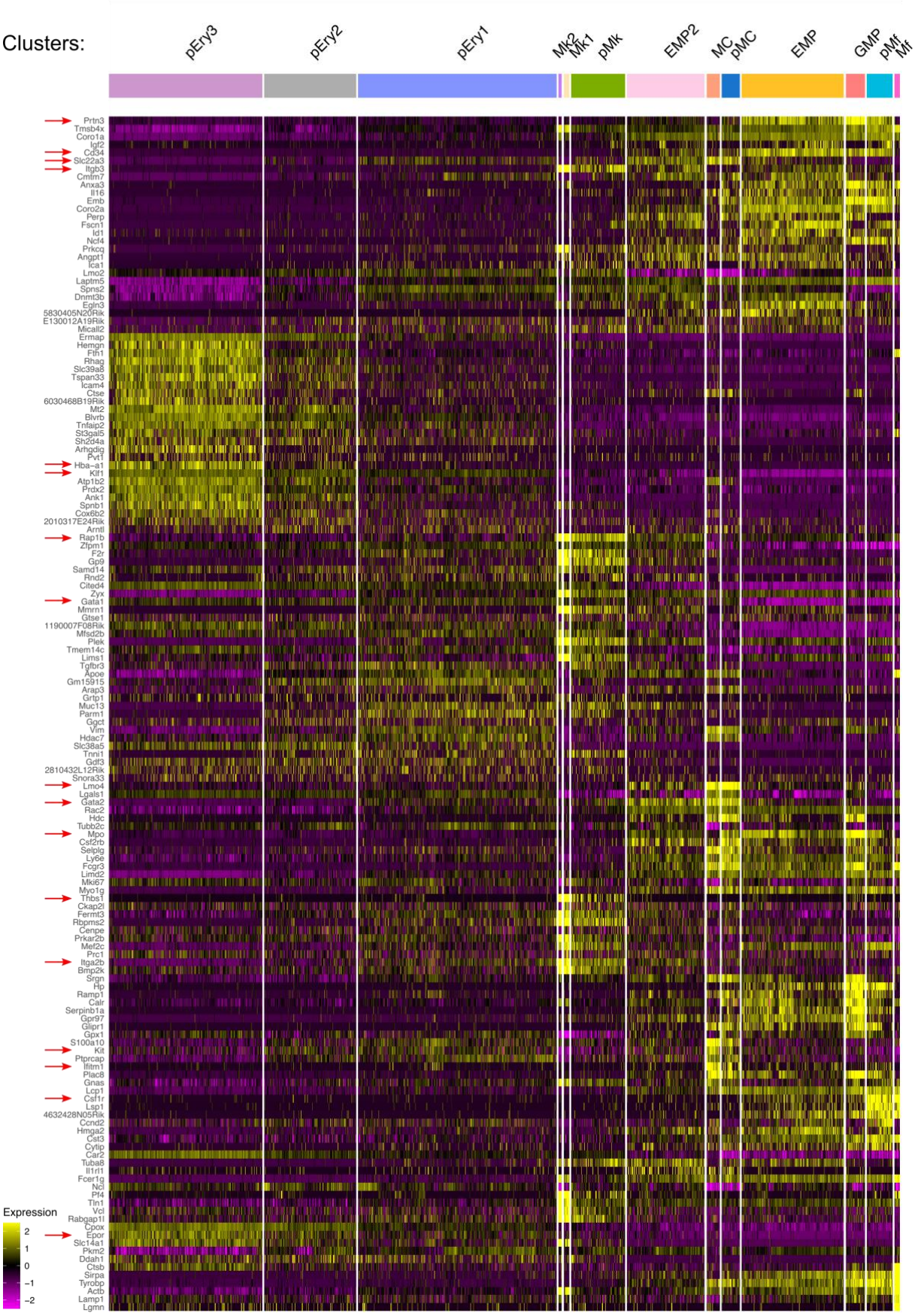

Figure 12. Heatmap displaying the top three differentially expressed genes in each pairwise comparison (ordered by p-value, always less than 0.01) used for clustering with shared nearest-neighbor graph (SNN) and random walks method (FAST-MNN). Modularity was set to k=11. pEry1-3, erythroid progenitor 1-3; pMk; megakaryocyte progenitor; EMP2, erythromyeloid progenitor 2; MC, mast cell; pMC, mast cell progenitor; EMP, erythromyeloid progenitor; GMP, granulocyte/monocyte progenitor; pMf, macrophage progenitor; Mf, macrophage. Red arrows point towards genes mentioned in the text.

Mast cell clusters (pMC and MC) were annotated based on the higher expression of *Kit*, *Gata1* and *Gata2*, as well as expression of mast cell- specific genes: organic cation transporter 3 (*Slc22a3,* histamine and organic cation transporter), interferon induced transmembrane protein 1 (*Ifitm1*) and integrin alpha-4/beta-7 (*Itgb7*) (Figure 13A). High expression of *Lmo4* was also found to be a marker of pMC and MC in the dataset. MC cluster also showed lower number of expressed genes, which is generally a marker of differentiated cells when compared to progenitors(Banerji et al., 2013; Gaspar-Maia et al., 2011) (Figure 13B). Further, MC cells were mostly in the G1 cell cycle phase, together with mature Mk2 and a part of mature Mf (Figure 13C). Collectively, these characteristics of the MC cluster pointed to a set of differentiated mast cells or mast cell precursors produced early by EMP hematopoiesis.

Finally, we analysed the contribution of the different sorted conditions, defined by stage and tissue, to the clusters (Figure 14). As previously observed, E9.5 YS solely contained undifferentiated EMPs (EMP1 and EMP2), macrophage progenitors (pMf) and megakaryocyte progenitors (pMk). E10.5 YS contained in addition more myeloid progenitors, some in the GMP cluster, mast cell progenitors and early erythroid progenitors.

E10.5 FL was the main source for pEry1 and pEry2 (Figure 14B), while it barely contributed to EMP and myeloid progenitor compartments (GMP and pMf). They also contributed to pMC and pMk and low number of cells were found in EMP2. Interestingly, E10.5 FL did contribute significantly to mature Mf, and co-clustered with E10.5 YS counterparts. This

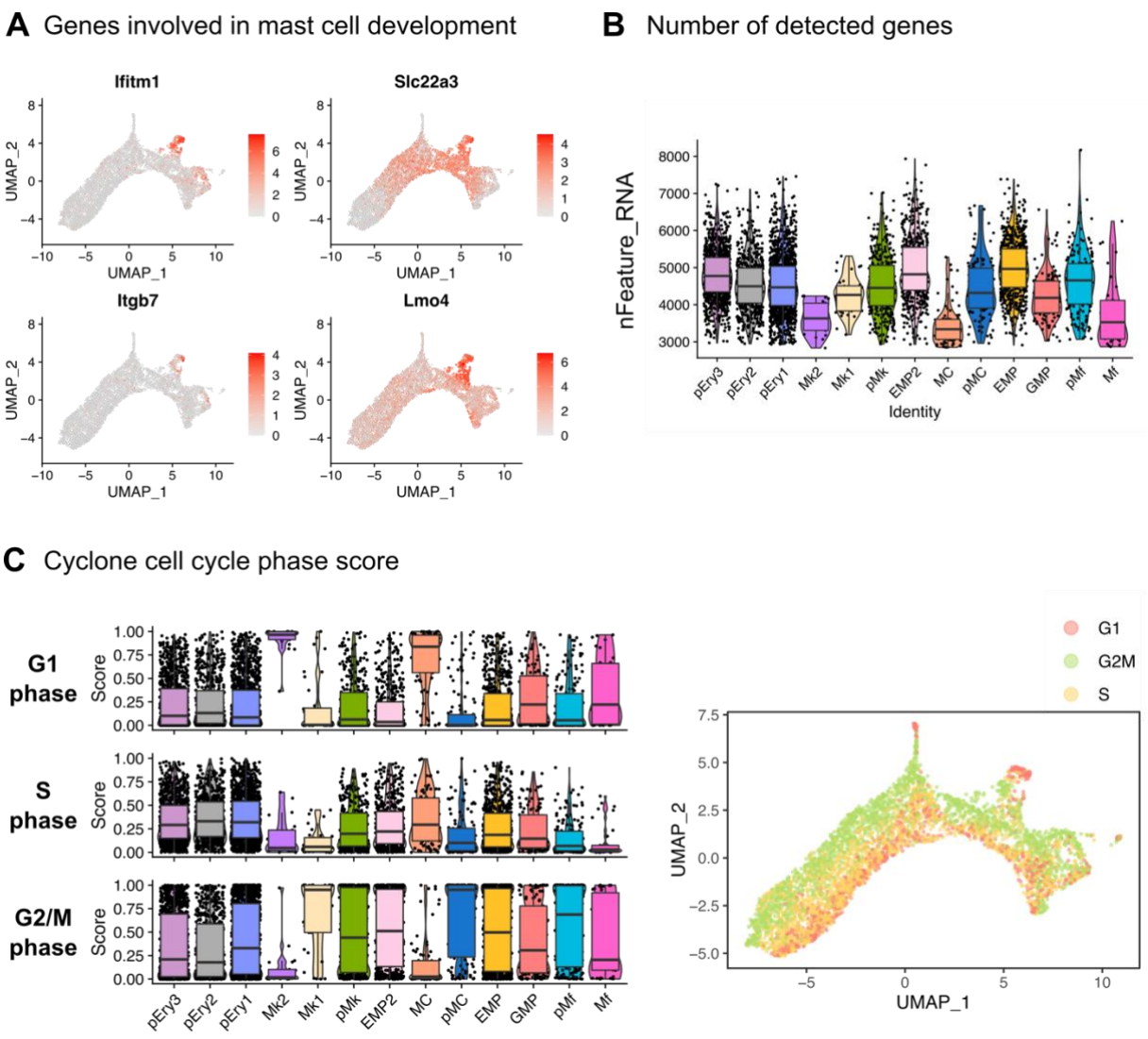

Figure 13. MC cluster has differentiated mast cell characteristics. (A) Expression of mast cell differentiation associated genes in UMAP representation. (B) Number of genes detected per cell in each cluster. Mk1, Mk2, Mf and MC express less genes than progenitor cells. (C) Cell cycle phase score given by cyclone across clusters (Right) shows that MC is uniquely in G1, together with terminally differentiated Mk, while pMC is mostly in mitotic state. (Right) Cell cycle phase was annotated and represented in the UMAP. Although G1 and S cells were found in all clusters, MC is composed only of cells in G1.

could be consequent to a technical limitation of the MARS-Seq pipeline (lack of gene detection), or it could indicate that FL E10.5 macrophages might be circulating macrophages coming from the yolk sac that just seeded and did not significantly change gene expression profile in response to their new niche. The low number of cells available (11 from the YS and 23 from the FL) unfortunately did not allow us to conclude further. E12.5 FL contribution offered

a complementary inverted picture to E10.5: undifferentiated cells were barely present when compared to the large amount of committed cells, as late erythroid progenitors pEry3, mast cells (MC) and GMPs.

This dataset clearly suggested that EMP commitment and differentiation was not only time-specific but also niche-specific. The YS niche favoured exclusively Mk and Mf differentiation at early stages, while early erythroid and broad myeloid fate (pMC, GMP and pMF) were only evidenced a day later there. In the FL, Mk differentiation was mainly observed at E10.5. However, macrophage differentiation (pMf) is almost virtually absent from the FL, regardless of the stage, and it thus appeared as if macrophage differentiation from early pulsed EMP was YS-specific.

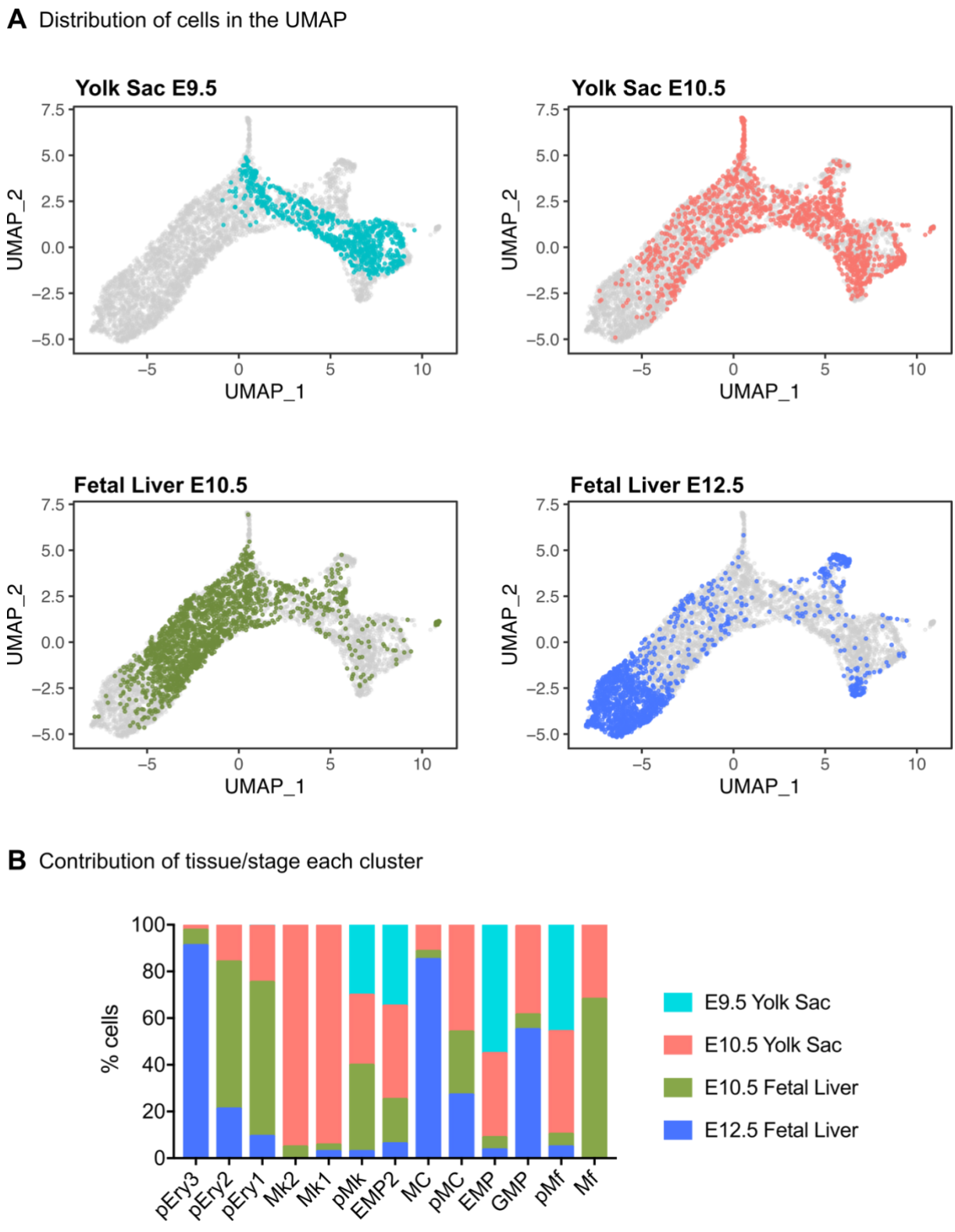

Figure 14. Contribution of embryonic stage and niche to the cell clusters. (A) Distribution of the cells per each condition in the UMAP: E9.5 YS, E10.5 YS, E10.5 FL and E12.5 FL. (B) Quantification of the contribution of each condition to the clusters, showing percentage of cells in each cluster.

DISCUSSION

The contribution of different embryonic hematopoietic waves to the hematopoietic system of the embryo and adult is a fascinating field of research. Several studies over the past decade have demonstrated that EMPs, although a transient population of progenitors, are essential to ensure fetal survival (Chen et al., 2011), as they give rise to the first burst of definitive erythrocytes and to the first set of definitive myeloid populations of the embryo (Gomez Perdiguero et al., 2015; McGrath et al., 2015a). Importantly, EMPs are also the origin of some adult resident myeloid populations, as they have been shown to give rise to tissue resident macrophages (Gomez Perdiguero et al., 2015; Hoeffel et al., 2015), and to some tissue mast cells (Gentek et al., 2018a; Li et al., 2018). These myeloid subsets are able to self-renew in their tissue of residency, without contribution from HSC-derived hematopoiesis in steady-state.

Yet, little is known about the differentiation pathways that EMPs undertake during their existence, as well as the extent of their contribution to the developing embryo. In the course of my PhD, I aimed to decipher the spatio-temporal differentiation dynamics of EMPs throughout embryonic development.

In this section, I will discuss the results we obtained on the phenotype of yolk sac definitive MEPs, on the novel direct pathway of megakaryopoiesis I identified in the yolk sac and on the macrophage and mast cell differentiation from EMPs. Finally, I will discuss the observed differences of EMPs that emerged at E8.5 and at E9.5.

1.- Phenotype of yolk sac definitive MEPs

An initial objective of the project was to identify the phenotype of EMP-derived progenitors. In this study, we showed a distinct phenotype of MEP progenitors produced in the yolk sac by EMPs.

We showed that these MEP progenitors can be isolated within Kit+ CD41+ CD34^{neg} cells and further subdivided into populations C and D following downregulation of CD45. They first appear at E9.5 (C, 79.22 ± 20.23 sem; D, 72.97 ± 21.41 sem) and are more abundant at E10.5 (C, 262.49 ± 54,36 sem; D, 153.39 ± 22.86 sem). This is in accordance with the previous observation of BFU-E and CFU-E producing progenitors starting at E9.5 in the yolk sac, preceding the fetal liver (Palis et al., 1999). The analysis of scRNA-Seq Kit+ CD41+ cells in *Csf1r*^{MeriCreMer} *Rosa*^{YFP} embryos, pulsed at E8.5, confirmed that cell populations losing CD34 and CD45 gradually enriched in more terminally differentiated erythroid progenitors. Erythroid clusters were composed of B, C and D cells, displaying a continuum of differentiation along the trajectory. It is important to note that both C and D, although mostly erythroid, contained cells in the clusters of megakaryocyte progenitors, and that the culture of these cells gave rise to both RBC and Mk. Thus, these populations have not yet committed fully to red blood cells production. The observation of CD34 downregulation is consistent with the phenotype of MEP potential in the bone marrow and the fetal liver (Akashi et al., 2000; Traver et al., 2001). Additionally, the loss of CD45 has been very recently reported to be a signature of EMP-derived MEPs in the fetal liver (Soares-da-Silva et al., 2020).

Csf2rb/CD131 as a marker of early MEP commitment in the yolk sac

The pairwise statistical comparison of E9.5 and E10.5 MEP-committed progenitors in the scRNA-Seq dataset was performed to resolve Ery/Mk pathways of differentiation, after the observation that E9.5 and E10.5 cells segregated inside the MEP cluster and contributed differently to the trajectories of megakaryocyte and erythrocytes. *Csf2rb* was found to be expressed 2.4 fold more in E10.5 cells and it was expressed higher in those cells when compared to other clusters. Since this gene encodes for the common β chain of the high affinity receptor subunit CD131, we investigated the phenotype and colony forming potential of the cells expressing CD131 at their surface. This led us to conclude that CD131 was a marker of MEP commitment that was situated upstream of CD34 loss.

CD131 is the common β chain of the granulocyte-macrophage colony-stimulating factor (GM-CSF/CSF2), interleukin-3 (IL-3) and interleukin 5 (IL-5) receptors. Each of the three receptors is a heterodimer comprising a cytokine-binding α chain, and a common β chain (βc/CD131) that converts the low-affinity interaction between ligand and α chain to one of high affinity (Scott and Begley, 1999). It is involved in the differentiation and survival of progenitor cells and the growth and differentiation of myeloid cells and megakaryocytes.

A recent publication using scRNASeq proposed that CD131 expression in a subset of human CMPs marks progenitors that were able to specifically generate megakaryocytes, erythroid cells and *Gata1*-expressing myeloid cell types (basophils/mast cells and eosinophils), but not monocytes or neutrophils. They designated CD131+ CMPs as EMPP (erythroid/megakaryocyte-primed MPP) and also found CD131 expression in the MEP compartment (Drissen et al., 2019). However, the mechanism governing this remains unknown.

A possible explanation for these results may reside in the interaction of CD131 with erythropoietin receptor (EpoR), since it is expressed early during MEP commitment. It has been suggested that CD131/EpoR heterodimer regulates cellular stress responses in mesenchymal cells of different tissues through alternative erythropoietin (EPO) signalling (Bohr et al., 2015; Brines et al., 2004; Leis et al., 2004). However, the interaction of EpoR and CD131 is not yet clear and rather controversial. A recent report claimed that the biophysical interaction of the two proteins does not occur with EPO (Cheung Tung Shing et al., 2018). On the other hand, a recent screening of artificial transmembrane protein aptamers, extremely short proteins designed to bind to transmembrane proteins, demonstrated that the combination of the transmembrane domain and JAK2-binding sites of the EpoR with the transmembrane and cytoplasmic domains of CD131 induced cell proliferation when activated by EPO (He et al., 2019).

Another possible explanation would be in the GM-CSFR/CSF2R complex itself, since it is known that GM-CSF stimulates the maintenance of multipotential progenitor cells, the initial proliferation of progenitors of the erythroid, eosinophil, and megakaryocyte lineage, as well as mature cells of the granulocyte/monocyte lineage (Burgess and Metcalf, 1980). Indeed, single cell cloning studies showed that GM-CSF could stimulate at least five divisions of cells that subsequently formed mixed or pure erythroid, eosinophil, or megakaryocyte colonies but that it was not required for the terminal cell divisions in these pathways (Metcalf et al., 1980). Interestingly, human GM-CSF does supports terminal maturation of erythrocyte colonies in the absence of EPO (Nishijima et al., 1997).

Since CD131 is only expressed early during MEP commitment but is downregulated in pEry1 and pMk1 cell clusters, is it possible to hypothesize that CD131 is involved in the proliferation of the progenitors before their maturation via EPO, GM-CSF or another ligand that could activate the receptor signalling cascade. CD131 upregulation could be part of the differentiation process of MEP-biased progenitors in order to proliferate, or it could be the result of a stochastic expression of CD131 in EMPs, which in turn biases their differentiation towards MEP differentiation.

2.- EMP-derived megakaryopoiesis

The fate-mapping of *Csf1r*^{MeriCreMer} *Rosa*^{YFP} embryos combined with the deletion of *Myb*, a key transcription factor for definitive erythropoiesis, showed that EMPs produce megakaryocytes in the yolk sac that do not transit through a CD131+ MEP stage. Also, it demonstrated that MEP-independent differentiation occurs rapidly after EMP emergence, since yolk sac megakaryocytes were practically only labelled when the OHT pulse was given at E8.5.

These results share similarities with the observation of (i) Mk-primed HSC (vWF+ CD150+) that are placed at the top of the differentiation tree and that directly differentiate into

Mk (Sanjuan-Pla et al., 2013), and (ii) HSC and MPP priming towards megakaryocytes that has been observed in single cell studies combining clonal studies with gene expression analysis (Rodriguez-Fraticelli et al., 2018). Additionally, Mk-primed HSC have been shown to occupy a distinct niche in the bone marrow and to be regulated by megakaryocytes (Pinho et al., 2018). We currently ignore whether EMP-direct megakaryopoiesis is produced by a phenotypically different subset of EMP or if it emerges in specific regions of the yolk sac vasculature.

As it has been mentioned in the introduction, megakaryocyte potential emerges in the mouse yolk sac at E8 (4-6sp), peaks at E9.5 (Tober et al., 2007) and most embryonic megakaryocytes and platelets are formed after E10.5 (Potts et al., 2014). The distinct phenotype of yolk sac-derived megakaryocytes (Cortegano et al., 2019; Potts et al., 2014), the association of Mk colonies with primitive erythroid colonies at E8-E9 (Tober et al., 2007) and the independence of yolk sac megakaryopoiesis from Myb (Tober et al., 2008) has led to the conclusion that this first wave of megakaryopoiesis is of primitive origin.

Our results raise the possibility that yolk sac megakaryopoiesis is, to a great extent, of EMP origin. Unfortunately, labelling using the *Csf1r*^{MeriCreMer} inducible construct underestimates the contribution of the pulsed EMP progenitors, since only 40% of the progenitors are labelled. Similarly, the inability to label primitive megakaryocytes does not allow us either to resolve their quantitative contribution *in vivo* to megakaryopoiesis.

Regarding the independence from the transcription factor Myb, an initial study reported that no megakaryocyte progenitors were produced in the absence of *Myb*, since both *Myb -/-* CFU assays and ES cell chimeras failed to produce megakaryocytes (Sumner et al., 2000). In contrast, a later report stated that *Myb* depletion did not affect yolk sac megakaryopoiesis specifically (Tober et al., 2008). We could confirm both reports, since the number of megakaryocytes were normal in *Myb*-deficient yolk sacs *in vivo* but we did not observe any megakaryocyte colony development *ex vivo*. One hypothesis to reconcile such conflicting

findings is that Myb might be important in the colony environment during Mk differentiation. In mice with single point mutations in the *c-Myb* gene (Metcalf et al., 2005), *Myb*-disrupted progenitors generated CFU-Mk colonies in regular culture conditions that were distinctively small, containing 2-20 cells per well, when compared to the average colony of 100-200 cells. If this was also the case in the *Myb-/-* mutant, Mk colonies would have been missed by our colony counting method, flow cytometry.

Altogether, these results demonstrate that EMPs can differentiate into megakaryocytes in the yolk sac very rapidly (in 24-48h) and that they do not depend on a MEP intermediate to do so. These results uncover two pathways to produce definitive megakaryocytes: a direct yolk sac-specific pathway that starts at E9.5 directly from EMP progenitors in a *Myb*-independent manner, and a second adult-like pathway, where EMP produce first MEP in the yolk sac in a *Myb*-dependent manner and that terminally differentiate into both erythrocytes and megakaryocytes in the fetal liver.

3.- Production of macrophages by EMPs

Contrary to the observation of sophisticated maturation levels of erythrocyte and megakaryocyte progenitors, the transcriptional analysis of EMP-derived progenitors in the yolk sac showed a distinctively short macrophage differentiation continuum in both E9.5 and E10.5 yolk sac cells. This was embodied by the similarity of EMP1/EMP2 and myeloid clusters in the yolk sac, both containing also A cells (AA4.1+). There are several possible explanations for this result that will be discussed here.

One possible interpretation is that the differentiation of EMPs towards macrophages is very rapid in the yolk sac. This is contrary to a report that performed scRNA-Seq from E9-E10.25 $CD45^{+/low}$ cells, which showed a differentiation continuum from a non-primed EMP through a pMac intermediate towards a differentiated macrophage (Mass et al., 2016). The key difference with our study is that they also sorted all the CD45+ cells, which could support the

idea that Kit downregulation is very rapid during macrophage differentiation and that the following steps are performed through a Kit^{neg} precursor, the pre-mac, that would probably also be responsible for expansion of the macrophage population. In this case, more cells would need to be sorted to observe intermediate progenitor levels, maybe focusing on A and/or $CD131^{neg}$ B cells to enrich in myeloid-biased cells, and adding more Kit^{neg} $CD45^{+}$ cells.

Another possible interpretation is that the technique has an insufficient level of gene detection. A comparative analysis of single-cell RNA sequencing methods found that MARS-Seq had a high probability of gene dropout (fraction of cells with zero counts) and a lower sequencing depth than other methods like Smart-seq, Smart-seq2 and CEL-seq2 (Ziegenhain et al., 2017). A third possible interpretation would be that *bona fide* EMP gene expression is very similar to macrophage progenitor gene profile, which, together with a lower detection capacity, would not allow to properly resolve the two progenitor populations. In order to address this problem, we could resort to use a complementary scRNA sequencing technique such a 10X Chromium, which can now be combined with surface protein detection (CITE-Seq), or perform single cell RT-qPCR in a microfluidic-based platform such as BioMark.

We did, nevertheless, identify a myeloid progenitor cluster (My in the YS analysis, pMf in the analysis of YS and FL) with a higher expression of *Csf1r*, *Cx3cr1* and *Irf8* and a lower expression of *Myb*, which was also observed in the study of Mass and colleagues (Mass et al., 2016).

Macrophage cluster in the single cell analysis

It was interesting to notice a big separation in the UMAP between the My and macrophage (Mf) clusters. This could be, as mentioned before, because intermediate precursors were not sorted. But it could also indicate that the sorted macrophages were of primitive origin. Indeed, the major caveat of *Csf1r*^{MeriCreMer} strain is that committed macrophage progenitors/precursors can recombine independently of their origin, as they also express

Csf1r. Also, within the Mf cluster, macrophages sorted from the E10.5 fetal liver clustered with those of the yolk sac, without any tissue-specific “signature”. This could also be due to a potential primitive origin or another possible explanation is that those cells had just colonized their tissue or were still in the internal circulation of the yolk sac and fetal liver, respectively, so they did not acquire yet the tissue-specific characteristics of their niche. Unfortunately, the plates of E12.5 macrophages, monocytes and granulocytes prepared in order to address this further failed in the sequencing step, so we were unable to compare the expression of E12.5 fetal liver myeloid cells with the E10.5 YS and FL macrophages or the different myeloid progenitor subsets identified in the FL.

4. EMP-derived mast cell production

One unanticipated finding of the study was the presence of mast cell-committed progenitors starting from the E10.5 yolk sac, and the large amount of mast cell progenitor (or precursor) numbers in the E12.5 fetal liver.

Both the YS and FL cells from the MC clusters (pMC and MC) expressed genes involved in the differentiation of mast cells, such as *Gata1*, *Gata2*, *Scl22a3* and *Itgb7* (Figure 9-11). However, due to the expression of *Kit* in differentiated mast cells and the lack of mature mast cell gene expression in embryonic mast cells, specially FcεRI (McGrath et al., 2015a), we could not formally conclude on the degree of differentiation of this cluster. Instead, we analysed cell cycle status and the number of genes detected in the cluster to decide between progenitor/precursor and mature mast cells.

First, the cell cycle score given by the Cyclone package showed that 80% of cells in the MC cluster were in cell cycle arrest (G1), thus in favour with more mature differentiated cells. Second, MC progenitors (pMC) cells expressed on average 4500-5000 genes/cell, indicating a higher signalling promiscuity, or entropy, while Mk2, Mf and MC clusters contained around 3500 genes/cell. As a general rule, the low basal expression of a wide range of

developmental transcription factors is a marker of stem and progenitor cells, related to the openness of the chromatin in these cells (Efroni et al., 2008; Gaspar-Maia et al., 2011; Lee et al., 2006), therefore, they can be distinguished from differentiated cells that highly express a lower number of lineage-specific genes and genes implicated in mRNA splicing(Banerji et al., 2013). Of note, signalling promiscuity is now used in computational methods in order to infer the inherent potency of different cells in single cell analysis algorithms like SCENT (Chen and Teschendorff, 2019; Teschendorff and Enver, 2017). Collectively, these findings, associated to the higher expression of mast cell related genes, indicated that the cluster annotated as MC was more terminally differentiated that pMC (MC progenitor) and could therefore contain mast cells and/or mast cell precursors.

The idea that the YS could harbour mast cell precursors was first introduced by Sonoda and colleagues in 1983 (Sonoda et al., 1983). They showed that the injection of E9.5 or E11 yolk sac cells directly into the skin of adult mice produced mast cells that could be observed in the skin 5 months after the graft, at a higher efficiency than the fetal liver cells of the same stages. In the fetal liver, the number of cells with mast cell potential explode from E11.5 to E17.5 (Gentek et al., 2018a; Sonoda et al., 1983), which could be explained with the big contribution of E12.5 EMP-derived cells to the more differentiated MC cluster in our dataset.

Differentiation hierarchy of mast cell progenitors

Mast cell clusters (pMC and MC) are found adjacent to MEP in the UMAP, which could suggest that they share a differentiation trajectory or just be the consequence of similar expression of Gata1 and Gata2 gene sets, among others, during differentiation. This adjacent clustering has already been observed for mast cell progenitors in several single cell expression studies. A novel megakaryocyte-erythroid-mast cell (MEMP) progenitor has been proposed from human FL scRNA-seq analysis (Popescu et al., 2019), just based on UMAP proximity and force-directed graph (FDG) inferred-trajectory analysis, but without any functional validation. Similarly, mast cell and basophil potential within the CMP population has been

observed to be more correlated to MEP-biased CMPs than to granulocyte/monocyte-biased CMPs (Drissen et al., 2019; Franco et al., 2010), suggesting that mast cells could be generated in the course of MEP differentiation. Other studies have claimed that the potential to give rise to pure mast cell colonies in the bone marrow resides only in GMPs, through a bipotent basophil/mast cell progenitor (Arinobu et al., 2005; Iwasaki et al., 2006; Qi et al., 2013). Unfortunately, since we could not distinguish basophil progenitor signature in our dataset and we did not evaluate mast cell potential in the CFU-assays, we are not able yet to conclude on this matter.

5. Similarities and differences between EMPs emerging at E8.5 and at E9.5

Phenotype of bona fide EMPs in the yolk sac

EMPs had been characterised as Kit$^+$ CD41$^+$ CD16/32$^+$ cells at E9.5 by McGrath and colleagues (McGrath et al., 2015a) and as Kit$^+$ CD45^{low} AA4.1$^+$ cells from E9 to E10.5 (Bertrand et al., 2005a; Gomez Perdiguero et al., 2015). As for the latter, AA4.1 expression during development is found in vascular endothelial cells, aorta-associated hematopoietic clusters and fetal liver hematopoietic progenitors (Petrenko et al., 1999) but its function in not known. Indeed, CD45$^{neg/low}$ Kit$^+$ AA4.1$^+$ cells were enriched mostly for multipotent cells with LTR activity, or HSC, in the E10.5 AGM (Bertrand et al., 2005a) and for erythromyeloid progenitors in the E9 and E10.5 YS (Bertrand et al., 2005a; Gomez Perdiguero et al., 2015). I thus performed an unbiased approach of high parameter flow cytometry and scRNA-Seq analysis of Kit+ CD41+ cells using AA4.1, CD34 and CD45 fluorophore-conjugated antibodies.

While CD16/32-defined EMPs were found all across the EMP differentiation spectrum, including certain erythroid-committed progenitors, AA4.1-defined EMPs (named population A in this study) were relatively homogeneous at the gene expression level, and expressed *Pu.1* but not *Gata1*. Among YS progenitor populations, AA4.1-defined EMPs were the first to appear, between E8 and E8.75, and subsequently gave rise to the other progenitor

populations. Therefore, this study confirms that AA4.1 is a marker of early emerging EMPs that is rapidly downregulated in 24 hours as EMPs advance in the differentiation process. Careful analysis of differentially expressed genes (DEGs) in the scRNAseq dataset has not allowed us thus far to identify (and test) novel surface markers for EMPs, which could dramatically improve our toolset for EMP studies.

Observation of "early" and "late" emerging EMPs

The different output observed between E8.5 and E9.5 OHT-pulsed progenitors in *Csf1r*^{MeriCreMer} *Rosa*^{YFP} embryos raises interesting possibilities. The differences and similarities have been summarised in Table 2.

EMP that were pulsed with *Csf1r*^{MeriCreMer} at E8.5 had different potential *in vivo* than the ones pulsed at E9.5. EMPs pulsed at E8.5 gave rise to a rapidly maturing wave of MEP-independent megakaryocytes and to erythroid progenitors that generated millions of red blood cells that were exhausted by E14-15 in the FL. The pulse at E9.5, on the other hand, seemed to give rise to a more classical pathway of differentiation, in which megakaryocytes are produced in the FL together with red blood cells. The maintenance of EMP-derived progenitors in the fetal liver for a longer period of time suggests that more undifferentiated progenitors colonize the FL in this wave.

The differences between the two pulses could be explained (i) by a temporal specialization of progenitors in the yolk sac, in response to changes in the hematopoietic niche over time, or due to different signals provided by the microenvironment through the emergence in different locations (cell extrinsic hypothesis), or (ii) by the emergence of two waves of EMP progenitors (cell intrinsic hypothesis). Indeed, as commented in the literature review, the vascular niche is very different at E8.5 and E9.5, since the vascular plexus is being remodeled into a network of blood vessels and arteries, and could harbor different local microenvironment along the remodelling procedure.

	OHT E8.5	OHT E9.5
Similarities	They give rise to cells of the erythromyeloid lineages	
	They label population A, which differentiates in 24 hours	
	They produce erythrocytes in the liver three days after pulse and release them to circulation in five days	
	AA4.1+ cells of E9.5 and E10.5 YS (pulsed at E8.5) did not cluster separately in scRNASeq analysis	
Differences	40% maximum of progenitor labelling	10% maximum of progenitor labelling
	Labels YS population D at E10.5	No YS D labelling is observed
	Labels YS specific MEP-independent Mk production	Mk production is mostly localized in the FL
	Labels a wave of large erythrocyte production that exhausts rapidly	Labels a wave of erythrocyte production that is maintained longer
	YFP+ FL progenitors are rapidly exhausted	YFP+ FL progenitors are maintained for a longer time
	No labelling of LSK	No labelling of LSK, although 1-1.5% in some litters

Table 2. Comparison of the results obtained in *Csf1r*^{MeriCreMer} *Rosa*^{YFP} embryos pulsed at E8.5 or E9.5. Population A was defined as AA4.1^{+} CD34^{+} CD45^{+}; population D as AA4.1^{neg} CD34^{neg} CD45^{neg} CD71^{+}; YS, yolk sac; FL, fetal liver; MEP, megakaryocyte/erythrocyte progenitors; LSK, Lin^{neg} Kit^{+} Sca-1^{+}.

The existence of two waves of EMP potential was claimed by Hoeffel and colleagues in 2015 (Hoeffel et al., 2015). In their study, they reported that EMP emerging at E7.5 were expressing *Csf1r* but not *Myb*, and gave rise to yolk sac macrophages and microglia. They denominated this wave “early” or “primitive” EMPs, due to the possibility that it embodied primitive macrophage precursors. On the other hand, they reported a wave of “late” or “definitive" EMPs that expressed *Myb* but not *Csf1r*. To set the stages for each EMP wave, they used the OHT induction timing from *Runx1*^{MerCreMer} (E7.5, E8.5 or E9.5) and they assumed that the *Runx1*^{MerCreMer} OHT E7.5 pulse corresponded (i.e. labelled the same cells) to the *Csf1r*^{MeriCreMer} E8.5 pulse. To our knowledge, no erythromyeloid potential has been observed in the literature in progenitors emerging at E7.5 (Gomez Perdiguero et al., 2015; McGrath et al., 2015a; Palis et al., 1999), therefore there are not “early” EMPs that could emerge that early (E7.5). Further, the authors did not assess themselves for erythromyeloid potential in the different stages or pulses (by CFU assays and/or quantifying red blood cell labelling). The confusion is likely explained by the fact that *Runx1* labels endothelial cells with hemogenic potential at E7.5, but not directly emerging progenitor cells at this stage (Samokhvalov et al., 2007).

A note of caution is due here also, since the *Csf1r*^{MeriCreMer} strain was generated by a classical additive transgenesis, and it is not a knock-in like the *Runx1*^{MerCreMer} or *Kit*^{MerCreMer} strains, thus the expression of the Cre may not fully recapitulate endogenous expression of *Csf1r*. However, all E8.5 *Csf1r*+ labeled cells in *Csf1r*^{iCre} embryos expressed the Csf1r protein, as did most, but not all, of the E9.5 cells, indicating that some EMP-derived cell did lose *Csf1r* expression as they differentiated (Kasaai et al., 2017). This observation contradicted the study by Hoeffel an colleagues, which stated that no Csf1r protein was expressed by Kit+ CD41+ cells at E9.5 (E8.5 cells were not tested), although some mRNA was expressed at E9.5 and even less mRNA was found at E10.5 using Csf1r-GFP mice as a proxy for gene expression (Hoeffel et al., 2015). Similarly, they found that more Myb mRNA was found in E10.5 Kit+ CD41+ cells compared to E9.5 cells (again, E8.5 cells were not tested).

Our study offers an explanation for the observation of a decrease in *Csf1r* expression and an increase in *Myb* expression in Kit+ CD41+ progenitor cells over time when sorted as bulk. This is, in fact, due to an increase of progenitor heterogeneity in the yolk sac, and in particular the large production of yolk sac MEP progenitors, which express high levels of *Myb* and no *Csf1r*. Therefore, if two waves of EMP exist, expression of *Csf1r* or *Myb* at the EMP level is most probably not a distinctive marker of each wave.

The reason why the labelling efficiency is different between the two pulses is not yet clear. One possibility is indeed that the EMPs emerging from E8.5 to E9.5 are expressing higher levels of *Csf1r* transcript than the ones emerging from E9.5 to 10.5. A second possibility is that more EMPs are emerging from E8.5 to E9.5 than later. A third possibility involves the pharmacological kinetics of OHT in utero.

As for the first possibility, it is fundamental to assess the levels of *Csf1r* and other interacting factors by single cell qPCR, i.e. using the BioMark technology. Regarding the second possibility, the maximum number of A and B (putative *Csf1r*+ expressing cells) was found at E9.5, which is consistent with the maximum number of clusters in the yolk sac found by Frame and colleagues (Frame et al., 2016). We thus do not observe a decrease in EMP production that would explain the results. Finally, it is important to notice that the lack of fine understanding on the precise pharmacological kinetics of OHT in utero makes it very difficult to conclude, as OHT induced recombination in time may not follow a symmetrical Gaussian distribution, which could severely impact on the interpretation of such close-by pulses.

In any case, in order to assess the intrinsic hematopoietic potential of the two EMP waves single cell clonal analysis should be performed. First, colony forming assay (CFU) from EMPs at E8.5 and E9.5 should be performed to verify the potential of the progenitors *ex vivo*, in a controlled environment. Alternatively, we could verify the potential of E8.5 versus E9.5 pulsed AA4.1+ progenitors at E10.5. Second, we could take advantage of novel cell barcoding technologies such as the *PolyloxExpress* barcoding recently developed by Pei and colleagues

(Pei et al., 2020). This system combines lineage tracing and single progenitor cell barcoding (single cell fate) with single cell RNA-Sequencing (transcriptomics of the produced cells), and could be fundamental to observe the dynamics of differentiation *in vivo* of the two pulses in the yolk sac and the fetal liver. Ideally, it would resolve the question on whether E8.5 cells tend to have a uni-lineage potential compared to E9.5 cells, and would particularly resolve the input of MEP-independent or dependent megakaryopoiesis to the pool of labelled megakaryocytes.

Once the inherent potential of the two pulses is characterised, a greater focus on the location of the different emerging progenitors in the yolk sac (arterial/venous or distal/proximal vasculature) could produce interesting findings that could account for the specifications of each wave.

Altogether, we evidenced that EMPs with different *in vivo* potential exist in the embryo, either corresponding to the emergence of two distinct waves of EMP progenitors or as a result of a temporal specialization of progenitors in the yolk sac, in response to changes in the signals provided by the niche over time. Several questions remain unanswered at present and further work is required to establish the identity of the progenitors emerging at E8.5 or E9.5.

CONCLUSION

The purpose of my thesis was to decipher the spatio-temporal differentiation dynamics of erythromyeloid progenitors (EMP) and to characterize the phenotype of EMP and EMP-derived progenitors throughout development. In order to do so, we embarked upon an extensive characterization of EMP and EMP-derived progenitors using high parameter flow cytometry, fate mapping approaches and single cell expression analysis. In particular, we focused on their niche of origin, the yolk sac (YS), where we resolved the heterogeneity of EMP-derived progenitors and demonstrated the existence of a direct pathway of definitive megakaryopoiesis.

First, we observed the segregation of four different EMP-derived progenitors in the E10.5 yolk sac, based on AA4.1, CD34 and CD45 expression, which are distinct at a potency and gene expression level, and identified among them AA4.1^{+} CD34^{+} CD45$^{low/+}$ as a marker of bona fide EMPs.

Second, we identified the intermediate steps in the erythroid/megakaryocyte pathway, thanks to a cell surface marker identified with the scRNA-seq analysis, CD131, which was upregulated between E9.5 and E10.5. We validated this marker in functional assays and demonstrated that CD131 is a marker of early megakaryocyte/erythrocyte progenitor (MEP) commitment, that is expressed before the complete downregulation of CD34 and CD45 in late MEP.

Additionally, the combination of *Myb* deficiency with EMP pulse labelling using the *Csf1r*^{MeriCreMer} strain showed that EMPs emerge normally in *Myb-/-* embryos and differentiate directly into megakaryocytes, bypassing yolk sac CD131+ MEP progenitors. Importantly, we showed that this novel direct MEP-independent megakaryopoiesis is part of the unperturbed *in vivo* differentiation dynamics of EMPs, since it was also present in *Myb*-competent embryos,

as evidenced during EMP fate mapping and scRNAseq studies. Therefore, we demonstrated that EMPs can differentiate into megakaryocytes in the yolk sac very rapidly (in 24-48h) and that they do not depend on a MEP intermediate to do so.

Finally, the results in this study indicated that the timing of EMP emergence in the yolk sac could impact its differentiation potential and contribution to the hematopoietic system of the embryo. Yolk sac MEP-independent megakaryopoiesis was produced in a limited time window, as evidenced by the fact that yolk sac Mks were only labeled when EMP were pulsed at E8.5 and not at E9.5. Further, the different labelling dynamics of fetal liver progenitors, and red blood cells particularly, suggested that the cells colonizing this niche had different potential depending on their time of production.

Taken together, the findings of this thesis provide insights into the ontogeny of early embryonic hematopoiesis and specially contribute to our understanding of the hematopoiesis of the yolk sac. As a result, we can build a EMP-lineage tree that embodies yolk sac definitive hematopoiesis (Figure 15).

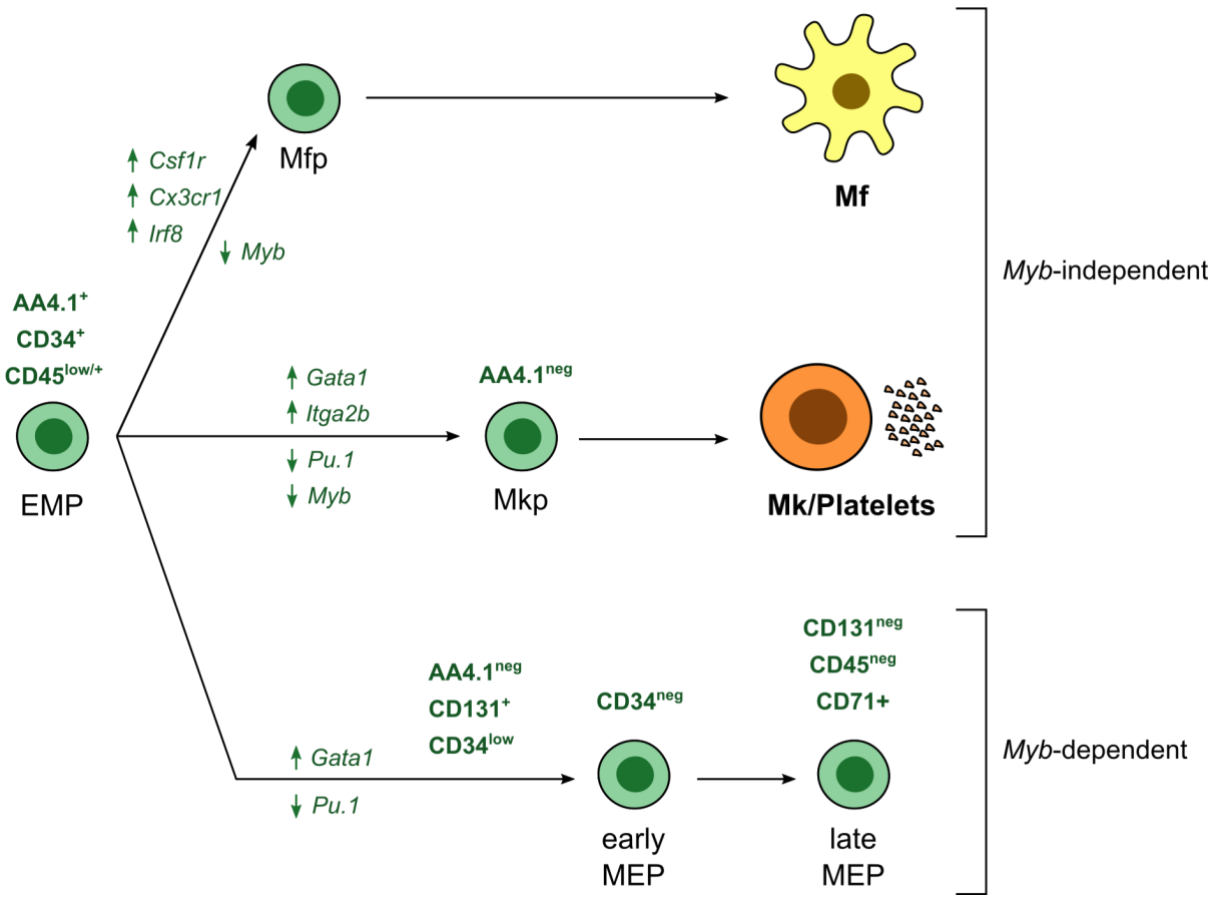

Figure 15. Hallmarks of yolk sac definitive hematopoiesis depicted as a lineage tree. *Bona fide* EMPs are characterised by the expression of AA4.1, and they sequentially give rise to macrophage precursors (Mfp), megakaryocyte precursors (Mkp) and definitive megakaryocyte/erythrocyte progenitors (MEP). EMP give rise both to macrophages and megakaryocytes/platelets in the yolk sac in a *Myb*-independent manner, while MEP differentiation requires *Myb* expression. Cell surface phenotype is shown in bold green, upregulated or downregulated genes are shown in green italics and the green vertical arrows indicate the up or downregulation of the genes in the differentiation steps, illustrated by horizontal black arrows.

REFERENCES

Adamo, L., Naveiras, O., Wenzel, P.L., McKinney-Freeman, S., Mack, P.J., Gracia-Sancho, J., Suchy-Dicey, A., Yoshimoto, M., Lensch, M.W., Yoder, M.C., et al. (2009). Biomechanical forces promote embryonic haematopoiesis. Nature *459*, 1131–1135.

Ajami, B., Bennett, J.L., Krieger, C., Tetzlaff, W., and Rossi, F.M.V. (2007). Local self-renewal can sustain CNS microglia maintenance and function throughout adult life. Nat. Neurosci. *10*, 1538–1543.

Akashi, K., Traver, D., Miyamoto, T., and Weissman, I.L. (2000). A clonogenic common myeloid progenitor that gives rise to all myeloid lineages. Nature *404*, 193–197.

Alberts, B., Johnson, A., Lewis, J., Raff, M., Roberts, K., and Walter, P. (2002). Molecular Biology of the Cell (New York).

Allakhverdi, Z., Smith, D.E., Comeau, M.R., and Delespesse, G. (2007). Cutting Edge: The ST2 Ligand IL-33 Potently Activates and Drives Maturation of Human Mast Cells. J. Immunol. *179*, 2051–2054.

Arinobu, Y., Iwasaki, H., Gurish, M.F., Mizuno, S.I., Shigematsu, H., Ozawa, H., Tenen, D.G., Austen, K.F., and Akashi, K. (2005). Developmental checkpoints of the basophil/mast cell lineages in adult murine hematopoiesis. Proc. Natl. Acad. Sci. U. S. A. *102*, 18105–18110.

Athens, J.W., Haab, O.P., Raab, S.O., Mauer, A.M., Ashenbrucker, H., Cartwright, G.E., and Wintrobe, M.M. (1961). Leukokinetic studies. IV. The total blood, circulating and marginal granulocyte pools and the granulocyte turnover rate in normal subjects. J. Clin. Invest. *40*, 989–995.

Auffray, C., Fogg, D., Garfa, M., Elain, G., Join-Lambert, O., Kayal, S., Sarnacki, S., Cumano, A., Lauvau, G., and Geissmann, F. (2007). Monitoring of blood vessels and tissues by a population of monocytes with patrolling behavior. Science (80-.). *317*, 666–670.

Auffray, C., Fogg, D.K., Narni-Mancinelli, E., Senechal, B., Trouillet, C., Saederup, N., Leemput, J., Bigot, K., Campisi, L., Abitbol, M., et al. (2009). CX3CR1+ CD115+ CD135+ common macrophage/DC precursors and the role of CX3CR1 in their response to inflammation. J. Exp. Med. *206*, 595–606.

Avecilla, S.T., Hattori, K., Heissig, B., Tejada, R., Liao, F., Shido, K., Jin, D.K., Dias, S., Zhang, F., Hartman, T.E., et al. (2004). Chemokine-mediated interaction of hematopoietic progenitors with the bone marrow vascular niche is required for thrombopoiesis. Nat. Med. *10*, 64–71.

Bain, C.C., Bravo-Blas, A., Scott, C.L., Gomez Perdiguero, E., Geissmann, F., Henri, S., Malissen, B., Osborne, L.C., Artis, D., and Mowat, A.M.I. (2014). Constant replenishment from circulating monocytes maintains the macrophage pool in the intestine of adult mice. Nat. Immunol. *15*, 929–937.

Bainton, D.F., Ullyot, J.L., and Farquhar, M.G. (1971). The development of neutrophilic polymorphonuclear leukocytes in human bone marrow: Origin and content of azurophil and specific granules. J. Exp. Med. *134*, 907–934.

Banaei-Bouchareb, L., Gouon-Evans, V., Samara-Boustani, D., Castellotti, M.C., Czernichow, P., Pollard, J.W., and Polak, M. (2004). Insulin cell mass is altered in *Csf1* ^{op} */Csf1* ^{op} macrophage-deficient mice. J. Leukoc. Biol. *76*, 359–367.

Banerji, C.R.S., Miranda-Saavedra, D., Severini, S., Widschwendter, M., Enver, T., Zhou, J.X., and Teschendorff, A.E. (2013). Cellular network entropy as the energy potential in

Waddington's differentiation landscape. Sci. Rep. *3*, 3039.

Bartels, M., Govers, A.M., Fleskens, V., Lourenço, A.R., Pals, C.E., Vervoort, S.J., Van Gent, R., Brenkman, A.B., Bierings, M.B., Ackerman, S.J., et al. (2015). Acetylation of C/EBPε is a prerequisite for terminal neutrophil differentiation. Blood *125*, 1782–1792.

Batta, K., Florkowska, M., Kouskoff, V., and Lacaud, G. (2014). Direct Reprogramming of Murine Fibroblasts to Hematopoietic Progenitor Cells. Cell Rep. *9*, 1871–1884.

Beaudin, A.E., Boyer, S.W., Perez-Cunningham, J., Hernandez, G.E., Derderian, S.C., Jujjavarapu, C., Aaserude, E., MacKenzie, T., and Forsberg, E.C. (2016). A Transient Developmental Hematopoietic Stem Cell Gives Rise to Innate-like B and T Cells. Cell Stem Cell *19*, 768–783.

Bender, M., Thon, J.N., Ehrlicher, A.J., Wu, S., Mazutis, L., Deschmann, E., Sola-Visner, M., Italiano, J.E., and Hartwig, J.H. (2015). Microtubule sliding drives proplatelet elongation and is dependent on cytoplasmic dynein. Blood *125*, 860–868.

Bertozzi, C.C., Schmaier, A.A., Mericko, P., Hess, P.R., Zou, Z., Chen, M., Chen, C.Y., Xu, B., Lu, M.M., Zhou, D., et al. (2010). Platelets regulate lymphatic vascular development through CLEC-2-SLP-76 signaling. Blood *116*, 661–670.

Bertrand, J.Y., and Traver, D. (2009). Hematopoietic cell development in the zebrafish embryo. Curr. Opin. Hematol. *16*, 243–248.

Bertrand, J.Y., Giroux, S., Golub, R., Klaine, M., Jalil, A., Boucontet, L., Godin, I., and Cumano, A. (2005a). Characterization of purified intraembryonic hematopoietic stem cells as a tool to define their site of origin. Proc. Natl. Acad. Sci. U. S. A. *102*, 134–139.

Bertrand, J.Y., Jalil, A., Le Klaine, M., Jung, S., Cumano, A., Godin, I., Klaine, M., Jung, S., Cumano, A., and Godin, I. (2005b). Three pathways to mature macrophages in the early mouse yolk sac. Blood *106*, 3004 LP – 3011.

Bertrand, J.Y., Kim, A.D., Violette, E.P., Stachura, D.L., Cisson, J.L., and Traver, D. (2007). Definitive hematopoiesis initiates through a committed erythromyeloid progenitor in the zebrafish embryo. Development *134*, 4147–4156.

Bertrand, J.Y., Chi, N.C., Santoso, B., Teng, S., Stainier, D.Y.R., and Traver, D. (2010). Haematopoietic stem cells derive directly from aortic endothelium during development. Nature *464*, 108–111.

Bianchi, E., Zini, R., Salati, S., Tenedini, E., Norfo, R., Tagliafico, E., Manfredini, R., and Ferrari, S. (2010). c-myb supports erythropoiesis through the transactivation of KLF1 and LMO2 expression. Blood *116*, e99–e110.

Bianconi, E., Piovesan, A., Facchin, F., Beraudi, A., Casadei, R., Frabetti, F., Vitale, L., Pelleri, M.C., Tassani, S., Piva, F., et al. (2013). An estimation of the number of cells in the human body. Ann. Hum. Biol. *40*, 463–471.

Bigas, A., Guiu, J., and Gama-Norton, L. (2013). Notch and Wnt signaling in the emergence of hematopoietic stem cells. Blood Cells, Mol. Dis. *51*, 264–270.

Blackwell, T.S., Hipps, A.N., Yamamoto, Y., Han, W., Barham, W.J., Ostrowski, M.C., Yull, F.E., and Prince, L.S. (2011). NF-κB Signaling in Fetal Lung Macrophages Disrupts Airway Morphogenesis. J. Immunol. *187*, 2740–2747.

Blatter, D., Lui, B., Stone, D., and Wyatt, B. (2017). The Denucleation of the Mammalian Erythrocyte: An Evolutionary Mechanism.

Blériot, C., Dupuis, T., Jouvion, G., Eberl, G., Disson, O., and Lecuit, M. (2015). Liver-Resident Macrophage Necroptosis Orchestrates Type 1 Microbicidal Inflammation and Type-2-Mediated Tissue Repair during Bacterial Infection. Immunity *42*, 145–158.

Bloom, W., and Bartelmez, G.W. (1940). Hematopoiesis in young human embryos. Am. J. Anat. *67*, 21–53.

Bohr, S., Patel, S.J., Vasko, R., Shen, K., Iracheta-Vellve, A., Lee, J., Bale, S.S., Chakraborty, N., Brines, M., Cerami, A., et al. (2015). Modulation of cellular stress response via the erythropoietin/CD131 heteroreceptor complex in mouse mesenchymal-derived cells. J. Mol. Med. *93*, 199–210.

Böiers, C., Carrelha, J., Lutteropp, M., Luc, S., Green, J.C.A., Azzoni, E., Woll, P.S., Mead, A.J., Hultquist, A., Swiers, G., et al. (2013). Lymphomyeloid contribution of an immune-restricted progenitor emerging prior to definitive hematopoietic stem cells. Cell Stem Cell *13*, 535–548.

Boisset, J.C., Van Cappellen, W., Andrieu-Soler, C., Galjart, N., Dzierzak, E., and Robin, C. (2010). In vivo imaging of haematopoietic cells emerging from the mouse aortic endothelium. Nature *464*, 116–120.

Boltjes, A., and van Wijk, F. (2014). Human dendritic cell functional specialization in steady-state and inflammation. Front. Immunol. *5*, 131.

Borst, K., Frenz, T., Spanier, J., Tegtmeyer, P.K., Chhatbar, C., Skerra, J., Ghita, L., Namineni, S., Lienenklaus, S., Köster, M., et al. (2018). Type I interferon receptor signaling delays Kupffer cell replenishment during acute fulminant viral hepatitis. J. Hepatol. *68*, 682–690.

Boulais, P.E., Mizoguchi, T., Zimmerman, S., Nakahara, F., Vivié, J., Mar, J.C., van Oudenaarden, A., and Frenette, P.S. (2018). The Majority of CD45– Ter119– CD31– Bone Marrow Cell Fraction Is of Hematopoietic Origin and Contains Erythroid and Lymphoid Progenitors. Immunity *49*, 627-639.e6.

Bouwens, L., Baekeland, M., de Zanger, R., and Wisse, E. (1986). Quantitation, tissue distribution and proliferation kinetics of kupffer cells in normal rat liver. Hepatology *6*, 718–722.

Boyer, S.W., Schroeder, A. V., Smith-Berdan, S., and Forsberg, E.C. (2011). All Hematopoietic Cells Develop from Hematopoietic Stem Cells through Flk2/Flt3-Positive Progenitor Cells. Cell Stem Cell *9*, 64–73.

Branehög, I., Ridell, B., Swolin, B., and Weinfeld, A. (1975). Megakaryocyte Quantifications in Relation to Thrombokinetics in Primary Thrombocythaemia and Allied Diseases. Scand. J. Haematol. *15*, 321–332.

Bratosin, D., Mazurier, J., Tissier, J.P., Estaquier, J., Huart, J.J., Ameisen, J.C., Aminoff, D., and Montreuil, J. (1998). Cellular and molecular mechanisms of senescent erythrocyte phagocytosis by macrophages. A review. Biochimie *80*, 173–195.

Brines, M., Grasso, G., Fiordaliso, F., Sfacteria, A., Ghezzi, P., Fratelli, M., Latini, R., Xie, Q.W., Smart, J., Su-Rick, C.J., et al. (2004). Erythropoietin mediates tissue protection through an erythropoietin and common β-subunit heteroreceptor. Proc. Natl. Acad. Sci. U. S. A. *101*, 14907–14912.

Brinkmann, V., Reichard, U., Goosmann, C., Fauler, B., Uhlemann, Y., Weiss, D.S., Weinrauch, Y., and Zychlinsky, A. (2004). Neutrophil Extracellular Traps Kill Bacteria. Science (80-.). *303*, 1532–1535.

Briseño, C.G., Haldar, M., Kretzer, N.M., Wu, X., Theisen, D.J., Wumesh, K.C., Durai, V., Grajales-Reyes, G.E., Iwata, A., Bagadia, P., et al. (2016). Distinct Transcriptional Programs Control Cross-Priming in Classical and Monocyte-Derived Dendritic Cells. Cell Rep. *15*, 2462–2474.

De Bruijn, M.F.T.R., Ma, X., Robin, C., Ottersbach, K., Sanchez, M.J., and Dzierzak, E. (2002). Hematopoietic stem cells localize to the endothelial cell layer in the midgestation

mouse aorta. Immunity *16*, 673–683.

Burger, P., Hilarius-Stokman, P., De Korte, D., Van Den Berg, T.K., and Van Bruggen, R. (2012). CD47 functions as a molecular switch for erythrocyte phagocytosis. Blood *119*, 5512–5521.

Burgess, A.W., and Metcalf, D. (1980). The nature and action of granulocyte - macrophage colony stimulating factors. Blood *56*, 947–958.

Cabezas-Wallscheid, N., Klimmeck, D., Hansson, J., Lipka, D.B., Reyes, A., Wang, Q., Weichenhan, D., Lier, A., Von Paleske, L., Renders, S., et al. (2014). Identification of regulatory networks in HSCs and their immediate progeny via integrated proteome, transcriptome, and DNA methylome analysis. Cell Stem Cell *15*, 507–522.

Cai, Z., de Bruijn, M., Ma, X., Dortland, B., Luteijn, T., Downing, J.R., and Dzierzak, E. (2000). Haploinsufficiency of AML1 Affects the Temporal and Spatial Generation of Hematopoietic Stem Cells in the Mouse Embryo specific genes, including IL-3, GM-CSF, CSF-1R, the subunits of the T cell antigen receptor, myeloperoxi-dase, and neutrophil elastase (.

Calderon, B., Carrero, J.A., Ferris, S.T., Sojka, D.K., Moore, L., Epelman, S., Murphy, K.M., Yokoyama, W.M., Randolph, G.J., and Unanue, E.R. (2015). The pancreas anatomy conditions the origin and properties of resident macrophages. J. Exp. Med. *212*, 1497–1512.

Carlin, L.M., Stamatiades, E.G., Auffray, C., Hanna, R.N., Glover, L., Vizcay-Barrena, G., Hedrick, C.C., Cook, H.T., Diebold, S., and Geissmann, F. (2013). Nr4a1-dependent Ly6Clow monocytes monitor endothelial cells and orchestrate their disposal. Cell *153*, 362–375.

Carramolino, L., Fuentes, J., García-Andrés, C., Azcoitia, V., Riethmacher, D., and Torres, M. (2010). Platelets play an essential role in separating the blood and lymphatic vasculatures during embryonic angiogenesis. Circ. Res. *106*, 1197–1201.

Carrelha, J., Meng, Y., Kettyle, L.M., Luis, T.C., Norfo, R., Alcolea, V., Boukarabila, H., Grasso, F., Gambardella, A., Grover, A., et al. (2018). Hierarchically related lineage-restricted fates of multipotent haematopoietic stem cells. Nature *554*, 106–111.

Charbord, P., Tavian, M., Humeau, L., and Péault, B. (1996). Early ontogeny of the human marrow from long bones: An immunohistochemical study of hematopoiesis and its microenvironment. Blood *87*, 4109–4119.

Chen, W., and Teschendorff, A.E. (2019). Estimating differentiation potency of single cells using single-cell entropy (SCENT). In Methods in Molecular Biology, (Humana Press Inc.), pp. 125–139.

Chen, M.J., Yokomizo, T., Zeigler, B.M., Dzierzak, E., and Speck, N.A. (2009). Runx1 is required for the endothelial to haematopoietic cell transition but not thereafter. Nature *457*, 887–891.

Chen, M.J., Li, Y., De Obaldia, M.E., Yang, Q., Yzaguirre, A.D., Yamada-Inagawa, T., Vink, C.S., Bhandoola, A., Dzierzak, E., and Speck, N.A. (2011). Erythroid/myeloid progenitors and hematopoietic stem cells originate from distinct populations of endothelial cells. Cell Stem Cell *9*, 541–552.

Cheung Tung Shing, K.S., Broughton, S.E., Nero, T.L., Gillinder, K., Ilsley, M.D., Ramshaw, H., Lopez, A.F., Griffin, M.D.W., Parker, M.W., Perkins, A.C., et al. (2018). EPO does not promote interaction between the erythropoietin and beta-common receptors. Sci. Rep. *8*, 1–16.

Chopin, M., and Nutt, S.L. (2015). Establishing and maintaining the Langerhans cell network.

Semin. Cell Dev. Biol. *41*, 23–29.

Chorro, L., Sarde, A., Li, M., Woollard, K.J., Chambon, P., Malissen, B., Kissenpfennig, A., Barbaroux, J.B., Groves, R., and Geissmann, F. (2009). Langerhans cell (LC) proliferation mediates neonatal development, homeostasis, and inflammation-associated expansion of the epidermal LC network. J. Exp. Med. *206*, 3089–3100.

Christensen, J.L., Wright, D.E., Wagers, A.J., and Weissman, I.L. (2004). Circulation and Chemotaxis of Fetal Hematopoietic Stem Cells. PLoS Biol. *2*, e75.

Ciau-Uitz, A., Walmsley, M., and Patient, R. (2000). Distinct origins of adult and embryonic blood in Xenopus. Cell *102*, 787–796.

Collin, M., and Bigley, V. (2018). Human dendritic cell subsets: an update. Immunology *154*, 3–20.

Corada, M., Nyqvist, D., Orsenigo, F., Caprini, A., Giampietro, C., Taketo, M.M., Iruela-Arispe, M.L., Adams, R.H., and Dejana, E. (2010). The Wnt/β-catenin pathway modulates vascular remodeling and specification by upregulating Dll4/notch signaling. Dev. Cell *18*, 938–949.

Corada, M., Orsenigo, F., Morini, M.F., Pitulescu, M.E., Bhat, G., Nyqvist, D., Breviario, F., Conti, V., Briot, A., Iruela-Arispe, M.L., et al. (2013). Sox17 is indispensable for acquisition and maintenance of arterial identity. Nat. Commun. *4*, 1–14.

Cortegano, I., Serrano, N., Ruiz, C., Rodríguez, M., Prado, C., Alía, M., Hidalgo, A., Cano, E., De Andrés, B., and Gaspar, M.L. (2019). CD45 expression discriminates waves of embryonic megakaryocytes in the mouse. Haematologica *104*, 1853–1865.

Coşkun, S., Chao, H., Vasavada, H., Heydari, K., Gonzales, N., Zhou, X., de Crombrugghe, B., and Hirschi, K.K. (2014). Development of the fetal bone marrow niche and regulation of HSC quiescence and homing ability by emerging osteolineage cells. Cell Rep. *9*, 581–590.

Costa, J.J. (1997). The Cells of the Allergic Response. JAMA *278*, 1815.

Cronkite, E.P., and Fliedner, T.M. (1964). GRANULOCYTOPOIESIS. N. Engl. J. Med. *270*, 1244–1248.

Cumano, A., Dieterlen-Lievre, F., and Godin, I. (1996). Lymphoid potential, probed before circulation in mouse, is restricted to caudal intraembryonic splanchnopleura. Cell *86*, 907–916.

Cumano, A., Ferraz, J.C., Klaine, M., Di Santo, J.P., and Godin, I. (2001). Intraembryonic, but not yolk sac hematopoietic precursors, isolated before circulation, provide long-term multilineage reconstitution. Immunity *15*, 477–485.

Dahlin, J.S., and Hallgren, J. (2015). Mast cell progenitors: Origin, development and migration to tissues. Mol. Immunol. *63*, 9–17.

Dakic, A., Shao, Q., D'Amico, A., O'Keeffe, M., Chen, W., Shortman, K., and Wu, L. (2004). Development of the Dendritic Cell System during Mouse Ontogeny. J. Immunol. *172*, 1018–1027.

Dautry Varsat, A., Ciechanover, A., and Lodish, H.F. (1983). pH and the recycling of transferrin during receptor-mediated endocytosis. Proc. Natl. Acad. Sci. U. S. A. *80*, 2258–2262.

Davidson, A.J., and Zon, L.I. (2004). The "definitive" (and 'primitive') guide to zebrafish hematopoiesis. Oncogene *23*, 7233–7246.

Debili, N., Coulombel, L., Croisille, L., Katz, A., Guichard, J., Breton-Gorius, J., and Vainchenker, W. (1996). Characterization of a bipotent erythro-megakaryocytic progenitor in human bone marrow. Blood *88*, 1284–1296.

DeFalco, T., Bhattacharya, I., Williams, A. V., Sams, D.M., and Capel, B. (2014). Yolk-sac-derived macrophages regulate fetal testis vascularization and morphogenesis. Proc. Natl. Acad. Sci. U. S. A. *111*, E2384–E2393.

Denzel, A., Maus, U.A., Gomez, M.R., Moll, C., Niedermeier, M., Winter, C., Maus, R., Hollingshead, S., Briles, D.E., Kunz-Schughart, L.A., et al. (2008). Basophils enhance immunological memory responses. Nat. Immunol. *9*, 733–742.

Dieterlen-Lievre, F. (1975). On the origin of haemopoietic stem cells in the avian embryo: an experimental approach.

Downard, C.D., Lewicke, S., and Ziegler, M.M. (2004). Meckel's Diverticulum. In Encyclopedia of Gastroenterology, (Elsevier), pp. 638–640.

Drake, C.J., and Fleming, P.A. (2000). Vasculogenesis in the day 6.5 to 9.5 mouse embryo. Blood *95*, 1671–1679.

Drissen, R., Thongjuea, S., Theilgaard-Mönch, K., and Nerlov, C. (2019). Identification of two distinct pathways of human myelopoiesis. Sci. Immunol. *4*, 7148.

Dunay, I.R., Fuchs, A., and Sibley, L.D. (2010). Inflammatory Monocytes but Not Neutrophils Are Necessary To Control Infection with Toxoplasma gondii in Mice. Infect. Immun. *78*, 1564–1570.

Dzierzak, E., and Speck, N.A. (2008). Of lineage and legacy: The development of mammalian hematopoietic stem cells. Nat. Immunol. *9*, 129–136.

Efroni, S., Duttagupta, R., Cheng, J., Dehghani, H., Hoeppner, D.J., Dash, C., Bazett-Jones, D.P., Le Grice, S., McKay, R.D.G., Buetow, K.H., et al. (2008). Global Transcription in Pluripotent Embryonic Stem Cells. Cell Stem Cell *2*, 437–447.

Elsaid, R., Meunier, S., Defranoux, O., Soraes-da-Silva, F., Perchet, T., Iturri, L., Freyer, L., Vieira, P., Pereira, P., Golub, R., et al. (2019). A wave of hematopoietic stem cell-derived T/ILC-restricted progenitors initiates thymopoiesis and shapes the embryonic thymus architecture. BioRxiv 791103.

England, S.J., McGrath, K.E., Frame, J.M., and Palis, J. (2011). Immature erythroblasts with extensive ex vivo self-renewal capacity emerge from the early mammalian fetus. Blood *117*, 2708–2717.

Enzan, H. (1986). ELECTRON MICROSCOPIC STUDIES OF MACROPHAGES IN EARLY HUMAN YOLK SACS. Pathol. Int. *36*, 49–64.

Epelman, S., Lavine, K.J., Beaudin, A.E., Sojka, D.K., Carrero, J.A., Calderon, B., Brija, T., Gautier, E.L., Ivanov, S., Satpathy, A.T., et al. (2014). Embryonic and adult-derived resident cardiac macrophages are maintained through distinct mechanisms at steady state and during inflammation. Immunity *40*, 91–104.

Espín-Palazón, R., Stachura, D.L., Campbell, C.A., García-Moreno, D., Del Cid, N., Kim, A.D., Candel, S., Meseguer, J., Mulero, V., and Traver, D. (2014). Proinflammatory signaling regulates hematopoietic stem cell emergence. Cell *159*, 1070–1085.

Evans, C.J., Hartenstein, V., and Banerjee, U. (2003). Thicker than blood: Conserved mechanisms in Drosophila and vertebrate hematopoiesis. Dev. Cell *5*, 673–690.

Everett, J.W. (1935). Morphological and physiological studies of the placenta in the albino rat. J. Exp. Zool. *70*, 243–285.

Faltusová, K., Chen, C.-L., Heizer, T., Báječný, M., Szikszai, K., Páral, P., Savvulidi, F., Renešová, N., and Nečas, E. (2020). Altered Erythro-Myeloid Progenitor Cells Are Highly Expanded in Intensively Regenerating Hematopoiesis. Front. Cell Dev. Biol. *8*, 98.

Fantin, A., Vieira, J.M., Gestri, G., Denti, L., Schwarz, Q., Prykhozhij, S., Peri, F., Wilson, S.W.,

and Ruhrberg, C. (2010). Tissue macrophages act as cellular chaperones for vascular anastomosis downstream of VEGF-mediated endothelial tip cell induction. Blood *116*, 829–840.

Ferkowicz, M.J., and Yoder, M.C. (2005). Blood island formation: Longstanding observations and modern interpretations. Exp. Hematol. *33*, 1041–1047.

Ferkowicz, M.J., Starr, M., Xie, X., Li, W., Johnson, S.A., Shelley, W.C., Morrison, P.R., and Yoder, M.C. (2003). CD41 expression defines the onset of primitive and definitive hematopoiesis in the murine embryo. Development *130*, 4393–4403.

Ferrero, G., Mahony, C.B., Traver, D., Bertrand, J.Y., and Rie Wittamer, V. (2018). Embryonic Microglia Derive from Primitive Macrophages and Are Replaced by cmyb-Dependent Definitive Microglia in Zebrafish.

Fiedler, K., and Brunner, C. (2012). The role of transcription factors in the guidance of granulopoiesis. Am. J. Blood Res. *2*, 57–65.

Flamme, I., Frölich, T., and Risau, W. (1997). Molecular mechanisms of vasculogenesis and embryonic angiogenesis. J. Cell. Physiol. *173*, 206–210.

Fogg, D.K., Sibon, C., Miled, C., Jung, S., Aucouturier, P., Littman, D.R., Cumano, A., and Geissmann, F. (2006). A clonogenic bone harrow progenitor specific for macrophages and dendritic cells. Science (80-.). *311*, 83–87.

Frame, J.M., Fegan, K.H., Conway, S.J., McGrath, K.E., and Palis, J. (2016). Definitive Hematopoiesis in the Yolk Sac Emerges from Wnt-Responsive Hemogenic Endothelium Independently of Circulation and Arterial Identity. Stem Cells *34*, 431–444.

Franco, R.S. (2012). Measurement of Red Cell Lifespan and Aging. Transfus. Med. Hemotherapy *39*, 302–307.

Franco, C.B., Chen, C.-C., Drukker, M., Weissman, I.L., and Galli, S.J. (2010). Distinguishing Mast Cell and Granulocyte Differentiation at the Single-Cell Level. Cell Stem Cell *6*, 361–368.

Fraser, S.T., Isern, J., and Baron, M.H. (2007). Maturation and enucleation of primitive erythroblasts during mouse embryogenesis is accompanied by changes in cell-surface antigen expression. Blood *109*, 343–352.

Fujimoto, T.T., Kohata, S., Suzuki, H., Miyazaki, H., and Fujimura, K. (2003). Production of functional platelets by differentiated embryonic stem (ES) cells in vitro. Blood *102*, 4044–4051.

Fujiwara, Y., Browne, C.P., Cunniff, K., Goff, S.C., and Orkin, S.H. (1996). Arrested development of embryonic red cell precursors in mouse embryos lacking transcription factor GATA-1. Proc. Natl. Acad. Sci. U. S. A. *93*, 12355–12358.

van Furth, R., Cohn, Z.A., Hirsch, J.G., Humphrey, J.H., Spector, W.G., and Langevoort, H.L. (1972). The mononuclear phagocyte system: a new classification of macrophages, monocytes, and their precursor cells. Bull. World Health Organ. *46*, 845–852.

Galli, S.J., Kalesnikoff, J., Grimbaldeston, M.A., Piliponsky, A.M., Williams, C.M.M., and Tsai, M. (2005). MAST CELLS AS “TUNABLE” EFFECTOR AND IMMUNOREGULATORY CELLS: Recent Advances. Annu. Rev. Immunol. *23*, 749–786.

Garcia-Alegria, E., Menegatti, S., Fadlullah, M.Z.H., Menendez, P., Lacaud, G., and Kouskoff, V. (2018). Early Human Hemogenic Endothelium Generates Primitive and Definitive Hematopoiesis In Vitro. Stem Cell Reports *11*, 1061–1074.

Garcia-Porrero, J.A., Godin, I.E., and Dieterlen-Libvre, F. (1995). Potential intraembryonic

hemogenic sites at pre-liver stages in the mouse (Springer-Verlag).

Garcia, M.D., Lopez, A.L., Larin, K. V., and Larina, I. V. (2015). Imaging of cardiovascular development in mammalian embryos using optical coherence tomography. Methods Mol. Biol. *1214*, 151–161.

Gaspar-Maia, A., Alajem, A., Meshorer, E., and Ramalho-Santos, M. (2011). Open chromatin in pluripotency and reprogramming. Nat. Rev. Mol. Cell Biol. *12*, 36–47.

Gasteiger, G., Fan, X., Dikiy, S., Lee, S.Y., and Rudensky, A.Y. (2015). Tissue residency of innate lymphoid cells in lymphoid and nonlymphoid organs. Science (80-.). *350*, 981–985.

Gautier, E.L., Shay, T., Miller, J., Greter, M., Jakubzick, C., Ivanov, S., Helft, J., Chow, A., Elpek, K.G., Gordonov, S., et al. (2012). Gene-expression profiles and transcriptional regulatory pathways that underlie the identity and diversity of mouse tissue macrophages. Nat. Immunol. *13*, 1118–1128.

Geissmann, F., Manz, M.G., Jung, S., Sieweke, M.H., Merad, M., and Ley, K. (2010). Development of monocytes, macrophages, and dendritic cells. Science (80-.). *327*, 656–661.

Gentek, R., Ghigo, C., Hoeffel, G., Bulle, M.J., Msallam, R., Gautier, G., Launay, P., Chen, J., Ginhoux, F., and Bajénoff, M. (2018a). Hemogenic Endothelial Fate Mapping Reveals Dual Developmental Origin of Mast Cells. Immunity *48*, 1160-1171.e5.

Gentek, R., Ghigo, C., Hoeffel, G., Jorquera, A., Msallam, R., Wienert, S., Klauschen, F., Ginhoux, F., and Bajénoff, M. (2018b). Epidermal γδ T cells originate from yolk sac hematopoiesis and clonally self-renew in the adult. J. Exp. Med. *215*, 2994–3005.

Germain, P.-L. (2020). scDblFinder: scDblFinder. R package version 1.1.8.

Ghigo, C., Mondor, I., Jorquera, A., Nowak, N.J., Wienert, S., Zahner, S.P., Clausen, B.E., Luche, H., Malissen, B., Klauschen, F., et al. (2013). Multicolor fate mapping of langerhans cell homeostasis. J. Exp. Med. *210*, 1657–1664.

Gibbs, B.F. (2005). Human basophils as effectors and immunomodulators of allergic inflammation and innate immunity. Clin. Exp. Med. *5*, 43–49.

Ginhoux, F., Greter, M., Leboeuf, M., Nandi, S., See, P., Gokhan, S., Mehler, M.F., Conway, S.J., Ng, L.G., Stanley, E.R., et al. (2010). Fate mapping analysis reveals that adult microglia derive from primitive macrophages. Science (80-.). *330*, 841–845.

Godin, I., and Cumano, A. (2002). The hare and the tortoise: An embryonic haematopoietic race. Nat. Rev. Immunol. *2*, 593–604.

Godin, I., Garcia-Porrero, J.A., Dieterlen-Lièvre, F., and Cumano, A. (1999). Stem cell emergence and hemopoietic activity are incompatible in mouse intraembryonic sites. J. Exp. Med. *190*, 43–52.

Godin, I.E., Garcia-Porrero, J.A., Coutinho, A., Dieterlen-Lièvre, F., and Marcos, M.A.R. (1993). Para-aortic splanchnopleura from early mouse embryos contains B1a cell progenitors. Nature *364*, 67–70.

Golfier, F., Barcena, A., Harrison, M.R., and Muench, M.O. (2000). Fetal bone marrow as a source of stem cells for in utero or postnatal transplantation. Br. J. Haematol. *109*, 173–181.

Gomez Perdiguero, E., Klapproth, K., Schulz, C., Busch, K., Azzoni, E., Crozet, L., Garner, H., Trouillet, C., De Bruijn, M.F., Geissmann, F., et al. (2015). Tissue-resident macrophages originate from yolk-sac-derived erythro-myeloid progenitors. Nature *518*, 547–551.

Gordon, E.J., Rao, S., Pollard, J.W., Nutt, S.L., Lang, R.A., and Harvey, N.L. (2010).

Macrophages define dermal lymphatic vessel calibre during development by regulating lymphatic endothelial cell proliferation. Development *137*, 3899–3910.

Graf, T., and Enver, T. (2009). Forcing cells to change lineages. Nature *462*, 587–594.

Grajales-Reyes, G.E., Iwata, A., Albring, J., Wu, X., Tussiwand, R., Kc, W., Kretzer, N.M., Briseño, C.G., Durai, V., Bagadia, P., et al. (2015). Batf3 maintains autoactivation of Irf8 for commitment of a CD8α + conventional DC clonogenic progenitor. Nat. Immunol. *16*, 708–717.

Grover, A., Sanjuan-Pla, A., Thongjuea, S., Carrelha, J., Giustacchini, A., Gambardella, A., Macaulay, I., Mancini, E., Luis, T.C., Mead, A., et al. (2016). Single-cell RNA sequencing reveals molecular and functional platelet bias of aged haematopoietic stem cells. Nat. Commun. *7*, 1–12.

Grozovsky, R., Giannini, S., Falet, H., and Hoffmeister, K.M. (2015). Regulating billions of blood platelets: Glycans and beyond. Blood *126*, 1877–1884.

Guilliams, M., and Scott, C.L. (2017). Does niche competition determine the origin of tissue-resident macrophages? Nat. Rev. Immunol. *17*, 451–460.

Guilliams, M., Ginhoux, F., Jakubzick, C., Naik, S.H., Onai, N., Schraml, B.U., Segura, E., Tussiwand, R., and Yona, S. (2014). Dendritic cells, monocytes and macrophages: a unified nomenclature based on ontogeny. Nat. Rev. Immunol. *14*, 571–578.

Guilliams, M., Dutertre, C.A., Scott, C.L., McGovern, N., Sichien, D., Chakarov, S., Van Gassen, S., Chen, J., Poidinger, M., De Prijck, S., et al. (2016). Unsupervised High-Dimensional Analysis Aligns Dendritic Cells across Tissues and Species. Immunity *45*, 669–684.

Guilliams, M., Mildner, A., and Yona, S. (2018). Developmental and Functional Heterogeneity of Monocytes. Immunity *49*, 595–613.

Gulliver, G. (1875). Observations on the sizes and shapes of the red corpuscles of the blood of vertebrates, with drawings of them to a uniform scale, and extended and revised tables of measurements. Proc Zool Soc London 474–495.

Haas, K.M., Poe, J.C., Steeber, D.A., and Tedder, T.F. (2005). B-1a and B-1b cells exhibit distinct developmental requirements and have unique functional roles in innate and adaptive immunity to S. pneumoniae. Immunity *23*, 7–18.

Haas, S., Hansson, J., Klimmeck, D., Loeffler, D., Velten, L., Uckelmann, H., Wurzer, S., Prendergast, Á.M., Schnell, A., Hexel, K., et al. (2015). Inflammation-Induced Emergency Megakaryopoiesis Driven by Hematopoietic Stem Cell-like Megakaryocyte Progenitors. Cell Stem Cell *17*, 422–434.

Hadland, B.K., Huppert, S.S., Kanungo, J., Xue, Y., Jiang, R., Gridley, T., Conlon, R.A., Cheng, A.M., Kopan, R., and Longmore, G.D. (2004). A requirement for Notch1 distinguishes 2 phases of definitive hematopoiesis during development. Blood *104*, 3097–3105.

Haghverdi, L., Lun, A.T.L., Morgan, M.D., and Marioni, J.C. (2018). Batch effects in single-cell RNA-sequencing data are corrected by matching mutual nearest neighbors. Nat. Biotechnol. *36*, 421–427.

Harigae, H., Takahashi, S., Suwabe, N., Ohtsu, H., Gu, L., Yang, Z., Tsai, F., Kitamura, Y., Douglas Engel, J., and Yamamoto, M. (1998). Differential roles of GATA-1 and GATA-2 in growth and differentiation of mast cells. Genes to Cells *3*, 39–50.

Harrison, D.E., Zhong, R.K., Jordan, C.T., Lemischka, I.R., and Astle, C.M. (1997). Relative to adult marrow, fetal liver repopulates nearly five times more effectively long-term than short-term. Exp. Hematol. *25*, 293–297.

Hashimoto, D., Chow, A., Noizat, C., Teo, P., Beasley, M.B., Leboeuf, M., Becker, C.D., See, P., Price, J., Lucas, D., et al. (2013). Tissue-resident macrophages self-maintain locally throughout adult life with minimal contribution from circulating monocytes. Immunity *38*, 792–804.

Hatanaka, K., Kitamura, Y., and Nishimune, Y. (1979). Local development of mast cells from bone marrow-derived precursors in the skin of mice. Blood *53*, 142–147.

Hayashi, C., Sonoda, T., Nakano, T., Nakayama, H., and Kitamura, Y. (1985). Mast-cell precursors in the skin of mouse embryos and their deficiency in embryos of Sl Sld genotype. Dev. Biol. *109*, 234–241.

He, L., Cohen, E.B., Edwards, A.P.B., Kragelund, B.B., Krause, D.S., and Dimaio, D. (2019). Transmembrane Protein Aptamer Induces Cooperative Signaling by the EPO Receptor and the Cytokine Receptor β-Common Subunit. ISCIENCE *17*, 167–181.

Hentze, M.W., Muckenthaler, M.U., Galy, B., and Camaschella, C. (2010). Two to Tango: Regulation of Mammalian Iron Metabolism. Cell *142*, 24–38.

Hettinger, J., Richards, D.M., Hansson, J., Barra, M.M., Joschko, A.C., Krijgsveld, J., and Feuerer, M. (2013). Origin of monocytes and macrophages in a committed progenitor. Nat. Immunol. *14*, 821–830.

Hirai, H., Zhang, P., Dayaram, T., Hetherington, C.J., Mizuno, S.I., Imanishi, J., Akashi, K., and Tenen, D.G. (2006). C/EBPβ is required for “emergency” granulopoiesis. Nat. Immunol. *7*, 732–739.

Hirai, H., Yokota, A., Tamura, A., Sato, A., and Maekawa, T. (2015). Non-steady-state hematopoiesis regulated by the C/EBPβ transcription factor. Cancer Sci. *106*, 797–802.

Hitchcock, I.S., and Kaushansky, K. (2014). Thrombopoietin from beginning to end. Br. J. Haematol. *165*, 259–268.

Hoeffel, G., Wang, Y., Greter, M., See, P., Teo, P., Malleret, B., Leboeuf, M., Low, D., Oller, G., Almeida, F., et al. (2012). Adult Langerhans cells derive predominantly from embryonic fetal liver monocytes with a minor contribution of yolk sac-derived macrophages. J. Exp. Med. *209*, 1167–1181.

Hoeffel, G., Chen, J., Lavin, Y., Low, D., Almeida, F.F., See, P., Beaudin, A.E., Lum, J., Low, I., Forsberg, E.C., et al. (2015). C-Myb+ Erythro-Myeloid Progenitor-Derived Fetal Monocytes Give Rise to Adult Tissue-Resident Macrophages. Immunity *42*, 665–678.

Höfer, T., Busch, K., Klapproth, K., and Rodewald, H.R. (2016). Fate Mapping and Quantitation of Hematopoiesis in Vivo. Annu. Rev. Immunol. *34*, 449–478.

Holz, A., Bossinger, B., Strasser, T., Janning, W., and Klapper, R. (2003). The two origins of hemocytes in Drosophila. Development *130*, 4955–4962.

Hoppe, P.S., Schwarzfischer, M., Loeffler, D., Kokkaliaris, K.D., Hilsenbeck, O., Moritz, N., Endele, M., Filipczyk, A., Gambardella, A., Ahmed, N., et al. (2016). Early myeloid lineage choice is not initiated by random PU.1 to GATA1 protein ratios. Nature *535*, 299–302.

Hou, S., Li, Z., Zheng, X., Gao, Y., Dong, J., Ni, Y., Wang, X., Li, Y., Ding, X., Chang, Z., et al. (2020). Embryonic endothelial evolution towards first hematopoietic stem cells revealed by single-cell transcriptomic and functional analyses. Cell Res. *30*, 376–392.

Hume, D.A., Irvine, K.M., and Pridans, C. (2019). The Mononuclear Phagocyte System: The Relationship between Monocytes and Macrophages. Trends Immunol. *40*, 98–112.

Ikeda, N., Asano, K., Kikuchi, K., Uchida, Y., Ikegami, H., Takagi, R., Yotsumoto, S., Shibuya, T., Makino-Okamura, C., Fukuyama, H., et al. (2018). Emergence of immunoregulatory Ym1+Ly6Chi monocytes during recovery phase of tissue injury. Sci. Immunol. *3*, 207.

Ikuta, K., Kina, T., MacNeil, I., Uchida, N., Peault, B., Chien, Y. hsiu, and Weissman, I.L. (1990). A developmental switch in thymic lymphocyte maturation potential occurs at the level of hematopoietic stem cells. Cell *62*, 863–874.

Ingman, W. V., Wyckoff, J., Gouon-Evans, V., Condeelis, J., and Pollard, J.W. (2006). Macrophages promote collagen fibrillogenesis around terminal end buds of the developing mammary gland. Dev. Dyn. *235*, 3222–3229.

Irion, S., Clarke, R.L., Luche, H., Kim, I., Morrison, S.J., Fehling, H.J., and Keller, G.M. (2010). Temporal specification of blood progenitors from mouse embryonic stem cells and induced pluripotent stem cells. Development *137*, 2829–2839.

Italiano, J.E., Lecine, P., Shivdasani, R.A., and Hartwig, J.H. (1999). Blood platelets are assembled principally at the ends of proplatelet processes produced by differentiated megakaryocytes. J. Cell Biol. *147*, 1299–1312.

Iturri, L., Saenz Coronilla, J., Lallemand, Y., and Gomez Perdiguero, E. (2017). Identification of erythromyeloid progenitors and their progeny in the mouse embryo by flow cytometry. J. Vis. Exp. *2017*.

Ivanovs, A., Rybtsov, S., Welch, L., Anderson, R.A., Turner, M.L., and Medvinsky, A. (2011). Highly potent human hematopoietic stem cells first emerge in the intraembryonic aorta-gonad-mesonephros region. J. Exp. Med. *208*, 2417–2427.

Ivanovs, A., Rybtsov, S., Ng, E.S., Stanley, E.G., Elefanty, A.G., and Medvinsky, A. (2017). Human haematopoietic stem cell development: From the embryo to the dish. Dev. *144*, 2323–2337.

Iwasaki, H., and Akashi, K. (2007). Myeloid Lineage Commitment from the Hematopoietic Stem Cell (Cell Press).

Iwasaki, H., Mizuno, S.I., Arinobu, Y., Ozawa, H., Mori, Y., Shigematsu, H., Takatsu, K., Tenen, D.G., and Akashi, K. (2006). The order of expression of transcription factors directs hierarchical specification of hematopoietic lineages. Genes Dev. *20*, 3010–3021.

Jaffredo, T., Gautier, R., Eichmann, A., and Dieterlen-Lievre, F. (1998). Intraaortic hemopoietic cells are derived from endothelial cells during ontogeny. Development *125*, 4575 LP – 4583.

Jaffredo, T., Gautier, R., Brajeul, V., and Dieterlen-Lièvre, F. (2000). Tracing the progeny of the aortic hemangioblast in the avian embryo. Dev. Biol. *224*, 204–214.

Jameson, J.M., Cauvi, G., Witherden, D.A., and Havran, W.L. (2004). A Keratinocyte-Responsive γδ TCR Is Necessary for Dendritic Epidermal T Cell Activation by Damaged Keratinocytes and Maintenance in the Epidermis. J. Immunol. *172*, 3573–3579.

Jenkins, S.J., Ruckerl, D., Cook, P.C., Jones, L.H., Finkelman, F.D., Van Rooijen, N., MacDonald, A.S., and Allen, J.E. (2011). Local macrophage proliferation, rather than recruitment from the blood, is a signature of T H2 inflammation. Science (80-.). *332*, 1284–1288.

Ji, P., Murata-Hori, M., and Lodish, H.F. (2011). Formation of mammalian erythrocytes: Chromatin condensation and enucleation. Trends Cell Biol. *21*, 409–415.

Johansen, L.M., Iwama, A., Lodie, T.A., Sasaki, K., Felsher, D.W., Golub, T.R., and Tenen, D.G. (2001). c-Myc Is a Critical Target for C/EBPα in Granulopoiesis. Mol. Cell. Biol. *21*, 3789–3806.

Jollie, W.P. (1990). Development, morphology, and function of the yolk-sac placenta of laboratory rodents. Teratology *41*, 361–381.

Kanaji, T., Vo, M.-N., Kanaji, S., Zarpellon, A., Shapiro, R., Morodomi, Y., Yuzuriha, A., Eto, K., Belani, R., Do, M.-H., et al. (2018). Tyrosyl-tRNA synthetase stimulates thrombopoietin-independent hematopoiesis accelerating recovery from thrombocytopenia. Proc. Natl. Acad. Sci. *115*, E8228–E8235.

Kanda, H., Tateya, S., Tamori, Y., Kotani, K., Hiasa, K.I., Kitazawa, R., Kitazawa, S., Miyachi, H., Maeda, S., Egashira, K., et al. (2006). MCP-1 contributes to macrophage infiltration into adipose tissue, insulin resistance, and hepatic steatosis in obesity. J. Clin. Invest. *116*, 1494–1505.

Karasuyama, H., and Yamanishi, Y. (2014). Basophils have emerged as a key player in immunity. Curr. Opin. Immunol. *31*, 1–7.

Karsunky, H., Merad, M., Cozzio, A., Weissman, I.L., and Manz, M.G. (2003). Flt3 ligand regulates dendritic cell development from Flt3+ lymphoid and myeloid-committed progenitors to Flt3+ dendritic cells in vivo. J. Exp. Med. *198*, 305–313.

Kasaai, B., Caolo, V., Peacock, H.M., Lehoux, S., Gomez-Perdiguero, E., Luttun, A., and Jones, E.A.V. (2017). Erythro-myeloid progenitors can differentiate from endothelial cells and modulate embryonic vascular remodeling. Sci. Rep. *7*, 1–12.

Katz, S.I., Tamaki, K., and Sachs, D.H. (1979). Epidermal Langerhans cells are derived from cells originating in bone marrow [30]. Nature *282*, 324–326.

Kauts, M.L., De Leo, B., Rodríguez-Seoane, C., Ronn, R., Glykofrydis, F., Maglitto, A., Kaimakis, P., Basi, M., Taylor, H., Forrester, L., et al. (2018). Rapid Mast Cell Generation from Gata2 Reporter Pluripotent Stem Cells. Stem Cell Reports *11*, 1009–1020.

Kennedy, A.D., and Deleo, F.R. (2009). Neutrophil apoptosis and the resolution of infection. Immunol. Res. *43*, 25–61.

Kennedy, M., D'Souza, S.L., Lynch-Kattman, M., Schwantz, S., and Keller, G. (2007). Development of the hemangioblast defines the onset of hematopoiesis in human ES cell differentiation cultures. In Blood, (American Society of Hematology), pp. 2679–2687.

Kierdorf, K., Erny, D., Goldmann, T., Sander, V., Schulz, C., Perdiguero, E.G., Wieghofer, P., Heinrich, A., Riemke, P., Hölscher, C., et al. (2013). Microglia emerge from erythromyeloid precursors via Pu.1-and Irf8-dependent pathways. Nat. Neurosci. *16*, 273–280.

Kierdorf, K., Prinz, M., Geissmann, F., and Gomez Perdiguero, E. (2015). Development and function of tissue resident macrophages in mice. Semin. Immunol. *27*, 369–378.

Kieusseian, A., de la Grange, P.B., Burlen-Defranoux, O., Godin, I., and Cumano, A. (2012). Immature hematopoietic stem cells undergo maturation in the fetal liver. Dev. *139*, 3521–3530.

Kingsley, P.D., Malik, J., Fantauzzo, K.A., and Palis, J. (2004). Yolk sac-derived primitive erythroblasts enucleate during mammalian embryogenesis. Blood *104*, 19–25.

Kingsley, P.D., Malik, J., Emerson, R.L., Bushnell, T.P., Mcgrath, K.E., Bloedorn, L.A., Bulger, M., and Palis, J. (2006). "Maturational" globin switching in primary primitive erythroid cells.

Kissa, K., and Herbomel, P. (2010). Blood stem cells emerge from aortic endothelium by a novel type of cell transition. Nature *464*, 112–115.

Kita, H. (2011). Eosinophils: Multifaceted biological properties and roles in health and disease.

Immunol. Rev. *242*, 161–177.

Kitamura, Y., Shimada, M., Hatanaka, K., and Miyano, Y. (1977). Development of mast cells from grafted bone marrow cells in irradiated mice. Nature *268*, 442–443.

Kohyama, M., Ise, W., Edelson, B.T., Wilker, P.R., Hildner, K., Mejia, C., Frazier, W.A., Murphy, T.L., and Murphy, K.M. (2009). Role for Spi-C in the development of red pulp macrophages and splenic iron homeostasis. Nature *457*, 318–321.

Koury, M.J., and Bondurant, M.C. (1990). Erythropoietin retards DNA breakdown and prevents programmed death in erythroid progenitor cells. Science (80-.). *248*, 378–381.

Koury, M.J., and Bondurant, M.C. (1992). The molecular mechanism of erythropoietin action. Eur. J. Biochem. *210*, 649–663.

Kubota, Y., Takubo, K., Shimizu, T., Ohno, H., Kishi, K., Shibuya, M., Saya, H., and Suda, T. (2009). M-CSF inhibition selectively targets pathological angiogenesis and lymphangiogenesis. J. Exp. Med. *206*, 1089–1102.

Kucia, M., Reca, R., Campbell, F.R., Zuba-Surma, E., Majka, M., Ratajczak, J., and Ratajczak, M.Z. (2006). A population of very small embryonic-like (VSEL) CXCR4+ SSEA-1+Oct-4+ stem cells identified in adult bone marrow. Leukemia *20*, 857–869.

Kumano, K., Chiba, S., Kunisato, A., Sata, M., Saito, T., Nakagami-Yamaguchi, E., Yamaguchi, T., Masuda, S., Shimizu, K., Takahashi, T., et al. (2003). Notch1 but not Notch2 is essential for generating hematopoietic stem cells from endothelial cells. Immunity *18*, 699–711.

Kwok, I., Becht, E., Xia, Y., Ng, M., Teh, Y.C., Tan, L., Evrard, M., Li, J.L.Y., Tran, H.T.N., Tan, Y., et al. (2020). Combinatorial Single-Cell Analyses of Granulocyte-Monocyte Progenitor Heterogeneity Reveals an Early Uni-potent Neutrophil Progenitor. Immunity.

Lacaud, G., and Kouskoff, V. (2017). Hemangioblast, hemogenic endothelium, and primitive versus definitive hematopoiesis. Exp. Hematol. *49*, 19–24.

Lacaud, G., Gore, L., Kennedy, M., Kouskoff, V., Kingsley, P., Hogan, C., Carlsson, L., Speck, N., Palis, J., and Keller, G. (2002). Runx1 is essential for hematopoietic commitment at the hemangioblast stage of development in vitro. Blood *100*, 458–466.

Lancino, M., Majello, S., Herbert, S., De Chaumont, F., Tinevez, J.Y., Olivo-Marin, J.C., Herbomel, P., and Schmidt, A. (2018). Anisotropic organization of circumferential actomyosin characterizes hematopoietic stem cells emergence in the zebrafish. Elife *7*.

Lantz, C.S., Boeslger, J., Song, C.H., Mach, N., Kobayashi, T., Mulligan, R.C., Nawa, Y., Dranoff, G., and Galli, S.J. (1998). Role for interleukin-3 in mast cell and basophil development and in immunity to parasites. Nature *392*, 90–93.

Lassila, O., Eskola, J., Toivanen, P., Martin, C., and Dieterlen-lievre, F. (1978). The origin of lymphoid stem cells studied in chick yolk sac-embryo chimaeras. Nature *272*, 353–354.

Lavin, Y., Winter, D., Blecher-Gonen, R., David, E., Keren-Shaul, H., Merad, M., Jung, S., and Amit, I. (2014). Tissue-resident macrophage enhancer landscapes are shaped by the local microenvironment. Cell *159*, 1312–1326.

Lee, L.K., Ghorbanian, Y., Wang, W., Wang, Y., Kim, Y.J., Weissman, I.L., Inlay, M.A., and Mikkola, H.K.A. (2016). LYVE1 Marks the Divergence of Yolk Sac Definitive Hemogenic Endothelium from the Primitive Erythroid Lineage. Cell Rep. *17*, 2286–2298.

Lee, T.I., Jenner, R.G., Boyer, L.A., Guenther, M.G., Levine, S.S., Kumar, R.M., Chevalier, B.,

Johnstone, S.E., Cole, M.F., Isono, K. ichi, et al. (2006). Control of Developmental Regulators by Polycomb in Human Embryonic Stem Cells. Cell *125*, 301–313.

Leimberg, M.J., Prus, E., Konijn, A.M., and Fibach, E. (2008). Macrophages function as a ferritin iron source for cultured human erythroid precursors. J. Cell. Biochem. *103*, 1211–1218.

Leis, M., Gliezzi, P., Grasso, G., Bianchi, R., Vilia, P., Fratelli, M., Savino, C., Bianchi, M., Nielsen, J., Gerwien, J., et al. (2004). Derivatives of erythropoitein that are tissue protective but not erythropoietic. Science (80-.). *305*, 239–242.

Li, J., Hale, J., Bhagia, P., Xue, F., Chen, L., Jaffray, J., Yan, H., Lane, J., Gallagher, P.G., Mohandas, N., et al. (2014a). Isolation and transcriptome analyses of human erythroid progenitors: BFU-E and CFU-E. Blood *124*, 3636–3645.

Li, Y., Esain, V., Teng, L., Xu, J., Kwan, W., Frost, I.M., Yzaguirre, A.D., Cai, X., Cortes, M., Maijenburg, M.W., et al. (2014b). Inflammatory signaling regulates embryonic hematopoietic stem and progenitor cell production. Genes Dev. *28*, 2597–2612.

Li, Z., Liu, S., Xu, J., Zhang, X., Han, D., Liu, J., Xia, M., Yi, L., Shen, Q., Xu, S., et al. (2018). Adult Connective Tissue-Resident Mast Cells Originate from Late Erythro-Myeloid Progenitors. Immunity *49*, 640-653.e5.

Lichtinger, M., Ingram, R., Hannah, R., Müller, D., Clarke, D., Assi, S.A., Lie-A-Ling, M., Noailles, L., Vijayabaskar, M.S., Wu, M., et al. (2012). RUNX1 reshapes the epigenetic landscape at the onset of haematopoiesis. EMBO J. *31*, 4318–4333.

Liu, C.-P., and Auerbach, R. (1991). In vitro development of murine T cells from prethymic and preliver embryonic yolk sac hematopoietic stem cells.

Liu, J., Fu, T., Song, F., Xue, Y., Xia, C., Liu, P., Wang, H., Zhong, J., Li, Q., Chen, J., et al. (2015). Mast Cells Participate in Corneal Development in Mice. Sci. Rep. *5*, 17569.

Liu, K., Victora, G.D., Schwickert, T.A., Guermonprez, P., Meredith, M.M., Yao, K., Chu, F.-F., Randolph, G.J., Rudensky, A.Y., and Nussenzweig, M. (2009). In Vivo Analysis of Dendritic Cell Development and Homeostasis. Science (80-.). *431*, 530.

Liu, Z., Gu, Y., Chakarov, S., Bleriot, C., Kwok, I., Chen, X., Shin, A., Huang, W., Dress, R.J., Dutertre, C.A., et al. (2019). Fate Mapping via Ms4a3-Expression History Traces Monocyte-Derived Cells. Cell *178*, 1509-1525.e19.

Lopez, A.L., Garcia, M.D., Dickinson, M.E., and Larina, I. V. (2015). Live confocal microscopy of the developing mouse embryonic yolk sac vasculature. Methods Mol. Biol. *1214*, 163–172.

Louis, C., Cook, A.D., Lacey, D., Fleetwood, A.J., Vlahos, R., Anderson, G.P., and Hamilton, J.A. (2015). Specific Contributions of CSF-1 and GM-CSF to the Dynamics of the Mononuclear Phagocyte System. J. Immunol. *195*, 134–144.

Lucitti, J.L., Jones, E.A.V., Huang, C., Chen, J., Fraser, S.E., and Dickinson, M.E. (2007). Vascular remodeling of the mouse yolk sac requires hemodynamic force. Development *134*, 3317–3326.

Luckett, W.P. (1978). Origin and differentiation of the yolk sac and extraembryonic mesoderm in presomite human and rhesus monkey embryos. Am. J. Anat. *152*, 59–97.

Lux, C.T., Yoshimoto, M., McGrath, K., Conway, S.J., Palis, J., and Yoder, M.C. (2008). All primitive and definitive hematopoietic progenitor cells emerging before E10 in the mouse embryo are products of the yolk sac. Blood *111*, 3435–3438.

Ma, O., Hong, S., Guo, H., Ghiaur, G., and Friedman, A.D. (2014). Granulopoiesis Requires Increased C/EBPα Compared to Monopoiesis, Correlated with Elevated Cebpa in Immature G-CSF Receptor versus M-CSF Receptor Expressing Cells. PLoS One *9*,

e95784.

Mantovani, A., Cassatella, M.A., Costantini, C., and Jaillon, S. (2011). Neutrophils in the activation and regulation of innate and adaptive immunity. Nat. Rev. Immunol. *11*, 519–531.

Manz, M.G., and Boettcher, S. (2014). Emergency granulopoiesis. Nat. Rev. Immunol. *14*, 302–314.

Mariani, S.A., Li, Z., Rice, S., Krieg, C., Fragkogianni, S., Robinson, M., Vink, C.S., Pollard, J.W., and Dzierzak, E. (2019). Pro-inflammatory Aorta-Associated Macrophages Are Involved in Embryonic Development of Hematopoietic Stem Cells. Immunity *50*, 1439-1452.e5.

Mass, E., Ballesteros, I., Farlik, M., Halbritter, F., Günther, P., Crozet, L., Jacome-Galarza, C.E., Händler, K., Klughammer, J., Kobayashi, Y., et al. (2016). Specification of tissue-resident macrophages during organogenesis. Science (80-.). *353*.

Mass, E., Jacome-Galarza, C.E., Blank, T., Lazarov, T., Durham, B.H., Ozkaya, N., Pastore, A., Schwabenland, M., Chung, Y.R., Rosenblum, M.K., et al. (2017). A somatic mutation in erythro-myeloid progenitors causes neurodegenerative disease. Nature *549*, 389–393.

Matcovitch-Natan, O., Winter, D.R., Giladi, A., Aguilar, S.V., Spinrad, A., Sarrazin, S., Ben-Yehuda, H., David, E., González, F.Z., Perrin, P., et al. (2016). Microglia development follows a stepwise program to regulate brain homeostasis. Science (80-.). *353*.

Matsuda, H., Kitamura, Y., Sonoda, T., and Imori, T. (1981). Precursor of mast cells fixed in the skin of mice. J. Cell. Physiol. *108*, 409–415.

McGovern, N., Shin, A., Low, G., Low, D., Duan, K., Yao, L.J., Msallam, R., Low, I., Shadan, N.B., Sumatoh, H.R., et al. (2017). Human fetal dendritic cells promote prenatal T-cell immune suppression through arginase-2. Nature *546*, 662–666.

McGrath, K.E., Frame, J.M., Fromm, G.J., Koniski, A.D., Kingsley, P.D., Little, J., Bulger, M., and Palis, J. (2011). A transient definitive erythroid lineage with unique regulation of the β-globin locus in the mammalian embryo. Blood *117*, 4600–4608.

McGrath, K.E., Frame, J.M., Fegan, K.H., Bowen, J.R., Conway, S.J., Catherman, S.C., Kingsley, P.D., Koniski, A.D., and Palis, J. (2015a). Distinct Sources of Hematopoietic Progenitors Emerge before HSCs and Provide Functional Blood Cells in the Mammalian Embryo. Cell Rep. *11*, 1892–1904.

McGrath, K.E., Frame, J.M., and Palis, J. (2015b). Early hematopoiesis and macrophage development. Semin. Immunol. *27*, 379–387.

McKenna, H.J., Stocking, K.L., Miller, R.E., Brasel, K., De Smedt, T., Maraskovsky, E., Maliszewski, C.R., Lynch, D.H., Smith, J., Pulendran, B., et al. (2000). Mice lacking flt3 ligand have deficient hematopoiesis affecting hematopoietic progenitor cells, dendritic cells, and natural killer cells. Blood *95*, 3489–3497.

Mebius, R.E., and Kraal, G. (2005). Structure and function of the spleen. Nat. Rev. Immunol. *5*, 606–616.

Medvinsky, A., and Dzierzak, E. (1996). Definitive hematopoiesis is autonomously initiated by the AGM region. Cell *86*, 897–906.

Metcalf, D., Johnson, G.R., and Burgess, A.W. (1980). Direct stimulation by purified GM-CSF of the proliferation of multipotential and erythroid precursor cells. Blood *55*, 138–147.

Metcalf, D., Carpinelli, M.R., Hyland, C., Mifsud, S., DiRago, L., Nicola, N.A., Hilton, D.J., and

Alexander, W.S. (2005). Anomalous megakaryocytopoiesis in mice with mutations in the c-Myb gene. Blood *105*, 3480–3487.

Metzger, D., Clifford, J., Chiba, H., and Chambon, P. (1995). Conditional site-specific recombination in mammalian cells using a ligand- dependent chimeric Cre recombinase. Proc. Natl. Acad. Sci. U. S. A. *92*, 6991–6995.

Meyer, N., Woidacki, K., Knöfler, M., Meinhardt, G., Nowak, D., Velicky, P., Pollheimer, J., and Zenclussen, A.C. (2017). Chymase-producing cells of the innate immune system are required for decidual vascular remodeling and fetal growth. Sci. Rep. *7*, 1–14.

Migliaccio, A.R., Rana, R.A., Sanchez, M., Lorenzini, R., Centurione, L., Bianchi, L., Vannucchi, A.M., Migliaccio, G., and Orkin, S.H. (2003). GATA-1 as a regulator of mast cell differentiation revealed by the phenotype of the GATA-1low mouse mutant. J. Exp. Med. *197*, 281–296.

Migliaccio, G., Migliaccio, A.R., Petti, S., Mavilio, F., Russo, G., Lazzaro, D., Testa, U., Marinucci, M., and Peschle, C. (1986). Human embryonic hemopoiesis. Kinetics of progenitors and precursors underlying the yolk sac-liver transition. J. Clin. Invest. *78*, 51–60.

Mikkola, H.K.A., and Orkin, S.H. (2006). The journey of developing hematopoietic stem cells. Development *133*, 3733–3744.

Mikkola, H.K.A.A., Fujiwara, Y., Schlaeger, T.M., Traver, D., and Orkin, S.H. (2003). Expression of CD41 marks the initiation of definitive hematopoiesis in the mouse embryo. Blood *101*, 508–516.

Min, B., Brown, M.A., and LeGros, G. (2012). Understanding the roles of basophils: breaking dawn. Immunology *135*, 192–197.

Molawi, K., Wolf, Y., Kandalla, P.K., Favret, J., Hagemeyer, N., Frenzel, K., Pinto, A.R., Klapproth, K., Henri, S., Malissen, B., et al. (2014). Progressive replacement of embryo-derived cardiac macrophages with age. J. Exp. Med. *211*, 2151–2158.

Moore, M.A.S., and Metcalf, D. (1970). Ontogeny of the Haemopoietic System: Yolk Sac Origin of In Vivo and In Vitro Colony Forming Cells in the Developing Mouse Embryo. Br. J. Haematol. *18*, 279–296.

Morera, D., and MacKenzie, S.A. (2011). Is there a direct role for erythrocytes in the immune response? Vet. Res. *42*, 89.

Morrison, S.J., Uchida, N., and Weissman, I.L. (1995a). The Biology of Hematopoietic Stem Cells. Annu. Rev. Cell Dev. Biol. *11*, 35–71.

Morrison, S.J., Hemmati, H.D., Wandycz, A.M., and Weissman, I.L. (1995b). The purification and characterization of fetal liver hematopoietic stem cells. Proc. Natl. Acad. Sci. U. S. A. *92*, 10302–10306.

Mucenski, M.L., McLain, K., Kier, A.B., Swerdlow, S.H., Schreiner, C.M., Miller, T.A., Pietryga, D.W., Scott Jr., W.J., and Potter, S.S. (1991). A functional c-myb gene is required for normal murine fetal hepatic hematopoiesis. Cell *65*, 677–689.

Müller, A.M., Medvinsky, A., Strouboulis, J., Grosveld, F., and Dzierzakt, E. (1994). Development of hematopoietic stem cell activity in the mouse embryo. Immunity *1*, 291–301.

Muñoz-Espín, D., Cañamero, M., Maraver, A., Gómez-López, G., Contreras, J., Murillo-Cuesta, S., Rodríguez-Baeza, A., Varela-Nieto, I., Ruberte, J., Collado, M., et al. (2013). Programmed cell senescence during mammalian embryonic development. Cell *155*, 1104.

Murray, P.J., Allen, J.E., Biswas, S.K., Fisher, E.A., Gilroy, D.W., Goerdt, S., Gordon, S.,

Hamilton, J.A., Ivashkiv, L.B., Lawrence, T., et al. (2014). Macrophage Activation and Polarization: Nomenclature and Experimental Guidelines. Immunity *41*, 14–20.

Nahrendorf, M., Swirski, F.K., Aikawa, E., Stangenberg, L., Wurdinger, T., Figueiredo, J.L., Libby, P., Weissleder, R., and Pittet, M.J. (2007). The healing myocardium sequentially mobilizes two monocyte subsets with divergent and complementary functions. J. Exp. Med. *204*, 3037–3047.

Naik, S.H., Metcalf, D., van Nieuwenhuijze, A., Wicks, I., Wu, L., O'Keeffe, M., and Shortman, K. (2006). Intrasplenic steady-state dendritic cell precursors that are distinct from monocytes. Nat. Immunol. *7*, 663–671.

Naito, M., Yamamura, F., Nishikawa, S., and Takahashi, K. (1989). Development, Differentiation, and Maturation of Fetal Mouse Yolk Sac Macrophages in Cultures. J. Leukoc. Biol. *46*, 1–10.

Naito, M., Umeda, S., Yamamoto, T., Moriyama, H., Umezu, H., Hasegawa, G., Usuda, H., Shultz, L.D., and Takahashi, K. (1996). Development, differentiation, and phenotypic heterogeneity of murine tissue macrophages. J. Leukoc. Biol. *59*, 133–138.

Narula, J., Williams, C.J., Tiwari, A., Marks-Bluth, J., Pimanda, J.E., and Igoshin, O.A. (2013). Mathematical model of a gene regulatory network reconciles effects of genetic perturbations on hematopoietic stem cell emergence. Dev. Biol. *379*, 258–269.

Nerlov, C., and Graf, T. (1998). PU.1 induces myeloid lineage commitment in multipotent hematopoietic progenitors. *12*, 2403–2412.

Nerlov, C., Querfurth, E., Kulessa, H., and Graf, T. (2000). GATA-1 interacts with the myeloid PU.1 transcription factor and represses PU.1-dependent transcription. Blood *95*, 2543–2551.

Ngkelo, A., Richart, A., Kirk, J.A., Bonnin, P., Vilar, J., Lemitre, M., Marck, P., Branchereau, M., Le Gall, S., Renault, N., et al. (2016). Mast cells regulate myofilament calcium sensitization and heart function after myocardial infarction. J. Exp. Med. *213*, 1353–1374.

Nguyen, P.T., Dorman, L.C., Pan, S., Vainchtein, I.D., Han, R.T., Nakao-Inoue, H., Taloma, S.E., Barron, J.J., Molofsky, A.B., Kheirbek, M.A., et al. (2020). Microglial Remodeling of the Extracellular Matrix Promotes Synapse Plasticity. Cell *182*, 388-403.e15.

Nimmerjahn, A., Kirchhoff, F., and Helmchen, F. (2005). Neuroscience: Resting microglial cells are highly dynamic surveillants of brain parenchyma in vivo. Science (80-.). *308*, 1314–1318.

Nishijima, I., Watanabe, S., Nakahata, T., and Arai, K.I. (1997). Human granulocyte-macrophage colony-stimulating factor (hGM-CSF)-dependent in vitro and in vivo proliferation and differentiation of all hematopoietic progenitor cells in hGM-CSF receptor transgenic mice. J. Allergy Clin. Immunol. *100*, S79–S86.

North, T., Gu, T.L., Stacy, T., Wang, Q., Howard, L., Binder, M., Marin-Padilla, M., and Speck, N.A. (1999). Cbfa2 is required for the formation of intra-aortic hematopoietic clusters. Development *126*, 2563 LP – 2575.

North, T.E., De Bruijn, M.F.T.R., Stacy, T., Talebian, L., Lind, E., Robin, C., Binder, M., Dzierzak, E., and Speck, N.A. (2002). Runx1 expression marks long-term repopulating hematopoietic stem cells in the midgestation mouse embryo. Immunity *16*, 661–672.

North, T.E., Goessling, W., Peeters, M., Li, P., Ceol, C., Lord, A.M., Weber, G.J., Harris, J., Cutting, C.C., Huang, P., et al. (2009). Hematopoietic Stem Cell Development Is Dependent on Blood Flow. Cell *137*, 736–748.

O'Keeffe, M., Hochrein, H., Vremec, D., Caminschi, I., Miller, J.L., Anders, E.M., Wu, L., Lahoud, M.H., Henri, S., Scott, B., et al. (2002). Mouse plasmacytoid cells: Long-lived cells, heterogeneous in surface phenotype and function, that differentiate into CD8- dendritic cells only after microbial stimulus. J. Exp. Med. *196*, 1307–1319.

Oatley, M., Bölükbası, Ö.V., Svensson, V., Shvartsman, M., Ganter, K., Zirngibl, K., Pavlovich, P. V., Milchevskaya, V., Foteva, V., Natarajan, K.N., et al. (2020). Single-cell transcriptomics identifies CD44 as a marker and regulator of endothelial to haematopoietic transition. Nat. Commun. *11*, 1–18.

Oberlin, E., Tavian, M., Blazsek, I., and Péault, B. (2002). Blood-forming potential of vascular endothelium in the human embryo. Development *129*, 4147 LP – 4157.

Ogawa, M., Tajima, F., Ito, T., Sato, T., Laver, J.H., and Deguchi, T. (2001). CD34 Expression by Murine Hematopoietic Stem Cells. Ann. N. Y. Acad. Sci. *938*, 139–145.

Ohls, R.K., Li, Y., Abdel-Mageed, A., Buchanan, G., Mandell, L., and Christensen, R.D. (1995). Neutrophil pool sizes and granulocyte colony-stimulating factor production in human mid-trimester fetuses. Pediatr. Res. *37*, 806–811.

Okabe, Y., and Medzhitov, R. (2014). Tissue-specific signals control reversible program of localization and functional polarization of macrophages. Cell *157*, 832–844.

Okabe, Y., and Medzhitov, R. (2016). Tissue biology perspective on macrophages. Nat. Immunol. *17*, 9–17.

Okuda, T., Van Deursen, J., and Hiebert, S.W. (1996). AML1, the Target of Multiple Chromosomal Translocations in Human Leukemia, Is Essential for Normal Fetal Liver Hematopoiesis.

Onai, N., Obata-Onai, A., Schmid, M.A., and Manz, M.G. (2007). Flt3 in Regulation of Type I Interferon-Producing Cell and Dendritic Cell Development. Ann. N. Y. Acad. Sci. *1106*, 253–261.

Orkin, S.H., and Zon, L.I. (2008). Hematopoiesis: An Evolving Paradigm for Stem Cell Biology. Cell *132*, 631–644.

Ottersbach, K. (2019). Endothelial-to-haematopoietic transition: An update on the process of making blood. Biochem. Soc. Trans. *47*, 591–601.

Palis, J. (2006). Yolk Sac Development in Mice. In Hematopoietic Stem Cell Development, (Boston, MA: Springer US), pp. 62–71.

Palis, J. (2014). Primitive and definitive erythropoiesis in mammals. Front. Physiol. *5 JAN*, 3.

Palis, J., and Yoder, M.C. (2001). Yolk-sac hematopoiesis: The first blood cells of mouse and man. Exp. Hematol. *29*, 927–936.

Palis, J., Robertson, S., Kennedy, M., Wall, C., and Keller, G. (1999). Development of erythroid and myeloid progenitors in the yolk sac and embryo proper of the mouse. Development *126*, 5073–5084.

Palis, J., Chan, R.J., Koniski, A., Patel, R., Starr, M., and Yoder, M.C. (2001). Spatial and temporal emergence of high proliferative potential hematopoietic precursors during murine embryogenesis. Proc. Natl. Acad. Sci. U. S. A. *98*, 4528–4533.

van Panhuys, N., Prout, M., Forbes, E., Min, B., Paul, W.E., and Le Gros, G. (2011). Basophils Are the Major Producers of IL-4 during Primary Helminth Infection. J. Immunol. *186*, 2719–2728.

Paolicelli, R.C., Bolasco, G., Pagani, F., Maggi, L., Scianni, M., Panzanelli, P., Giustetto, M., Ferreira, T.A., Guiducci, E., Dumas, L., et al. (2011). Synaptic pruning by microglia is necessary for normal brain development. Science (80-.). *333*, 1456–1458.

Parwaresch, M.R., and Wacker, H.-H. (1984). Origin and Kinetics of Resident Tissue Macrophages. Cell Prolif. *17*, 25–39.

Passegué, E., Wagers, A.J., Giuriato, S., Anderson, W.C., and Weissman, I.L. (2005). Global analysis of proliferation and cell cycle gene expression in the regulation of hematopoietic stem and progenitor cell fates. J. Exp. Med. *202*, 1599–1611.

Patel, S.R., Hartwig, J.H., and Italiano, J.E. (2005). The biogenesis of platelets from megakaryocyte proplatelets. J. Clin. Invest. *115*, 3348–3354.

Paul, F., Arkin, Y., Giladi, A., Jaitin, D.A., Kenigsberg, E., Keren-Shaul, H., Winter, D., Lara-Astiaso, D., Gury, M., Weiner, A., et al. (2015). Transcriptional Heterogeneity and Lineage Commitment in Myeloid Progenitors. Cell *163*, 1663–1677.

Payer, E., Elbe, A., and Stingl, G. (1991). Circulating CD3+/T cell receptor V gamma 3+ fetal murine thymocytes home to the skin and give rise to proliferating dendritic epidermal T cells. J. Immunol. *146*, 2536–2543.

Pei, W., Shang, F., Wang, X., Fanti, A.-K., Greco, A., Busch, K., Klapproth, K., Zhang, Q., Quedenau, C., Sauer, S., et al. (2020). Resolving Fates and Single-Cell Transcriptomes of Hematopoietic Stem Cell Clones by PolyloxExpress Barcoding. Cell Stem Cell *0*.

Peschle, C., Mavilio, F., Carè, A., Migliaccio, G., Migliaccio, A.R., Salvo, G., Samoggia, P., Petti, S., Guerriero, R., Marinucci, M., et al. (1985). Haemoglobin switching in human embryos: Asynchrony of ζ → α and ε → γ-globin switches in primitive and definitive erythropoietic lineage. Nature *313*, 235–238.

Peters, W., Cyster, J.G., Mack, M., Schlöndorff, D., Wolf, A.J., Ernst, J.D., and Charo, I.F. (2004). CCR2-Dependent Trafficking of F4/80dim Macrophages and CD11cdim/intermediate Dendritic Cells Is Crucial for T Cell Recruitment to Lungs Infected with Mycobacterium tuberculosis. J. Immunol. *172*, 7647 LP – 7653.

Petrenko, O., Beavis, A., Klaine, M., Kittappa, R., Godin, I., and Lemischka, I.R. (1999). The molecular characterization of the fetal stem cell marker AA4. Immunity *10*, 691–700.

Pietras, E.M., Reynaud, D., Kang, Y.A., Carlin, D., Calero-Nieto, F.J., Leavitt, A.D., Stuart, J.A., Göttgens, B., and Passegué, E. (2015). Functionally Distinct Subsets of Lineage-Biased Multipotent Progenitors Control Blood Production in Normal and Regenerative Conditions. Cell Stem Cell *17*, 35–46.

Pinho, S., Marchand, T., Yang, E., Wei, Q., Nerlov, C., and Frenette, P.S. (2018). Lineage-Biased Hematopoietic Stem Cells Are Regulated by Distinct Niches. Dev. Cell *44*, 634-641.e4.

Plantinga, M., Guilliams, M., Vanheerswynghels, M., Deswarte, K., Branco-Madeira, F., Toussaint, W., Vanhoutte, L., Neyt, K., Killeen, N., Malissen, B., et al. (2013). Conventional and Monocyte-Derived CD11b+ Dendritic Cells Initiate and Maintain T Helper 2 Cell-Mediated Immunity to House Dust Mite Allergen. Immunity *38*, 322–335.

Pons, P., and Latapy, M. (2006). Computing communities in large networks using random walks. J. Graph Algorithms Appl. *10*, 191–218.

Popescu, D.M., Botting, R.A., Stephenson, E., Green, K., Webb, S., Jardine, L., Calderbank, E.F., Polanski, K., Goh, I., Efremova, M., et al. (2019). Decoding human fetal liver haematopoiesis. Nature *574*, 365–371.

Potts, K.S., Sargeant, T.J., Markham, J.F., Shi, W., Biben, C., Josefsson, E.C., Whitehead, L.W., Rogers, K.L., Liakhovitskaia, A., Smyth, G.K., et al. (2014). A lineage of diploid platelet-forming cells precedes polyploid megakaryocyte formation in the mouse embryo. Blood *124*, 2725–2729.

Prussin, C., and Metcalfe, D.D. (2006). 5. IgE, mast cells, basophils, and eosinophils. J. Allergy Clin. Immunol. *117*, S450–S456.

Qi, X., Hong, J., Chaves, L., Zhuang, Y., Chen, Y., Wang, D., Chabon, J., Graham, B., Ohmori, K., Li, Y., et al. (2013). Antagonistic Regulation by the Transcription Factors C/EBPα and MITF Specifies Basophil and Mast Cell Fates. Immunity *39*, 97–110.

Rebel, V.I., Miller, C.L., Eaves, C.J., and Lansdorp, P.M. (1996). The repopulation potential of fetal liver hematopoietic stem cells in mice exceeds that of their adult bone marrow counterparts. Blood *87*, 3500–3507.

Reizis, B., Bunin, A., Ghosh, H.S., Lewis, K.L., and Sisirak, V. (2011). Plasmacytoid dendritic cells: Recent progress and open questions. Annu. Rev. Immunol. *29*, 163–183.

Robb, L., Lyons, I., Li, R., Hartley, L., Köntgen, F., Harvey, R.P., Metcalf, D., and Begley, C.G. (1995). Absence of yolk sac hematopoiesis from mice with a targeted disruption of the scl gene. Proc. Natl. Acad. Sci. U. S. A. *92*, 7075–7079.

Robert-Moreno, À., Espinosa, L., de la Pompa, J.L., and Bigas, A. (2005). RBPjκ-dependent Notch function regulates Gata2 and is essential for the formation of intra-embryonic hematopoietic cells. Development *132*, 1117–1126.

Robert-Moreno, À., Guiu, J., Ruiz-Herguido, C., López, M.E., Inglés-Esteve, J., Riera, L., Tipping, A., Enver, T., Dzierzak, E., Gridley, T., et al. (2008). Impaired embryonic haematopoiesis yet normal arterial development in the absence of the Notch ligand Jagged1. EMBO J. *27*, 1886–1895.

Rodrigues, P.F., Alberti-Servera, L., Eremin, A., Grajales-Reyes, G.E., Ivanek, R., and Tussiwand, R. (2018). Distinct progenitor lineages contribute to the heterogeneity of plasmacytoid dendritic cells. Nat. Immunol. *19*, 711–722.

Rodriguez-Fraticelli, A.E., Wolock, S.L., Weinreb, C.S., Panero, R., Patel, S.H., Jankovic, M., Sun, J., Calogero, R.A., Klein, A.M., and Camargo, F.D. (2018). Clonal analysis of lineage fate in native haematopoiesis. Nature *553*, 212–216.

Rosas, M., Davies, L.C., Giles, P.J., Liao, C. Te, Kharfan, B., Stone, T.C., O'Donnell, V.B., Fraser, D.J., Jones, S.A., and Taylor, P.R. (2014). The transcription factor Gata6 links tissue macrophage phenotype and proliferative renewal. Science (80-.). *344*, 645–648.

Ruiz-Herguido, C., Guiu, J., D'Altri, T., Inglés-Esteve, J., Dzierzak, E., Espinosa, L., and Bigas, A. (2012). Hematopoietic stem cell development requires transient Wnt/β-catenin activity. J. Exp. Med. *209*, 1457–1468.

Russell, E.S., and Seldon E. Bernstein (1966). Blood and Blood Formation.

Rybtsov, S., Sobiesiak, M., Taoudi, S., Souilhol, C., Senserrich, J., Liakhovitskaia, A., Ivanovs, A., Frampton, J., Zhao, S., and Medvinsky, A. (2011). Hierarchical organization and early hematopoietic specification of the developing HSC lineage in the AGM region. J. Exp. Med. *208*, 1305–1315.

Sabin, F.R. (1920). Studies on the origin of blood-vessels and ofred blood-corpuscles as seen in the living blastoderm of chicks during the second day of incubation.

Salvermoser, J., van Blijswijk, J., Papaioannou, N.E., Rambichler, S., Pasztoi, M., Pakalniškyte, D., Rogers, N.C., Keppler, S.J., Straub, T., Reis e Sousa, C., et al. (2018). Clec9a-mediated ablation of conventional dendritic cells suggests a lymphoid path to generating dendritic cells in vivo. Front. Immunol. *9*, 16.

Samokhvalov, I.M., Samokhvalova, N.I., and Nishikawa, S.I. (2007). Cell tracing shows the contribution of the yolk sac to adult haematopoiesis. Nature *446*, 1056–1061.

Samstein, M., Schreiber, H.A., Leiner, I.M., Sušac, B., Glickman, M.S., and Pamer, E.G.

(2013). Essential yet limited role for CCR2+ inflammatory monocytes during Mycobacterium tuberculosis-specific T cell priming. Elife *2013*.

Sánchez, M.J., Holmes, A., Miles, C., and Dzierzak, E. (1996). Characterization of the first definitive hematopoietic stem cells in the AGM and liver of the mouse embryo. Immunity *5*, 513–525.

Sanjuan-Pla, A., Macaulay, I.C., Jensen, C.T., Woll, P.S., Luis, T.C., Mead, A., Moore, S., Carella, C., Matsuoka, S., Jones, T.B., et al. (2013). Platelet-biased stem cells reside at the apex of the haematopoietic stem-cell hierarchy. Nature *502*, 232–236.

Sasaki, K., and Sonoda, Y. (2000). Histometrical and Three-Dimensional Analyses of Liver Hematopoiesis in the Mouse Embryo. Arch. Histol. Cytol. *63*, 137–146.

Satpathy, A.T., KC, W., Albring, J.C., Edelson, B.T., Kretzer, N.M., Bhattacharya, D., Murphy, T.L., and Murphy, K.M. (2012). Zbtb46 expression distinguishes classical dendritic cells and their committed progenitors from other immune lineages. J. Exp. Med. *209*, 1135–1152.

Savill, J.S., Henson, P.M., and Haslett, C. (1989a). Phagocytosis of aged human neutrophils by macrophages is mediated by a novel 'charge-sensitive'recognition mechanism. J. Clin. Invest. *84*, 1518–1527.

Savill, J.S., Wyllie, A.H., Henson, J.E., Walport, M.J., Henson, P.M., and Haslett, C. (1989b). Macrophage phagocytosis of aging neutrophils in inflammation. Programmed cell death in the neutrophil leads to its recognition by macrophages. J. Clin. Invest. *83*, 865–875.

Sawamiphak, S., Kontarakis, Z., and Stainier, D.Y.R. (2014). Interferon Gamma Signaling Positively Regulates Hematopoietic Stem Cell Emergence. Dev. Cell *31*, 640–653.

Schlitzer, A., Sivakamasundari, V., Chen, J., Sumatoh, H.R. Bin, Schreuder, J., Lum, J., Malleret, B., Zhang, S., Larbi, A., Zolezzi, F., et al. (2015). Identification of cDC1- and cDC2-committed DC progenitors reveals early lineage priming at the common DC progenitor stage in the bone marrow. Nat. Immunol. *16*, 718–728.

Schüler, A., Schwieger, M., Engelmann, A., Weber, K., Horn, S., Müller, U., Arnold, M.A., Olson, E.N., Stocking, C., Schü, A., et al. (2008). The MADS transcription factor Mef2c is a pivotal modulator of myeloid cell fate. Blood *111*, 4532–4541.

Schüller, S.S., Sadeghi, K., Wisgrill, L., Dangl, A., Diesner, S.C., Prusa, A.R., Klebermasz-Schrehof, K., Greber-Platzer, S., Neumüller, J., Helmer, H., et al. (2013). Preterm neonates display altered plasmacytoid dendritic cell function and morphology. J. Leukoc. Biol. *93*, 781–788.

Schulz, C., Perdiguero, E.G., Chorro, L., Szabo-Rogers, H., Cagnard, N., Kierdorf, K., Prinz, M., Wu, B., Jacobsen, S.E.W., Pollard, J.W., et al. (2012). A Lineage of Myeloid Cells Independent of Myb and Hematopoietic Stem Cells. Science (80-.). *336*, 86 LP – 90.

Scialdone, A., Natarajan, K.N., Saraiva, L.R., Proserpio, V., Teichmann, S.A., Stegle, O., Marioni, J.C., and Buettner, F. (2015). Computational assignment of cell-cycle stage from single-cell transcriptome data. Methods *85*, 54–61.

Scott, C.L., and Begley, C.G. (1999). The beta common chain (βc) of the granulocyte macrophage-colony stimulating factor, interleukin-3 and interleukin-5 receptors. Int. J. Biochem. Cell Biol. *31*, 1011–1015.

Scott, C.L., Zheng, F., De Baetselier, P., Martens, L., Saeys, Y., De Prijck, S., Lippens, S., Abels, C., Schoonooghe, S., Raes, G., et al. (2016). Bone marrow-derived monocytes give rise to self-renewing and fully differentiated Kupffer cells. Nat. Commun. *7*, 1–10.

Scott, C.L., T'Jonck, W., Martens, L., Todorov, H., Sichien, D., Soen, B., Bonnardel, J., De Prijck, S., Vandamme, N., Cannoodt, R., et al. (2018). The Transcription Factor ZEB2 Is Required to Maintain the Tissue-Specific Identities of Macrophages. Immunity *49*, 312-325.e5.

Segura, E., and Amigorena, S. (2013). Inflammatory dendritic cells in mice and humans. Trends Immunol. *34*, 440–445.

Serbina, N. V., Kuziel, W., Flavell, R., Akira, S., Rollins, B., and Pamer, E.G. (2003). Sequential MyD88-Independent and -Dependent Activation of Innate Immune Responses to Intracellular Bacterial Infection. Immunity *19*, 891–901.

Shivdasanl, R.A., Mayer, E.L., and Orkin, S.H. (1995). Absence of blood formation in mice lacking the T-cell leukaemia oncoprotein tal-1/SCL. Nature *373*, 432–434.

Siegal, F.P., Kadowaki, N., Shodell, M., Fitzgerald-Bocarsly, P.A., Shah, K., Ho, S., Antonenko, S., and Liu, Y.J. (1999). The nature of the principal Type 1 interferon-producing cells in human blood. Science (80-.). *284*, 1835–1837.

Silver, L., and Palis, J. (1997). Initiation of murine embryonic erythropoiesis: A spatial analysis. Blood *89*, 1154–1164.

Slayton, W.B., Juul, S.E., Calhoun, D.A., Li, Y., Braylan, R.C., and Christensen, R.D. (1998). Hematopoiesisis the liver and marrow of human fetuses at 5 to 16 weeks postconception: Quantitative assessment of macrophage and neutrophil populations. Pediatr. Res. *43*, 774–782.

Snell, G.D., and Stevens, L.C. (1966). Early Embryology.

Soares-da-Silva, F., Burlen-Defranoux, O., Elsaid, R., Iturri, L., Freyer, L., Sismeiro, O., Pinto-do-Ó, P., Gomez-Perdiguero, E., and Cumano, A. (2020). Yolk sac erythromyeloid progenitors sustain erythropoiesis throughout embryonic life. BioRxiv 2020.02.27.968230.

Soehnlein, O., Steffens, S., Hidalgo, A., and Weber, C. (2017). Neutrophils as protagonists and targets in chronic inflammation. Nat. Rev. Immunol. *17*, 248–261.

Sonoda, T., Hayashi, C., and Kitamura, Y. (1983). Presence of mast cell precursors in the yolk sac of mice. Dev. Biol. *97*, 89–94.

Stamatoyannopoulos, G. (2005). Control of globin gene expression during development and erythroid differentiation. Exp. Hematol. *33*, 259–271.

Stamatoyannopoulos, G., and Nienhuis, A.W. (1983). Globin Gene Expression and Hematopoietic Differentiation. Liss, New York.

Stefanska, M., Batta, K., Patel, R., Florkowska, M., Kouskoff, V., and Lacaud, G. (2017). Primitive erythrocytes are generated from hemogenic endothelial cells. Sci. Rep. *7*, 1–10.

Stegner, D., Vaneeuwijk, J.M.M., Angay, O., Gorelashvili, M.G., Semeniak, D., Pinnecker, J., Schmithausen, P., Meyer, I., Friedrich, M., Dütting, S., et al. (2017). Thrombopoiesis is spatially regulated by the bone marrow vasculature. Nat. Commun. *8*, 1–11.

Stremmel, C., Schuchert, R., Wagner, F., Thaler, R., Weinberger, T., Pick, R., Mass, E., Ishikawa-Ankerhold, H.C., Margraf, A., Hutter, S., et al. (2018). Yolk sac macrophage progenitors traffic to the embryo during defined stages of development. Nat. Commun. *9*, 75.

Stuart, T., Butler, A., Hoffman, P., Hafemeister, C., Papalexi, E., Mauck, W.M., Hao, Y., Stoeckius, M., Smibert, P., and Satija, R. (2019). Comprehensive Integration of Single-Cell Data. Cell *177*, 1888-1902.e21.

Summers, K.M., and Hume, D.A. (2017). Identification of the macrophage-specific promoter

signature in FANTOM5 mouse embryo developmental time course data. J. Leukoc. Biol. *102*, 1081–1092.

Summers, C., Rankin, S.M., Condliffe, A.M., Singh, N., Peters, A.M., and Chilvers, E.R. (2010). Neutrophil kinetics in health and disease. Trends Immunol. *31*, 318–324.

Sumner, R., Crawford, A., Mucenski, M., and Frampton, J. (2000). Initiation of adult myelopoiesis can occur in the absence of c-Myb whereas subsequent development is strictly dependent on the transcription factor. Oncogene *19*, 3335–3342.

Sun, C.M., Fiette, L., Tanguy, M., Leclerc, C., and Lo-Man, R. (2003). Ontogeny and innate properties of neonatal dendritic cells. Blood *102*, 585–591.

Swirski, F.K., Nahrendorf, M., Etzrodt, M., Wildgruber, M., Cortez-Retamozo, V., Panizzi, P., Figueiredo, J.L., Kohler, R.H., Chudnovskiy, A., Waterman, P., et al. (2009). Identification of splenic reservoir monocytes and their deployment to inflammatory sites. Science (80-.). *325*, 612–616.

Takahashi, K., Yamamura, F., and Naito, M. (1989). Differentiation, maturation, and proliferation of macrophages in the mouse yolk sac: A light-microscopic, enzyme-cytochemical, immunohistochemical, and ultrastructural study. J. Leukoc. Biol. *45*, 87–96.

Tamoutounour, S., Guilliams, M., MontananaSanchis, F., Liu, H., Terhorst, D., Malosse, C., Pollet, E., Ardouin, L., Luche, H., Sanchez, C., et al. (2013). Origins and functional specialization of macrophages and of conventional and monocyte-derived dendritic cells in mouse skin. Immunity *39*, 925–938.

Tang, Y., Harrington, A., Yang, X., Friesel, R.E., and Liaw, L. (2010). The contribution of the Tie2+ lineage to primitive and definitive hematopoietic cells. Genesis *48*, 563–567.

Taoudi, S., Gonneau, C., Moore, K., Sheridan, J.M., Blackburn, C.C., Taylor, E., and Medvinsky, A. (2008). Extensive hematopoietic stem cell generation in the AGM region via maturation of VE-Cadherin+CD45+ pre-definitive HSCs. Cell Stem Cell *3*, 99–108.

Tavian, M., Coulombel, L., Luton, D., Clemente, H., Dieterlen-Lievre, F., and Peault, B. (1996). Aorta-associated CD34+ hematopoietic cells in the early human embryo. Blood *87*, 67–72.

Tavian, M., Robin, C., Coulombel, L., and Péault, B. (2001). The human embryo, but not its yolk sac, generates lympho-myeloid stem cells: Mapping multipotent hematopoietic cell fate in intraembryonic mesoderm. Immunity *15*, 487–495.

Teschendorff, A.E., and Enver, T. (2017). Single-cell entropy for accurate estimation of differentiation potency from a cell's transcriptome. Nat. Commun. *8*, 1–15.

Tober, J., Koniski, A., McGrath, K.E., Vemishetti, R., Emerson, R., De Mesy-Bentley, K.K.L., Waugh, R., and Palis, J. (2007). The megakaryocyte lineage originates from hemangioblast precursors and is an integral component both of primitive and of definitive hematopoiesis. Blood *109*, 1433–1441.

Tober, J., McGrath, K.E., and Palis, J. (2008). Primitive erythropoiesis and megakaryopoiesis in the yolk sac are independent of c-myb. Blood *111*, 2636–2639.

Tran, S., Baba, I., Poupel, L., Dussaud, S., Moreau, M., Gélineau, A., Marcelin, G., Magréau-Davy, E., Ouhachi, M., Lesnik, P., et al. (2020). Impaired Kupffer Cell Self-Renewal Alters the Liver Response to Lipid Overload during Non-alcoholic Steatohepatitis. Immunity *0*.

Traver, D., Miyamoto, T., Christensen, J., Iwasaki-Arai, J., Akashi, K., and Weissman, I.L. (2001). Fetal liver myelopoiesis occurs through distinct, prospectively isolatable progenitor subsets.

Traynor, T.R., Kuziel, W.A., Toews, G.B., and Huffnagle, G.B. (2000). CCR2 Expression Determines T1 Versus T2 Polarization During Pulmonary Cryptococcus neoformans Infection . J. Immunol. *164*, 2021–2027.

Trimborn, T., Gribnau, J., Grosveld, F., and Fraser, P. (1999). Mechanisms of developmental control transcription in the murine α and β-globin loci. Genes Dev. *13*, 112–124.

Turpen, J.B., and Smith, P.B. (1985). Dorsal lateral plate mesoderm influences proliferation and differentiation of hemopoietic stem cells derived from ventral lateral plate mesoderm during early development of Xenopus laevis embryos. J. Leukoc. Biol. *38*, 415–427.

Turpen, J.B., Kelley, C.M., Mead, P.E., and Zon, L.I. (1997). Bipotential primitive-definitive hematopoietic progenitors in the vertebrate embryo. Immunity *7*, 325–334.

Udan, R.S., Vadakkan, T.J., and Dickinson, M.E. (2013). Dynamic responses of endothelial cells to changes in blood flow during vascular remodeling of the mouse yolk sac. Dev. *140*, 4041–4050.

Vink, C.S., Calero-Nieto, F.J., Wang, X., Maglitto, A., Mariani, S.A., Jawaid, W., Göttgens, B., and Dzierzak, E. (2020). Iterative Single-Cell Analyses Define the Transcriptome of the First Functional Hematopoietic Stem Cells. Cell Rep. *31*, 107627.

Warren, A.J., Colledge, W.H., Carlton, M.B.L., Evans, M.J., Smith, A.J.H., and Rabbitts, T.H. (1994). The Oncogenic Cysteine-rich LIM domain protein Rbtn2 is essential for erythroid development. Cell *78*, 45–57.

Waskow, C., Liu, K., Darrasse-Jèze, G., Guermonprez, P., Ginhoux, F., Merad, M., Shengelia, T., Yao, K., and Nussenzweig, M. (2008). The receptor tyrosine kinase Flt3 is required for dendritic cell development in peripheral lymphoid tissues. Nat. Immunol. *9*, 676–683.

Weisberg, S.P., Hunter, D., Huber, R., Lemieux, J., Slaymaker, S., Vaddi, K., Charo, I., Leibel, R.L., and Ferrante, A.W. (2006). CCR2 modulates inflammatory and metabolic effects of high-fat feeding. J. Clin. Invest. *116*, 115–124.

Williams, T.J., and Hellewell, P.G. (1995). Mechanisms and pharmacological manipulation of eosinophil accumulation in vivo. Trends Pharmacol. Sci. *16*, 418–423.

Wislocki, G.B., Deane, H.W., and Dempsey, E.W. (1946). The histochemistry of the rodent's placenta. Am. J. Anat. *78*, 281–345.

Woidacki, K., Popovic, M., Metz, M., Schumacher, A., Linzke, N., Teles, A., Poirier, F., Fest, S., Jensen, F., Rabinovich, G.A., et al. (2013). Mast cells rescue implantation defects caused by c-kit Deficiency. Cell Death Dis. *4*, 462.

Wojtasiak, M., Pickett, D.L., Tate, M.D., Bedoui, S., Job, E.R., Whitney, P.G., Brooks, A.G., and Reading, P.C. (2010). Gr-1+ cells, but not neutrophils, limit virus replication and lesion development following flank infection of mice with herpes simplex virus type-1. Virology *407*, 143–151.

Wolber, F.M., Leonard, E., Michael, S., Orschell-Traycoff, C.M., Yoder, M.C., and Srour, E.F. (2002). Roles of spleen and liver in development of the murine hematopoietic system. Exp. Hematol. *30*, 1010–1019.

Wong, P., Chung, S., Reicheld, S., and Chui, D. (1986). Hemoglobin switching during murine embryonic development: evidence for two populations of embryonic erythropoietic progenitor cells. Blood *67*, 716–721.

Wynn, T.A., and Vannella, K.M. (2016). Macrophages in Tissue Repair, Regeneration, and Fibrosis. Immunity *44*, 450–462.

Xu, M.J., Matsuoka, S., Yang, F.C., Ebihara, Y., Manabe, A., Tanaka, R., Eguchi, M., Asano,

S., Nakahata, T., and Tsuji, K. (2001). Evidence for the presence of murine primitive megakarycytopoiesis in the early yolk sac. Blood *97*, 2016–2022.

Yáñez, A., Coetzee, S.G., Olsson, A., Muench, D.E., Berman, B.P., Hazelett, D.J., Salomonis, N., Grimes, H.L., and Goodridge, H.S. (2017). Granulocyte-Monocyte Progenitors and Monocyte-Dendritic Cell Progenitors Independently Produce Functionally Distinct Monocytes. Immunity *47*, 890-902.e4.

Yoder, M.C., Hiatt, K., Dutt, P., Mukherjee, P., Bodine, D.M., and Orlic, D. (1997). Characterization of definitive lymphohematopoietic stem cells in the day 9 murine yolk sac. Immunity *7*, 335–344.

Yokomizo, T., and Dzierzak, E. (2010). Three-dimensional cartography of hematopoietic clusters in the vasculature of whole mouse embryos. Development *137*, 3651–3661.

Yokomizo, T., Hasegawa, K., Ishitobi, H., Osato, M., Ema, M., Ito, Y., Yamamoto, M., and Takahashi, S. (2008). Runx1 is involved in primitive erythropoiesis in the mouse. Blood *111*, 4075–4080.

Yona, S., Kim, K.W., Wolf, Y., Mildner, A., Varol, D., Breker, M., Strauss-Ayali, D., Viukov, S., Guilliams, M., Misharin, A., et al. (2013). Fate Mapping Reveals Origins and Dynamics of Monocytes and Tissue Macrophages under Homeostasis. Immunity *38*, 79–91.

Yoshida, H., Kawane, K., Koike, M., Mori, Y., Uchiyama, Y., and Nagata, S. (2005). Phosphatidylserine-dependent engulfment by macrophages of nuclei from erythroid precursor cells. Nature *437*, 754–758.

Yoshimoto, M., Montecino-Rodriguez, E., Ferkowicz, M.J., Porayette, P., Shelley, W.C., Conway, S.J., Dorshkind, K., and Yoder, M.C. (2011). Embryonic day 9 yolk sac and intra-embryonic hemogenic endothelium independently generate a B-1 and marginal zone progenitor lacking B-2 potential. Proc. Natl. Acad. Sci. U. S. A. *108*, 1468–1473.

Yvan-Charvet, L., and Ng, L.G. (2019). Granulopoiesis and Neutrophil Homeostasis: A Metabolic, Daily Balancing Act. Trends Immunol. *40*, 598–612.

Yzaguirre, A.D., de Bruijn, M.F.T.R., and Speck, N.A. (2017). The Role of Runx1 in Embryonic Blood Cell Formation. In Advances in Experimental Medicine and Biology, (Springer New York LLC), pp. 47–64.

Zambidis, E.T., Peault, B., Park, T.S., Bunz, F., and Civin, C.I. (2005). Hematopoietic differentiation of human embryonic stem cells progresses through sequential hematoendothelial, primitive, and definitive stages resembling human yolk sac development. Blood *106*, 860–870.

Zhang, P., Zhang, X., Iwama, A., Yu, C., Smith, K.A., Mueller, B.U., Narravula, S., Torbett, B.E., Orkin, S.H., and Tenen, D.G. (2000). PU.1 inhibits GATA-1 function and erythroid differentiation by blocking GATA-1 DNA binding. Blood *96*, 2641–2648.

Zhang, Y., Riesterer, C., Ayrall, A.M., Sablitzky, F., Littlewood, T.D., and Reth, M. (1996). Inducible site-directed recombination in mouse embryonic stem cells. Nucleic Acids Res. *24*, 543–548.

Zhou, F., Li, X., Wang, W., Zhu, P., Zhou, J., He, W., Ding, M., Xiong, F., Zheng, X., Li, Z., et al. (2016). Tracing haematopoietic stem cell formation at single-cell resolution. Nature *533*, 487–492.

Ziegenhain, C., Vieth, B., Parekh, S., Reinius, B., Guillaumet-Adkins, A., Smets, M., Leonhardt, H., Heyn, H., Hellmann, I., and Enard, W. (2017). Comparative Analysis of Single-Cell RNA Sequencing Methods. Mol. Cell *65*, 631-643.e4.

Zigmond, E., Samia-Grinberg, S., Pasmanik-Chor, M., Brazowski, E., Shibolet, O., Halpern,

Z., and Varol, C. (2014). Infiltrating Monocyte-Derived Macrophages and Resident Kupffer Cells Display Different Ontogeny and Functions in Acute Liver Injury. J. Immunol. *193*, 344–353.

LIST OF FIGURES

Figure 1. Illustration of the three hematopoietic waves during mammal development. 13

Figure 2. Illustrations of murine yolk sacs after gastrulation 26

Figure 3. Illustration of E9.5 murine embryo 28

Figure 4. Illustration of events taking place in EHT 31

Figure 5. Schematic illustration of commitment steps of HSC towards erythroid and myeloid lineages 34

Figure 6. Maturation steps of definitive erythroid precursors deriving from BFU-E progenitors.. 37

Figure 7. Schematic illustration of progenitor steps leading to the production of monocytes.. 42

Figure 8. Schematic illustration of the development of the three types of granulocytes and mast cells in steady state. 53

Figure 9. Erythroid and/or myeloid progenitor populations in the fetal liver. 121

Figure 10. Single cell RNA-Sequencing of yolk sac and fetal liver EMP-derived progenitors 123

Figure 11. Distribution of clusters in the UMAP and expression of manually picked genes. 125

Figure 12. Heatmap displaying the top three differentially expressed genes. 128

Figure 13. MC cluster has differentiated mast cell characteristics.. 129

Figure 14. Contribution of embryonic stage and niche to the cell clusters. 131

Figure 15. Hallmarks of yolk sac definitive hematopoiesis depicted as a lineage tree 151

LIST OF TABLES

Table 1. Summary of main characteristics of the three hematopoietic waves.....24

Table 2. Comparison of the results obtained in *Csf1r*^{MeriCreMer} *Rosa*^{YFP} embryos pulsed at E8.5 or E9.5.....144

ABSTRACT

English

Erythro-myeloid progenitors (EMP) are developmentally restricted hematopoietic progenitors that produce the first definitive hematopoietic cells in the embryo. Importantly, it has been shown that they give rise to tissue-resident macrophages and mast cells that colonize organs during gestation and self-maintain during adult life without contribution from the bone marrow. These cells are specialized immune cells that contribute to the homeostasis of the tissues throughout steady state and tissue challenge (wounds or infections). This PhD project aimed to characterise the contribution of EMPs to the hematopoietic system of the embryo, with special focus to their niche of origin, the yolk sac. With the use of genetic mouse models, high parameter flow cytometry and single cell expression analysis, this project i) characterises the major definitive progenitor populations in the yolk sac, ii) identifies a novel pathway of direct megakaryopoiesis from EMPs and iii) uncovers two waves of EMP potential emerging at different stages. This work sheds light on the poorly characterised early definitive embryonic haematopoiesis and could have potential implications on macrophage ontogeny studies and early childhood myeloproliferative disorders.

Français

Les progéniteurs érythro-myéloïdes (EMP) sont des progéniteurs hématopoïétiques restreints au développement qui produisent les premières cellules hématopoïétiques définitives de l'embryon. Surtout, ils donnent naissance aux macrophages résidents et mastocytes qui colonisent les différents organes pendant la gestation et s'auto-renouvellent pendant la vie adulte sans apport de la moelle osseuse. Ces cellules sont des cellules immunitaires spécialisées qui contribuent à l'homéostasie des tissus aussi bien dans les tissus sains que suite à des blessures ou des infections. Ce projet de doctorat visait à caractériser la contribution des EMP au système hématopoïétique de l'embryon, avec un accent particulier sur leur niche d'origine, le sac vitellin. En utilisant des modèles génétiques de souris, la cytométrie de flux à paramètres élevés et l'analyse de l'expression au niveau unicellulaire, ce projet i) caractérise les principales populations de progéniteurs définitifs dans le sac vitellin, ii) identifie une nouvelle voie de mégacaryopoïèse directe à partir des EMP et iii) découvre deux vagues de potentiel EMP émergeant à des stades différents du développement. Ce projet a pour but de mieux comprendre la complexité de l'hématopoïèse embryonnaire et pourrait avoir des implications sur les études d'ontogenèse des macrophages et les troubles myéloprolifératifs infantiles.